Investigating the Role of Protein Arginine Methyltransferases in Breast Cancer Etiology

Alan James Morettin, B.Sc., M.Sc.

A Thesis
Presented to
The University of Ottawa

In partial fulfillment of requirements
for the degree of
Doctor of Philosophy
in
Cellular and Molecular Medicine

ABSTRACT

Breast cancer is the most commonly diagnosed cancer amongst Canadian women. Though numerous treatments are available, in many instances tumours become refractory or recur. Therefore, understanding the biological events that lead to the progression and therapeutic resistance of breast cancer is essential for the development of novel treatment options for this disease. Numerous members of the protein arginine methyltransferase (PRMT) family, which are the enzymes responsible for catalyzing methylation on arginine residues are aberrantly regulated in breast cancer. Hence, understanding the precise contribution of PRMTs to the development and progression of breast cancer is important. This Thesis will present my findings on the alternatively spliced PRMT1 isoform, PRMT1v2, previously identified to be overexpressed in breast cancer cell lines and here shown to promote breast cancer cell survival and invasion. Second, a novel role is ascribed to PRMT6, another PRMT aberrantly expressed in breast cancer. PRMT6 promotes chemoresistance to the drug bortezomib by mediating stress granule formation through down-regulation of eIF4E. Increased stress granule formation in bortezomib-resistant cancer cells promotes cell survival. Third, DDX3, a prototypical PRMT substrate which is overexpressed in breast cancer cell lines and stimulates transformation of mammary epithelial cells is a novel substrate of PRMT1, CARM1, and PRMT6. Lastly, TDRD3, a reader/effector of arginine methylation also overexpressed in breast tumours regulates breast cancer cell proliferation, anchorage-independent growth and cell motility and invasion.

ACKNOWLEDGEMENTS

First, I would like to thank my supervisor Dr. Jocelyn Cote for providing me with the chance to pursue my PhD degree in his laboratory and the opportunity to work on novel, stimulating and innovative projects. I would also like to thank Jocelyn for providing me with the latitude to follow different research angles that may not always have been correct and for his patience in allowing me to learn from my mistakes. Lastly, I would like to thank him for challenging me and having the faith in me that I would meet those challenges.

I would also like to acknowledge my thesis advisory committee members: Dr. Stephen Lee, Dr. David Lohnes, and Dr. Laura Trinkle-Mulcahy. I would like to thank them for providing helpful insight and constructive criticism; facilitating the movement of my research project forward. Their advice will make me a better scientist through allowing me to examine every potential angle to make my research as concrete as possible.

I would like to thank Cote lab members too numerous to mention both past and present for making my graduate experience in Jocelyn's lab as pleasant and as entertaining as possible. I would like to thank those who provided me with technical assistance that I required over the years. Specifically, I would like to thank Dr. Mitch Baldwin for his assistance and advice throughout the years, in addition to our numerous hockey conversations. I would especially like to thank both Helina Tadesse and Emma Bondy-Chorney for their friendship. Only someone who is undergoing the same process

as you can appreciate the varying degrees of emotions that one endures in this process. I am indebted to both of you.

Lastly, I would like to thank my family for their love and support throughout this process. It is your continual support that gave me the strength and determination to accomplish my goals.

STATEMENT OF CONTRIBUTION OF COLLABORATORS

In Chapter 3 of the dissertation, MCF7 GFP, GFP-PRMT1v1, and GFP-PRMT1v2 stably expressing cell lines were generated by Isabelle Goulet. Mitch Baldwin performed the characterization of the MCF7 GFP expressing cell lines (Figure 3.12A, 13.12B & 3.12D), motility, invasion and MTT assays (Figure 3.13), immunofluorescence images (Figures 3.16 & 3.19) and β-catenin experiments in Figures 3.20 & 3.21. Quantification of the colony scattering assay (Figure 3.17) was performed by Mitch Baldwin, Genevieve Paris and myself.

In Chapter 5, data mining of SILAC mass spectrometry databases was performed by Dr. Laura Trinkle-Mulcahy (Figure 5.2). Mass spectrometry analysis of DDX3 samples immunoprecipitated from HeLa scramble and PRMT6 shRNA expressing cells was performed at the Ottawa Hospital Research Institute Proteomics Core Facility.

In Chapter 6, the colony formation assays in Figure 6.3 were performed by Tyler Murray. The pCMV myc TDRD3 deletion mutants used in Figure 6.6 were generated by Isabelle Goulet. The tail vein injection mouse model (Appendix Iq) was performed by Mitch Baldwin and Genevieve Paris.

TABLE OF CONTENTS

LIST OF FIGURES AND ILLUSTRATIONS

List of Abbreviations

PRMT	Protein arginine methyltransferase
AdoMet	S-adenosylmethionine
AdoHcy	S-adenosylhomocysteine
ADMA	asymmetric dimethylarginine
SMDA	symmetric dimethylarginine
MMA	monomethylarginine
GAR	glycine- and arginine-rich
CARM1	Co-activator of arginine methyltransferase 1
PGM	proline-, glycine- and methionine-rich
H3R17	histone 3 arginine 17
ERα	estrogen receptor α
JMJD6	Jumonji domain-containing protein 6
miRNA	micro RNA
HIV	human immunodeficiency virus
JAK2	janus kinase 2
MEP50	methylosome protein 50
H3K18	histone 3 lysine 18
H3K8	histone 3 lysine 8
H3R8	histone 3 arginine 8
H4K5	histone 4 lysine 5
H4R3	histone 4 arginine 3
BTG2	B-cell translocation gene 2
hCAF1	CCR4-associated factor 1
NF-κB	Nuclear Factor κB
PR	progesterone receptor
RBPs	RNA-binding proteins
Sam68	Src associated substrate in mitosis of 68 kDa
DNA	deoxyribonucleic acid
DSBs	DNA double strand breaks
MRN complex	MRE11/Rad50/Nsb1 complex
53BP1	p53 binding protein 1
Pol-β	DNA polymerase β
SMN	survival of motor neuron
SPF30	survival of motor neuron-related splicing factor 30
TDRD3	Tudor domain containing protein 3
STAT1	signal transducer and activator of transcription 1
mRNA	messenger ribonucleic acid
PI3K	phosphoinositide 3-kinase
FAK	focal adhesion kinase
BRCA1	breast cancer 1, early onset
FOXO1	forkhead box O1
BAD	BCL-2 antagonist of cell death
ASK1	apoptotic signalling kinase 1
GSK-3β	glycogen synthase kinase 3β

APC	adenomatous polyposis coli
CK1	casein kinase 1
NES	nuclear export sequence
PELP1	proline-, glutamic acid- and leucine-rich protein 1
RNP	ribonucleoprotein
VEGF	vascular endothelial growth factor
Syk	spleen tyrosine kinase
H3R2	histone 3 arginine 2
TSP-1	thromobospondin 1
H3K4	histone 3 lysine 4
H2AR29	histone 2A arginine 29
H3K27	histone 3 lysine 27
H3R42	histone 3 arginine 42
CDK	cyclin-dependent kinase
MEF	mouse embryonic fibroblast
eIF	eukaryotic initiation factor
GTP	guanosine-5'-triphosphate
tRNA	transfer RNA
MET	methionine
PKR	protein kinase R
PERK	PKR-like endoplasmic reticulum kinase
GCN	general control nonderepressible 2
HRI	heme regulated initiation factor 2α kinase
PABP1	Poly A binding protein 1
TIA-1	T cell internal antigen 1
FMRP	Fragile X Mental Retardation Protein
DDX3	DEAD-box RNA Helicase 3
UTR	untranslated region
RACK1	receptor for activated C kinase 1
MAPK	mitogen-activated protein kinase
hnRNP	heterogenous nuclear ribonucleoprotein
snRNP	small nuclear ribonucleoprotein
ATP	adenosine-5'-triphosphate
mRNPs	messenger ribonucleprotein
EJC	exon junction complex
CBC	cap binding complex
IRES	internal ribosome entry site
HCV	hepatitis C virus
cDNA	complementary DNA
GC	guanosine cytosine
4E-BP1	4E binding protein 1
HBV	hepatitis B virus
HCC	hepatocellular carcinoma
HIF1α	hypoxia inducible factor 1α
cIAP-1	cellular inhibitor of apoptosis 1
SMA	spinal muscular atrophy

UBA	ubiquitin binding domain
EBM	EJC-binding motif
GST	glutathione-S-transferase
H3R17	histone 3 arginine 17
DMEM	Dulbecco's Modified Eagles Medium
FBS	fetal bovine serum
GFP	green fluorescence protein
PARP	poly-ADP-ribose polymerase
PBS	phosphate buffer saline
siRNA	small interfering ribonucleic acid
shRNA	short hairpin ribonucleic acid
PEI	polyethyleneimine
DEPC	diethylpyrocarbonate
RT-PCR	reverse transcription polymerase chain reaction
GAPDH	glyceraldehyde 3-phosphate dehydrogenase
MTT	thiazolyl blue tetrazolium bromide
IPTG	isopropyl-β-D-thiogalactopyranoside
SAM	S-adenosyl-L-[methyl-^{3}H] methionine
RIPA	radioimmunoprecipitation
PVDF	polyvinylidene difluoride
PMSF	phenylmethanesulfonylfluoride
PBS-T	PBS-Tween
ANOVA	analysis of variance
mTORC1	mammalian target of rapamycin complex 1
SILAC	Stable Isotope Labelling of Amino Acids in Culture
Adox	adenosine 2', 3'-dialdehyde
MTA	methylthioadenosine
Mnk-1	MAP kinase-interacting protein kinase-1
PSMB5	β5 subunit of the proteasome
HSP	heat shock protein
ES	embryonic stem cells
TOP3β	DNA topoisomerase 3β

Chapter 1: Introduction

1.1 Arginine Methylation

Protein arginine methylation is a common post-translation modification catalyzed by a family of enzymes called the protein arginine methyltransferases (PRMTs). PRMTs catalyze the transfer of a methyl group from *S*-adenosylmethionine (AdoMet or SAM) to the guanidino nitrogen of arginine, resulting in the formation of a methylarginine and *S*-adenosylhomocysteine (AdoHcy or SAH) as a by-product (Bedford and Richard, 2005). The transfer of each methyl group to a substrate removes the potential for an additional hydrogen bond while changing the shape of the arginine. Therefore, arginine methylation conveys increased local bulkiness and hydrophobicity to a protein, thus potentially affecting protein-protein interactions, albeit without actually changing the cationic charge of the arginine residue (Tripsianes et al., 2011).

Members of the PRMT family contain four conserved sequence motifs (I, post-I, II, and III) and a "double E" and "THW" loop (Katz et al., 2003), with motifs I, post-I and the THW loop forming part of the AdoMet-binding pocket (Cheng et al., 2005). There are currently nine identified human PRMTs (PRMT 1-9). PRMTs are classified based on the type of arginine methylation that they catalyze. Both type I and type II PRMTs produce monomethylarginines as an intermediate, with type I PRMTs (PRMT1, 2, 3, 4(CARM1), 6, 8) catalyzing the formation of asymmetric dimethylarginines (ADMA), while type II PRMTs (PRMT5) form symmetric dimethylarginines (SDMA). Type III PRMTs (PRMT7) are capable of forming monomethylarginine (MMA) products (Zurita-Lopez et al., 2012), while the enzymatic activity of PRMT9 has yet to be characterized (Lee et al., 2005) (Figure 1.1).

Most PRMTs methylate arginine residues within a glycine- and arginine-rich (GAR) motif (Boffa et al., 1977). However, PRMT4 or coactivator-associated of arginine methyltransferase 1 (CARM1) and PRMT7 display unique substrate specificity, as CARM1 methylates an arginine residue in the vicinity of a proline-, glycine- and methionine-rich (PGM) motif (Lee and Bedford, 2002), and PRMT7 methylates arginine residues in a RXR motif (Feng et al., 2013). Additionally, PRMT5 can methylate arginine residues in both a GAR and PGM motif (Cheng et al., 2007; Branscombe et al., 2001), while PRMT6 is efficient at methylating both arginine residues within a GAR protein sequence and those outside of this sequence (Frankel et al., 2002; Sgarra et al., 2006; El-Andaloussi et al., 2006; Boulanger et al., 2005).

Although arginine methylation is a stable post-translation modification, a number of studies have shown the dynamic nature of this modification. Asymmetric methylation of histone 3 on arginine residue 17 (H3R17) occurs in a cyclic manner in response to estrogen stimulation at the pS2 promoter (Metivier et al., 2003). Additionally, estrogen stimulation results in methylation of the estrogen receptor α (ERα) by PRMT1 within five minutes of stimulation, with the methylation mark being lost ten minutes later (Le Romancer et al., 2008). Furthermore, H3R17 methylation catalyzed by CARM1 is high in mitotic cells and decreases as cells proceed through the cell cycle (Sakabe and Hart, 2010). Initially, Jumonji domain-containing protein 6 (JMJD6) was characterized as an arginine demethylase (Chang et al., 2007), however, its categorization as one has come into debate (Webby et al., 2009).

1.2 Regulation of Arginine Methylation

1.1)

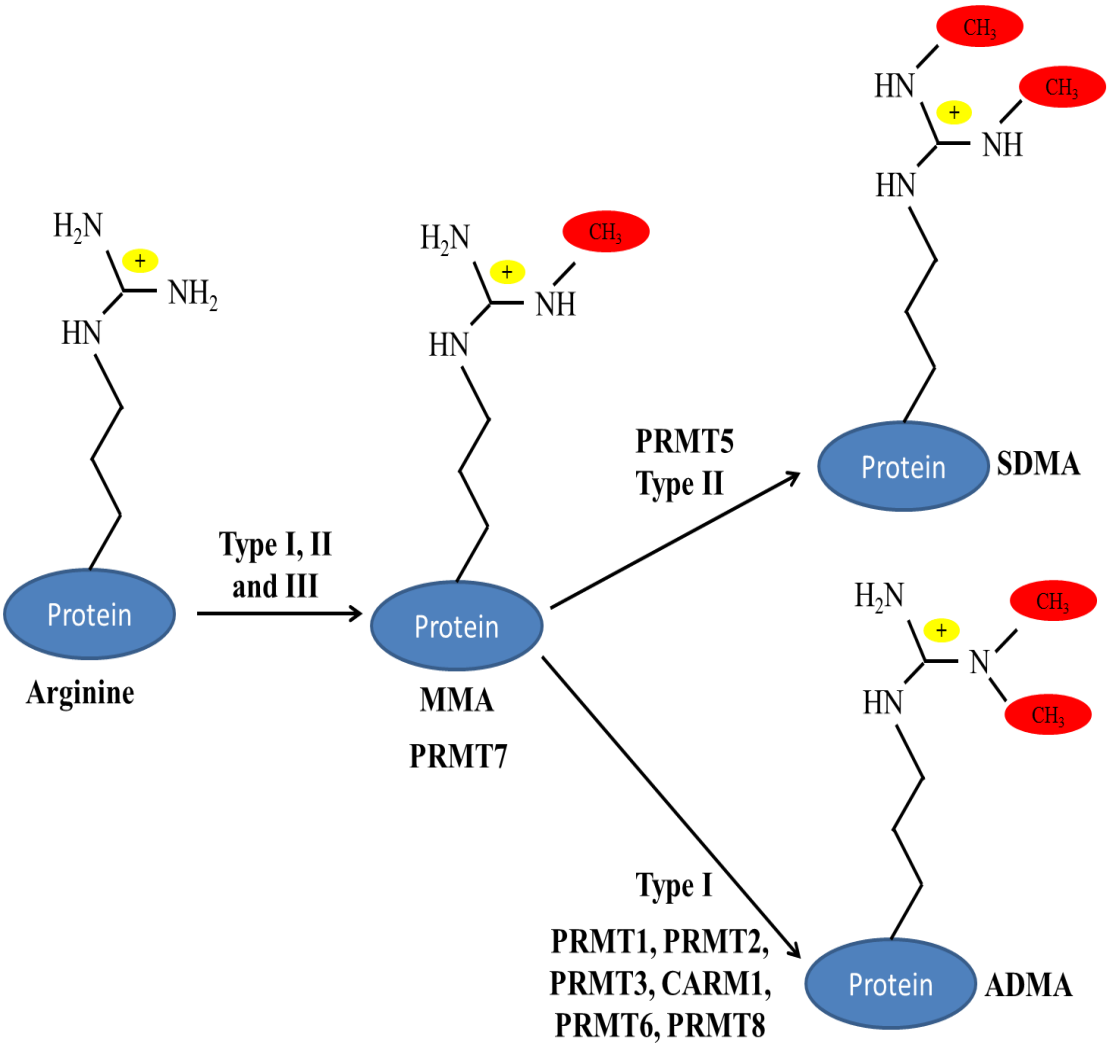
Protein
Arginine
Type I, II
and III
Protein
MMA
PRMT7
PRMT5
Type II
Protein
SDMA
Type I
PRMT1, PRMT2,
PRMT3, CARM1,
PRMT6, PRMT8
Protein
ADMA

Figure 1.1: Mammalian Protein Arginine Methyltransferases (PRMTs)

There are currently nine identified members of the PRMT family. Type I, II, and III PRMTs catalyze monomethylarginines (MMA). Type I and II PRMTs form MMA as an intermediate before the second methylgroup is placed on the substrate. Type I PRMTs catalyze asymmetric methylarginines (aDMA), while type II PRMTs form symmetric methylarginines (sDMA). Type I PRMTs include PRMTs 1, 2, 3, 4, 6, and 8. PRMT5 is a Type II PRMT and PRMT7 is a Type III PRMT. The enzymatic activity of PRMT9 has yet to be characterized.

A number of PRMT regulatory mechanisms have been identified including post-translation modifications, association with regulatory proteins, subcellular localization and micro RNA (miRNA) regulation.

Post-translation modifications

A number of studies have reported that PRMT activity is regulated by post-translation modifications, including through auto-methylation. PRMT6, PRMT8 and CARM1 have all been shown to be auto-methylated. Auto-methylation by PRMT6 on arginine residue 35 is required for protein stability and facilitates its ability to inhibit human immunodeficiency virus (HIV) replication (Frankel et al., 2002; Singhroy et al., 2013). Auto-methylation by PRMT8 in the N-terminus of the protein decreases its capacity to bind AdoMet (Sayegh et al., 2007; Dillon et al., 2013). Alternatively, auto-methylation of CARM1 does not affect its enzymatic activity but plays a role in regulating CARM1-activated transcription and pre-mRNA splicing (Kuhn et al., 2011).

CARM1 is additionally regulated by both phosphorylation and glycosylation. Phosphorylation of CARM1 on serine 217 by a yet unidentified kinase prevents its binding to AdoMet, thus blocking methyltransferase activity (Feng et al., 2009; Higashimoto et al., 2007). Glycosylation by N-acetylglucosamine transferase prevents CARM1 phosphorylation causing its cellular mis-localization (Cheung et al., 2008; Sakabe and Hart, 2010). In addition to CARM1, phosphorylation of PRMT5 by a janus kinase 2 (JAK2) mutant, JAK2-V617F abrogates its interaction with the methylosome protein 50 (MEP50), preventing PRMT5 methyltransferase activity (Liu et al., 2011).

Methylation of substrates by PRMTs can be influenced by surrounding post-

translational modifications on their substrates. For example, acetylation of lysine 18 on histone 3 (H3K18) primes the histone tail for H3R17 methylation by CARM1 (An et al., 2004; Daujat et al., 2002; Yue et al., 2007). Conversely, acetylation of lysine 8 on histone 3 (H3K8) prevents symmetric dimethylation by PRMT5 on histone 3 arginine residue 8 (H3R8) (Pal et al., 2004) . Furthermore, acetylation of histone 4 on lysine residue 5 (H4K5) allows PRMT5 to methylate histone 4 arginine 3 (H4R3), thus promoting a repressive SDMA mark instead of an activating ADMA mark by PRMT1 (Feng et al., 2011).

Regulatory Proteins

The binding of accessory proteins to PRMTs can regulate their activity. For example, PRMT5 is catalytically inactive as a bacterially expressed recombinant protein and requires the binding of MEP50 to modulate its methyltransferase activity (Martin et al., 2010). Likewise, in mammalian cells, MEP50 binds PRMT5 to regulate its activity (Friesen et al., 2002). In addition to MEP50, other proteins can also modulate PRMT5 activity. The SWI/SNF chromatin remodelling complex enhances the activity of MEP50-PRMT5 toward histone substrates (Pal et al., 2004), while the RNA binding protein Y14 regulates MEP50-PRMT5 activity toward Sm proteins (Chuang et al., 2011). Furthermore, RIO kinase 1 and ICLN can regulate PRMT5 substrate specificity (Guderian et al., 2011), whereas the histone-binding protein cooperator of PRMT5 (COPR5) targets MEP50-PRMT5 to methylate H4R3 instead of H3R8 (Lacroix et al., 2008).

In addition to PRMT5, mechanisms have also been elucidated characterizing the regulation of other PRMTs. PRMT1 forms a heterodimer with PRMT2 increasing its methyltransferase activity (Pak et al., 2011). B-cell translocation gene 2 (BTG2) can stimulate PRMT1 activity towards specific substrates while CCR4-associated factor 1 (hCAF1) can inhibit PRMT1 activity (Lin et al., 1996; Robin-Lespinasse et al., 2007). Similarly, the tumor suppressor protein DAL1/4.1B can interact with and inhibit the methyltransferase activity of PRMT3 (Singh et al., 2004), and modulate PRMT5 enzymatic activity in a substrate-dependent manner (Jiang et al., 2005).

Subcellular Localization

Proper cellular localization of PRMTs can regulate their enzymatic activity. Myristoylation in the N-terminus of PRMT8 targets it to the plasma membrane with PRMT8 exhibiting weak enzymatic activity. However, removal of this myristoyl group by proteolysis results in increased PRMT8 methyltransferase activity (Sayegh et al., 2007). Alternative splicing of the N-terminus of PRMT1 yields seven distinct isoforms with each exhibiting distinct subcellular localization, and unique substrate specificity. PRMT1v2 isoform is the only isoform to localize exclusively to the cytoplasm. PRMT1v3, -v4, v5, and v6 localize to both the nucleus and the cytoplasm, while PRMT1v1 and –v7 localize predominantly to the nucleus (Goulet et al., 2007) . Furthermore, enzymatic activity of PRMT1v2 is required for its nuclear-cytoplasmic shuttling ability as enzymatically dead mutants accumulate within the nucleus (Herrmann and Fackelmayer, 2009) .

1.3 Biological Roles of Arginine Methylation

PRMTs function in a myriad of cellular processes including transcription regulation, pre-mRNA splicing, nuclear-cytoplasmic shuttling, DNA repair, and mediating protein-protein interactions.

Transcription Regulation

PRMTs can serve as either transcriptional co-activators or as co-repressors. PRMTs have been identified as co-activators of a number of transcription factors including p53 (An et al., 2004), YY1 (Rezai-Zadeh et al., 2003), nuclear factor κB (NF-κB) (Hassa et al., 2008), PPARγ (Yadav et al., 2008), RUNX1 (Zhao et al., 2008) and E2F1 (Yadav et al., 2003). PRMT1, PRMT2, CARM1, and PRMT6 can trans activate the ER, with PRMT2 and PRMT6 modulating the activity of the progesterone receptor (PR) (Qi et al., 2002; Klinge et al., 2004; Frietze et al., 2008; Carascossa et al., 2010; Harrison et al., 2010). In addition to functioning as co-activators to regulate transcription, PRMTs can methylate transcriptional co-activators including p300/CBP (An et al., 2004), and SRC3 (Klinge et al., 2004), providing an indirect mechanism to impact a gene's epigenetic state.

Conversely, PRMT5 has been implicated to function as a general transcriptional repressor. PRMT5 functions synergistically with E2F1 to repress the transcription of cyclin E1 (Fabbrizio et al., 2002). Also, PRMT5 works with co-repressors to inhibit transcription of BRG1 and hBRM (Pal et al., 2003), Blimp1 (Ancelin et al., 2006) and Snail (Hou et al., 2008). Moreover, PRMT5 methylates H4R3, an arginine residue also methylated by PRMT1. PRMT5 methylation of H4R3 serves as a repressive transcription mark, while PRMT1 methylation functions as an activating mark (Pal et al., 2004; Feng

et al., 2011). PRMT6 can also promote or suppress transcription of target genes through methylation of H3R2 (Hyllus et al., 2007; Michaud-Levesque and Richard, 2009; Neault et al., 2012; Phalke et al., 2012; Herglotz et al., 2013), H3R42 (Casadio et al., 2013), and H2AR29 (Waldmann et al., 2011).

Pre-mRNA Splicing

Arginine methylation was initially implicated in pre-mRNA splicing as *in vitro* splicing reactions were inhibited when pan SDMA-specific antibodies were added to the reaction (Boisvert et al., 2002). Furthermore, splicing efficiency was found to be reduced in hypomethylated nuclear extracts. CARM1 has been identified as a regulator of alternative splicing and methylates the splicing factors CA150, SAP49, SmB and U1C. Moreover, CARM1 promotes exon skipping in an enzyme-dependent manner (Ohkura et al., 2005; Cheng et al., 2007). PRMT5 also regulates alternative splicing with PRMT5 depletion leading to reduced methylation of Sm proteins in the spliceosome, aberrant constitutive splicing, and the alternative splicing of specific mRNAs with a weak 5' donor site (Bezzi et al., 2013). Similarly to CARM1 and PRMT5, PRMT6 has also been shown to regulate mRNA splicing (Harrison et al., 2010; Dowhan et al., 2012).

Nuclear-Cytoplasmic Shuttling

PRMTs can facilitate the nuclear-cytoplasmic shutting of RNA-binding proteins (RBPs) through the methylation of arginine residue on these substrates. Sixty percent of ADMA marks are contained on RBPs in the nucleus (Bedford and Richard, 2005). In yeast cells lacking the PRMT1 homolog Hmt1/Rmt1, two RBPs Npl3 and Hrp1 become sequestered in the nucleus (Shen et al., 1998). In mammalian cells, inhibition of

methylation causes the nuclear accumulation of fibroblast growth factor 2 (Pintucci et al., 1996) and Sam68 (Cote et al., 2003). Additionally, methylation of the adenovirus 100K protein causes protein shuttling from the cytoplasm to the nucleus (Iacovides et al., 2007). Intriguingly, some hypomethylated proteins accumulate in the nucleus while others accrue in the cytoplasm. The exact mechanism by which arginine methylation may facilitate nuclear-cytoplasmic shuttling has yet to be elucidated.

DNA Repair

PRMT1 is linked with the repair of DNA double strand breaks (DSBs) through mediation of the MRE11/Rad50/NSB1 (MRN) complex which repairs DSBs through either homologous recombination or non-homologous end joining. PRMT1 methylates MRE11 to mediate the localization of the MRN complex to DSBs, while additionally regulating its 3' to 5' exonuclease activity (Boisvert et al., 2005a; Boisvert et al., 2005b). Also, PRMT1 methylates the p53-binding protein 1 (53BP1), a protein that is rapidly recruited to the site of DSBs upon DNA damage, regulating its localization to these sites (Boisvert et al., 2005c).

Arginine methylation is also involved in base excision repair through methylation of the DNA polymerase β (Pol-β). PRMT1 and PRMT6 play distinct, non-redundant roles in the regulation of Pol-β. PRMT6 methylates Pol-β on arginine residues 83 and 152 increasing its polymerase activity by enhancing its DNA binding ability and processivity (El-Andaloussi et al., 2006). Conversely, PRMT1 methylates Pol-β on arginine residue 137, blocking the interaction between Pol-β and proliferating cell nuclear antigen which facilitates Pol-β mediated base excision repair (El-Andaloussi et al., 2007).

Protein-Protein Interaction

PRMTs can impact protein-protein interactions, as the addition of a methyl group can increase or decrease the interaction between two proteins. The first example of methyl arginines affecting protein-protein interactions was demonstrated with the methylated arginines of Sam68 inhibiting its interaction with the SH3 domain of p59 (Bedford et al., 2000). A class of proteins containing Tudor domains have been identified which recognize methyl arginines. The Tudor domains of the survival of motor neuron (SMN) protein, survival of motor neuron-related splicing factor 30 (SPF30) and the Tudor domain-containing protein 3 (TDRD3) recognize methylated arginine residues and may serve as physiological ligands for arginine methylated marks. The role of Tudor domains in the reading of methylated arginines will be elaborated on below. Additional protein domains can also recognize methylated arginines. The BRCT domains of BRCA1 can recognize CARM1-mediated methylation of p300, facilitating a p53-dependent DNA damage response (Lee et al., 2011).

1.4 Arginine Methylation and Breast Cancer

Altered PRMT expression has been shown to correlate with the development and progression of malignancy, including in the etiology and/or progression of breast cancer. Specifically, PRMT1 mRNA expression is up-regulated in breast cancer tumour samples compared to adjacent normal tissue with PRMT1 expression correlating with patient age, menopausal status, tumour grade and status of the progesterone receptor (Yoshimatsu et al., 2011; Mathioudaki et al., 2011). In one study, low PRMT1v1 mRNA expression correlated with a longer disease free survival, whereas PRMT1v2 or PRMT1v3

expression did not correlate with any clinical or pathological indicators, at least at the RNA level (Mathioudaki et al., 2011). However, in a panel of breast cancer cell lines, all PRMT1 isoforms were over-expressed, though PRMT1v2 expression was increased to a greater extent than PRMT1v1, the main isoform (Goulet et al., 2007).

PRMT1 influences cellular pathways aberrantly regulated in breast cancer pathology. Presence of the ER in a breast tumour is an important prognostic and predictive biomarker (Harvey et al., 1999). Upon rapid estrogen stimulation, PRMT1 methylates ERα on arginine residue 260. This methylation results in the assembly of a complex containing ERα, the p85 subunit of phosphoinositide 3-kinase (PI3K), Src and focal adhesion kinase (FAK), which promotes phosphorylation of Akt on serine 473, a downstream target of this pathway whose activation promotes cellular proliferation and the anti-apoptotic response. Furthermore, an increase in the methylation of the ERα was observed in breast cancer tumour samples relative to normal breast tissue (Le Romancer et al., 2008).

PRMT1 also methylates breast cancer 1, early onset (BRCA1), a tumour suppressor protein involved in DNA damage pathways. Genetic mutation of the *BRCA1* gene results in increased predisposition to the development of breast cancer (Shattuck-Eidens et al., 1995). BRCA1 was shown to be methylated in both breast cancer cell lines and patient breast tumour samples. PRMT1 methylation of BRCA1 occurs within the DNA binding region, impacting not only BRCA1's ability to bind its target genes but also its ability to interact with other proteins (Guendel et al., 2010).

In addition to PRMT1, other PRMTs are also implicated in breast cancer. PRMT2 contains five alternatively spliced variants: full length PRMT2 and four truncated isoforms PRMT2L2, PRMT2α, β, and γ whose mRNA expression is up-regulated in breast cancer tissue and correlates with ER status. PRMT2 modulates the transcriptional expression of ERα target genes Snail and E-cadherin, two proteins whose expression is commonly altered in breast cancer (Zhong et al., 2011; Zhong et al., 2012). DAL1/4.1B, a tumor suppressor protein whose expression is frequently lost in breast cancer samples (Heller et al., 2007; Takahashi et al., 2012), represses PRMT3 methyltransferase activity (Singh et al., 2004), while modulating PRMT5 activity in a substrate-dependent manner (Jiang et al., 2005). Furthermore, over-expression of PRMT5 and programmed cell death 4 results in increased tumour growth in a mouse xenograft model (Powers et al., 2011). CARM1 can regulate ER transactivation in a ligand-dependent and independent manner (Frietze et al., 2008; Carascossa et al., 2010), and patient breast tumour samples display increased CARM1 expression (Cheng et al., 2013; Habashy et al., 2013; Davis et al., 2013). Additionally, PRMT6 expression is altered in breast cancer cell lines and patient samples (Yoshimatsu et al., 2011; Dowhan et al., 2012) and lastly, amplification of chromosome 16q22 which contains the PRMT7 gene is consistently observed in metastatic breast cancer (Thomassen et al., 2009). A more thorough examination of the role of arginine methylation in breast cancer is reviewed in Morettin *et al*. (Morettin,A., Baldwin,RM., Cote,J., In Press).

1.5 Protein Arginine Methyltransferase 1 (PRMT1)

PRMT1 is the main methyltransferase in human cells (Pahlich et al., 2006). Results from cultured RAT1 fibroblast cells and extracts from mouse liver cells illustrates

that PRMT1 is responsible for about 85 percent of protein arginine methylation activity (Tang et al., 2000). With PRMT1 responsible for the bulk of methyltransferase activity, and PRMTs involved in a myriad of cellular pathways, aberrant regulation of this enzyme represents a strong candidate that could promote malignant transformation of cells.

In additional to its correlative role in breast cancer, aberrant PRMT1 expression has also been observed in prostate (Seligson et al., 2005), lung (Yoshimatsu et al., 2011), colon and bladder cancers (Mathioudaki et al., 2008; Papadokostopoulou et al., 2009; Yoshimatsu et al., 2011) and leukemia (Zou et al., 2012). Furthermore, the role that PRMT1 plays in the repair of DNA double strand breaks (Boisvert et al., 2005a; Boisvert et al., 2005b; Boisvert et al., 2005c), and its ability to regulate genomic stability through methylation of the shelterin complex component, telomeric repeat binding factor 2 (TRF2) which promotes telomere maintenance (Mitchell et al., 2009), may contribute to malignancy.

PRMT1 also functions in signalling pathways whose aberrant regulation are key factors in cancer development. PRMT1 induces Akt activation through methylation of the ERα, with Akt activation promoting cell proliferation and survival (Le Romancer et al., 2008). Interestingly, however, PRMT1 also methylates forkhead box O1 (FOXO1), preventing its phosphorylation by Akt, which induces its nuclear localization, thus promoting oxidative-stress induced apoptosis (Yamagata et al., 2008). This study and others have identified conflicting roles for PRMT1 in regulating apoptotic signalling. In accordance with the above study, PRMT1 methylates the pro-apoptotic protein BCL-2 antagonist of cell death (BAD). This methylation prevents BAD's phosphorylation by Akt which would result in its mitochondrial sequestration and binding to the anti-

apoptotic protein BCL-X_L, which would inhibit apoptosis (Sakamaki et al., 2011). In contrast, an inhibitory methylation mark by PRMT1 on the apoptotic signal-regulating kinase 1 (ASK1) prevents its activation protecting cells from stress induced apoptosis (Cho et al., 2011).

PRMT1 has also been implicated in WNT signalling, where perturbations are prevalent in cancer. PRMT1 methylates Axin, a negative regulator of β-catenin which is involved in cell-cell adhesion and gene transcription. PRMT1 methylation of Axin enhances its stability and increases its affinity for glycogen synthase kinase 3β (GSK-3β), which along with Axin forms a complex with adenomatous polyposis coli (APC) and casein kinase 1 (CK1). This complex phosphorylates β-catenin, promoting its degradation. In addition, PRMT1 knockdown enhances β-catenin-dependent gene transcription (Cha et al., 2011). Therefore, the involvement of PRMT1 in cellular pathways linked with cancer etiology potentially implicates it in cellular transformation and cancer development.

Alternative splicing of the 5' region of the PRMT1 pre-mRNA yields seven distinct isoforms with each isoform having a unique N-terminal sequence and a slightly different molecular weight (Figure 1.2). Each PRMT1 isoform has distinct enzymatic properties, substrate specificity and sub-cellular localization, and thus should be functionally different. The N-terminal sequence of PRMT1 contributes to enzymatic activity and/or substrate specificity as the N-terminal sequence is juxtaposed with an exposed alpha helix located in the space between the AdoMet and substrate binding pockets (Goulet et al., 2007).

1.2)

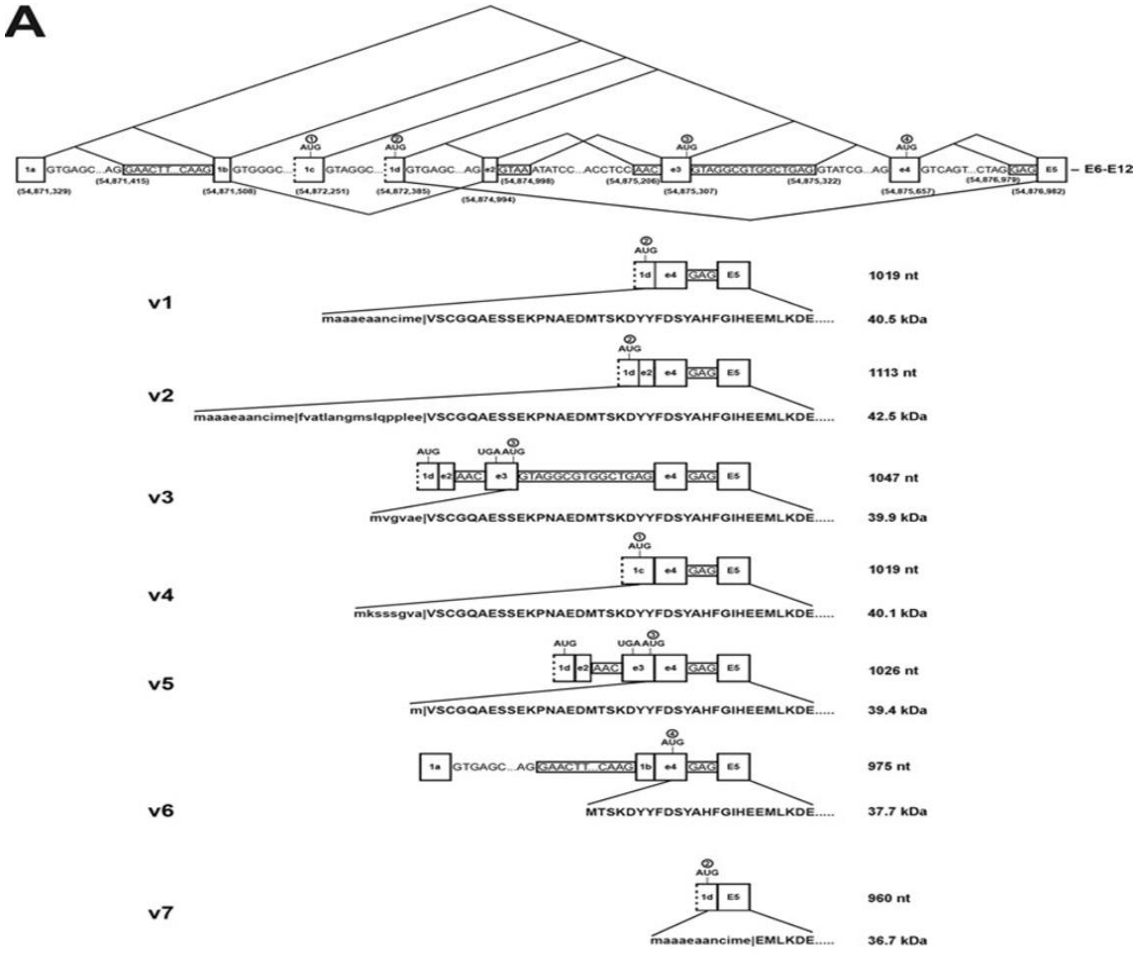
A
E6-E12
v1
1019 nt
maaaeaancime|VSCGQAESSEKPNAEDMTSKDYYFDSYAHFGIHEEMLKDE.....
40.5 kDa
v2
1113 nt
maaaeaancime|fvatlangmslqpplee|VSCGQAESSEKPNAEDMTSKDYYFDSYAHFGIHEEMLKDE.....
42.5 kDa
v3
1047 nt
mvgvae|VSCGQAESSEKPNAEDMTSKDYYFDSYAHFGIHEEMLKDE.....
39.9 kDa
v4
1019 nt
mksssgva|VSCGQAESSEKPNAEDMTSKDYYFDSYAHFGIHEEMLKDE.....
40.1 kDa
v5
1026 nt
m|VSCGQAESSEKPNAEDMTSKDYYFDSYAHFGIHEEMLKDE.....
39.4 kDa
v6
975 nt
MTSKDYYFDSYAHFGIHEEMLKDE.....
37.7 kDa
v7
960 nt
maaaeaancime|EMLKDE.....
36.7 kDa

Figure 1.2: Alternative Splicing of PRMT1 yields Seven Distinct Isoforms

Alternative splicing of the N-terminus of PRMT1 yields sevens distinct isoforms with slightly different molecular weights. Each PRMT1 isoform has distinct substrate specificity and sub-cellular localization, and thus should be functionally different. PRMT1v2 differs from the other isoforms as it is the only isoform that contains exon 2 within its translated sequence. (Taken from Goulet *et al*. 2007 *J. Biol. Chem.* 282: 33009-33021)

PRMT1v2 is the only isoform that shows exclusive cytoplasmic localization. Isoforms v3, v4, v5, and v6 localize to both nucleus and the cytoplasm, while PRMT1v1 and v7 localize predominantly to the nucleus. Sequence analysis shows that PRMT1v2 retains exon 2 within its coding sequence, a 54 base pair (bp) sequence encoding an 18 amino acid insert in the protein. This 18 amino acid sequence contains a leucine rich, CRM1-dependent nuclear export sequence (NES), which when mutated results in nuclear retention of PRMT1v2. Individual examination of expression levels of the PRMT1 isoforms in breast cancer cell lines reveals a significantly higher increase in expression of PRMT1v2 compared to PRMT1v1; the main isoform which is also over-expressed (Goulet et al., 2007).

1.6 Protein Arginine Methyltransferase 6 (PRMT6)

PRMT6, a predominantly nuclear protein, is a type I PRMT which was identified as the first PRMT capable of auto-methylation (Frankel et al., 2002). Subsequently, it has been shown that this auto-methylation, which occurs on arginine residue 35, is necessary to maintain PRMT6 protein stability (Singhroy et al., 2013). PRMT6 shares a high sequence similarity with the other PRMTs within the main AdoMet-catalytic domain. Similar to PRMT1, PRMT6 contains only the core PRMT catalytic domain with no additional recognizable domains present within its sequence. However, in contrast to PRMT1 which is ubiquitously expressed, PRMT6 is highly expressed only in the kidney and testes (Frankel et al., 2002). Enzymatically, PRMT6 is efficient at methylating both arginine residues within a GAR protein sequence and those outside of this sequence (Frankel et al., 2002; Sgarra et al., 2006; El-Andaloussi et al., 2006; Boulanger et al., 2005). PRMT6 displays distinct substrate specificity from other PRMTs and has been

implicated in a variety of cellular processes including DNA repair, alternative splicing, transcription regulation, cell cycle regulation and viral immunity. Furthermore, a role for PRMT6 in cancer has also been ascribed.

DNA Repair

PRMT6 through its methylation of Pol β is implicated in DNA repair. PRMT6 methylates Pol β on arginine residues 83 and 152 increasing Pol β's DNA binding capacity and its processivity (El-Andaloussi et al., 2006).

Alternative Splicing

PRMT6 through modulation by proline-, glutamic acid- and leucine-rich protein 1 (PELP1) regulates the alternative splicing of 449 specific genes (Dowhan et al., 2012). Specifically, PRMT6 depletion alters the alternative splicing of vascular endothelial growth factor (VEGF) and spleen tyrosine kinase (Syk). VEGF yields three isoforms: full length VEGF ($VEGF_{189}$), VEGF excluding exon 6 ($VEGF_{165}$) and VEGF excluding exons 6 and 7 ($VEGF_{121}$). While PRMT6 depletion has no effect on the levels of $VEGF_{121}$, a significant increase in the levels of $VEGF_{189}$ corresponded with a decrease in the levels of $VEGF_{165}$. Likewise, PRMT6 knockdown results in an increase in the ratio of full length Syk to a shorter form of Syk lacking a 69-bp sequence comprising exon 7 (Harrison et al., 2010).

Transcription Regulation

PRMT6 has been ascribed a role in transcriptional regulation; although most evidence shows PRMT6 functioning as a transcriptional repressor, data has also been

reported attributing a role for it as a transcriptional activator. Over-expression of PRMT6 contributes to the transcriptional repression of HoxA genes, HoxA2 and HoxA10, as well as myc target genes TERT, nucleolin, Golph3, and prothymosin α upon PRMT6 methylation of arginine residue 2 on histone 3 (H3R2). Methylation of H3R2 negatively impacts the ability of lysine methylases to methylate lysine residue 4 on histone 3 (H3K4), which promotes transcriptional activation of these genes (Hyllus et al., 2007). Similarly, PRMT6 transcriptionally represses the anti-angiogenic factor thrombospondin-1 (TSP-1) through binding to its promoter, influencing the balance between H3R2 and H3K4 methylation (Michaud-Levesque and Richard, 2009). However, PRMT6 overexpression inducing TSP-1 expression has also been documented (Kim et al., 2013). PRMT6 negatively regulates p53's transcription through H3R2 methylation (Neault et al., 2012), while methylation on arginine 29 on histone 2A (H2AR29) results in the transcriptional repression of PRMT6 target genes: eIF1B, MMP9, THBS1, and TNFRSF11B (Waldmann et al., 2011). Additionally, PRMT6 functions as an integral component of the RUNX1 co-repressor complex which contains Sin3a and HDAC1 and binds to the promoters of RUNX1 target genes. PRMT6-mediated methylation of H3R2 functions concomitantly with the dimethyl lysine mark on H3K4 and the tri-methyl lysine mark on H3K27, inhibiting tri-methyl lysine methylation of H3K4 to repress RUNX1 target genes (Herglotz et al., 2013).

Contrarily to its function as a transcriptional repressor, PRMT6 enhances the transcriptional activity of the progesterone and glucocorticoid receptors, and works synergistically with CARM1 to promote expression of the estrogen receptor (Harrison et

al., 2010). Additionally, PRMT6 was shown to stimulate transcription through methylation of arginine residue 42 on histone 3 (H3R42) (Casadio et al., 2013).

Cell Cycle Regulation

PRMT6 additionally regulates cell proliferation through regulation of p53, and the cyclin-dependent kinase (CDK) inhibitors p16, p21 and p27 (Neault et al., 2012; Stein et al., 2012; Wang et al., 2012; Kleinschmidt et al., 2012; Phalke et al., 2012). PRMT6 null mouse embryonic fibroblasts (MEFs) display a cell cycle profile with a decrease in the percentage of cells in S phase and an increase of cells in G_0/G_1 compared to wild type MEFs. Furthermore, PRMT6 null MEFs have increased levels of β-galatosidase staining, a hallmark of cellular senescence, as well as increased mRNA and protein levels of p53 and its transcriptional targets p21 and PML (Neault et al., 2012). Enhanced PML expression, in addition to an increase in PML nuclear bodies, is also a hallmark of senescent cells (Ferbeyre et al., 2000). Similarly, in breast cancer cells, PRMT6 depletion results in cell cycle arrest and senescence, albeit in a p53-independent manner. PRMT6 directly binds to the p21 promoter corresponding with an increase in the transcriptional repressive mark on H3R2 (Phalke et al., 2012). Consistently, increased cellular senescence was demonstrated in human osteosarcoma cells upon PRMT6 depletion, with a subsequent up-regulation of p16 and p21 expression (Stein et al., 2012). Also in osteosarcoma cells, PRMT6 knockdown results in accumulation of cells at the G_2/M checkpoint, consistent with up-regulation of the CDK inhibitors p21 and p27. Promoter analysis indicated that both p21 and p27 are transcriptional targets of PRMT6 involving methylation of H3R2 (Kleinschmidt et al., 2012). Furthermore, Wang *et al*. demonstrate that PRMT6 methylation of p16 impedes the p16-CDK4 interaction, promoting cell

proliferation (Wang et al., 2012). However, Kim *et al.* show PRMT6 overexpression inhibiting cell proliferation through p21 induction (Kim et al., 2013).

Viral Immunity

PRMT6 distinguishes itself from other members of the PRMT family through its involvement in viral immunity. Corresponding with the inconsistency in published data regarding the function of PRMT6 in transcription regulation and the cell cycle, discrepancies have arisen about its role pertaining to viral immunity. PRMT6 methylates the HIV-1 proteins Tat, Rev, and nucleocapsid protein (Boulanger et al., 2005; Invernizzi et al., 2006; Xie et al., 2007; Invernizzi et al., 2007; Sivakumaran et al., 2009). Methylation of Tat on arginine residues 52 and 53 inhibits its ability to form a ternary complex with TAR and cyclin T1, diminishing cyclin T1-mediated Tat transcriptional activation, thus impeding viral replication (Boulanger et al., 2005; Xie et al., 2007). Similarly, PRMT6 methylation of the nucleocapsid protein constrains its capacity to promote RNA annealing, resulting in diminished viral replication (Invernizzi et al., 2007). However, PRMT6 methylation of Tat was shown to promote protein stability potentially enabling HIV-1 to persist within the cell and the extracellular environment for extended periods (Sivakumaran et al., 2009; Sivakumaran et al., 2013). Moreover, methylation of the HIV-1 Rev protein inhibits its ability to bind viral RNA and promote its export from the nucleus to the cytoplasm (Invernizzi et al., 2006).

PRMT6 and Cancer

Like other PRMTs, PRMT6 has been implicated in tumorigenesis. PRMT6 protein expression is up-regulated in a number of cancer types including lymphoma,

osteosarcoma, cervical, bladder, prostate, and breast cancers, both small cell and non-small cell lung carcinomas (Yoshimatsu et al., 2011), melanomas (Limm et al., 2013) and hepatocellular carcinoma (Meerzaman et al., 2014). PRMT6 depletion in bladder and lung cancer cell lines results in a decrease in cell proliferation (Yoshimatsu et al., 2011). Whereas PRMT6 expression was correlated with a poor prognosis in breast cancer (Yoshimatsu et al., 2011), Dowhan *et al*. demonstrate that PRMT6 expression was significantly down-regulated in invasive ductal carcinomas (Dowhan et al., 2012)

PRMT6 functions in numerous cellular pathways including DNA repair, transcription regulation, cell cycle regulation and alternative splicing, all of which have been linked to cancer etiology. PRMT6 methylates Pol β regulating its capacity to operate in the DNA base excision repair pathway (El-Andaloussi et al., 2006). Additionally, PRMT6 transcriptionally represses the anti-angiogenic factor TSP-1 in osteosarcoma cells concurring with an increase in cell migration and invasion (Michaud-Levesque and Richard, 2009); however, in prostate cancer cells, overexpression of PRMT6 was also shown to induce TSP-1 expression, coinciding with a decrease in cellular migration and invasion due to down-regulation of the matrix metalloproteinases 2 and 9 (Kim et al., 2013). PRMT6 transcriptionally regulates numerous genes whose expression pattern may be altered in different cancers (Dowhan et al., 2012). Also, PRMT6 impacts the cell cycle through regulation of p16, p21, p27, and p53 (Neault et al., 2012; Stein et al., 2012; Wang et al., 2012; Kleinschmidt et al., 2012; Phalke et al., 2012), however discrepancies have arisen in terms of the precise function that PRMT6 performs in this process. Moreover, proto-oncogene PELP1 modulates PRMT6 function influencing the alternative splicing of PRMT6 target genes (Mann et al., 2014).

1.7 Stress Granules

The formation of cytoplasmic stress granules (Figure 1.3) occurs when environmental stresses such as heat shock, oxidative stress, osmotic stress, UV irradiation, or viral infection trigger a sudden translation arrest leading to rapid polysome disassembly (Anderson and Kedersha, 2002). This results in numerous proteins which normally function in mRNA processing assuming additional emergency functions, activating a process of sorting which determines the fate of the mRNA from the disassembling polysomes (Anderson and Kedersha, 2002; Anderson and Kedersha, 2006). Stress granules are dynamic structures of mRNA triage where individual mRNAs are sorted for storage, degradation, or translation during recovery from stress (Anderson and Kedersha, 2009).

Stress Granule Formation

Stress granule formation is predominantly initiated by the stress-induced phosphorylation of the eukaryotic initiation factor 2α (eIF2α) (Figure 1.3). Phosphorylation of eIF2α on serine 51 inhibits global protein translation by reducing the levels of the eIF2-GTP-$tRNA_i^{MET}$ complex that is required for cap-dependent translation initiation (Anderson and Kedersha, 2002). Five kinases are responsible for monitoring environmental stresses and modulating the translation machinery through eIF2α phosphorylation. These include (i) protein kinase R (PKR) which becomes activated by viral infection, heat shock and UV irradiation (Srivastava et al., 1998), (ii) PKR-like endoplasmic reticulum kinase (PERK) is initiated when unfolded proteins accumulate in the endoplasmic reticulum lumen (Harding et al., 2000b; Harding et al., 2000a), (iii)

1.3)

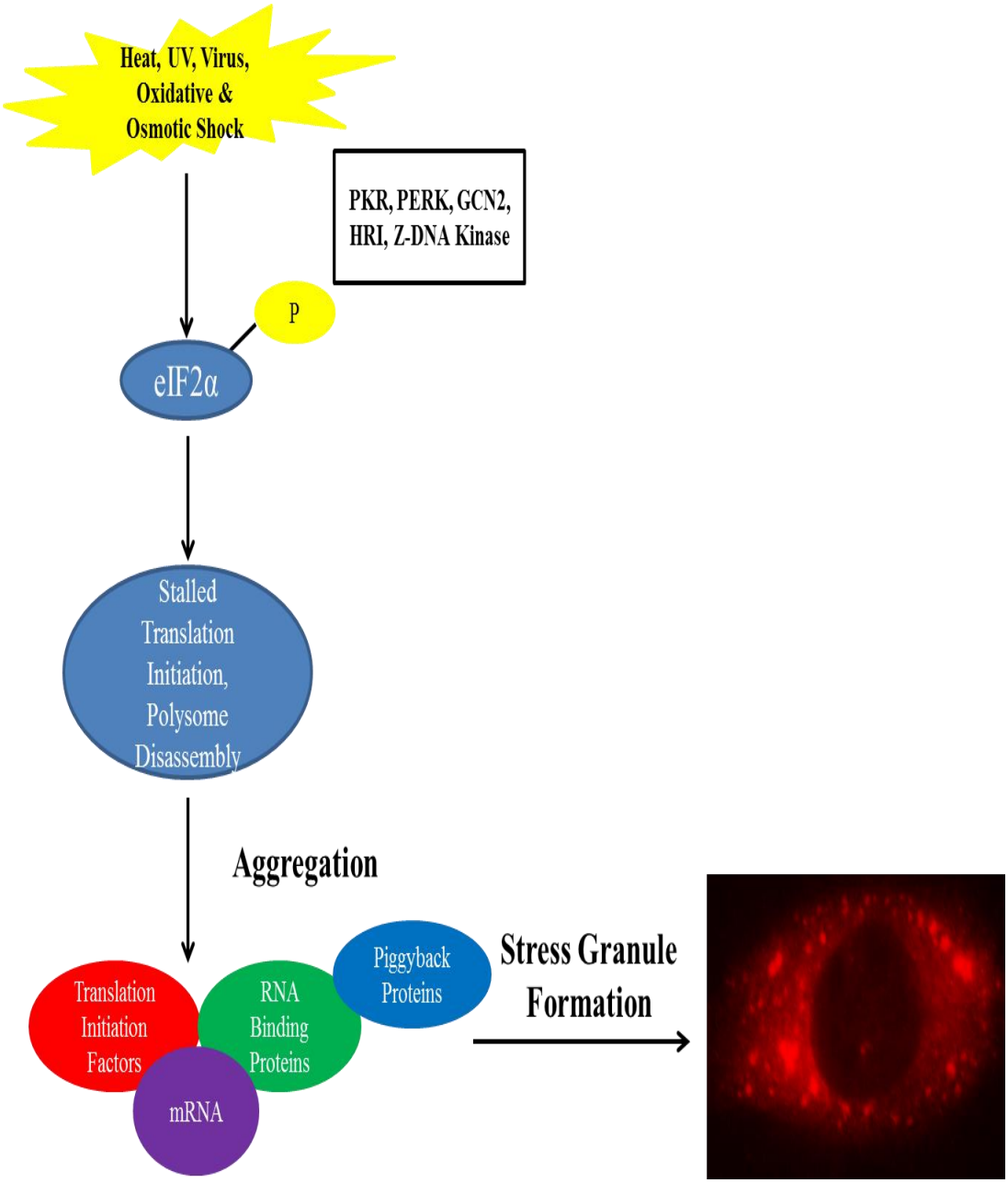
Heat, UV, Virus,
Oxidative &
Osmotic Shock
PKR, PERK, GCN2,
HRI, Z-DNA Kinase
P
eIF2α
Stalled
Translation
Initiation,
Polysome
Disassembly
Aggregation
Translation
Initiation
Factors
RNA
Binding
Proteins
Piggyback
Proteins
mRNA
Stress Granule
Formation

Figure 1.3: Stress Granule Formation

Exposure of the cell to environmental stress including heat shock, UV irradiation, viral infection and oxidative and osmotic stress results in the phosphorylation of eIF2α by stress kinases (PKR, PERK, GCN2, HRI, Z-DNA kinase). Phosphorylation of eIF2α leads to depletion of the eIF2-GTP-$tRNA_i^{MET}$ ternary complex causing inhibition of translation initiation resulting in polysomes running off the mRNA and polysome disassembly. Next, components of the translation initiation complex still coupled to mRNA, as well as RNA binding proteins and additional proteins which are bound to these RNA binding proteins accumulate and form visible stress granules.

general control nonderepressible 2 (GCN) monitors amino acid levels in the cell and responds to amino acid deprivation (Wek et al., 1995), (iv) heme regulated initiation factor 2α kinase (HRI) which responds to oxidative stress (McEwen et al., 2005) and (v) Z-DNA kinase, an enzyme involved in the anti-viral response (Wek et al., 1995). These kinases function duly as overseers of cellular stress, and through the regulation of cap-dependent translation initiation (Anderson and Kedersha, 2008).

Although stress granule formation is predominantly regulated through phosphorylation of eIF2α, eIF2α-independent stress granule formation has also been documented. Stress granule formation can be induced via depletion of eIF4A, eIF4B, eIF4H and Poly A binding protein (PABP1). Additionally, depletion of the cap binding protein eIF4E or prevention of its binding to eIF4G triggers stress granule formation (Dang et al., 2006; Mazroui et al., 2006; Mokas et al., 2009). Furthermore, stress granules can be induced through treatment with the translation initiation inhibitors pateamine and hippuristanol or through poliovirus-mediated cleavage of eIF4G (Dang et al., 2006; Mazroui et al., 2006).

Components of Stress Granules

Stress granules consist of diverse classes of proteins which constitute its components. The first class of proteins contains components of the stalled initiation complexes still bound to mRNA which are recruited to stress granules from disassembling polysomes. These components include eIF3, eIF4F complex proteins including eIF4e, eIF4a and eIF4G, eIF4B, the small ribosomal subunits, and PABP1 (Anderson and Kedersha, 2002; Kedersha et al., 2002). These core components are

universal to stress granules induced from all types of cellular stresses. The second class of components entails mRNA-binding proteins associated with translational silencing or mRNA stability. These components are reliable stress granule markers that are present in stress granules assembled in response to all stresses. Examples include, but are not limited to, T cell internal antigen-1 (TIA-1), TIA-1-related (Kedersha et al., 1999), Fragile X Mental Retardation Protein (FMRP) (Mazroui et al., 2002) and DEAD-box RNA Helicase 3 (DDX3) (Shih et al., 2012). A third class of stress granule associated proteins include RNA binding proteins that regulate aspects of RNA metabolism including splicing, RNA editing, and RNA localization. A fourth class of constituents include components recruited to stress granules that interact with stress granule core components and thus localize to stress granules. These include SRC3, FAST, KSRP, and PMR1, all which bind to TIA-1, promoting their recruitment to stress granules (Anderson and Kedersha, 2008).

Processing Bodies and the mRNA Cycle

Following induction of environmental stress and subsequent inhibition of translation, mRNAs are transported to stress granules for storage or to processing bodies for mRNA degradation. Processing bodies are distinct, dynamic cytoplasmic granules whose constituent components include proteins involved in mRNA degradation (Brengues and Parker, 2007; Hoyle et al., 2007). Though their number and size increases upon induction of stress, processing bodies are observed in the cell under normal physiological conditions, distinguishing themselves from stress granules which form only under conditions of cellular stress (Bashkirov et al., 1997; van Dijk et al., 2002; Ingelfinger et al., 2002; Eystathioy et al., 2002).

Analysis of the role of stress granules and processing bodies and their regulation of cytoplasmic mRNA has produced a model describing the processivity of mRNAs upon the induction of cellular stress entitled the mRNA cycle. Exposure of cells to environmental stress results in termination of translation initiation, polysome disassembly and accumulation of the translation pre-initiation complexes. RNA binding proteins promote the aggregation of these translation initiation complexes into stress granules. Processing bodies are observed in close proximity to stress granules, where RNA binding proteins shuttle mRNAs between the two entities. mRNAs presenting either a premature termination codon or AU-rich elements are shuttled to processing bodies where they are degraded. Specifically, TTP and BRF1, two RNA binding proteins which are associated with both stress granules and processing bodies bind to mRNAs with AU-rich elements within their 3'- UTR promoting their decay. On removal of the stress, stress granules disassemble, translation initiation complexes reassemble, and mRNAs stored within stress granules are translated (Stoecklin and Kedersha, 2013).

Stress Granules and Cancer

Stress granules have been implicated in promoting cancer cell survival. Formation of stress granules in cancer cells exposed to hypoxic conditions inhibits etoposide-mediated apoptosis through the sequestration of the signalling scaffold protein, receptor for activated C kinase 1 (RACK1), resulting in inhibition of mitogen-activated protein kinase (MAPK) stress response pathways (Arimoto et al., 2008). Furthermore, in breast cancer cells, the mitogen-activated kinase RSK2 is also sequestered in stress granules promoting cell survival (Eisinger-Mathason et al., 2008). Treatment of cells with either proteasome inhibitors or the chemotherapeutic drug bortezomib induces stress granule

formation in cells (Mazroui et al., 2007; Fournier et al., 2010). Finally, stress granules have been observed in the hypoxic core of breast tumours, with their presence hypothesized to promote tumour cell survival, and resistance to chemotherapeutic drugs (Baguet et al., 2007; Fournier et al., 2010).

Though no direct link has implicated PRMTs in stress granules dynamics to date, numerous PRMT substrates and other proteins containing GAR motifs localize, and are integral components of stress granules. Specifically, methylation of the RNA binding protein FUS promotes its localization to stress granules (De Leeuw et al., 2007; Tradewell et al., 2012; Matsumoto et al., 2012; Yamaguchi and Kitajo, 2012; Baron et al., 2013; Lee et al., 2014). Additionally, methylation of FMRP promotes its localization to stress granules (Dolzhanskaya et al., 2006), and a mutation in the Tudor domain of TDRD3, the methyl arginine binding region, inhibits its localization to stress granules (Goulet et al., 2008). Therefore, it is likely that PRMTs may perform a vital function in stress granule dynamics.

Bortezomib (Velcade)

The proteasome is a large multi-subunit complex responsible for the degradation of various proteins either through ubiquitin-dependent or –independent mechanisms (Adams, 2004a; Adams, 2004b). Proteasome inhibitors induce apoptosis in proliferating cells (Drexler, 1997; Imajoh-Ohmi et al., 1995; Lopes et al., 1997; Sloss et al., 2008). Bortezomib (Velcade), a chemotherapeutic drug which inhibits the proteasome has been successfully used in the treatment of mantle cell myeloma and multiple myeloma (Richardson et al., 2003; Richardson et al., 2004; McConkey and Zhu, 2008; Sterz et al.,

2008). However, various solid tumours are refractory to bortezomib treatment, and this resistance is observed in cancer cell lines derived from these tumours, *in vitro* (McConkey and Zhu, 2008; Codony-Servat et al., 2006; Rajkumar et al., 2005; Tang et al., 2008). Treatment of resistant cancer cell lines with bortezomib promotes the formation of stress granules, enhancing cancer cell survival (Fournier et al., 2010).

1.8 Arginine Methylation and RNA Binding Proteins

RNA binding proteins (RBPs) participate in the processing, folding, stabilization and localization of RNA and mRNA translation. Most RBPs harbor GAR motifs and a number of RBPs have been identified as substrates for PRMTs (Pahlich et al., 2006). Arginine residues within the binding sites of RBPs have been identified as key amino acids which mediate RNA-protein interactions (Ciriello et al., 2010; Ellis et al., 2007; Jones et al., 2001; Kim et al., 2003; Lejeune et al., 2005; Treger and Westhof, 2001). Methylation of these residues may result in the loss of a hydrogen bond that forms with RNA, or causes steric hindrance between RNA and protein molecules. Alternatively, methylation could result in the arginine residue becoming more hydrophobic in nature, thereby enhancing the association between RNA and protein by facilitating stacking with the bases of the RNA (Bedford and Richard, 2005).

Arginine methylation of specific RNA binding proteins results in distinct functional consequences within the cell. For example, methylation of heterogenous nuclear ribonucleoprotein A1 (hnRNP A1) reduces its ability to bind with single stranded nucleic acids (Rajpurohit et al., 1994). Methylation of Sm proteins SmD1, SmD3, and SmB, which are core components of the spliceosomal small nuclear ribonucleoproteins (snRNPs), by PRMT5 increases the affinity of Sm proteins for the SMN complex,

providing a regulatory mechanism for snRNP assembly (Brahms et al., 2000; Brahms et al., 2001; Friesen et al., 2001b; Selenko et al., 2001). Lastly, SMN binds with HuD in a CARM1-dependent manner, reducing HuD's ability to bind p21 mRNA and inhibiting its recruitment to neuronal RNA granules (Hubers et al., 2011).

1.9 DEAD-Box RNA Helicases

Numerous RNA helicases are present within both the prokaryotic and eukaryotic genomes that interact with RNA molecules to manipulate their folding and assist in the maturation of these molecules. DEAD-box RNA helicases belong to super-family 2 of the DNA and RNA helicase superfamilies' and are closely related to DEAH, DExH and DExD helicase families. These helicases are commonly referred to as the DExD/H helicase family and share eight conserved motifs. DExD/H family members are distinguishable based on variations within their conserved motifs (Tanner and Linder, 2001; Caruthers and McKay, 2002). The DEAD-box family is the largest of these families, and is characterized by the presence of nine conserved motifs shown to be essential for ATPase and helicase activities, as well as their overall regulation, with some of the conserved motifs required for RNA binding (Tanner, 2003).

DEAD-box proteins were first identified in the late 1980s through the identification of numerous conserved motifs within homologues of the yeast eIF4A translation initiation factor (Linder et al., 1989). Subsequently, DEAD-box proteins have been identified in a diverse array of organisms, including all eukaryotes and most prokaryotes (Aubourg et al., 1999; de la Cruz et al., 1999; Rocak and Linder, 2004). DEAD-box proteins were named based on the presence of the amino acid sequence D-E-

A-D (Asp-Glu-Ala-Asp). Consequently, over five hundred additional proteins have been identified containing the characteristic motifs of DEAD-box proteins, and these proteins are implicated in nearly all processes involving RNA, from transcription to RNA decay (Cordin et al., 2006). Members of the DEAD box family of RNA helicases function in numerous aspects of RNA metabolism including transcription, pre-mRNA splicing, mRNA export, ribosome biogenesis, translation initiation and RNA degradation.

1.10 DEAD-box RNA Helicase 3 (DDX3)

DDX3 (DDX3X) was identified as an X chromosome gene with a homologue, DDX3Y, which shares a ninety-three percent homology to DDX3, in the non-recombinant region of the Y chromosome (Park et al., 1998). DDX3 is ubiquitously expressed in tissues and its gene codes for a transcript of 5.3 kb, encoding a polypeptide of 662 amino acids in length (Kim et al., 2001). DDX3 is implicated in numerous cellular processes including playing predominant roles in RNA metabolism along with functioning in the innate immune system. Interestingly, DDX3 also functions in viral replication, along with involvement in cancer development and progression.

1.11 DDX3's Roles in RNA Metabolism

DDX3 functions in many aspects of RNA metabolism including splicing, nuclear export of RNA, protein translation, and formation of stress granules.

Splicing

Using affinity chromatography mass spectrometry; Zhou *et al*. identified DDX3 as a component of the human spliceosome (Zhou et al., 2002). Subsequently, Merz *et al*.

found DDX3 associated with purified messenger ribonucleoproteins (mRNPs) spliced *in vitro* (Merz et al., 2007). DDX3 association with nuclear mRNPs occurs through binding with components of both the exon junction complex (EJC) and the nuclear cap binding complex (CBC) (Masuda et al., 2005; Merz et al., 2007; Topisirovic et al., 2009). Though DDX3 binds both the EJC and the CBC, evidence suggests that it preferentially binds the EJC as its association with mRNPs requires both splicing and the presence of the EJC upstream of an exon-exon junction, but not binding of the CBC to the m^7GTP cap structure (Merz et al., 2007). DDX3 and the EJC are recruited to the pre-mRNP at the B*/C spliceosome complexes before the EJC is recruited to the processed mRNA. Though DDX3 is a component of the spliceosome and binds to nuclear mRNPs, cellular depletion of DDX3 does not affect global splicing (Lee et al., 2008). Therefore, the function that DDX3 perform as a component of the spliceosome requires clarification.

Nuclear Export of RNA

DDX3 is a nuclear-cytoplasmic shuttling protein which promotes the export of RNAs from the nucleus through its interaction with two of the mRNA export shuttling proteins, CRM1 and TAP (Yedavalli et al., 2004; Lai et al., 2008). CRM1 exports proteins from the nucleus which contain a leucine-rich NES. TAP is the main mRNA exporter, while CRM1 exports ribosomal and small nuclear RNAs (Kohler and Hurt, 2007). Though there is no evidence promoting a direct role for DDX3 in the bulk export of mRNA (Lai et al., 2008; Lee et al., 2008), DDX3 most likely functions in the export of specific mRNAs via the TAP-mediated mRNA export pathway (Tarn and Chang, 2009). Additionally, DDX3 can export incompletely spliced HIV RNA by the CRM1 export pathway in a Rev-dependent manner (Yedavalli et al., 2004).

Protein Translation

The yeast DDX3 homologue Ded1 has been identified as a general translation factor required for the translation of all yeast mRNAs (Chuang et al., 1997; de la Cruz et al., 1997). Though human DDX3 can rescue the lethality of the *ded1* null yeast (Mamiya and Worman, 1999), the functional role of DDX3 in translation is more ambiguous. DDX3 has been ascribed to be a general translation initiation factor (Lee et al., 2008; Geissler et al., 2012), while other groups have demonstrated that DDX3 has no effect on global translation (Lai et al., 2008; Soto-Rifo et al., 2012; Fukumura et al., 2003; Lai et al., 2010). Rather, it has been proposed that DDX3 facilitates the translation of a specific subset of mRNAs with highly structured 5'UTRs (Lai et al., 2008; Lai et al., 2010; Soto-Rifo et al., 2012). In contrast, Shih *et al*. have shown that DDX3 can inhibit cap-dependent translation through prevention of the eIF4E-eIF4G interaction (Shih et al., 2008). Therefore, discrepancies have arisen as to the precise role of DDX3 in translation.

DDX3 as a General Translation Initiation Factor

Using a β-globin reporter gene, Lee *et al*. show that DDX3 depletion results in β-globin protein levels being severely decreased. This reduction was attributed to DDX3 repressing translation as its depletion did not have an effect on transcription, mRNA export or splicing (Lee et al., 2008). Additionally, mass spectrometry analysis identified an interaction between DDX3 and ten of the thirteen subunits of the eIF3 complex (subunit j, l and m were not detected), with interactions between DDX3 and eIF3B and eIF3E confirmed, *in vivo* (Lee et al., 2008). The translation initiation factor eIF3 is the largest and most complex of the translation initiation factors. It is responsible for

mediating the interaction and stabilization of the eIF2-GTP-$tRNA_i^{MET}$ ternary complex, binding to the 40S ribosome, and promoting dissociation of the 40S and 60S ribosomal subunits (Marchione et al., 2013). The authors conclude based on the β-globin reporter gene data and the interaction between DDX3 and eIF3 that DDX3 functions to promote translation (Lee et al., 2008).

In support of this evidence, using luciferase-encoding reporter RNAs, Geissler *et al*. observed that DDX3 depletion resulted in a decrease in protein synthesis between thirty to sixty percent, while over-expression of wild type DDX3 stimulated translation of the reporter RNAs. Furthermore, DDX3 depletion inhibited internal ribosome entry site (IRES)-mediated translation of Hepatitis C virus (HCV) proteins as measured utilizing a bi-cistronic HCV replicon, whereby the IRES directs translation (Geissler et al., 2012). Using polysome sucrose gradients, DDX3 associated with the 40S and 80S ribosomal subunits, allowing the authors to reason that DDX3 functions in translation initiation and not in translation elongation or termination (Geissler et al., 2012). Confirming data observed by Lee *et al*., Geissler *et al*. observed that DDX3 interacts with components of the eIF3 translation subunit along with identifying eIF2 as a novel interactor (Geissler et al., 2012).

DDX3 Facilitates Translation of a Subset of mRNAs

In contradiction to the above data, Lai *et al*. demonstrate that DDX3 depletion does not affect general translation, as no changes in polysome profiles were observed upon depletion. However, DDX3 was shown to be necessary for efficient translation of mRNAs with long or structured 5'UTRs (Lai et al., 2008). Exploiting sucrose gradient

sedimentation in conjunction with cDNA microarray analysis to identify mRNAs translationally regulated by DDX3, Lai *et al*. identified 332 genes whose 5'UTRs were slightly longer and contained a higher GC content (Lai et al., 2010) . Specifically, DDX3 was shown to regulate cyclin E1 translation, mediating its control of the G_1/S transition in cells (Lai et al., 2010).

In support of this evidence, Soto-Rifo *et al*. discerned utilizing a Renilla luciferase reporter assay that DDX3 depletion repressed translation of specific viral mRNAs while having no effect on others. Soto-Rifo *et al*. elaborate on the results presented by Lai *et al*. by postulating that DDX3 regulation of mRNA translation is dependent on the presence of stem loop structures within the 5'UTRs of viral mRNA, as all regulated viral mRNAs examined contained 5'UTRs which are long, structured and GC-rich (Soto-Rifo et al., 2012). Moreover, DDX3 was observed to be associated with the eIF4F complex through an interaction with eIF4G and PABP1 in a RNA-independent manner (Soto-Rifo et al., 2012). The authors speculate that DDX3 may be a core component of the eIF4F complex and is required for translation when it interacts with an mRNA with a stem loop within its 5'UTR (Soto-Rifo et al., 2012). These results allude to a role for DDX3 in the translation of specific mRNAs.

DDX3 Inhibits Cap-Dependent Translation

Shih *et al*. observed that de novo protein synthesis upon ectopic expression of DDX3 was repressed in dose-dependent manner, while depletion of DDX3 enhanced protein synthesis. DDX3-mediated repression of protein translation occurred post-transcriptionally and did not result from a decrease in mRNA transcripts (Shih et al.,

2008). DDX3 repressed cap-dependent translation through binding to the cap binding protein, eIF4E, preventing its binding to eIF4G. It was hypothesized that DDX3 could function analogously to 4E binding protein 1 (4E-BP1) which binds to eIF4E preventing its association with eIF4G, inhibiting translation initiation (Shih et al., 2008). Conversely, DDX3 expression stimulated IRES-mediation translation, with its ability to enhance IRES-mediated translation dependent on its capacity to bind eIF4E. The authors speculate that DDX3 binding to eIF4E which prevents cap-dependent translation may free additional translation initiation factors shared by both cap- and IRES-containing mRNAs to promote IRES-mediated translation (Shih et al., 2008).

DDX3 and Stress Granules

DDX3 was identified as a component of cytoplasmic stress granules, through its localization with known stress granule markers, TIA-1 and HuR (Lai et al., 2008). The stress granule inducing capacity of DDX3 is dependent on its eIF4E-binding ability and is independent of its ATPase and helicase activities (Shih et al., 2012). DDX3 interacts with eIF4E and PABP1 and localizes to stress granules with these proteins upon the induction of environmental stresses. Knockdown of DDX3 inhibits stress granules assembly, causing nuclear retention of PABP1, and resulting in decreased cell viability upon removal of cellular stress (Shih et al., 2012).

Whereas the mechanism in human cells of how DDX3 may regulate translation through stress granule assembly has not been elucidated, a working hypothesis in yeast has been proposed. Consistent with DDX3 localization, Ded1 also localizes to stress granules. Ded1 accumulates in stress granules in a complex with mRNA and the eIF4F

complex through its direct interaction with eIF4G (Hilliker et al., 2011). Through Ded1 hydrolysis of an ATP molecule, the interaction between Ded1 and the bound mRNP is weakened. This permits the dissociation of the mRNP from Ded1, allowing the mRNP to proceed through translation initiation, suggesting that Ded1 may be part of an intermediate proof-reading complex during translation initiation (Hilliker et al., 2011).

1.12 DDX3 and Cancer

Numerous studies have implied a role for DDX3 in the development and/or progression of cancer, though contrary data exists whether DDX3 functions as a tumor suppressor protein or an oncogene. Chao *et al*. characterized DDX3 as a tumor suppressor as DDX3 mRNA levels were decreased in 57.8% of hepatocellular carcinoma (HCC) specimens, with DDX3 proteins levels decreased in 73% of HCC samples compared to normal liver tissue (Chao et al., 2006). This decrease in DDX3 levels corresponded with down-regulation of p21, a DDX3 transcriptional target. Over-expression of DDX3 suppressed cell growth in hepatocellular, cervical and colon carcinoma cell lines, as well as in mouse fibroblasts (Chao et al., 2006). In accordance with this study, Chang *et al*. observed a decrease in DDX3 protein levels in 59% of HCC samples. This decrease in DDX3 protein levels was accompanied by a two- to four-fold reduction in DDX3 mRNA levels. Additionally, down-regulation of DDX3 was highly prevalent in hepatitis B positive HCC samples. Moreover, DDX3 depletion in mouse fibroblasts accelerated cell growth corresponding with an increase in cyclin D1 protein levels and a decrease in p21 protein levels (Chang et al., 2006).

In agreement with the hypothesis that DDX3 functions as a tumor suppressor protein, Wu *et al*. observed DDX3 mRNA levels down-regulated in 53% of lung cancer samples compared to normal tissue. Furthermore, decreased DDX3 mRNA correlated positively with p21 levels, and negatively with the human papilloma virus E6 protein. Moreover, DDX3 transcription was discovered to be predominantly regulated by p53, whose activity is altered in E6 positive lung carcinomas (Wu et al., 2011). Consistent with these results, in lung carcinoma cells, DDX3 down-regulation via p53 inactivation results in an increase in both anchorage-independent growth and invasive potential. DDX3 down-regulation results in a loss of expression of MDM2, a regulator of p53, and increased expression of the transcription factor slug, which functions in the epithelial-mesenchymal transition. Increased Slug levels correlate with a reduction in E-cadherin levels. In the context of lung tumors, patients with low-DDX3 expressing tumors had poorer survival and an increased probability of tumor recurrence than patients with high-DDX3 expressing tumors (Wu et al., 2013).

In contrast to these studies, Huang *et al*. observed DDX3 mRNA levels increased in 64% of HCC samples. Additionally, over-expression of DDX3 resulted in a significant increase in cell growth in a hepatocellular carcinoma cell line (Huang et al., 2004). In breast cancer cells, Botlagunta *et al*. observed that DDX3 mRNA and protein levels were elevated in comparison to mammary epithelial cells. Treatment of mammary epithelial cells with Benzo[a]pyrene diol epoxide, a major cancer-causing agent in tobacco, induces DDX3 protein expression. Stable over-expression of DDX3 in mammary epithelial cells results in altered cell morphology, increased motility and invasion, altered β-catenin cellular localization, and E-cadherin repression, phenotypes indicative of an epithelial-

mesenchymal transition (Botlagunta et al., 2008). In breast cancer cells, DDX3 is a transcriptional target of hypoxia inducible factor 1α (HIF1α), which promotes elevated DDX3 expression in hypoxic conditions (Botlagunta et al., 2011). In gallbladder squamous cell/adenosquamous carcinoma, elevated DDX3 protein levels correlate with tumor size, lymph node metastasis and poor patient prognosis (Miao et al., 2013). DDX3 also promotes increased levels of the transcription factor Snail, which represses expression of cellular adhesion proteins leading to increased cell migration and invasion. Snail protein levels also correlated with DDX3 protein levels in glioblastoma multiforme samples (Sun et al., 2011). These contradictory findings characterizing DDX3 as both a tumor suppressor and an oncogene suggests that DDX3 exhibits tissue specific functions that either inhibit or promote malignancy.

DDX3 also functions in both the intrinsic and extrinsic apoptotic signalling pathways. DDX3 regulates the intrinsic apoptotic pathway by repressing apoptosis in p53 mutant cells, while promoting apoptosis in p53 wild type cells in response to the DNA damaging agent camptothecin. In p53 wild type cells, after DNA damage, DDX3 binds to p53 and promotes the accumulation of p53, thus allowing for the downstream activation of p21 (Sun et al., 2013). DDX3 regulates extrinsic apoptotic signalling by mediating the formation of a complex which includes GSK3 and cellular inhibitor of apoptosis protein-1 (cIAP-1) to cap the TRAIL-R2 death receptor, thus inhibiting caspase activation. This DDX3-GSK3-cIAP-1 complex provides a checkpoint for initiation of apoptotic signalling by forming a death-antagonizing signalling complex at the death receptor to function as a counterbalance to the death-inducing signalling complex (Sun et al., 2008).

1.13 Tudor Domain Containing Proteins

The Tudor family was originally identified in 1985 through the discovery of the *Drosophila melanogaster Tudor (Tud)* gene in a genetic screen characterizing maternally expressed genes resulting in lethality or sterility in progeny (Boswell and Mahowald, 1985). The Tudor domain was subsequently identified in the *Drosophila melanogaster* Tud protein based on the presence of ten repeated units of shared sequence homology (Ponting, 1997). Subsequently, Tudor domain containing proteins have been discovered in diverse eukaryotic organisms, including fungi, plants and animals, but not in prokaryotes (Lasko, 2010). Tudor domain containing proteins have been implicated in a diverse set of cellular functions including RNA metabolism, germ cell development, transposon silencing, the DNA damage response, histone modification and chromatin remodeling (Chen et al., 2011) .

Tudor domain containing proteins belong to the so-called "royal" domain superfamily, which also includes proteins with chromo, MBT, PWWP, and plant agenet domains. The royal domain superfamily recognizes proteins with arginine- and lysine-methylated residues (Maurer-Stroh et al., 2003). Members of the royal domain superfamily retain a structurally related barrel-like protein fold, composed of three to five anti-parallel β-sheets. These proteins from each royal domain subfamily bind to methylated arginine or lysine residues through a common binding mode, wherein an aromatic binding pocket in the barrel accepts the methylated side chain. This pocket is composed of two to four aromatic residues, which provides electrostatic and hydrophobic contacts to accept the methylated lysine or arginine residue (Taverna et al., 2007). About 30 mammalian Tudor proteins have been identified and can contain a single Tudor

domain, multiple tandem Tudor domain repeats or one or more Tudor domains in combination with other types of domains (Chen et al., 2011) .

Classification of Tudor Domains

Four subtypes of Tudor domains are distinguishable based on their flanking sequences and/or linkage to other conserved motifs, influencing their biological function (Jin et al., 2009). The original germ line type Tudor domain containing proteins (TDRD1, 2, 4, 5, 6, 7, 8, and 9) constitute one group; characterized by multiple Tudor domains which may be flanked on their amino-terminal side with an α helix and β sheet. The proteins within this group bind to either dimethylated arginine or lysine residues (Jin et al., 2009). These Tudor domain-containing proteins accrue within germline-specific ribonucleoprotein complexes called germinal granules, which recruit methylated Piwi-type proteins involved in retrotransposon silencing by Piwi-interacting RNAs during gametogenesis (Siomi et al., 2010). The second group encompasses Tudor domain containing proteins (ex. Staphylococcal nuclease domain-containing protein 1) with a Tudor domain inserted into the fifth domain of five tandem staphylococcal nuclease-like domains. These proteins bind to arginine methylated PIWI-like protein 1 in germ cells (Liu et al., 2010). Thirdly, Tudor domain-containing proteins labelled tandem Tudor or Jumonji domain-containing protein distinguish methylated lysines on histone tails (Charier et al., 2004; Kim et al., 2006a). Lastly, the fourth group contains Tudor domain containing proteins which recognize methylated arginine residues within the context of RG-rich repeat domains. This group includes the SMN protein, SPF30 and TDRD3 (Friesen et al., 2001a; Brahms et al., 2001; Rappsilber et al., 2001; Meister et al., 2001; Cote and Richard, 2005).

Tudor domains as Methylarginine Readers

SMN, the causative gene for spinal muscular atrophy (SMA) is the best characterized Tudor domain containing protein amongst this group. Recognition of symmetrically methylated Sm proteins by the Tudor domain of SMN promotes the cytoplasmic assembly of the core spliceosome machinery (Friesen et al., 2001a; Brahms et al., 2001; Cote and Richard, 2005). The Sm proteins (SmB, SmB', SmD1, SmD2, SmD3, SmE, SmF, and SmG) are components of small nuclear ribonucleoproteins (snRNPs). SMN, which recognizes symmetrically dimethylated arginine residues of SmB, SmB', SmD1 and SmD3 catalyzed by PRMT5, facilitates the formation of the Sm protein-based snRNP core structure through its interaction with the methylated Sm proteins (Friesen et al., 2001a; Brahms et al., 2001; Brahms et al., 2000; Friesen and Dreyfuss, 2000). The interaction between SMN and methylated Sm proteins promotes the efficient assembly of the mature snRNPs, which is crucial for pre-mRNA splicing. A SMA-causing mutation (Glu134Lys) within the SMN Tudor domain alters charge distribution within the methylarginine binding site, leading to the abolition of SMN binding to SmD1 and SmD3. Abrogation of SMN binding to Sm proteins results in the improper assembly of the spliceosome and defective mRNA splicing, contributing to the onset of SMA (Selenko et al., 2001; Tripsianes et al., 2011). While SMN recognizes symmetrically methylated Sm proteins, it is additionally capable of recognizing asymmetric dimethyl arginine residues. The SMN Tudor domain recognizes asymmetric methylation by CARM1 within the PGM motifs of CAP150, SAP49, SmB and U1C proteins (Cheng et al., 2007).

Like SMN, SPF30/SMNrp has also been implicated as an essential splicing factor. SPF30 is a U2 snRNP-associated protein that facilitates the recruitment of the U4/U5/U6 complex to the pre-spliceosome complex, with SPF30 depletion resulting in the spliceosome failing to form (Rappsilber et al., 2001; Meister et al., 2001). Like SMN, SPF30 and TDRD3 are also capable of recognizing symmetrically methylated Sm proteins (Cote and Richard, 2005). The Tudor domains of SMN, SPF30 and TDRD3 are closely related based on sequence homology (Jin et al., 2009), therefore, it is hypothesized that along with SMN and SPF30, TDRD3 may also be involved in spliceosome assembly and pre-mRNA splicing (Chen et al., 2011) .

1.14 Tudor domain containing protein 3 (TDRD3)

TDRD3 is a ubiquitously expressed, modular protein of unknown function which associates to cytoplasmic stress granules under conditions of cellular stress. TDRD3 is located on chromosome 13q21.2 and contains a 2.9 kb mRNA sequence encoding 13 coding exons. The TDRD3 protein sequence contains 744 amino acids and has a predicted molecular weight of 82.7 kDa (Goulet et al., 2008; Linder et al., 2008). In addition to its Tudor domain (amino acids 647-710), TDRD3 contains an DUF/OB-fold domain (amino acids 13-169), an ubiquitin binding (UBA) domain (amino acids 286-328), a FMRP binding domain (amino acids 711-723) and an exon junction complex-binding motif (EBM) (amino acids 725-744) (Figure 1.4). OB-folds are structural motifs consisting of five β-sheets that are often used for nucleic acid recognition, though they have also been observed at protein-protein interactions, while an UBA domain is a motif found in several proteins having connections to ubiquitin and the ubiquitination pathway (Theobald et al., 2003; Hurley et al., 2006). The UBA domain of TDRD3 was observed

1.4)

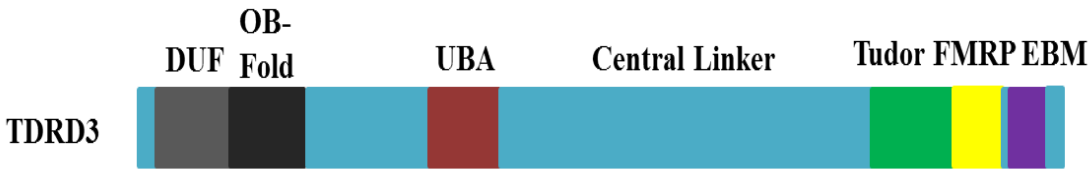

Figure 1.4: TDRD3 Structure

TDRD3 is a 744 amino acid protein containing a DUF/OB fold nucleic acid recognition motif (amino acids 13-169), an UBA domain which recognizes tetra ubiquitin (amino acids 286-328), an uncharacterized central linker region (amino acids 329-646), a Tudor domain which recognizes arginine methylated motifs (amino acids 647-710), a FMRP binding region (amino acids 711-723), and an exon junction complex-binding motif (EBM) (amino acids 725-744).

to be both necessary and sufficient for binding to Lys_{48}-linked tetra-ubiquitin (the signal for proteasome degradation of proteins), while TDRD3 was unable to bind either mono-ubiquitin or Lys_{63}-linked ubiquitin (a non-proteolytic signal) (Linder et al., 2008). Exon junction complex-binding motifs play a functional role in mRNA export and translation (Bono and Gehring, 2011).

Through both indirect immunofluorescence and cell fractionation methodology, TDRD3 was observed to be a predominantly cytoplasmic protein with diffuse nuclear expression (Goulet et al., 2008; Linder et al., 2008). Additionally, TDRD3 can function as a transcriptional activator for both estrogen- and androgen-receptor mediated transcription with the Tudor domain being indispensable for this function (Yang et al., 2010).

TDRD3 and Arginine Methylation

TDRD3 was initially characterized as a methylarginine binding protein through the propensity of a GST-tagged purified protein of the Tudor domain being able to bind methylated proteins from cell extracts (Cote and Richard, 2005). Further studies have shown that TDRD3 preferentially binds asymmetrically dimethylated arginine residues (Liu et al., 2012; Sikorsky et al., 2012), although TDRD3 recognition of methyl arginines could still be sequence or context-dependent. Specifically, TDRD3 reads the methylation marks deposited by CARM1 on H3R17 and by PRMT1 on H4R3. Conversely, weak binding to H3R17 was observed by the Tudor domains of SMN and SPF30. Moreover, TDRD3 is capable of discriminating between the H4R3 asymmetric methylation mark deposited by PRMT1 and the symmetric methylation mark deposited by PRMT5 (Yang

et al., 2010; Liu et al., 2012). Pull-down experiments have identified several proteins that interact with TDRD3's Tudor domain that have been identified as PRMT substrates or are proto-typical arginine methylated proteins (Goulet et al., 2008). Identified arginine methylated proteins include FUS (Rappsilber et al., 2003; Du et al., 2011; Tradewell et al., 2012), SERPB1 (Lee et al., 2012), while proto-typical arginine methylated proteins containing multiple GAR rich motifs include DDX3, eIF1A1, and EWS.

TDRD3 and Stress Granules

TDRD3 localizes to stress granules upon oxidative, heat and osmotic shock with a number of stress granule markers including TIA-1 and FMRP (Goulet et al., 2008; Linder et al., 2008). TDRD3 is detected in stress granules concurrently with TIA-1, a crucial mediator of stress granule assembly (Gilks et al., 2004), suggesting that TDRD3 may participate in early stress granule assembly (Goulet et al., 2008). Furthermore, the Tudor domain of TDRD3 was both necessary and sufficient for TDRD3 localization to stress granules (Goulet et al., 2008). Mutation in the Tudor domain of glutamic acid 691 to a lysine (E691K), a residue necessary to recognize arginine methylated motifs, results in a decrease in localization of the Tudor domain to stress granules. This implicates TDRD3's ability to recognize methylated arginine residues to its localization to stress granules (Goulet et al., 2008).

Interestingly, TDRD3 associates with actively translating polyribosomes in cycling cells. However, under stress conditions, TDRD3 associates with monomeric ribosomes (Goulet et al., 2008). This pattern of association is also observed with FMRP, which also localizes to stress granules (Mazroui et al., 2002; Dolzhanskaya et al., 2006;

Kim et al., 2006b; Anderson and Kedersha, 2008). TDRD3 interacts with FMRP and its paralogs FXR1 and FXR2, with the twenty amino acids C-terminal to the Tudor domain necessary for this interaction to occur (Linder et al., 2008). These results suggest that TDRD3 may play a functional role in translation regulation.

1.15 TDRD3 and Breast Cancer

In a patient screen examining survival rates in ER- breast cancer tumours five years post-operation, TDRD3 mRNA expression strongly correlates with patients who exhibited a poor prognosis (Nagahata et al., 2004). Furthermore, TDRD3 was among 14 genes associated with poor patient outcome in basal-like breast cancer (Hallett et al., 2012), and was overexpressed in 58 of 158 breast cancer patient samples in the Cancer Genome Atlas' Data Portal (http://tcga-portal.nci.nih.gov). Additionally, TDRD3 localizes to stress granules, a means that cancer cells use to promote cell survival. Therefore, since TDRD3 expression correlates with poor prognosis in patients and TDRD3 appears to be an early participant in stress granule formation, a mechanism used by cancer cells for survival, TDRD3 may contribute to breast cancer development and progression.

1.16 Rationale for Study

Work from this dissertation contributes to the expanding field of knowledge of how protein arginine methyltransferases function in the etiology and progression of cancer, specifically breast cancer. Research from other groups and ours has implicated aberrant regulation of PRMTs to breast cancer development and progression. Furthermore, PRMTs are implicated in numerous cellular processes including cell cycle

regulation, DNA damage repair and apoptotic pathways whose dysregulation are frequent occurrences in cancer. Specifically, PRMT1, the prominent PRMT member which accounts for the bulk of methylation in mammalian cells, yields seven distinct isoforms through alternative splicing which display distinct sub-cellular localization and substrate specificity. Therefore, it can be hypothesized that each PRMT isoform is functionally distinct. PRMT1 isoform 2 (PRMT1v2), the only isoform which contains exon 2 in it translated sequence is the only isoform with predominantly cytoplasmic cellular localization. In addition, its mRNA and protein levels are over-expressed in a panel of breast cancer cells to a higher extent than the other isoforms. Therefore, it is of importance to elucidate the function PRMT1v2 may perform in the development and/or progression of breast cancer.

Stress granules, sites of mRNA triage, form upon cellular exposure to environmental stress including chemotherapeutic drugs to promote cell survival at least in part through the sequestration of pro-apoptotic proteins. Though, to date, no study has directly shown an effect of PRMTs on stress granule dynamics, methylation of numerous PRMT substrates promotes their localization to stress granules. Therefore, delineating the role of PRMTs in stress granule formation, and the mechanism by which stress granules promote cancer cell survival is crucial to alleviate the problem of chemoresistance.

DDX3 is a prototypical PRMT substrate containing numerous glycine-, arginine-rich motifs, characteristic of PRMT substrates. Moreover, DDX3 mRNA and protein levels are up-regulated in breast cancer cells, while DDX3 overexpression in mammary epithelial cells represses E-cadherin expression leading to altered cell morphology, and increased motility and invasion. Consistent with the observation that numerous PRMTs

are overexpressed in breast tumors, it is essential to determine first if DDX3 is an arginine methylated protein and the PRMT(s) responsible for methylating DDX3, and second whether this methylation promotes DDX3-mediated altered cell morphology and increased migration and invasion in mammary epithelial cells.

Numerous PRMTs are aberrantly expressed in breast cancer corresponding with irregular expression of many of their substrates. Therefore, it would be hypothesized that atypical expression of TDRD3, a reader of arginine methylated marks would also be prevalent in breast cancer. Indeed, TDRD3 mRNA expression correlates with poor patient prognosis in recurrent estrogen receptor negative breast tumours. Furthermore, TDRD3 was amongst 14 genes associated with poor patient outcome in basal-like breast cancers. TDRD3 also localizes to stress granules, a mechanism cancer cells utilize to promote cell survival upon environmental stress. This evidence suggests TDRD3 may function in breast cell oncogenesis. Therefore, elucidating the contribution of TDRD3 to the development and/or progression of breast cancer is of importance.

Hypothesis and Objectives

Hypothesis: I hypothesize that aberrant regulation of protein arginine methyltransferases, their substrates and effectors contributes to the development of breast cancer tumors and subsequently to their growth and progression.

Objectives:

1) Assess the role of the PRMT1 alternatively spliced isoform v2 in breast cancer development and growth, one of the PRMTs known to be aberrantly regulated in breast cancer.

2) Elucidate the role of PRMT6 in chemoresistance through investigating its function in stress granule dynamics.
3) Identify the PRMT(s) responsible for DDX3 methylation and characterization of the potential functional impact on DDX3's function in breast cancer cells.
4) Assess the role of TDRD3, a reader/effector of arginine methylation that has been linked with poor prognosis of breast cancer, in breast cancer development and growth.

Chapter 2: Materials & Methods

2.1 Cell Lines

Cell lines were purchased from the American Type Culture Collection. HeLa, 293T, MDA MB 231, BT-20, and BT-474 cells lines were cultured with Dulbecco's Modified Eagles Medium (DMEM) with 2 mM glutamine and 10% fetal bovine serum (FBS). MCF7, T-47D, Hs578T, and BT-549 cells lines were supplemented with 2.75 µg/ml insulin. SK-BR-3 cells were cultured in McCoy's Medium supplemented with 10% FBS. MCF10A cells were cultured in DMEM/F12 medium supplemented with 5% horse serum, 20 ng/ml epidermal growth factor, 0.5 µg/ml hydrocortisone, 100 ng/ml cholera toxin and 10 µg/ml insulin.

2.2 Establishment of Stably-Expressing Cell Lines

To establish stably-expressing cell lines, DNA constructs were transfected using Lipofectamine 2000, according to the manufacturer's protocol. For GFP-tagged expressing constructs, transfection efficiency was determined 24 h post transfection. Selection for stable pools of cells was begun 48 h post-transfection using puromycin. The amount of puromycin used for selection was determined for each cell type by first performing a kill curve to determine the minimum concentration of puromycin required to kill all of the cells.

2.3 Antibodies

The following primary antibodies used were from Bethyl Laboratories: DDX3 (A300-474A), CARM1 (A300-421A), PRMT6 (A300-929A), eIF4G1 (A301-774A) and

eIF4E (A301-154A). The Tubulin (MAB1637), β-catenin (06-734), and FMRP (MAB2160) antibodies were from Millipore. The GST (G1160) and Flag (F3165) antibodies were from Sigma; PARP (9542) and phospho-β-catenin (9561) antibodies from Cell Signalling while the GAPDH (MMS-580S) antibody was from Covance. The His antibody (TAG 001) was from Bio Shop Canada Inc., p21 (05-345) from Upstate, GFP (11 814 460 001) from Roche, E-cadherin (610185) from BD Bioscience, TIA-1 (sc-1751) from Santa Cruz Biotechnology, and Alexa Fluor 594 nM Phallodin (A12381) from Life Technologies. The Myc 9E10 hybridoma cell line was from American Type Culture Collection and the PRMT1 C-terminal antibody was a gift from Dr. Stephane Richard (University of McGill).

The secondary horse radish peroxidase antibodies were purchased from Cappel: rabbit (55690) and mouse (55506). Alexa Fluor antibodies for immunofluorescence were purchased from Life Technologies: mouse Alexa Fluor 488 nm (A11001), mouse Alexa Fluor 594 nm (A11012), rabbit Alexa Fluor 488 nm (A11008), mouse Alexa Fluor 594 nm (A11005), and goat Alexa Fluor 594 nm (A11058).

2.4 Affinity Purification of PRMT1v2 Antibody

Synthetic PRMT1v2 peptide, ANC IME NFV ATL ANG MSL QPP L-EE, was synthesized at W.M. Keck Foundation Biotechnology Resource Laboratory. Polyclonal antibodies were generated by Cedarlane Laboratories using rabbits injected with the synthetic peptide coupled to KLH. Antibodies were affinity-purified over the antigenic peptide coupled to Affi-Gel 15 beads (Bio-Rad) following manufacturer's instructions, eluted in 100 mm Glycine pH 2.5, buffered with 1 M Tris–HCl pH 8.0, dialyzed against

1× phosphate-buffered saline (1× PBS: 137 mm NaCl, 2.7 mm KCl, 4.3 mm Na2HPO4, 1.4 mm KH2PO4, pH 7.4) and concentrated using a Centricon centrifugal device (Millipore). The PRMT1v2 antibody was used at a dilution of 1:1000 overnight at 4˚C for Western Blot analysis.

2.5 siRNA/shRNA Transfection

A PRMT1v2 Stealth siRNA duplex (Sense: CAUCCCAUUAGCAAGGUGGCUACA; Antisense: UGUAGCCACCUUGGCUAAUGGGAUG) (Life Technologies) was co-transfected with an shRNA, encoding the same target sequence as the siRNA to deplete PRMT1v2 levels using Xtreme Gene siRNA transfection reagent according to the manufacturer's protocol. A control siRNA (Life Technologies) was used individually, or in combination with a scramble shRNA in the pRS vector as a negative control. Briefly, 1 µg of siRNA and 2 µg of shRNA (6 well plates) were diluted in Opti-MEM media, combined with Xtreme Gene Transfection Reagent, incubated at room temperature for 15 minutes and added to the cells. Transfections were performed in the absence of antibiotics. Knockdown was assessed by either RT-PCR or Western Blot 24, 48, or 72 h post-transfection.

DDX3 siRNA (DDX3 siRNA #1: GGUAUUAGCACCAACGAGA; DDX3 siRNA #2: GAUGCUGGCUCGUGAUUUC) were purchased from Thermo Scientific and transfected into cells using Oligofectamine transfection reagent according to the manufacturer's protocol. A scramble siRNA was used as a control. Briefly, 1 µg of siRNA was diluted in Opti-MEM media, combined with Oligofectamine, mixed,

incubated for 20 minutes and added to cells. Transfections were performed in the absence of antibiotics and FBS. Media containing FBS was added to cells 4 hours post-transfection.

The pGIPz PRMT6 lentiviral shRNAmir was purchased from Open Biosystems (RHS4430-101515232) and was transfected using Lipofectamine 2000 according to the manufacturer's protocol.

2.6 Transfection of DNA Plasmids

DNA constructs were transfected into cells using either Lipofectamine 2000 (Life Technologies) or Polyethyleneimine (PEI). Lipofectamine 2000 transfections were performed according to the manufacturer's protocol. Briefly, 2 µg (6 well plates) or 10 µg (10 cm plates) of DNA were diluted in Opti-MEM media. Lipofectamine 2000 was diluted in Opti-MEM (ratio of Lipofectamine 2000 to DNA determined based on cell type) and incubated for 5 minutes at room temperature. Lipofectamine 2000 was added to DNA, mixed and incubated at room temperature for 20 minutes, then added to the cells. For PEI transfections, 3 µg (6 well plates) or 10 µg (10 cm plates) DNA was diluted in serum free media. PEI was added to the DNA (ratio of PEI to DNA used was 4:1 for 293T cells and 5:1 for HeLa cells), mixed and incubated 20 minutes at room temperature. Before addition of DNA and PEI complexes, cells were washed one time with 1X PBS and three times with serum free media. For PEI transfection, expression was assessed 48 h post transfection. Transfections were performed in the absence of antibiotics.

2.7 DNA Constructs

DDX3 was sub-cloned into the pGEX-4T2 expression plasmid utilizing the BamHI/EcoRI restriction sites, and pcDNA 3.1 myc expression plasmid using the EcoRI/XhoI restriction sites. DDX3 truncation mutants containing amino acids 1-181, 182-404, and 405-662 were created by PCR amplifying the fragments from full length DDX3 and sub-cloning them into the pGEX-4T2 expression plasmid or pcDNA 3.1 myc expression plasmid at the above mentioned restriction sites. PRMT6 was sub-cloned into the pET20b(+) expression construct utilizing the BamHI/EcoRI restriction sites. To create the pcDNA3 Flag PRMT6 construct, a Flag epitope (GAT TAC AAG GAT GAC GATGAC AAG) was PCR amplified N-terminal to the PRMT6 sequence and sub-cloned into pcDNA3 at the KpnI/BamHI restriction sites.

2.8 Site-Directed Mutagenesis

Mutation of DDX3 arginine residues 315, 532, 585, 587, 632, double 585/587 mutant, and triple 315/585/587 arginine to alanine mutant was performed by site-directed mutagenesis using PFU Turbo DNA Polymerase (Stratagene) utilizing primers designed using the Quick Change Primer Design Program (Agilent). The triple 315/585/587 mutant was created by mutating arginine residue 315 in the DDX3 585/587 mutant. Primers used for site-directed mutagenesis are in Appendix II.

2.9 RNA Isolation

RNA was isolated from cells using TRIzol (Life Technologies) according to the manufacturer's protocol. Briefly, cells were washed once with 1x PBS, then scraped and pelleted. The cell pellet was re-suspended in TRIzol and incubated at room temperature for 5 minutes. Chloroform was added to the suspension, mixed and incubated for 3

minutes at room temperature. The suspension was centrifuged, the upper phase was removed and isopropanol was added to this mixture. The suspension was mixed, incubated for 10 minutes at room temperature and centrifuged. The pellet was washed with 70% ethanol, and then re-suspended in Diethylpyrocarbonate (DEPC) water.

2.10 Reverse Transcription Polymerase Chain Reaction (RT-PCR)

Reverse transcription of RNA to make complementary DNA was performed using AMV reverse transcriptase (Promega). 500 ng of RNA was incubated with 1 µM oligo dT primer for 10 minutes at 65˚C, then for 60 seconds at 20˚C. 2 mM dNTPs were added to the RNA along with 20 units of RNasin and 5 units of AMV reverse transcriptase and incubated for 1 h at 42˚C.

PCR was performed in a 20 µL reaction using Go Taq Green Master Mix using 1 µL each of the following primers sets: 1) PRMT1 Forward 5'-GAGGCCGCGAACTGCATCAT-3'; Reverse 5'-TGGCTTTGACGATCTTCACC-3' 2) GAPDH Forward 5'-ACCACAGTCCATGCCATCAC-3'; Reverse 5'-TCCACCACCCTGTTGCTGTA-3' 3) E-cadherin Forward 5'-TGGGTTATTCCTCCCATCAG-3'; Reverse 5'-TTTGTCAGGGAGCTCAGGAT-3' 4) β-catenin Forward 5'-AAAATGGCAGTGCGTTTAG-3'; Reverse 5'-TTTGAAGGCAGTCTGTCGTA-3' 5) PRMT6 Forward 5'-GTTCCAGGTGACCTTCCCTGGAG-3'; Reverse 5'-CCGGCTCGTTCAGGTAGAGGAGC-3' 6) eIF4E Forward 5'-AAGCCTCTCGTTACTCACGA-3'; Reverse 5'-GTAGGGGTGGTTTCCGGTTC

2.11 Trypan Blue Exclusion Assay

Adherent and non-adherent cells were collected, pelleted, washed once with 1X PBS, re-pelleted and re-suspended in 500 µL 1X PBS. Trypan Blue was added to the cell suspension, mixed and incubated at room temperature for 2 minutes. The cell suspension was counted using a hemocytometer with 200 total cells counted for each condition assessed, and the number of blue cells representing non-viable cells was determined.

2.12 MTT Assays

Thiazolyl Blue Tetrazolium Bromide (MTT) reactions were performed in 96 well plates. MTT (5mg/mL dissolved in 1X PBS) was added to the cells, and the cells were incubated for 3.5 h at 37˚C. Media was removed and 150 µL of MTT solvent (4 mM HCl, 0.1% Nondet P-40 in isopropanol) was added. The 96 well plates were wrapped in aluminum foil and agitated on an orbital shaker for 15 minutes. Absorbance was read at 590 nm to determine intensity of the signal.

2.13 Flow Cytometry and Annexin V Staining

Flow cytometry was performed by collecting all adherent and non-adherent cells. Cells were pelleted and washed twice with 1X PBS. Cells were fixed in ice cold 70% ethanol and stored at -20˚C for at least 30 minutes. Cells were pelleted, washed once with 1X PBS and stained using a 1X propidium iodide solution (18 µg/mL propidium iodide, and 40 µg/mL RNase A dissolved in 1X PBS) for 30 minutes in the dark at 4˚C. Flow cytometry was performed using a Beckman Coulter Epics XL flow cytometer and data was analyzed using WinMDI 2.8. Annexin V staining was performed using the Annexin V-FITC Apoptosis Detection Kit (BioVision) according to the manufacturer's protocol. After washing of cells with 1X PBS, cells were co-stained with Annexin V-FITC and

propidium iodide for 5 minutes at room temperature in the dark. Annexin V/propidium iodide analysis quadrants were established according to individually stained Annexin V or propidium iodide controls.

2.14 Cell Motility and Invasion Assays

Control (for motility) and matrigel (for invasion) chambers were purchased from BD Biosciences and used according to the manufacturer's protocol. The chambers were rehydrated in serum free media in a 24 well plate in the incubator at 37˚C for 2 h. 50 000 cells in serum free media were added to the top of the chamber, while media containing a chemo attractant (FBS) was dispensed underneath the chamber. Chambers were incubated at 37˚C for 24 h to 72 h depending on the cell line. After incubation, the media was removed from the top of the chamber and cells that had not migrated to the bottom of the chamber were removed using a Q-tip. Chambers were stained with the Kwik Diff Staining Kit (Thermo) and washed twice in water. Chambers were imaged at 20X magnification and a minimum of 6 images per chamber were taken to determine the average number of cells that migrated through each chamber.

Scratch wound assays were performed by plating cells at 100% confluency 24 h prior to the experiment. A "scratch" was performed with a yellow pipette tip. Images of the wound were taken at 10X magnification at the time 0, 6, 12, and 24 h post "scratch" at the same place along the wound. The rate of the wound closure was measured and plotted.

2.15 Colony Scatter Assay

One thousand cells (MCF7) were counted and plated on 100 mm plates and allowed to form colonies for 5 days. One hundred phase contrast images were taken for each cell line and the number of colonies with compact, loose, or scattered formations was counted. Quantification was performed independently by three different people as not to bias the results.

2.16 Immunofluorescence

Cells were plated on coverslips in 6 well plates 24 h prior to immunofluorescence. Cells were washed three times with 1X PBS and fixed with 4% paraformaldehyde for 10 minutes. Cells were subsequently washed three times and permeabilized with 0.5% Triton X-100 in 1X PBS. Cells were washed three times and incubated with the primary antibody for 1 h. Cells were then washed once with 0.1% Triton X-100 in 1X PBS and twice with 1X PBS. The cells were incubated with secondary antibody for 1 h in the dark and washed as per incubation with the primary antibody. Finally, cells were mounted onto glass slides using Vectashield Mounting Media (Vector Labs). Fluorescence microscopy was performed using the Zeiss Axio Imager Z1 microscope and images were acquired with an AxioCam HRm camera utilizing Zeiss Axiovision 4.5 software.

2.17 Protein Purification

GST fusion proteins were overexpressed in *E. coli* BL-21 cells by induction with a final concentration of 0.1 mM isopropyl-β-D-thiogalactopyranoside (IPTG). Cells were lysed in 10 ml of 1X PBS, supplemented with complete protease inhibitor mixture (Roche Applied Science), by sonication. The GST fusion proteins were purified using glutathione-agarose beads (Sigma), and after extensive washes with PBS wash buffer (1X

PBS, 1% Triton X-100, complete protease inhibitor) were eluted from the beads with 60 mM glutathione in PBS adjusted to pH 7.5. His_6 fusion proteins were overexpressed in *E. coli* BL-21 cells by induction with a final concentration of 1 mM IPTG. Cells were lysed in 10 mL of lysis buffer (50 mM Na_2HPO_4, 300 mM NaCl, 10 mM imidazole, 20 mM 2-mercaptoethanol) by sonication. His_6-tagged proteins were purified using a nickel-nitrilotriacetic acid matrix (Qiagen) according the manufacturer's instructions and eluted from the beads using 250 mM imidazole. The purified tagged proteins were dialyzed against 1 L of 1X PBS at 4˚C overnight. The dialyzed proteins were concentrated using Centricon centrifugal devices (Millipore). Protein concentration was determined by Bradford Assay.

2.18 *In Vitro* Methylation Assays

In vitro methylation assays were performed by incubating 10 µg of the tagged PRMT enzyme with 10 µg of the substrate protein in the presence of 0.582 µM *S*-adenosyl-l-[methyl-^{3}H] methionine (^{3}H-SAM) (Perkin Elmer Life Sciences) in a reaction solution containing 25 mM Tris-HCl, pH 7.4 for 2 h at 37˚C. Reactions were terminated by adding Laemmli reducing buffer (25% glycerol, 125mM Tris-HCl pH 6.8, 4mM SDS, 700mM β-mercaptoethanol, 0.1% bromophenol blue). Methylated proteins were resolved by SDS-PAGE; following electrophoresis the gels were stained in Coomassie Brilliant Blue, and destained in a 10% methanol, 5% acetic acid solution to visualize protein bands, and then soaked in En^{3}Hance (Perkin Elmer Life Sciences) for 30 minutes and washed for 30 minutes in water. Gels were dried *in vacuo*, and ^{3}H-labeled proteins were visualized by fluorography.

2.19 *In Vivo* methylation assays

Cells were washed once with 1X PBS and twice with DMEM without methionine (Wisent). DMEM without methionine, 10% FBS, 100 µg/mL cycloheximide and 40 µg/mL chloramphenicol were added to cells which were incubated for 20 min at 37˚C-5% CO_2. 10 µCi/ml L-[Methyl-^{3}H]-methionine (Perkin Elmer Life Sciences) was added and cells were incubated for 3 h at 37˚C-5% CO_2. To ensure translation inhibition, control plates were treated as described above, and incubated with 10 µCi/ml ^{35}S-methionine (Perkin Elmer Life Sciences). Cells were lysed in radioimmunoprecipitation (RIPA) Lysis Buffer (10mM Tris pH 7.4, 100mM NaCl, 1mM EDTA, 1% NP-40, 0.5% NaDOC, 0.1% SDS) and immunoprecipitation was performed. Samples were resolved on SDS-PAGE gel and transferred to an Immunobilon-P polyvinylidene difluoride (PVDF; Millipore: 0.45 µm pores). The membrane was allowed to dry and sprayed with EN^{3}HANCE Spray (Perkin Elmer Life Sciences) three times allowing 20 minutes between sprays for the membrane to dry. ^{3}H-labeled proteins were visualized by fluorography.

2.20 Protein Isolation from Mammalian Cells

Cells were lysed in RIPA Lysis Buffer for 30 minutes rotating at 4˚C with debris cleared from the lysate by centrifugation at 13 000 rpm for 15 minutes at 4˚C. Protein concentration was measured by Bradford Assay.

2.21 Immunoprecipitation and Immunoblotting

Cells were lysed in Triton X-100 Lysis Buffer (10mM Tris pH 7.4, 150mM NaCl, 1% Triton X-100, 10ug/ml phenylmethanesulfonylfluoride (PMSF) with complete

protease inhibitor cocktail (Roche Applied Science)). Lysates were centrifuged 15 min at maximum speed to clear cellular debris. 1% or 5% of lysate was saved for input. The remaining lysate was equally divided between IgG control and the specific immunoprecipitation. 25 µl of a protein A sepharose bead slurry was added and the reaction was incubated rotating from 1 h to overnight at 4˚C. The beads were washed by rotating at 4˚C for 5 min three times with Triton X-100 Lysis Buffer and once with 1X PBS. 5X Laemmli reducing buffer was added and samples were boiled at 95˚C for 8 min. Proteins were resolved by SDS-PAGE and transferred onto a PVDF membrane. 5% non-fat milk in PBS containing 0.05% Tween-20 (PBS-T) was used to block the membrane for 1 h at room temperature. Membranes were incubated with primary antibody diluted in 2% non-fat milk in 0.05% PBS-T overnight at 4˚C, washed three times with PBS-T, incubated in the secondary antibody diluted in 2% non-fat milk in PBS-T for 1 h at room temperature, followed by three washes in 0.05% PBS-T. HRP was detected using chemiluminescent Luminata Crescendo Western HRP Substrate (Millipore) and exposed to film (Denville Scientific Inc).

2.22 GST pull down assay

GST fusion proteins were bound to glutathione agarose (GST) beads (Sigma Aldrich) in Triton X-100 Lysis Buffer (10mM Tris pH 7.4, 150mM NaCl, 1% Triton X-100, 10ug/ml PMSF with complete protease inhibitor cocktail) (Roche Applied Science) tumbling for 2 h at 4˚C. GST beads were washed three times with lysis buffer, one time with 1X PBS and re-suspended in a 1X PBS slurry supplemented with complete protease inhibitor cocktail. His-tagged fusion proteins or cell lysates were incubated with the GST bound fusion proteins for either 2 h or overnight, tumbling at 4˚C. GST beads were

washed four times with lysis buffer and one time with 1X PBS, re-suspended in 5X Laemmli buffer and resolved by SDS-Page.

2.23 CAP-binding Assay

Cells were lysed in Buffer A (50 mM Tris-HCl pH 7.4, 100 mM NaCl, 1 mM EDTA, and complete protease inhibitors supplemented with 0.5% NP-40). Five percent of cell lysate was keep for input with the remaining cell lysate incubated for 2 h at 4˚C with 30 µL of the mRNA cap analog m^7GTP-Sepharose (GE Healthcare) in buffer A. The m^7GTP-Sepharose-bound proteins were washed three times with buffer A, once with 1X PBS with cap-bound proteins eluted with 5X Laemmli buffer, resolved by SDS-PAGE and revealed by Western Blotting.

2.24 Mass Spectrometry

Three 15 cm plates of both HeLa scramble and PRMT6 shRNA stable cell lines were grown to eighty percent confluence. Cells were pelleted and lysed in 1 mL of RIPA lysis buffer rotating at 4˚C for thirty minutes with lysate cleared of debris by centrifugation at 16000 g for fifteen minutes. DDX3 was immunoprecipitated from both the scramble and PRMT6 shRNA lysates using 6 µg of DDX3 antibody. Two hundred microliters of 50:50 slurry of protein A sepharose slurry was added to the lysate and it was incubated overnight rotating at 4˚C. Protein A sepharose beads were washed three times with 1 mL of RIPA lysis buffer and one time with 1 mL of PBS, rotating for 5 min at 4˚C for each wash. Beads were centrifuged at 1300 g to collect the beads. Samples were re-suspended in 5X Laemmlli and boiled for 8 minutes at 100˚C. Samples were then run on an 8% SDS-PAGE gel. Post gel electrophoresis, the gel was washed three times

for 5 minutes in Milli-Q water. The gel was then stained for one hour with Simply Blue Self Stain, destained for one hour with Milli-Q water, and further destained in Milli-Q water overnight. Post destaining, the protein bands corresponding to DDX3 from both the scramble and PRMT6 shRNA cell lines were excised and stored in 1% acetic acid at 4˚C. Proteins were digested in-gel using chymotrypsin and extracted in 5% formic acid and 50% acetonitrile. The resulting peptide extracts were concentrated by vacufuge and re-suspended in 0.1% formic acid. Peptides were analysed by liquid chromatography tandem mass spectrometry on an UltiMate 3000 RSLC nano HPLC and an LTQ Orbitrap XL hybrid mass spectrometer with nanospray ionization source. Mass spectrometry was performed at the Ottawa Hospital Research Institute Proteomics Core Facility. MASCOT software version 2.4 was used to infer peptide and protein identities from the mass spectra.

2.25 Statistical Analysis

Statistical analysis was performed using a Student T-test, one way analysis of variance (ANOVA), or a two way ANOVA using a confidence interval of 95% or 99%.

Chapter 3: Protein Arginine Methyltransferase 1 Isoform 2 Promotes Breast Cancer Cell Survival and Invasiveness

(Work from this chapter of the dissertation was published in Cell Cycle (2012) 11:24 1-16. *Alternatively spliced protein arginine methyltransferase 1 isoform PRMT1v2 promotes the survival and invasiveness of breast cancer cells*. My contribution to this publication included the work presented in Figures 1, 2, 3, 4, 5(f, g), 6, and 7(c, d) of the manuscript.)

PRMT1 has been implicated in the development of numerous cancers including breast cancer (Goulet et al., 2007; Mathioudaki et al., 2011; Mathioudaki et al., 2008; Papadokostopoulou et al., 2009; Yoshimatsu et al., 2011). Alternative splicing of the N-terminal portion of PRMT 1 yields seven distinct isoforms which possess distinct cellular localization and *in vitro* substrate specificity (Goulet et al., 2007). Therefore, it can be hypothesized that each isoform is functionally distinct. PRMT1 isoform 2 (PRMT1v2), the only isoform which contains exon 2 in its translated sequence is the only isoform with predominantly cytoplasmic cellular localization, and its mRNA and protein levels are over-expressed in a panel of breast cancer cells to a higher extent than the other isoforms (Goulet et al., 2007). Therefore, it is important to elucidate the function PRMT1v2 may perform in the development and/or progression of breast cancer.

3.1 Characterization of a PRMT1v2 Specific Antibody

A PRMT1v2 specific polyclonal antibody was raised against the peptide sequence of exon 2 (Figure 3.1A). Via western blot, the PRMT1v2 specific antibody detected His-tagged PRMT1v2 purified protein, but did not detect His-tagged PRMT1v1 or PRMT1v3

purified proteins, which do not contain exon 2 (Figure 3.1B). Compared to a pan-PRMT1 antibody raised against the C-terminus of the protein (Cote, Boisvert et al. 2003), which recognizes two bands in MCF7 cell lysate for PRMT1, a lower band corresponding to 40.5 kDa for PRMT1v1 and an upper band corresponding to 42.5 kDa for PRMT1v2; the PRMT1v2 specific antibody only recognizes the upper band at 42.5 kDa (Figure 3.1C). Moreover, the specificity of the PRMT1v2 antibody was confirmed using RNA interference. MCF7 cells were mock transfected, transfected with a non-silencing siRNA, or co-transfected with si/shRNA targeting PRMT1v2. The PRMT1v2 siRNA and shRNA target the same sequence within exon 2 of PRMT1v2 (Figure 3.2A). This methodology was employed as transfection with either the PRMT1v2 siRNA or shRNA did not efficiently deplete PRMT1v2 levels. Efficient depletion of PRMT1v2 mRNA (Figure 3.2B) and protein (Figure 3.2C) levels in MCF7 cells was observed over the 72 h time period examined. PRMT1v1 mRNA and protein levels were not decreased upon PRMT1v2 depletion. Similar results were observed for PRMT1v2 depletion at the mRNA (Figure 3.2D) and protein (Figure 3.2E) level in T-47D cells and at the protein levels in Hs578T (Figure 3.2F) and MDA MB 231 (Figure 3.2G) cells.

Previous experimental data showed that PRMT1v2 proteins levels were over-expressed in a panel of breast cancer cells relative to mammary epithelial cells (Goulet et al., 2007). This result was observed using the pan-PRMT1 C-terminal antibody, and now subsequently confirmed using the PRMT1v2 specific antibody. In comparison to immortalized, normal mammary epithelial MCF10A cells, the protein expression of PRMT1v2 is elevated in all the breast cancer cell lines investigated (Figure 3.3A). Densitometry analysis shows between a two-fold and six-fold increase for PRMT1v2

3.1A)

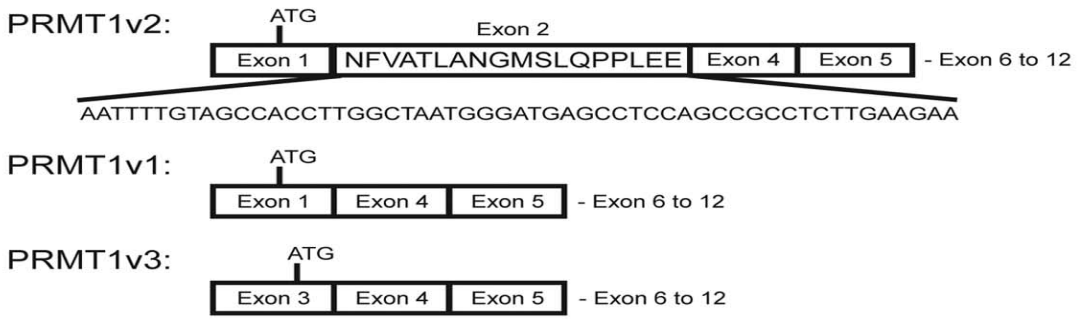
PRMT1v2:
ATG
Exon 2
Exon 1
NFVATLANGMSLQPPLEE
Exon 4
Exon 5
- Exon 6 to 12
AATTTTGTAGCCACCTTGGCTAATGGGATGAGCCTCCAGCCGCCTCTTGAAGAA
PRMT1v1:
ATG
Exon 1
Exon 4
Exon 5
- Exon 6 to 12
PRMT1v3:
ATG
Exon 3
Exon 4
Exon 5
- Exon 6 to 12

B)

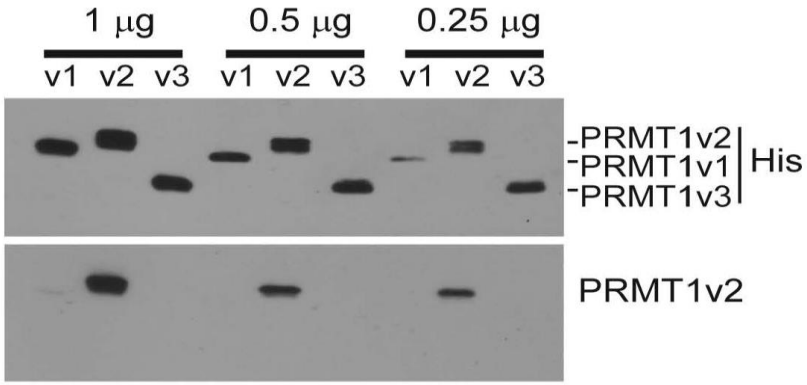
1 μg
0.5 μg
0.25 μg
v1 v2 v3 v1 v2 v3 v1 v2 v3
-PRMT1v2
-PRMT1v1
-PRMT1v3
His
PRMT1v2

C)

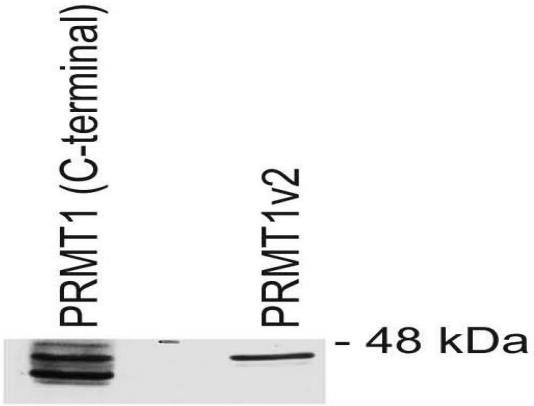
PRMT1 (C-terminal)
PRMT1v2
- 48 kDa

Figure 3.1: Characterization of PRMT1v2 Specific Antibody

(A)Schematic of PRMT1v2, PRMT1v1, and PRMT1v3. The PRMT1v2 specific antibody was raised against the peptide sequence of exon 2. (B) Western blot analysis of purified His-tagged PRMT1v1, PRMT1v2, and PRMT1v3 proteins. The His antibody recognizes all three His-tagged PRMT1 isoforms (top panel), while the PRMT1v2 specific antibody only recognizes His-tagged PRMT1v2 (bottom panel). (C) Western blot analysis of MCF7 lysate using a pan-PRMT1 antibody against the C-terminus of PRMT1 (lane 1) and the PRMT1v2 specific antibody (lane 2). The pan-PRMT1 antibody recognizes a lower band corresponding to 40.5 kDa for PRMT1v1 and an upper band corresponding to 42.5 kDa for PRMT1v2, while the PRMT1v2 specific band only recognizes the 42.5 kDa band for PRMT1v2.

3.2A)

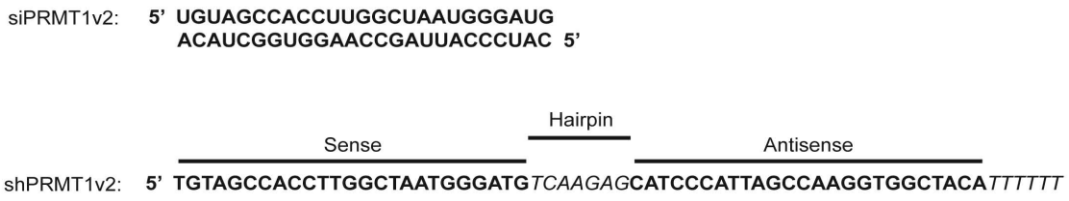
siPRMT1v2: 5' UGUAGCCACCUUGGCUAAUGGGAUG
ACAUCGGUGGAACCGAUUACCCUAC 5'
Hairpin
Sense
Antisense
shPRMT1v2: 5' TGTAGCCACCTTGGCTAATGGGATGTCAAGAGCATCCCATTAGCCAAGGTGGCTACATTTTTT

B)

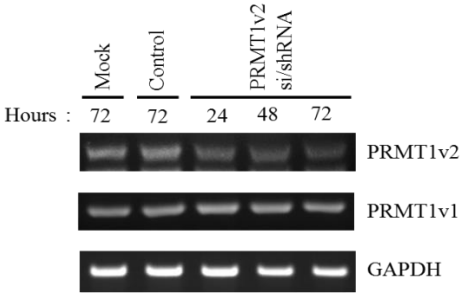
Mock
Control
PRMT1v2 si/shRNA
Hours : 72 72 24 48 72
PRMT1v2
PRMT1v1
GAPDH

C)

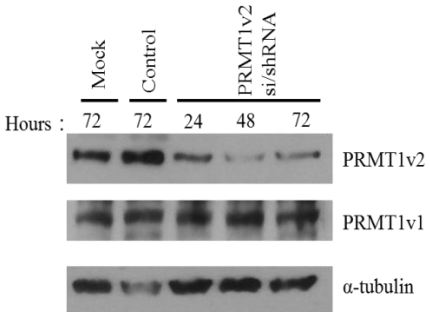
Mock
Control
PRMT1v2 si/shRNA
Hours : 72 72 24 48 72
PRMT1v2
PRMT1v1
α-tubulin

D)

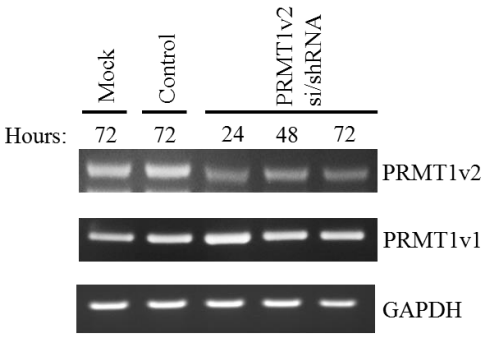
Mock
Control
PRMT1v2 si/shRNA
Hours: 72 72 24 48 72
PRMT1v2
PRMT1v1
GAPDH

E)

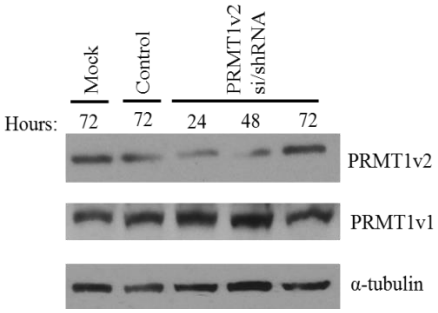
Mock
Control
PRMT1v2 si/shRNA
Hours: 72 72 24 48 72
PRMT1v2
PRMT1v1
α-tubulin

F)

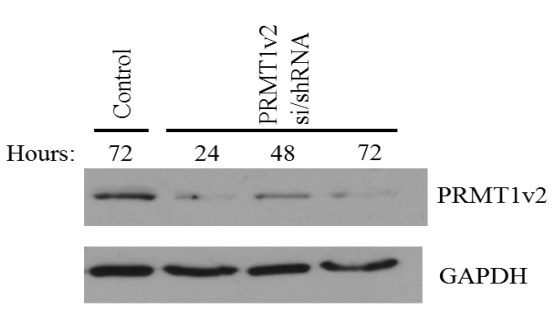
Control
PRMT1v2 si/shRNA
Hours: 72 24 48 72
PRMT1v2
GAPDH

G)

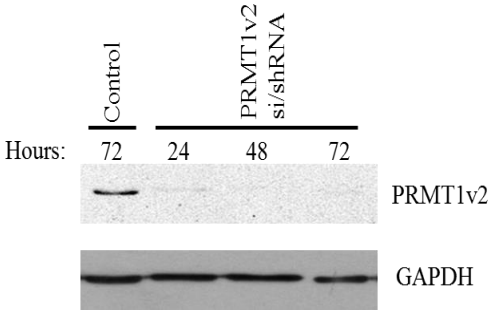
Control
PRMT1v2 si/shRNA
Hours: 72 24 48 72
PRMT1v2
GAPDH

Figure 3.2: Depletion of PRMT1v2 mRNA and Protein Levels by RNA Interference

(A) PRMT1v2 siRNA and shRNA targeting sequence. Total RNA was collected from MCF7 and T-47D cells transfected with PRMT1v2 si/shRNA at 24, 48, and 72 h post-transfection and at 72 h for mock transfected and control siRNA (control) transfected cells. PCR analysis of cDNA generated from total RNA with PRMT1 primers shows a depletion of PRMT1v2 mRNA in (B) MCF7 and (D) T-47D cells. No depletion of PRMT1v1 was observed upon PRMT1v2 depletion. GAPDH was used as a loading control. Total protein was collected from cells transfected with PRMT1v2 si/shRNA at 24, 48, and 72 h post-transfection and at 72 h for mock transfected and control siRNA (control) transfected cells. Western blot analysis of protein lysate with the PRMT1v2 antibody reveals a depletion of PRMT1v2 protein levels in (C) MCF7, (E) T-47D, (F) MDA MB 231 (G) Hs578T cells. No depletion of PRMT1v1 was observed upon PRMT1v2 depletion in (B) MCF7 and (D) T-47D cells, determined using the pan-PRMT1 antibody. GAPDH or α-tubulin was used as loading controls.

3.3A)

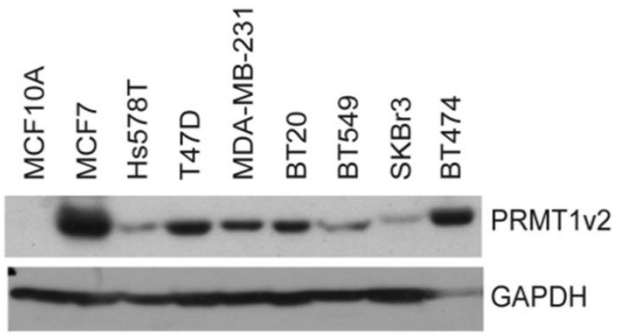
MCF10A
MCF7
Hs578T
T47D
MDA-MB-231
BT20
BT549
SKBr3
BT474
PRMT1v2
GAPDH

B)

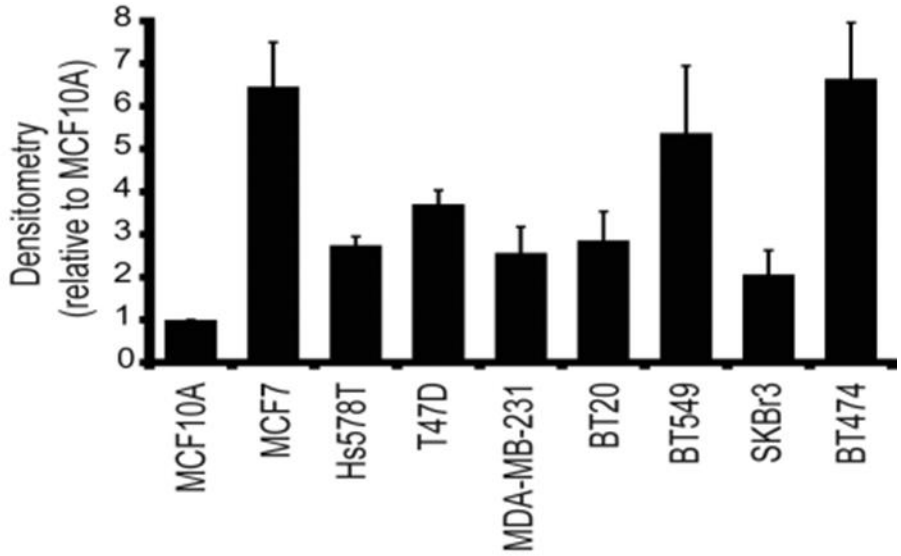
Densitometry
(relative to MCF10A)
0
1
2
3
4
5
6
7
8
MCF10A
MCF7
Hs578T
T47D
MDA-MB-231
BT20
BT549
SKBr3
BT474

Figure 3.3: PRMT1v2 Protein Levels are Increased in a Panel of Breast Cancer Cells

(A) Protein lysate was collected from different breast cancer cell lines. Western Blot analysis using the PRMT1v2 antibody shows elevated PRMT1v2 protein levels in all breast cancer cells examined in comparison to protein levels in MCF10A cells (top panel). GAPDH was used as a loading control (bottom panel). (B) Densitometry analysis was performed by normalizing PRMT1v2 protein levels to those of GAPDH. Relative to MCF10A cells, a two-fold to six-fold increase in PRMT1v2 protein levels was observed. Data represents the average +/- the standard error for three independent experiments.

protein levels in the breast cancer cell lines studied compared to the MCF10A cells (Figure 3.3B).

3.2 PRMT1v2 Depletion Affects Breast Cancer Cell Growth and Viability

To assess the effect of PRMT1v2 depletion on breast cancer cell growth and viability, MCF7, T-47D, and Hs578T were transfected with PRMT1v2 si/shRNA and assessed 24, 48, 72 h post-transfection. PRMT1v2 depletion resulted in a significant decrease in viable cells measured using the Trypan Blue Exclusion Assay in MCF7 (Figure 3.4A), T-47D (Figure 3.4B) and Hs578T (Figure 3.4C). In MCF7 cells, a 40% decrease in cell viability was observed 72 h post PRMT1v2 depletion, while in T-47D cells, a 35% to 40% decrease in viability was observed 48 h to 72 h post depletion. In Hs578T cells, a 60% decrease in viability was observed 48 h post-transfection. The results for all three cell lines examined, MCF7, T-47D and Hs578T were statistically significant in comparison to cells transfected with a non-silencing siRNA control as measured using a Student T Test with a 95% confidence interval.

Subsequently, the effect of PRMT1v2 depletion on cell growth over time was measured using an MTT assay. PRMT1v2 depletion resulted in a statistically significant decrease in cell growth 48 and 72 h post PRMT1v2 knockdown in MCF7 (Figure 3.5A), T-47D (Figure 3.5B), and Hs578T (Figure 3.5C) cell lines. In additional to a statistically significant decrease at 48 and 72 h, a statistically significant decrease in cell growth was observed 24 h post PRMT1v2 knockdown in MDA MB 231 cells (Figure 3.5D). To confirm that the decrease in cell growth was not due to transfection of a PRMT1v2 siRNA and shRNA combination, MCF7 cells were transfected with a non-silencing

3.4A)

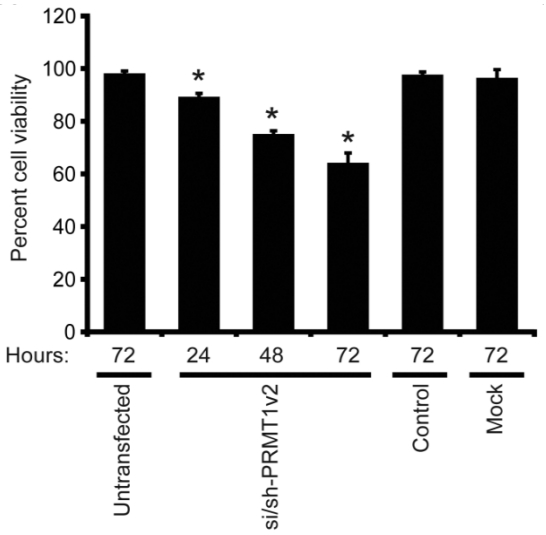
Percent cell viability
120
100
80
60
40
20
0
*
*
*
Hours:
72
24
48
72
72
72
Untransfected
si/sh-PRMT1v2
Control
Mock

B)

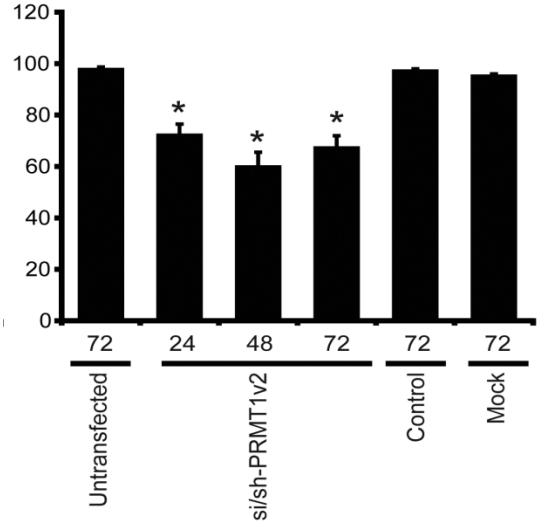
120
100
80
60
40
20
0
*
*
*
72
24
48
72
72
72
Untransfected
si/sh-PRMT1v2
Control
Mock

C)

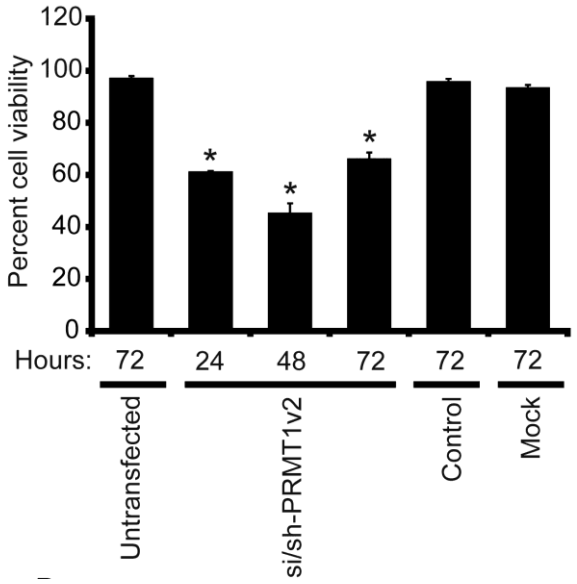
Percent cell viability
120
100
80
60
40
20
0
*
*
*
Hours:
72
24
48
72
72
72
Untransfected
si/sh-PRMT1v2
Control
Mock

Figure 3.4: Depletion of PRMT1v2 Affects Breast Cancer Cell Viability

(A) MCF7, (B) T-47D, or (C) Hs578T cells were transfected with PRMT1v2 si/shRNA for 24, 48, and 72 h, mock transfected for 72 h or transfected with a control siRNA (control) for 72 h. Adherent and non-adherent cells were collected and stained with Trypan Blue. 200 cells were counted and the percentage of viable cells (non-Trypan Blue stained cells) were counted. PRMT1v2 depletion results in a decrease in cell viability in all three cell lines examined. Data represents the average +/- the standard error of the mean for three independent experiments. * denotes statistical significance at $p<0.05$ determined using a Student T-test.

3.5A)

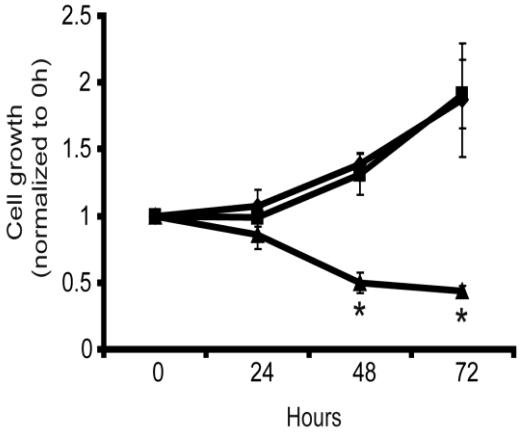
Cell growth
(normalized to 0h)
2.5
2
1.5
1
0.5
0
0
24
48
72
Hours
*
*

B)

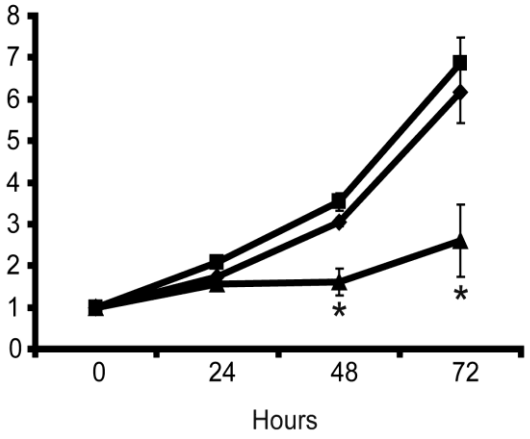
8
7
6
5
4
3
2
1
0
0
24
48
72
Hours
*
*

C)

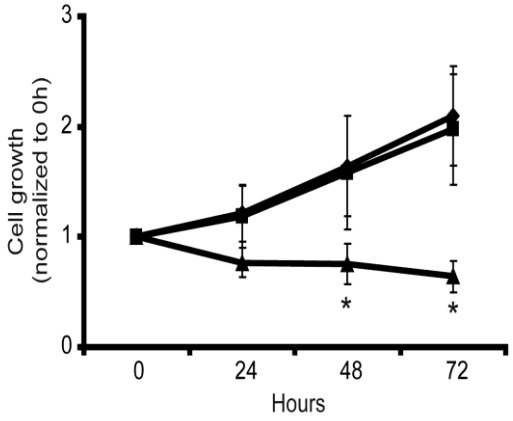
Cell growth
(normalized to 0h)
3
2
1
0
0
24
48
72
Hours
*
*

D)

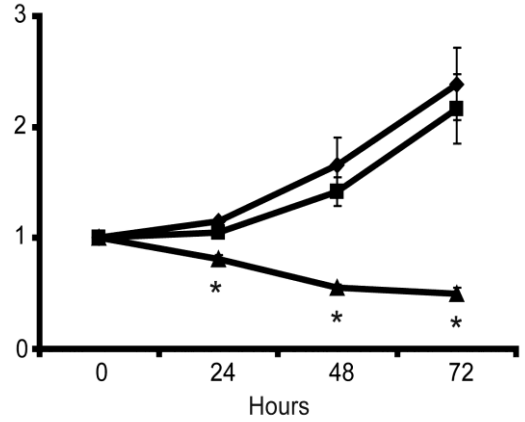
3
2
1
0
0
24
48
72
Hours
*
*
*

E)

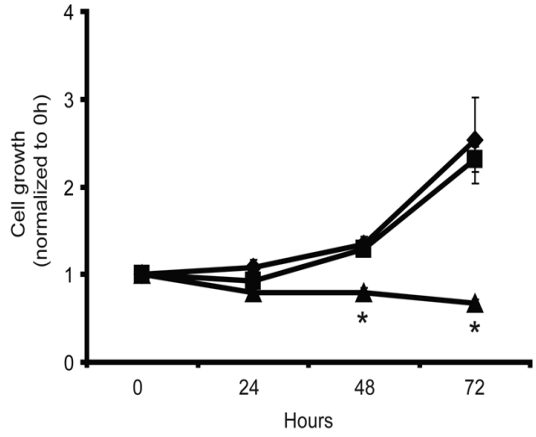
Cell growth
(normalized to 0h)
4
3
2
1
0
0
24
48
72
Hours
*
*

Figure 3.5: Depletion of PRMT1v2 affects Breast Cancer Cell Growth

(A) MCF7, (B) T-47D, (C) Hs578T, or (D) MDA MB 231 cells were plated at equal numbers and mock (♦), control (■) or PRMT1v2 si/shRNA (▲) transfected were assessed by MTT assay at 0, 24, 48, and 72 h post-transfection. (E) MCF7 cells were plated at equal numbers and mock (♦), control si/shRNA (■) or PRMT1v2 si/shRNA (▲) transfected and assessed by MTT assay at 0, 24, 48, and 72 h post-transfection. PRMT1v2 depletion results in a decrease in cell growth. Data are the mean of three independent experiments with six replicates per experiment. * denotes statistical significance determined using a Student T-test ($p<0.05$).

siRNA in tandem with a non-silencing shRNA. Transfection of this combination did not result in a decrease in cell growth compared to mock transfected cells (Figure 3.5E). Additionally, PRMT1v2 depletion results in an increase in the number of rounded cells and cells exhibiting membrane blebbing (MCF7 (Figure 3.6A), T-47D (Figure 3.6B), Hs578T (Figure 3.6C), MDA MB 231 (Figure 3.6D)); morphologies consistent with an increase in cell death.

3.3 Depletion of PRMT1v2 Induces Apoptosis

To determine if PRMT1v2 depletion resulted in increased cell death, flow cytometry was performed. MCF7 and T-47D cells were used for this analysis. Cells were stained with propidium iodide to measure the phase in the cell cycle in which the cells were present. PRMT1v2 depletion resulted in an increase in the percentage of cells exhibiting an increased sub-G_1 cell cycle profile in both MCF7 and T-47D cell lines, a phenotype often indicative of apoptotic cell death. In MCF7 cells, 24.5% of cells exhibited an increased sub-G_1 profile 24 h post PRMT1v2 depletion, 19.4% 48 h post depletion, and 15.7% 72 h post depletion. Contrarily, in cells transfected with the non-silencing control, 4.1%, 4%, and 5.5% of cells exhibited a sub-G1 profile 24 h, 48 h, and 72 h post transfection, while in mock transfected (control) cells, 3.9%, 3.6%, and 4.2% of cells exhibited a sub-G_1 profile 24, 48, and 72 h post-transfection, respectively (Figure 3.7A & 3.7B). The sub-G_1 percent of cells was statistically significant relative to the non-silencing control siRNA results at 24 h and 48 h post PRMT1v2 depletion, determined using a Student T test with a 95% confidence interval. In T-47D cells, 13.3% of cells exhibited an increased sub-G_1 profile 24 h post PRMT1v2 depletion, 15.2% 48 h post depletion, and 13.2% 72 h post depletion. This contrasts with 1.7%, 1.8%, and 1.1% of

3.6A)

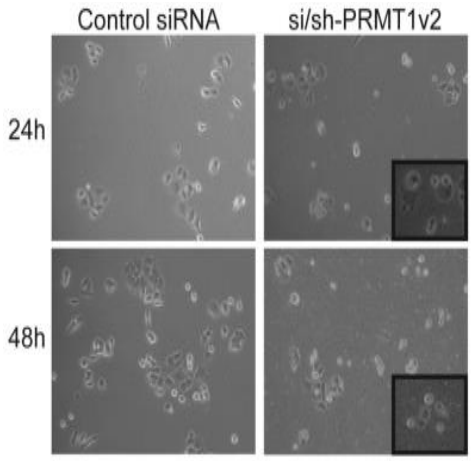
Control siRNA
si/sh-PRMT1v2
24h
48h

B)

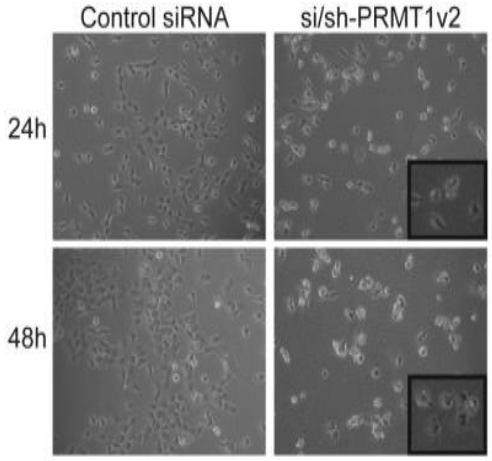
Control siRNA
si/sh-PRMT1v2
24h
48h

C)

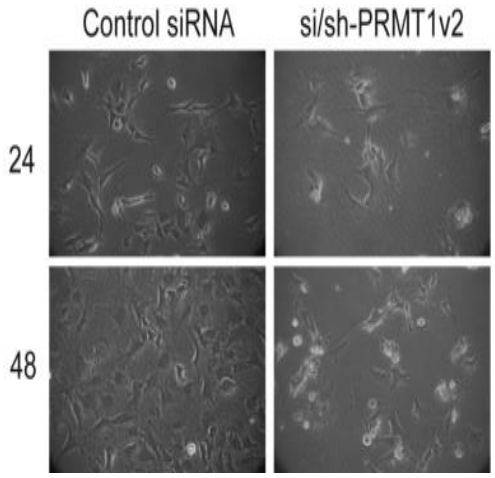
Control siRNA
si/sh-PRMT1v2
24
48

D)

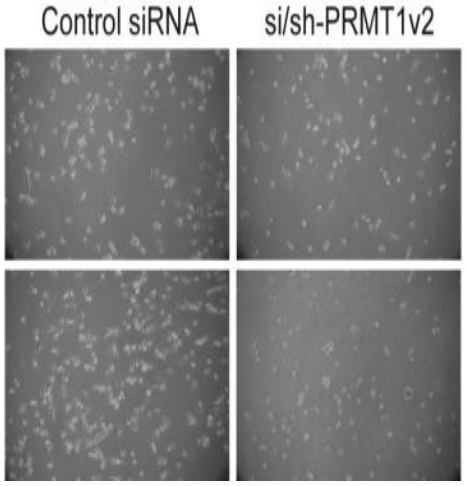
Control siRNA
si/sh-PRMT1v2

Figure 3.6: Depletion of PRMT1v2 Increases Membrane Blebbing and the Number of Rounded Cells

Morphology of (A) MCF7, (B) T-47D, (C) Hs578T, (D) MDA MB 231 cells upon transfection with control siRNA or PRMT1v2 si/shRNA 24 and 48 h post-transfection. Images were taken at 20X magnification with insets focused on an area in the field of view.

3.7A)

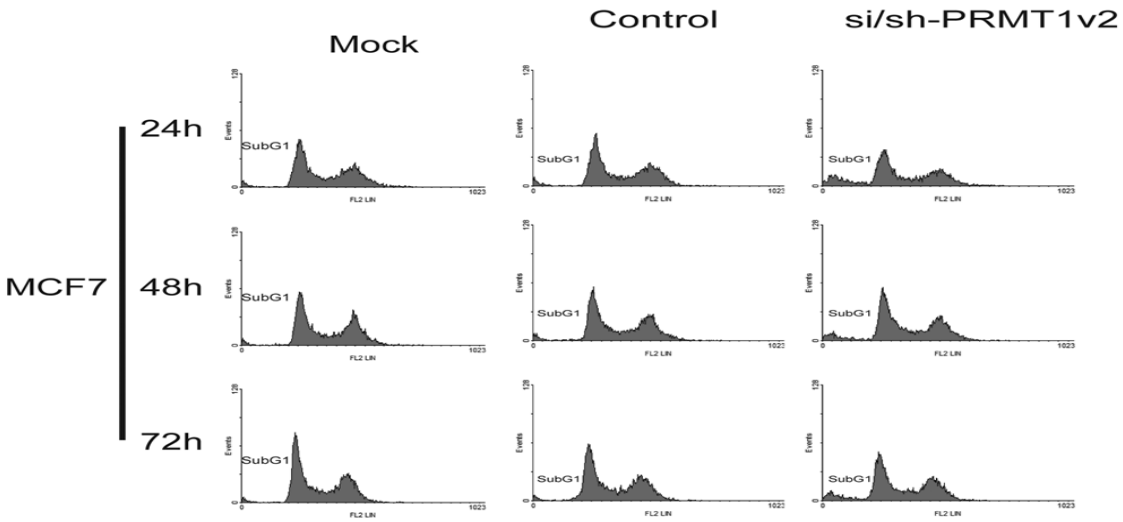
Mock
Control
si/sh-PRMT1v2
MCF7
24h
48h
72h
SubG1
Events
FL2 LIN

B)

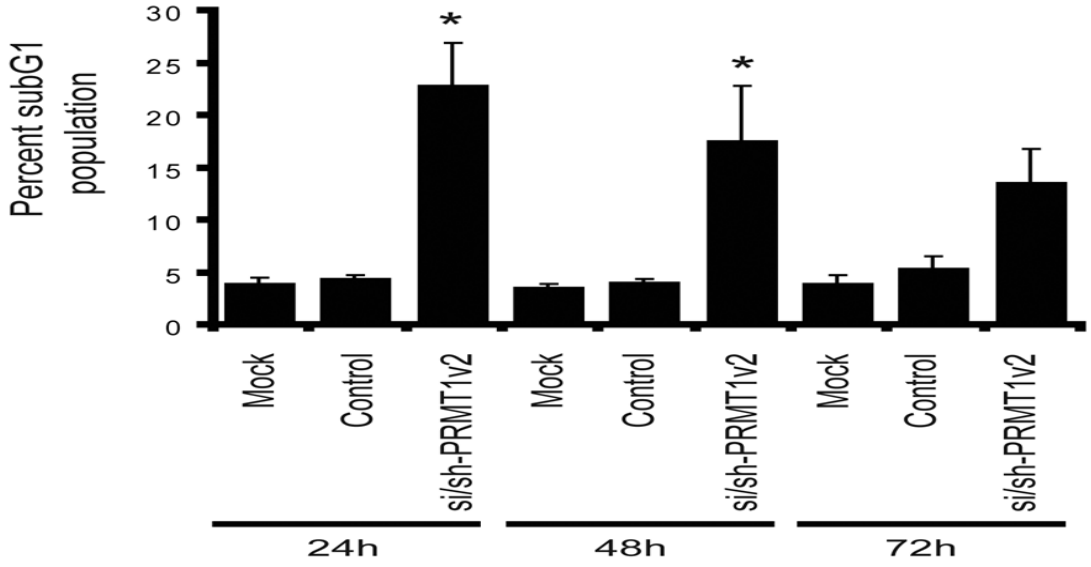
Percent subG1 population
30
25
20
15
10
5
0
*
*
Mock
Control
si/sh-PRMT1v2
24h
48h
72h

Figure 3.7: Depletion of PRMT1v2 Increases the Sub-G_1 Cell Cycle Profile in MCF7 Cells

(A) Representative flow cytometry analyses of propidium iodide (PI)-stained MCF7 cells following mock, control siRNA, and PRMT1v2 si/shRNA transfection at 24, 48, and 72 h. (B) Percentage of sub-G_1 population for MCF7 cells. Data are the mean +/- standard error of five independent experiments. * denotes statistically significance ($p<0.05$).

cells 24 h, 48 h, and 72 h, respectively, in non-silencing control siRNA transfected cells and 2.1%, 2.4%, and 1.1% in mock transfected (control) cells (Figure 3.8A & 3.8B). Similarly to MCF7 cells, a statistically significant difference in the sub-G_1 profile was observed between cells transfected with a non-silencing control siRNA and cells transfected with PRMT1v2 si/shRNA at 24 h and 48 h post-transfection.

To confirm that the observed increase in the percentage of sub-G_1 cells upon PRMT1v2 depletion was due to apoptosis, annexin V staining of cells was performed, with detection of annexin V by flow cytometry. Annexin V binds to phosphatidylserine which is located in the inner layer of the cell membrane, which translocates upon the induction of apoptosis (Martin et al., 1995). This phenotype is an early marker of apoptosis. Co-staining was performed with propidium iodide to differentiate between apoptotic staining with annexin V and necrosis with propidium iodide. Annexin V staining was assessed 24 h post PRMT1v2 depletion in MCF7 and T-47D cells, as at this time point the most efficient depletion in PRMT1v2 protein expression was observed. The green fluorescence gate (annexin V) for flow cytometry was set using MCF7 GFP stably-expressing cells, while the red fluorescence gate (propidium iodide) was set using MCF7 cells stained with propidium iodide (Figure 3.9A). In MCF7 cells transfected with a control siRNA, 97.6% +/- 1.1% of cells were unstained while 2.34% +/- 1.1% were stained with annexin V, while in mock transfected (control) cells, 97.6% +/- 1.2% of cells were unstained and 2.43% +/- 1.2% of cells were stained with annexin V. In contrast, in cells depleted of PRMT1v2, 81.2% +/- 2.1% of cells were unstained, 14.2% +/- 2.0% of cells were stained with annexin V and 4.62% +/- 0.11% of cells were co-stained with both annexin V and propodium iodide (Figure 3.9B). In T-47D cells, 97.3% +/- 1.2% of

3.8A)

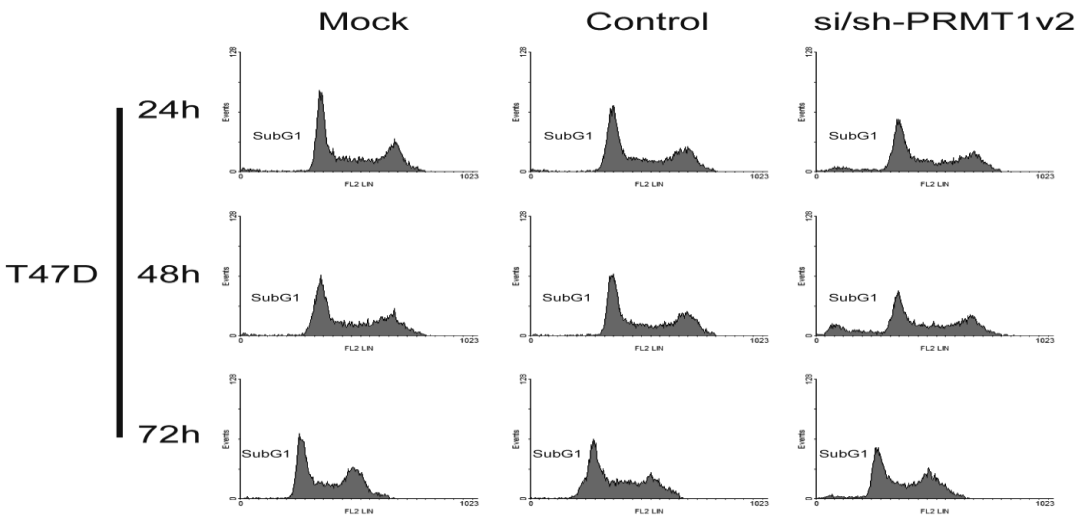
Mock
Control
si/sh-PRMT1v2
T47D
24h
48h
72h
SubG1
Events
FL2 LIN

B)

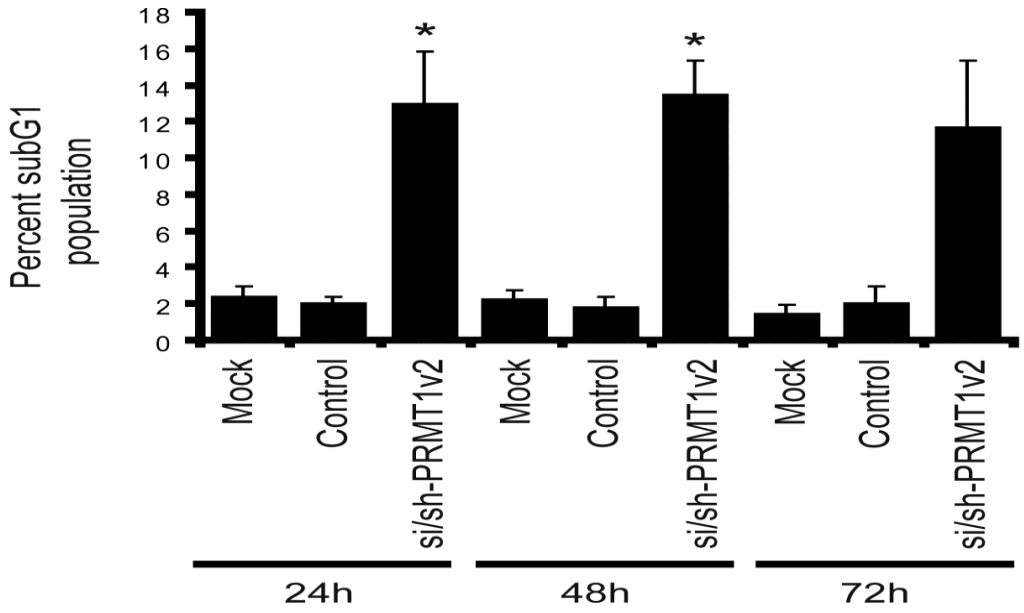
Percent subG1 population
0
2
4
6
8
10
12
14
16
18
*
*
Mock
Control
si/sh-PRMT1v2
24h
48h
72h

Figure 3.8: Depletion of PRMT1v2 Increases the Sub-G_1 Cell Cycle Profile in T-47D Cells

(A) Representative flow cytometry analyses of propidium iodide (PI)-stained T-47D cells following mock, control siRNA, and PRMT1v2 si/shRNA transfection at 24, 48, and 72 h. (B) Percentage of sub-G_1 population for T-47D cells. Data are the mean +/- standard error of four independent experiments. * denotes statistically significance ($p<0.05$).

3.9A)

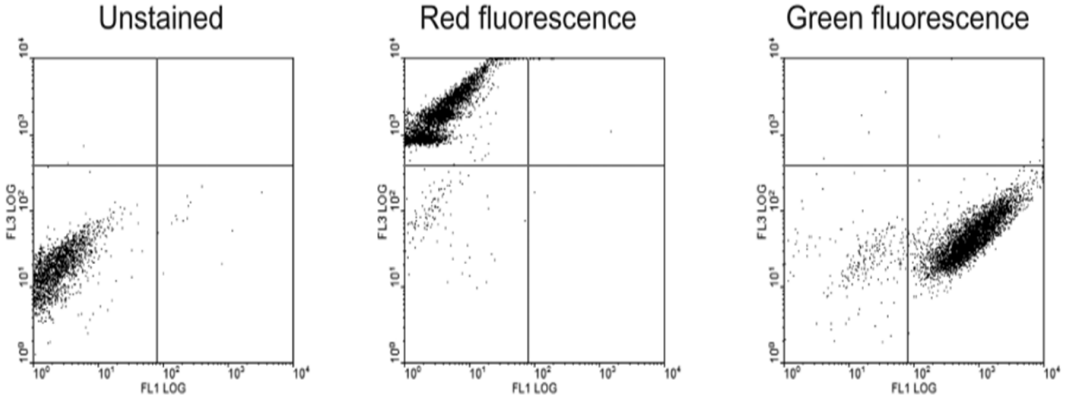
Unstained
Red fluorescence
Green fluorescence
FL3 LOG
FL1 LOG

B)

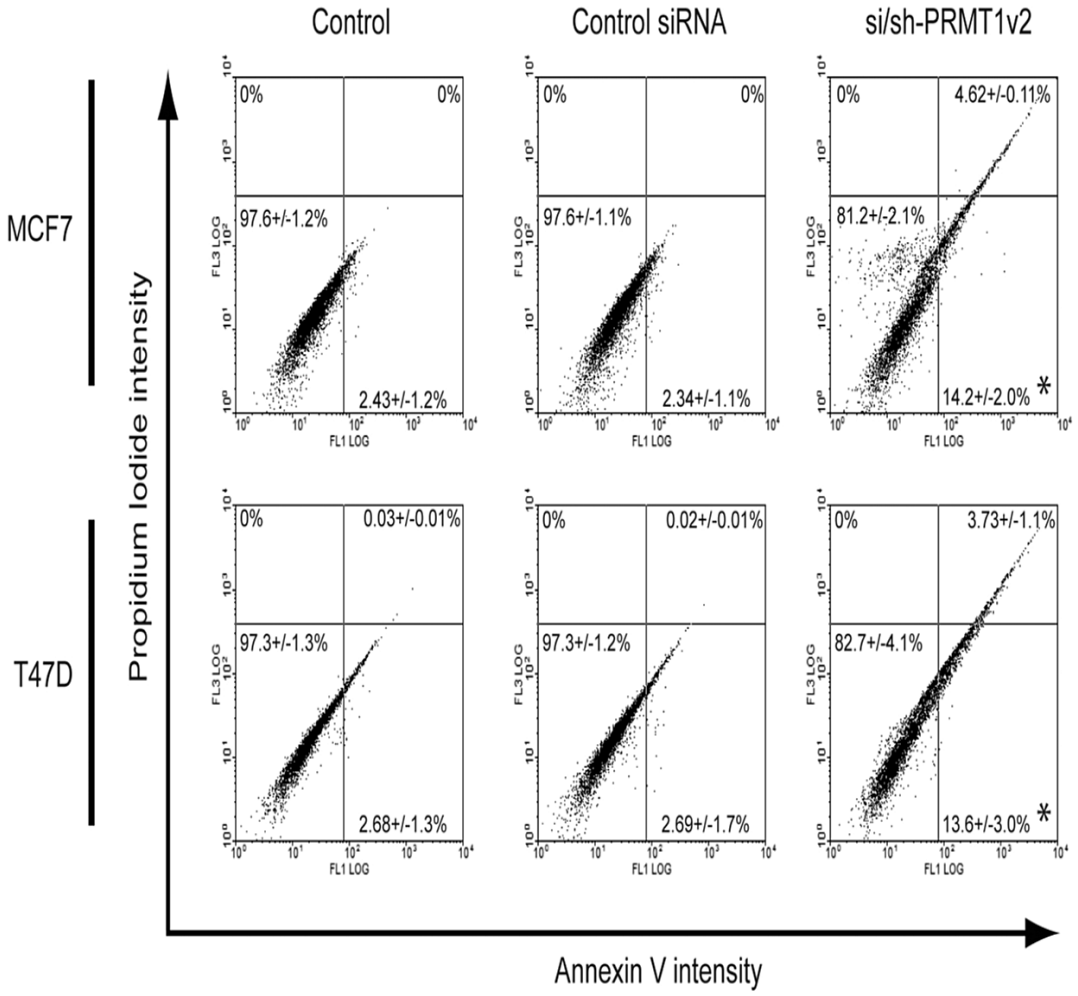
Control
Control siRNA
si/sh-PRMT1v2
MCF7
T47D
Propidium Iodide intensity
Annexin V intensity
FL3 LOG
FL1 LOG
0%
0%
97.6+/-1.2%
2.43+/-1.2%
0%
0%
97.6+/-1.1%
2.34+/-1.1%
0%
4.62+/-0.11%
81.2+/-2.1%
14.2+/-2.0%
*
0%
0.03+/-0.01%
97.3+/-1.3%
2.68+/-1.3%
0%
0.02+/-0.01%
97.3+/-1.2%
2.69+/-1.7%
0%
3.73+/-1.1%
82.7+/-4.1%
13.6+/-3.0%
*

Figure 3.9: Depletion of PRMT1v2 Induces Apoptosis

(A) Controls for annexin V and propidium iodide co-staining experiments for apoptosis. MCF7 unstained cells, red fluorescent cells, and green fluorescent cells were used for quadrant determination for flow cytometry. (B) Representative images for MCF7 and T-47D cells mock transfected (control), transfected with a control siRNA or PRMT1v2 si/shRNA and co-stained with annexin V and propidium iodide for flow cytometry analysis. Percentages within each quadrant represent the mean +/- the standard error for three independent experiments. * denotes statistical significance ($p<0.05$).

cells were unstained with 2.69% +/- 1.7% of cells stained with annexin V in cells transfected with the control siRNA. In mock transfected (control) cells, 97.3% +/- 1.3% of cells were unstained and 2.68% +/- 1.3% of cells were stained with annexin V. In comparison, 82.7% +/- 4.1% of cells were unstained, 13.6% +/- 3.0% of cells were stained with annexin V and 3.73% +/- 1.1% of cells were co-stained with annexin V and propidium iodide in cells co-transfected with PRMT1v2 si/shRNA (Figure 3.9B). For both the MCF7 and T-47D cell lines, upon PRMT1v2 depletion there was a statistically significant increase in the percentage of cells stained with annexin V compared with control siRNA transfected cells, as determined using a Student T-test with a 95% confidence interval.

To further validate that apoptosis was occurring upon PRMT1v2 depletion, cleavage of PARP, an additional early marker of apoptosis, was assessed. Both MCF7 and T-47D cells were mock transfected, transfected with a control siRNA or transfected with a PRMT1v2 si/shRNA. Protein samples were collected 6, 12, 18, and 24 h post PRMT1v2 transfection while protein samples were collected 24 h post mock and control siRNA transfection. Upon PRMT1v2 depletion, an increase in cleaved PARP was observed 18 h post transfection in both the MCF7 (Figure 3.10A) and T-47D (Figure 3.10B) cell lines in comparison to the control siRNA transfected cells. These results demonstrated that inhibition of PRMT1v2 expression induces apoptotic cell death.

3.4 PRMT1v2 Depletion Inhibits Breast Cancer Cell Motility and Invasion

3.10A)

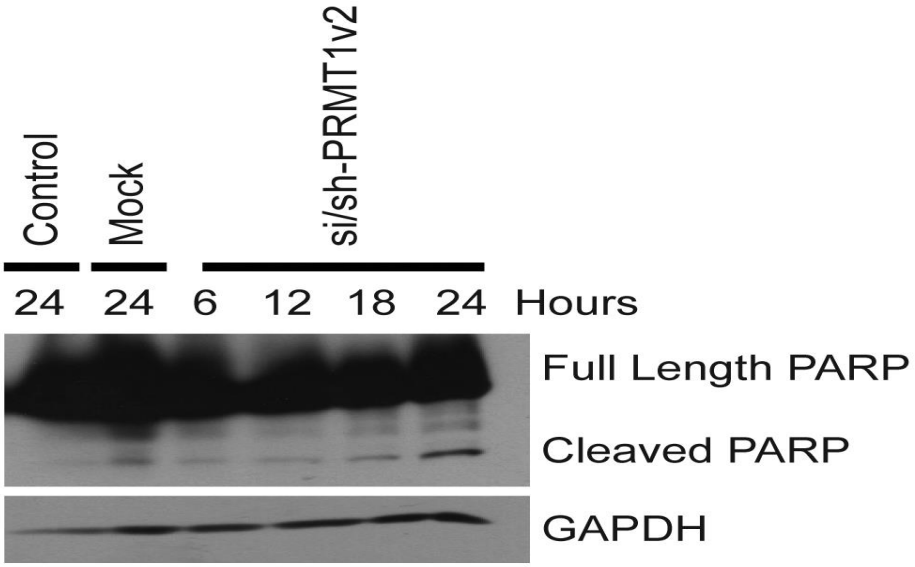
Control
Mock
si/sh-PRMT1v2
24 24 6 12 18 24 Hours
Full Length PARP
Cleaved PARP
GAPDH

B)

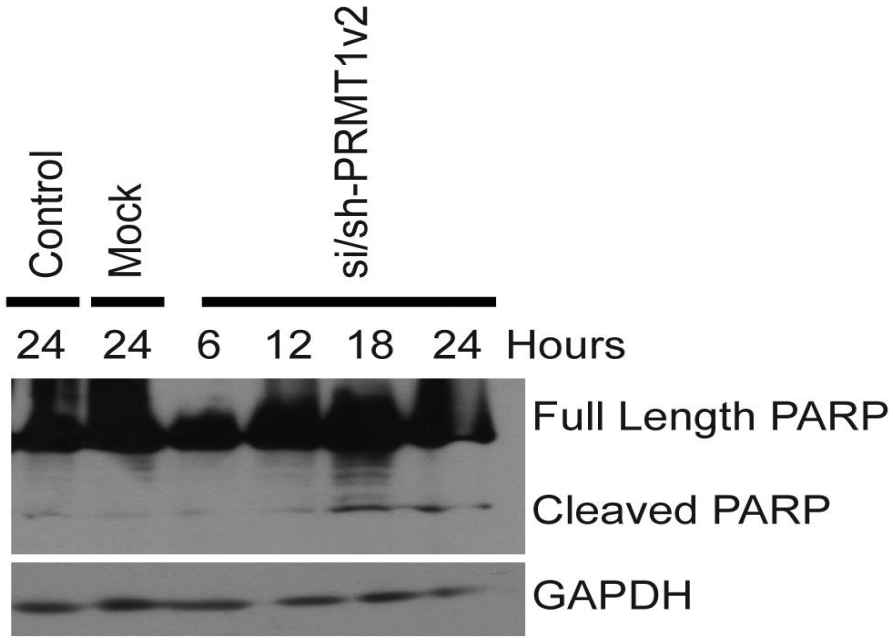
Control
Mock
si/sh-PRMT1v2
24 24 6 12 18 24 Hours
Full Length PARP
Cleaved PARP
GAPDH

Figure 3.10: Depletion of PRMT1v2 Induces PARP cleavage

A) MCF7 or (B) T-47D cells were transfected with PRMT1v2 si/shRNA for 6, 12, 18, and 24 h, and mock transfected or transfected with a control siRNA for 24 h and protein lysates were collected. Western blot analysis using an antibody for Poly-ADP ribose polymerase (PARP) shows an increase in cleaved PARP, an early marker of apoptosis. GAPDH was used as a loading control.

To examine the effect of PRMT1v2 depletion on cell line motility and invasion, the MDA MB 231 cell line, a highly invasive breast cancer cell line was utilized. Transwell chambers were employed to measure motility and invasion. Cells were placed within the top of the Transwell chamber in serum free media, with media containing a chemo-attractant (fetal bovine serum) below the chamber. Cells were allowed to migrate through the chamber for a 24 h incubation period. Following the 24 h incubation period, cells in the top of the chamber were removed, while the cells that migrated through the chamber were fixed, stained and counted (Figure 3.11A). The chambers used to measure invasion differ from the chambers utilized to measure motility as the invasion chambers contain a matrigel layer which mimics a reconstituted basement membrane *in vitro*.

Similarly as above, PRMT1v2 protein levels were reduced 24 h post transfection with the PRMT1v2 si/shRNA compared to cells mock transfected or transfected with a control siRNA (Figure 3.11B). PRMT1v1 protein levels were not decreased upon PRMT1v2 depletion. Twenty-four hours post-transfection, 50 000 mock transfected cells, control siRNA transfected cells, or cells co-transfected with the PRMT1v2 si/shRNA were incubated in the Transwell chambers to measure both the rate of motility (- matrigel layer) and invasion (+ matrigel layer). For motility, 177.6 +/- 2.5 mock transfected cells, 199.5 +/- 4.6 control siRNA transfected cells and 113.8 +/- 10.7 PRMT1v2 si/shRNA transfected cells passed through the Transwell chambers (Figure 3.11C & 3.11E). There is a statistically significant reduction in motility in the PRMT1v2 depleted cells compared to both the mock and control siRNA transfected cells, as determined using a Student T-test with a 99% confidence interval. For invasion, 84.4 +/- 8.4 mock transfected cells, 91.5 +/- 1.5 control siRNA transfected cells and 29.2 +/- 3.1 PRMT1v2

3.11A)

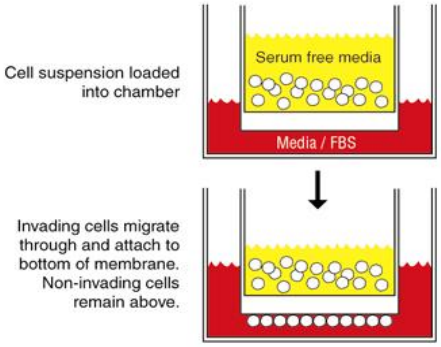
Cell suspension loaded into chamber
Serum free media
Media / FBS
Invading cells migrate through and attach to bottom of membrane. Non-invading cells remain above.

B)

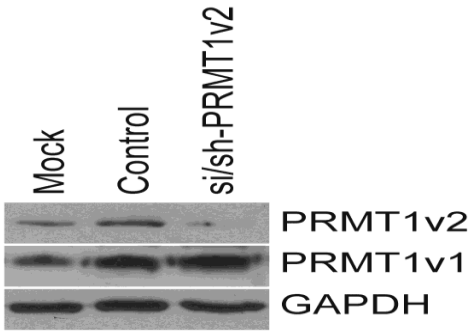
Mock
Control
si/sh-PRMT1v2
PRMT1v2
PRMT1v1
GAPDH

C)

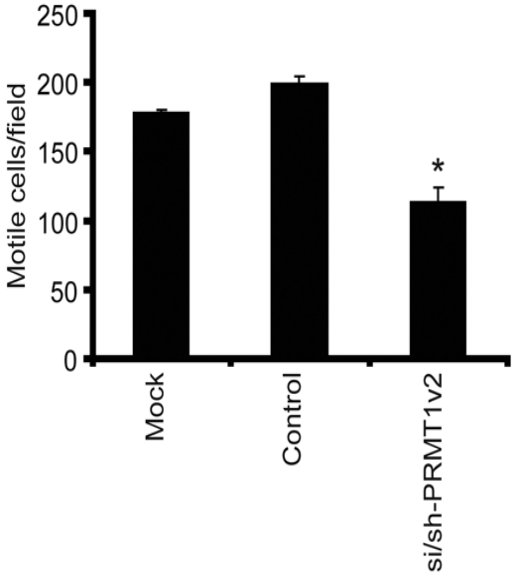
Motile cells/field
250
200
150
100
50
0
*
Mock
Control
si/sh-PRMT1v2

D)

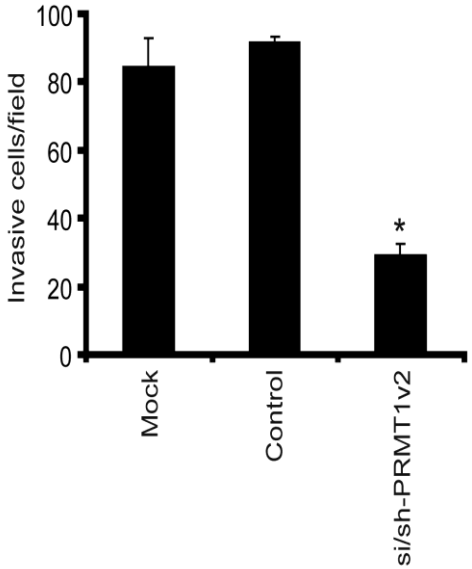
Invasive cells/field
100
80
60
40
20
0
*
Mock
Control
si/sh-PRMT1v2

E)

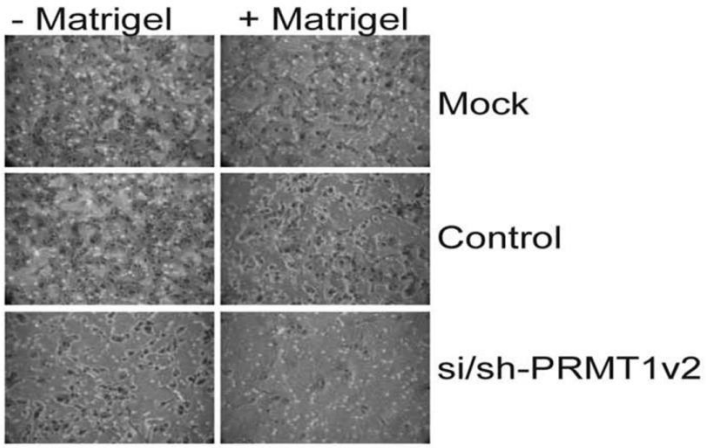
- Matrigel
+ Matrigel
Mock
Control
si/sh-PRMT1v2

Figure 3.11: Depletion of PRMT1v2 Decreases MDA MB 231 Motility and Invasion

(A) Schematic image representing a Transwell chamber. Cells are incubated in the top portion of the chamber in serum free media. Media containing fetal bovine serum, which serves as a chemoattract is placed in the bottom portion of the chamber. Cells migrate through the chamber during the incubation period and then are fixed, stained, and counted. (B) MDA MB 231 cells were mock transfected, transfected with a control siRNA or PRMT1v2 si/shRNA for 24 h and protein lysates were collected. Western blot analysis with the PRMT1v2 antibody shows a depletion of PRMT1v2 protein levels with no effect on PRMT1v1 protein levels. GAPDH serves as the loading control. 24 h post-transfection, cells were counted and incubated on Transwell chambers to measure motility or invasion for 24 h. Cells that passed through the chambers in the absence of matrigel (motility) (C) or presence of matrigel (invasion) (D) were counted. Data represents the mean +/- the standard error for three independent experiments ($p<0.05$ relative to control). (E) Photo images of cells that passed through the Transwell chambers in the absence/presence of matrigel. Images taken at 20X magnification.

depleted cells passed through the Transwell chambers (Figure 3.11D & 3.11E). Similarly to motility, there is a statistically significant reduction in the invasive potential of MDA MB 231 cells upon PRMT1v2 depletion, determined using a Student T-test with a 99% confidence interval.

3.5 Overexpression of PRMT1v2 Promotes Breast Cancer Cell Motility and Invasion

As it is impossible to measure the exact contribution that induction of apoptosis upon PRMT1v2 depletion has on the decrease in both motility and invasion in MDA MB 231 cells, the effect of PRMT1v2 overexpression on motility and invasion was assessed to corroborate the above results. MCF7 cells, which are a luminal epithelial-like breast cancer cell line considered to be weakly invasive, were utilized (Lacroix and Leclercq, 2004). Stably-expressing GFP-PRMT1v2 cell lines were established along with a GFP expressing and a GFP-PRMT1v1 expressing cell line as a control and for comparison, respectively. Expression of GFP was measured both through immunofluorescence (Figure 3.12A) and Western Blot (Figure 3.12B). Furthermore, expression of both PRMT1v1 and PRMT1v2 was measure by RT-PCR (Figure 3.12C) and Western Blot (Figure 3.12D). Localization of PRMT1v1 was predominantly nuclear while PRMT1v2 localized predominantly to the cytoplasm, consistent with previously published data (Goulet et al., 2007; Herrmann and Fackelmayer, 2009).

MCF7 expressing GFP, GFP-PRMT1v1, and GFP-PRMT1v2 cells were incubated on Transwell chambers for 72 h to measure the rate of both motility and invasion. For motility, 8.4 +/- 0.7 GFP expressing cells, 29.1 +/- 1.6 GFP-PRMT1v1

3.12A)

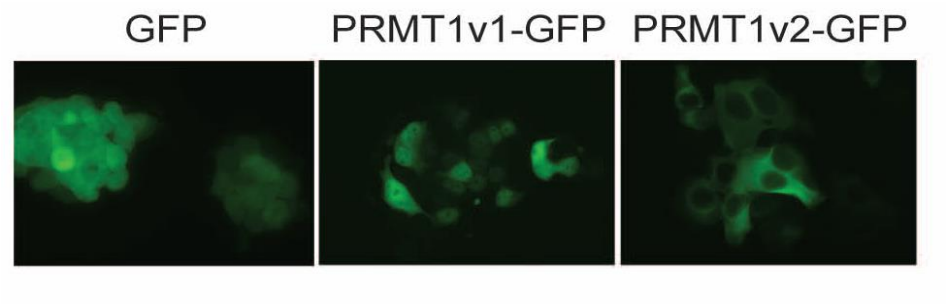
GFP
PRMT1v1-GFP
PRMT1v2-GFP

B)

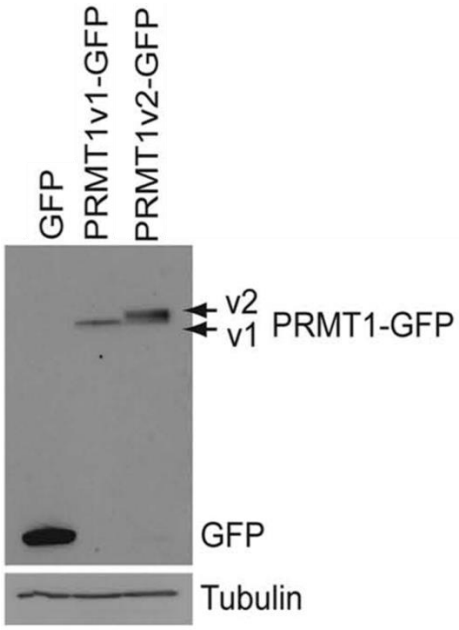
GFP
PRMT1v1-GFP
PRMT1v2-GFP
v2
v1
PRMT1-GFP
GFP
Tubulin

C)

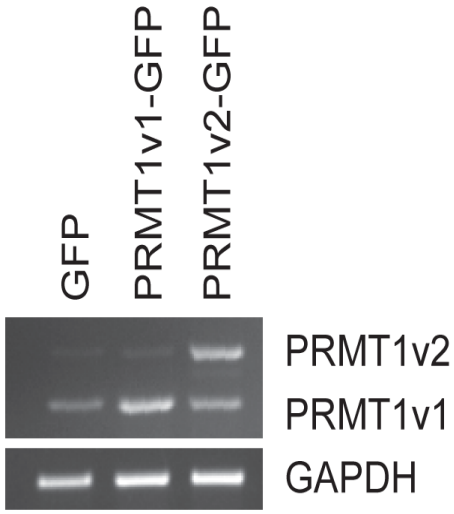
GFP
PRMT1v1-GFP
PRMT1v2-GFP
PRMT1v2
PRMT1v1
GAPDH

D)

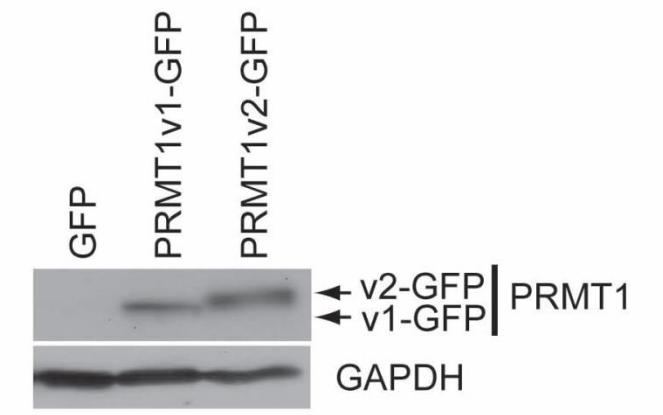
GFP
PRMT1v1-GFP
PRMT1v2-GFP
v2-GFP
v1-GFP
PRMT1
GAPDH

Figure 3.12: Establishment of Stably Expressing GFP-PRMT1v2 MCF7 Cell Lines

(A) Representative GFP fluorescent images of MCF7 cells stably expressing GFP, GFP-PRMT1v1 or GFP-PRMT1v2. Images were captured at 40X magnification. Protein lysates were collected from MCF7 cells stably expressing GFP, GFP-PRMT1v1 or GFP-PRMT1v2. Western blot analysis was performed with antibodies against (B) GFP and (D) PRMT1. Tubulin or GAPDH serve as loading controls. (C) Total RNA was isolated from MCF7 cells stably expressing GFP, GFP-PRMT1v1 or GFP-PRMT1v2. PCR analysis was performed from cDNA generated from the RNA using primers specific to PRMT1. GAPDH serves as a loading control.

expressing cells, and 26.9 +/- 1.2 GFP-PRMT1v2 expressing cells migrated through the chamber (Figure 3.13A & 3.13C). There was a statistically significant increase in both the MCF7 GFP-PRMT1v1 and GFP-PRMT1v2 cells migrating through the motility chambers, determined using a Student T-test with a 95% confidence interval. In contrast, for invasion 1.2 +/- 0.3 GFP expressing cells, 2.2 +/- 0.3 GFP-PRMT1v1 expressing cells, and 7.2 +/- 1.1 GFP-PRMT1v2 expressing cells migrated through the matrigel-containing chambers (Figure 3.13B & 3.13C). The increase in the number of GFP-PRMT1v2 expressing invasive cells relative to both the GFP and the GFP-PRMT1v1 expressing cells was statistically significant, as determined using a Student T-test with a 95% confidence interval. Furthermore, the difference in invasion between the GFP and GFP-PRMT1v1 expressing cells was not statistically significant. The increase in invasion in GFP-PRMT1v2 expressing cells is not due to any proliferative advantage MCF7 cells may have acquired due to overexpression of PRMT1v2 as no statistical difference in proliferation between GFP-PRMT1v2 and GFP or GFP-PRMT1v1 expressing cells measured via an MTT assay is observed 72 h post plating (Figure 3.13D). Although a statistically significant difference in proliferation is observed 144 h post plating.

The above result illustrating an increase in invasion in stably expressing GFP-PRMT1v2 MCF7 were further confirmed through transient overexpression of PRMT1v2 in parental MCF7 cells. GFP empty vector, GFP-PRMT1v1, -PRMT1v2, and –PRMT1v3 were overexpressed in MCF7 cells for 24 h (Figure 3.14A), counted and incubated in Transwell invasion chambers (+ matrigel layer) for 72 h. 6.4 +/- 1.2 MCF7 cells transiently transfected with GFP empty vector, 8.2 +/- 1.2 GFP-PRMT1v1 expressing, 16.3 +/- 1.8 GFP-PRMT1v2 expressing and 7.3 +/- 0.6 GFP-PRMT1v3 expressing cells

3.13A)

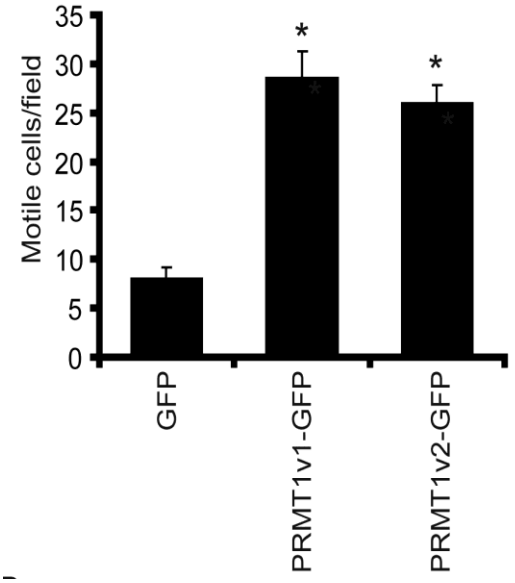
Motile cells/field
35
30
25
20
15
10
5
0
*
*
GFP
PRMT1v1-GFP
PRMT1v2-GFP

B)

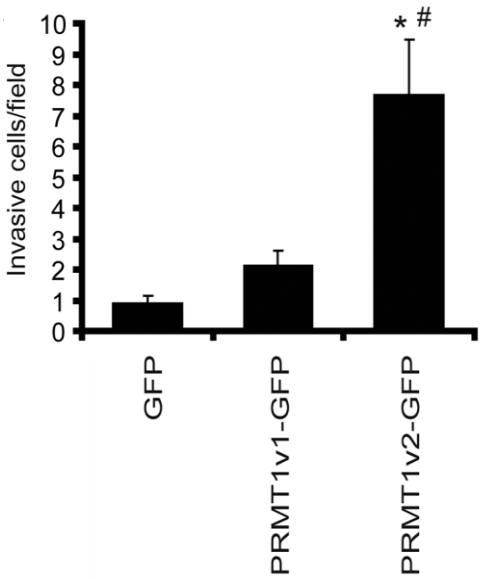
Invasive cells/field
10
9
8
7
6
5
4
3
2
1
0
* #
GFP
PRMT1v1-GFP
PRMT1v2-GFP

C)

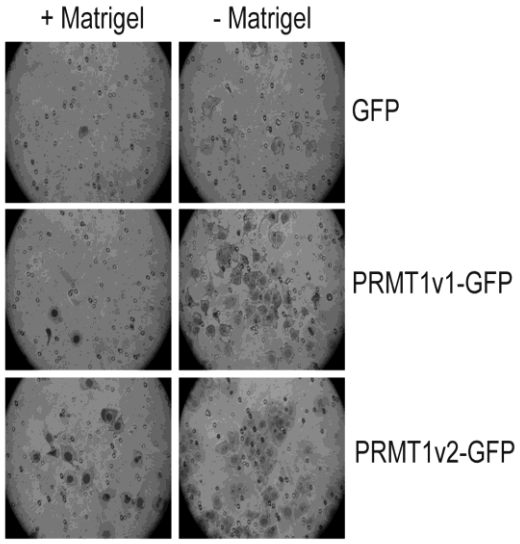
+ Matrigel
- Matrigel
GFP
PRMT1v1-GFP
PRMT1v2-GFP

D)

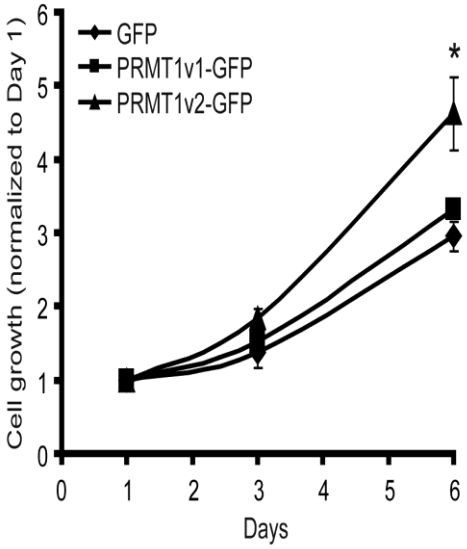
Cell growth (normalized to Day 1)
6
5
4
3
2
1
0
GFP
PRMT1v1-GFP
PRMT1v2-GFP
*
0
1
2
3
4
5
6
Days

Figure 3.13: Stable Overexpression of PRMT1v2 Increases the Invasive Potential of MCF7 Cells

MCF7 cells stably expressing GFP, GFP-PRMT1v1 or GFP-PRMT1v2 were counted and incubated on Transwell chambers for 72 h. Cells that migrated through the chamber in the absence/presence of matrigel were counted and the average number of cells per field for (A) motility and (B) invasion was determined. Data is the mean +/- the standard error for four independent experiments. * denotes statistical significance $p<0.05$ comparing to GFP, while # denotes statistical significance $p<0.05$ comparing to GFP-PRMT1v1. (C) Photo images of GFP, GFP-PRMT1v1 or GFP-PRMT1v2 cells that migrated through the Transwell chambers in the absence of matrigel (motility) or presence of matrigel (invasion). Photos captured at 20X magnification. (D) An equal number of GFP (♦), GFP-PRMT1v1 (■) or GFP-PRMT1v2 (▲) cells were plated and a MTT assay was performed 1, 3, and 6 days post plating. Data represents the mean +/- the standard error of three independent experiments with nine replicates per experiment. * denotes statistically significant $p<0.05$.

migrated through the Transwell chambers (Figure 3.14B). There is a statistically significant increase in GFP-PRMT1v2 expressing cells migrating through the Transwell chambers relative to GFP empty vector expressing cells, determined using a Student T-test with a 95% confidence interval. These results show that overexpression of both stably and transiently expressed PRMT1v2 is capable of promoting invasion in MCF7 cells.

Subsequently, it was determined if PRMT1v2's cytoplasmic localization and/or methyltransferase activity were required for promoting invasion using two PRMT1v2 mutant forms, an NES mutant and a methyltransferase dead mutant. The NES mutant was generated through point mutations of two hydrophobic residues (V15A/L18A) to alanines within the nuclear export sequence. Mutation of these residues results in increased nuclear retention of PRMT1v2 (Goulet et al., 2007). The methyltransferase dead mutant was generated through mutation of three amino acids (^{68}VLD^{70} $\rightarrow$ ^{68}AAA^{70}) within the S-adenosyl methionine binding region. This mutant results in the complete loss of enzymatic activity and results in the sequestration of PRMT1v2 in the nucleus (Herrmann and Fackelmayer, 2009; Wada et al., 2002). The PRMT1v2 NES and methyltransferase dead mutants were overexpressed in MCF7 cells for 24 h (Figure 3.14A), counted and incubated in Transwell invasion chambers for 72 h. 6.4 +/- 1.2 MCF7 cells transiently transfected with GFP empty vector, 16.3 +/- 1.8 GFP-PRMT1v2 expressing, 10.9 +/- 1.3 GFP-PRMT1v2 NES mutant, and 1.8 +/- 0.6 GFP-PRMT1v2 methyltransferase dead mutant cells migrated through the invasion chambers (Figure 3.14B). There was a statistically significant decrease in invasion of GFP-PRMT1v2 methyltransferase dead expressing cells relative to GFP empty vector expressing cells. Furthermore, there was

3.14A)

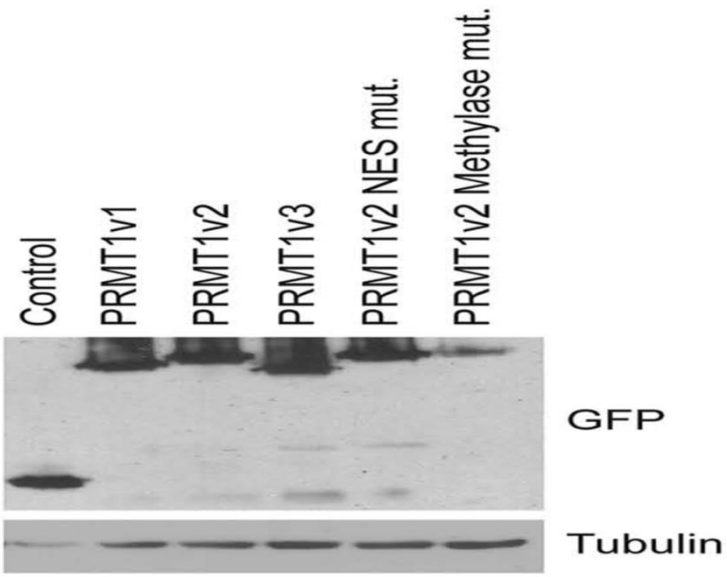
Control
PRMT1v1
PRMT1v2
PRMT1v3
PRMT1v2 NES mut.
PRMT1v2 Methylase mut.
GFP
Tubulin

B)

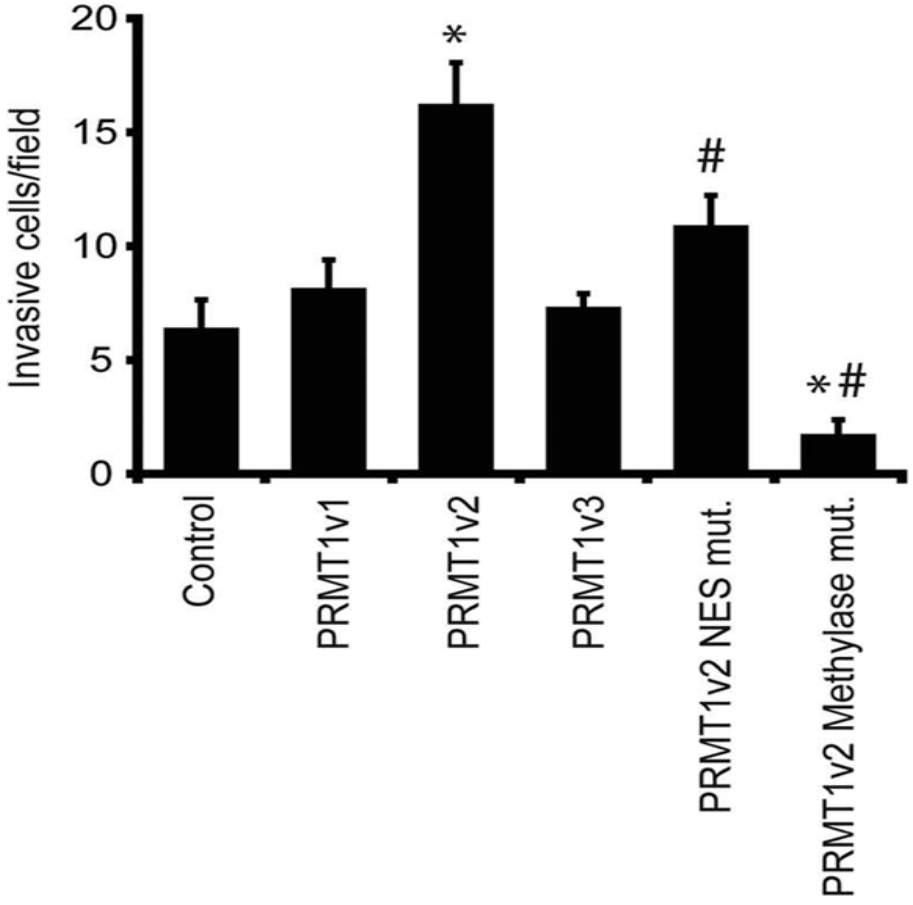
Invasive cells/field
20
15
10
5
0
*
#
*#
Control
PRMT1v1
PRMT1v2
PRMT1v3
PRMT1v2 NES mut.
PRMT1v2 Methylase mut.

Figure 3.14: PRMT1v2 Promotion of Invasion in MCF7 cells is Dependent on its Cytoplasmic Localization and Methyltransferase Activity

(A) A GFP empty vector (control), GFP-PRMT1v1, GFP-PRMT1v2, GFP-PRMT1v3, GFP-PRMT1v2 NES mutant and GFP-PRMT1v2 Methylase mutant were transfected into MCF7 cells for 24 h. Protein lysate were collected and Western blot analysis was performed with an antibody against GFP. Tubulin was used as a loading control. (B) 24 h post-transfection, cells were counted and an equal number were plated in Transwell chambers with matrigel for 72 h. Data represents the mean +/- standard error for three independent experiments. * denotes statistical significant $p<0.05$ comparing to control; # denotes statistical significant $p<0.05$ comparing PRMT1v2.

also a significant decrease in invading cells in GFP-PRMT1v2 NES and methyltransferase dead mutant expressing cells relative to GFP-PRMT1v2 expressing cells. Statistical significance was determined using a Student T-test with a 95% confidence interval. These results suggest that PRMT1v2 cytoplasmic localization and methyltransferase activity are required for PRMT1v2 to promote invasion.

To further validate that indeed PRMT1v2 promotes an increase in invasion in MCF7 cells, the following rescue experiment was performed. It was rationalized that stable overexpression of PRMT1v2 should confer resist to the inhibition of invasion observed upon transient depletion of PRMT1v2. Therefore, MCF7 stably expressing GFP, GFP-PRMT1v1, and GFP-PRMT1v2 were transiently transfected with PRMT1v2 si/shRNA. Through PCR analysis, it was determined that GFP-PRMT1v2 expressing cells maintained higher levels of PRMT1v2 mRNA upon transfection with PRMT1v2 si/shRNA through densitometry analysis relative to the mock control (Figure 3.15A). MCF7 stably expressing GFP, GFP-PRMT1v1, and GFP-PRMT1v2 cells were transfected with PRMT1v2 si/shRNA for 24 h, counted and incubated in Transwell invasion chambers for 72 h. To analyze the decrease in invasive potential upon transfection with PRMT1v2 si/shRNA, the values obtained for the GFP, GFP-PRMT1v1, and GFP-PRMT1v2 cell lines were normalized to their respective mock transfected controls. Upon PRMT1v2 depletion in each stably expressing MCF7 cell line (GFP, GFP-PRMT1v1, GFP-PRMT1v2) there was a statistically significant decrease in invasion relative to the invasive potential for control siRNA transfected cells in each respective cell line (Figure 3.15B). However, the decrease in invasion in the GFP and GFP-PRMT1v1 expressing cell lines was significantly greater than in the GFP-PRMT1v2

3.15A)

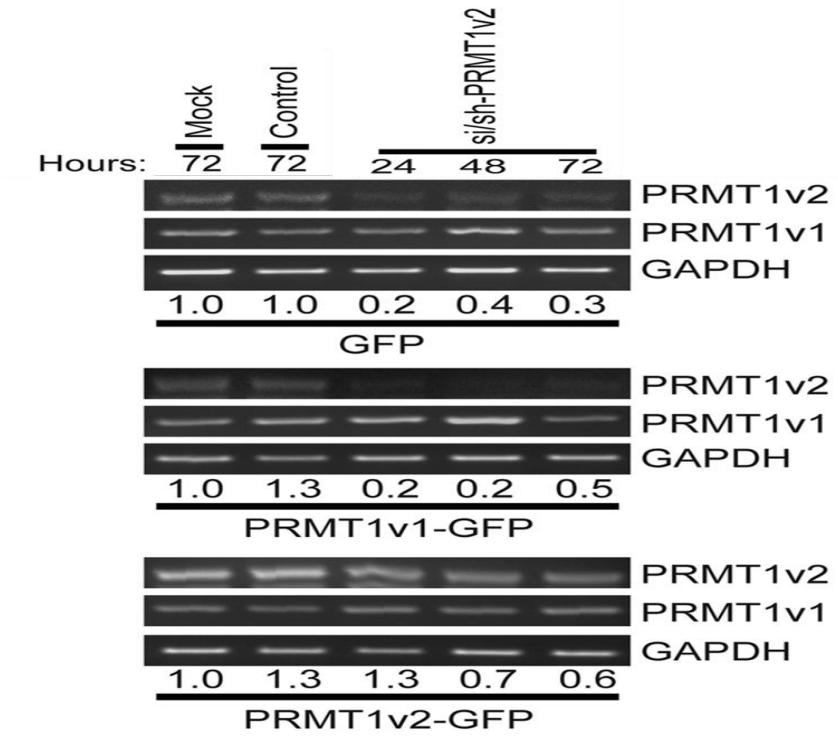
Mock
Control
si/sh-PRMT1v2
Hours:
72
72
24
48
72
PRMT1v2
PRMT1v1
GAPDH
1.0 1.0 0.2 0.4 0.3
GFP
PRMT1v2
PRMT1v1
GAPDH
1.0 1.3 0.2 0.2 0.5
PRMT1v1-GFP
PRMT1v2
PRMT1v1
GAPDH
1.0 1.3 1.3 0.7 0.6
PRMT1v2-GFP

B)

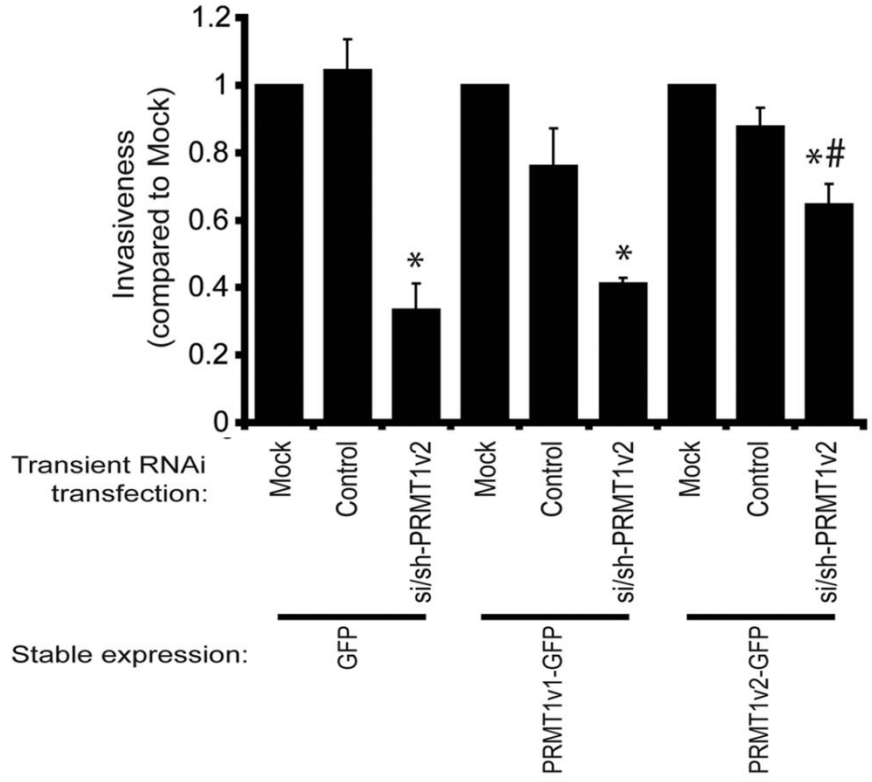
Invasiveness
(compared to Mock)
1.2
1
0.8
0.6
0.4
0.2
0
*
*
*#
Transient RNAi
transfection:
Mock
Control
si/sh-PRMT1v2
Mock
Control
si/sh-PRMT1v2
Mock
Control
si/sh-PRMT1v2
Stable expression:
GFP
PRMT1v1-GFP
PRMT1v2-GFP

Figure 3.15: Stable Overexpression of PRMT1v2 is Sufficient to Partially Rescue the Decrease in Invasion upon Transient Depletion of PRMT1v2

(A) Stably expressing MCF7 GFP, GFP-PRMT1v1, and GFP-PRMT1v2 cells were transiently transfected with PRMT1v2 si/shRNA for 24, 48, and 72 h or mock transfected and control siRNA for 72 h. Total RNA was isolated and PCR analysis was performed with cDNA generated from the RNA with primers specific to PRMT1. GAPDH was used as a loading control. Densitometry was performed to determine the relative level of PRMT1v2 mRNA expression upon transient depletion of PRMT1v2 by normalizing PRMT1v2 to GAPDH. (B) 24 h post-transfection, cells were counted and an equal number were incubated in Transwell chambers with matrigel for 72 h. Data represents the mean +/- standard error of three independent experiments. * denotes statistical significance $p<0.05$ compared with matched control transfection. # denotes statistical significance $p<0.05$ compared with MCF7 GFP cells transfected with PRMT1v2 si/shRNA.

expressing cells. Thus, stable overexpression of PRMT1v2 was sufficient to partially rescue the invasive phenotype observed in MCF7 cells. Statistical significance was performed using a Student T-test with a 95% confidence interval. Therefore, these results corroborate the previous evidence implicating PRMT1v2 in cell invasion.

3.6 Overexpression of PRMT1v2 Alters Breast Cancer Cell Morphology

MCF7 cells are polygonal in nature and form tight E-cadherin positive adherens junction colonies in culture (Lacroix and Leclercq, 2004; Shtutman et al., 2006). Examination of the MCF7 GFP, GFP-PRMT1v1, and GFP-PRMT1v2 stably expressing cell lines revealed an increase in the number of loose and disorganized colonies in GFP-PRMT1v2 cells (Figure 3.16A). Additionally, numerous cells displayed filopodia and small lamellipodia (Figure 3.16A), attributes consistent with cells exhibiting increased migratory potential (Hall, 2005; Jaffe and Hall, 2005; Schafer, 2004; Tomaskovic-Crook et al., 2009). Moreover, a cytoplasmic dispersion of F-actin, which localizes to cell-cell adherens junctions, was observed in GFP-PRMT1v2 cells, in contrast to localization at junctions in GFP cells (Figure 3.16B). In GFP-PRMT1v2 cells, F-actin localization to filopodia and lamellipodia structures was also observed. A similar phenotype, highly disorganized colonies with decreased F-actin localization to cell-cell junctions with increased filopodia and lamellipodia, was also observed in GFP-PRMT1v1 expressing cells (Figure 3.16A & 3.16B).

To quantify the changes in colony structure that were observed between the GFP, GFP-PRMT1v1 and GFP-PRMT1v2 expressing cells, a colony dispersion assay was performed. One thousand cells from each cell line were plated and allowed to grow for

3.16A)

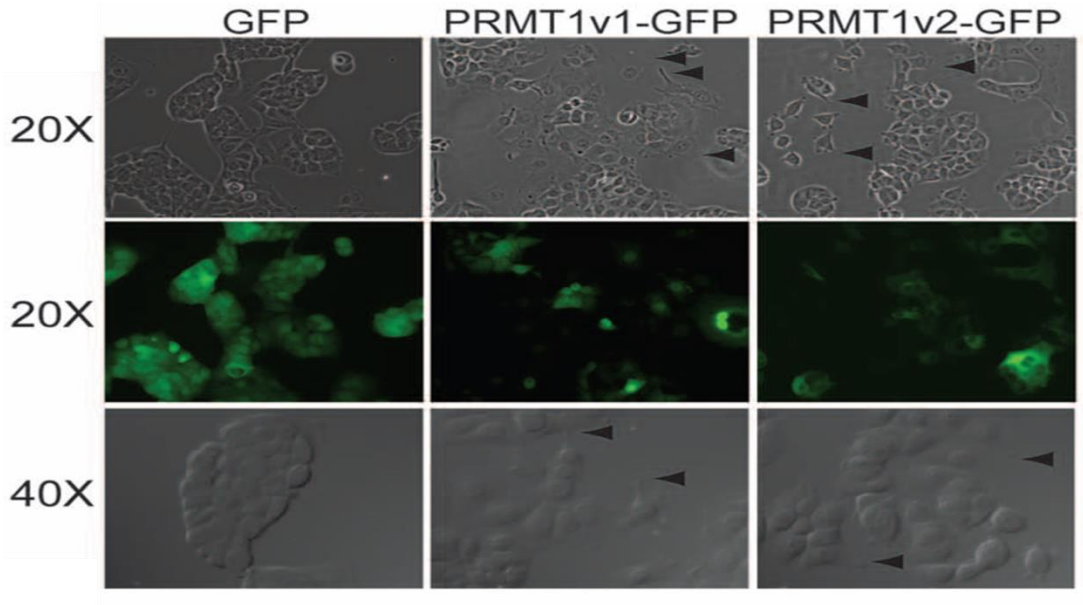
GFP
PRMT1v1-GFP
PRMT1v2-GFP
20X
20X
40X

B)

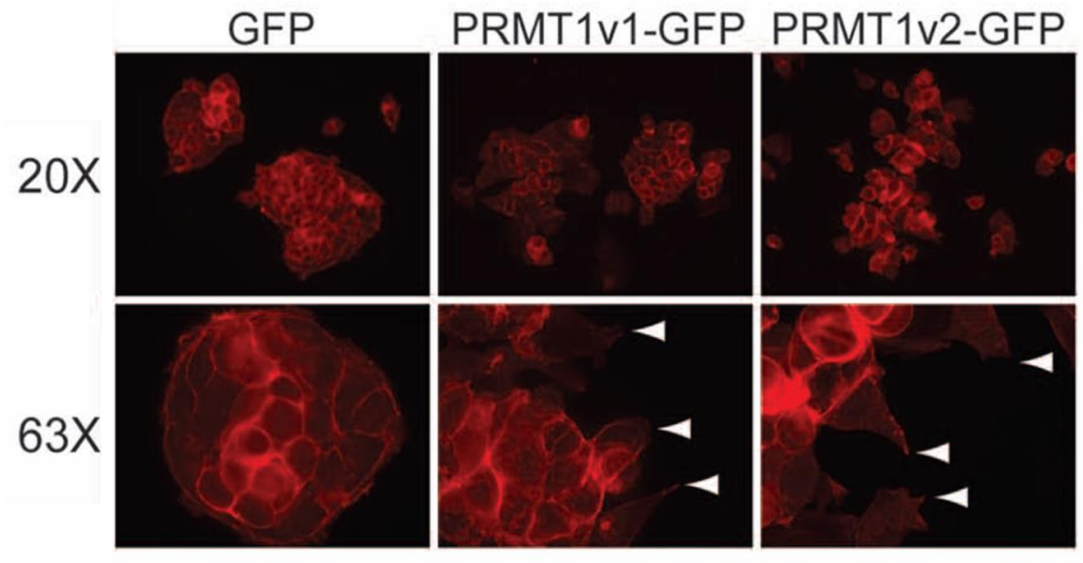
GFP
PRMT1v1-GFP
PRMT1v2-GFP
20X
63X

Figure 3.16: Overexpression of PRMT1v2 Results in Altered Morphology in MCF7 Cells

(A) Representative phase contrast and fluorescence images of MCF7 cells stably expressing GFP, GFP-PRMT1v1, or GFP-PRMT1v2. Arrowheads indicate the presence of filopodia and lamellipodia. Magnifications are indicated to the left. (B) Fluorescent images of actin filament using FITC-conjugated phalloidin in MCF7 cells stably expressing GFP, GFP-PRMT1v1, or GFP-PRMT1v2. Arrowheads indicate the presence of filopodia and lamellipodia. Magnifications are indicated to the left.

five days to allow colony formation. One hundred images of colonies were taken and the colonies were classified as compact, loose, or scattered (Figure 3.17A) independently by three different individuals. Relative to the GFP expressing cells, overexpression of PRMT1v2 resulted in a 45% decrease in compact colonies and a 28% increase in loose and a 15% increase in scattered colonies (Figure 3.17B). Similarly, overexpression of PRMT1v1 resulted in a 46% decrease in compact colonies and a 19% increase in loose and a 25% increase in scattered colonies. A statistically significant decrease in the number of compact colonies was observed in the GFP-PRMT1v1 and GFP-PRMT1v2 cell lines compared to the GFP cells, determined using a Student T-test with a 95% confidence interval. These results are consistent with the decrease in F-actin positive cell-cell junctions in GFP-PRMT1v1 and GFP-PRMT1v2 cell lines and the increased motility observed upon overexpression of both PRMT1v1 and PRMT1v2.

3.7 PRMT1v2 Represses β-catenin Expression Resulting in Increased Cell Invasion

The altered morphology observed in MCF7 GFP-PRMT1v2 overexpressing cells indicated that the disruption of cell-cell adherens junctions implicates PRMT1v2 in the promotion of invasion. MCF7 cells, which are epithelial-like in nature, exhibit tight cell-cell adherens junctions which are required for the maintenance of proper cell polarity and structure (Lacroix and Leclercq, 2004; Shtutman et al., 2006). To determine if a disruption in adherens junctions in PRMT1v2 expressing MCF7 cells contributes to the increased invasive phenotype, E-cadherin and β-catenin, two components of adherens junction were examined. No decrease in E-cadherin mRNA (Figure 3.18A) or protein (Figure 3.18A) levels was observed in GFP-PRMT1v2 cells, though a decrease in E-

3.17A)

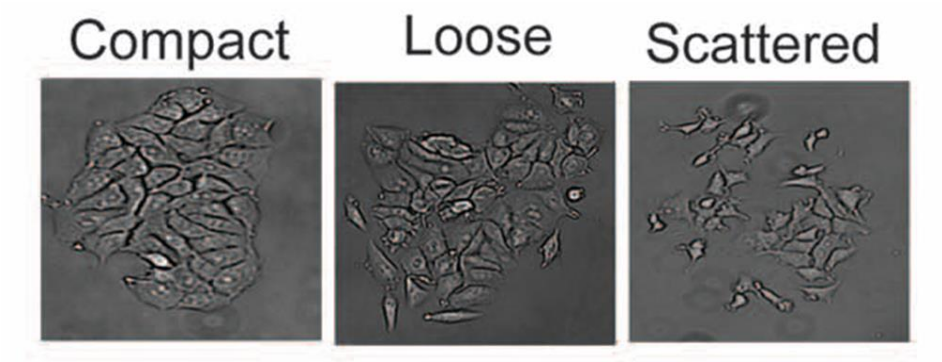
Compact
Loose
Scattered

B)

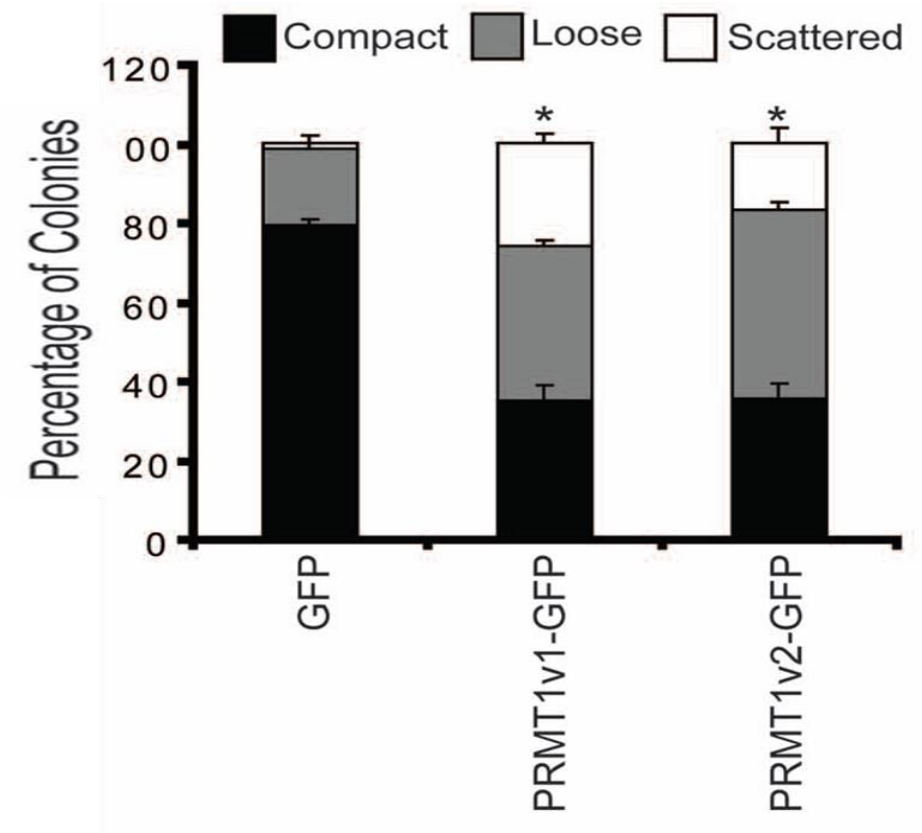
Compact
Loose
Scattered
Percentage of Colonies
120
00
80
60
40
20
0
*
*
GFP
PRMT1v1-GFP
PRMT1v2-GFP

Figure 3.17: Overexpression of PRMT1v2 Results in Altered Colony Formation in MCF7 Cells

(A) Distribution of compact, loose, and scattered MCF7 cells stably expressing GFP, GFP-PRMT1v1 or GFP-PRMT1v2. (B) One thousand GFP, GFP-PRMT1v1 or GFP-PRMT1v2 cells were plated and grown for five days. Approximately one hundred colonies were counted from each cell line per experiment and colonies were scored by three independent investigators. Data is the mean +/- the standard error for four independent experiments. * denotes statistical significance $p<0.05$ comparing compact colonies.

3.18A)

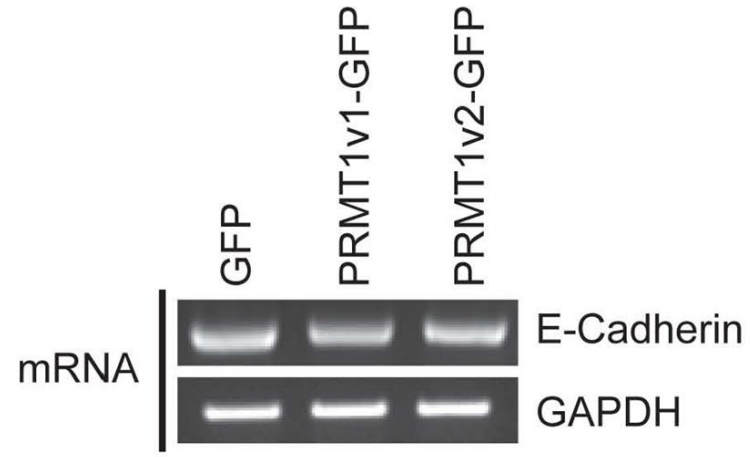
GFP
PRMT1v1-GFP
PRMT1v2-GFP
mRNA
E-Cadherin
GAPDH

B)

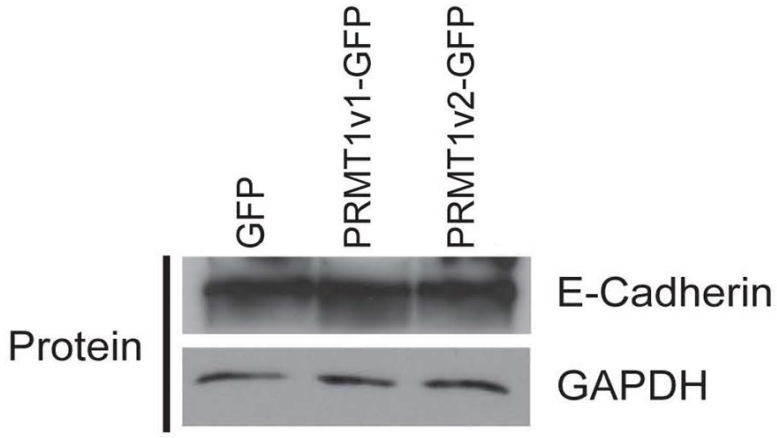
GFP
PRMT1v1-GFP
PRMT1v2-GFP
Protein
E-Cadherin
GAPDH

Figure 3.18: E-cadherin mRNA and Protein Levels are Unaltered in MCF7 cells Overexpressing PRMT1v2

(A) Total RNA was isolated from MCF7 cells stably overexpressing GFP, GFP-PRMT1v1, or GFP-PRMT1v2. PCR analysis was performed with cDNA generated from the total RNA using primers specific for E-cadherin. GAPDH was used as a loading control. (B) Protein lysate was collected from MCF7 cells stably overexpressing GFP, GFP-PRMT1v1, or GFP-PRMT1v2. Western blot analysis was performed using an antibody specific to E-cadherin. GAPDH was used as a loading control.

3.19A)

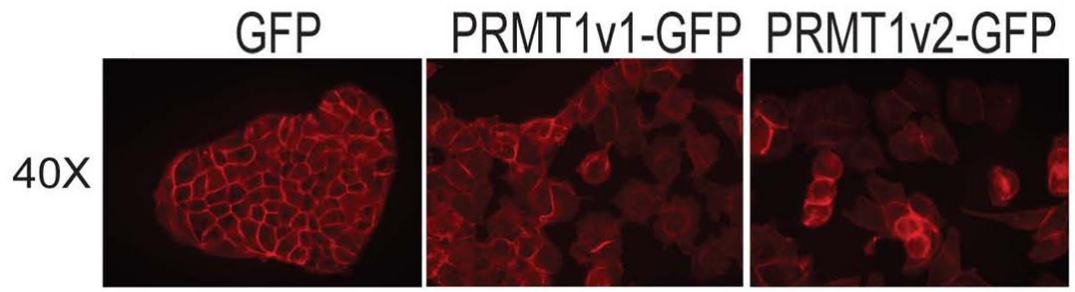
GFP
PRMT1v1-GFP
PRMT1v2-GFP
40X

B)

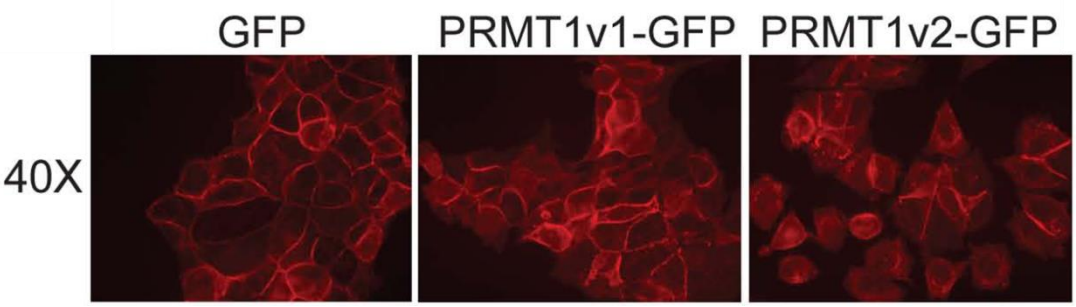
GFP
PRMT1v1-GFP
PRMT1v2-GFP
40X

Figure 3.19: E-cadherin and β-catenin is Dispersed from Cell-Cell Adherens Junctions in MCF7 cells Overexpressing PRMT1v2

Localization of (A) E-cadherin and (B) β-catenin in MCF7 cells stably overexpressing GFP, GFP-PRMT1v1, or GFP-PRMT1v2. Images were taken at 40X magnification.

cadherin (Figure 3.19A) and β-catenin (Figure 3.19B) localization at cell-cell adherens junctions was observed in GFP-PRMT1v2 cells, in comparison to GFP cells. While a decrease in β-catenin localization at cell-cell adherens junctions was observed, no nuclear accumulation of β-catenin was seen. Strikingly, a significant decrease in β-catenin protein levels was detected in GFP-PRMT1v2 cells (Figure 3.20A). Densitometry analysis revealed a 58% decrease in β-catenin protein levels in MCF7 GFP-PRMT1v2 overexpressing cells (Figure 3.20B). No change in β-catenin mRNA levels (Figure 3.20C) was detected, indicating that PRMT1v2 may be regulating β-catenin protein stability. β-catenin protein stability is negatively regulated through phosphorylation (Hart et al., 1999; Latres et al., 1999; Winston et al., 1999), therefore the phosphorylation status of β-catenin in GFP-PRMT1v2 cells was assessed. A lower level of phospho-β-catenin levels was observed in GFP-PRMT1v2 cells (Figure 3.20D), however, as GFP-PRMT1v2 contain a lower steady state level of β-catenin, the ratio of phosphorylated β-catenin to total β-catenin in each cell line was determined by densitometry. This revealed a statistically significant increase in the ratio of phosphorylated β-catenin to total β-catenin in the GFP-PRMT1v2 cells compared to the GFP and GFP-PRMT1v1 cells (Figure 3.20E). These results suggest that the lower levels of β-catenin observed in GFP-PRMT1v2 expressing cells is likely due to increased β-catenin phosphorylation-mediated protein degradation.

To determine if the reduction in β-catenin expression contributed to the increase in cell invasion detected in GFP-PRMT1v2 expressing cells, β-catenin was re-introduced in these cells. Flag-tagged β-catenin or an empty vector was transiently transfected in GFP, GFP-PRMT1v1, and GFP-PRMT1v2 expressing cell lines for 24 h. Equal

expression of flag-tagged β-catenin was observed in the three cell lines (Figure 3.21A). Twenty-four hours post-transfection, the cells were counted and placed in Transwell invasion chambers for 72 h. Transfection of cells with an empty vector yielded results similar to those previously observed with an increase in invasion in the GFP-PRMT1v2 expressing cells. Conversely, upon expression of flag-tagged β-catenin in GFP-PRMT1v2 cells, a reduction in invasion to levels similar to that of the GFP and GFP-PRMT1v1 expressing cells was observed (Figure 3.21B). These results suggest that PRMT1v2 contributes to breast cancer cell invasion through repression of β-catenin through regulation of its protein stability.

3.20A)

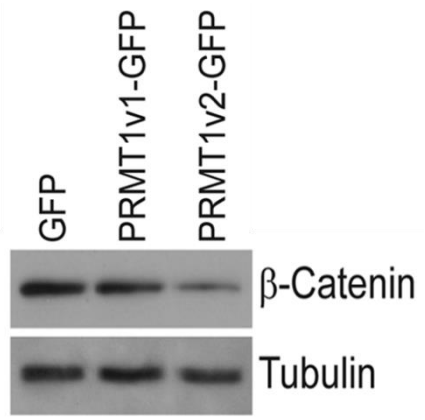
GFP
PRMT1v1-GFP
PRMT1v2-GFP
β-Catenin
Tubulin

B)

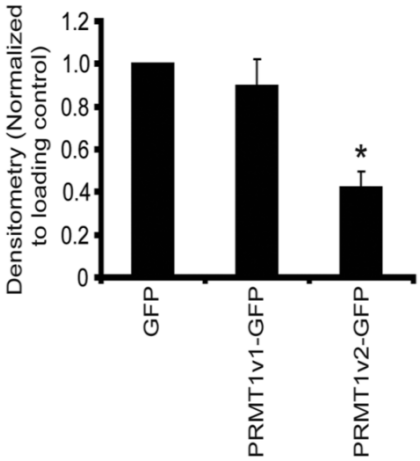
Densitometry (Normalized to loading control)
1.2
1.0
0.8
0.6
0.4
0.2
0
*
GFP
PRMT1v1-GFP
PRMT1v2-GFP

C)

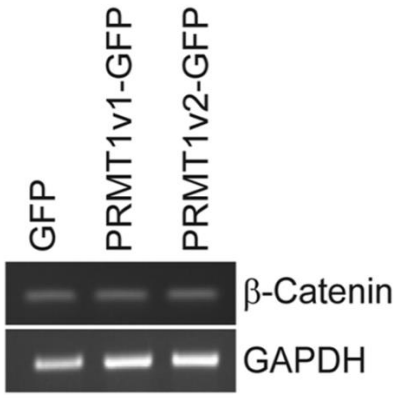
GFP
PRMT1v1-GFP
PRMT1v2-GFP
β-Catenin
GAPDH

D)

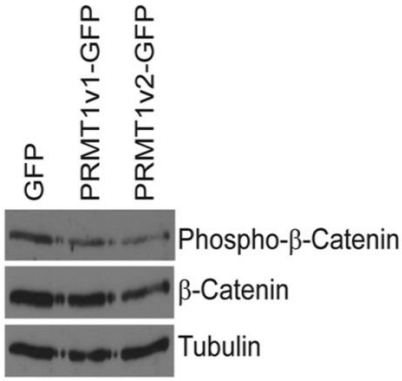
GFP
PRMT1v1-GFP
PRMT1v2-GFP
Phospho-β-Catenin
β-Catenin
Tubulin

E)

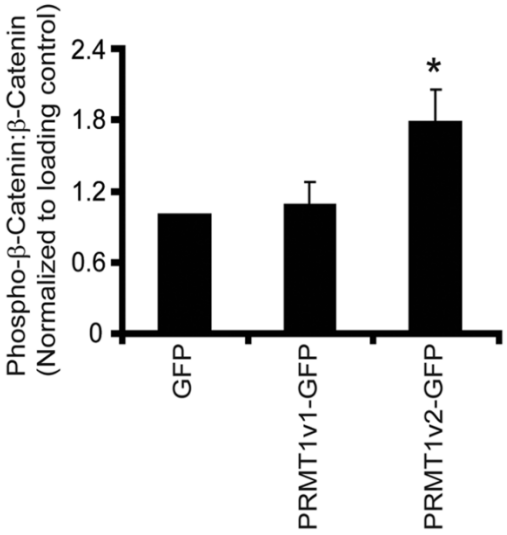
Phospho-β-Catenin:β-Catenin (Normalized to loading control)
2.4
1.8
1.2
0.6
0
*
GFP
PRMT1v1-GFP
PRMT1v2-GFP

Figure 3.20: PRMT1v2 Regulates β-catenin Protein Stability through β-catenin Phosphorylation-Mediated Protein Degradation

(A) Protein lysate was collected from MCF7 cells stably expressing GFP, GFP-PRMT1v1, and GFP-PRMT1v2 and Western blot analysis was performed using an antibody against β-catenin. Tubulin was used as a loading control. (B) Through densitometry the relative level of β-catenin protein was determined relative to MCF7 GFP expressing cells. β-catenin protein expression was normalized to the loading control. Data represents the mean +/- the standard error of seven independent experiments. * denotes statistical significance; $p<0.01$ compared to both GFP and GFP-PRMT1v1. (C) Total RNA was isolated from MCF cells stably expressing GFP, GFP-PRMT1v1, and GFP-PRMT1v2. PCR analysis of cDNA generated from total RNA using β-catenin specific primers. GAPDH serves as a loading control. (D) Western blot analysis for levels of phosphorylated β-catenin using a phospho-specific antibody that recognizes β-catenin phosphorylated residues (Ser 33, Ser 37, Thr 41). (E) Densitometry was performed to determine the ratio of phospho-β-catenin to β-catenin normalized to the loading control. Values are expressed relative to MCF7 GFP expressing cells. Data represents the mean +/- the standard error of the mean (* denote statistical significance; $p<0.05$ compared to both GFP and GFP-PRMT1v1).

3.21A)

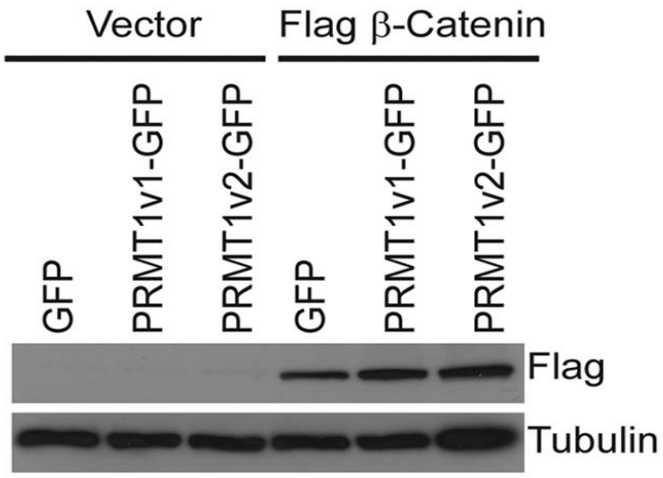
Vector
Flag β-Catenin
GFP
PRMT1v1-GFP
PRMT1v2-GFP
GFP
PRMT1v1-GFP
PRMT1v2-GFP
Flag
Tubulin

B)

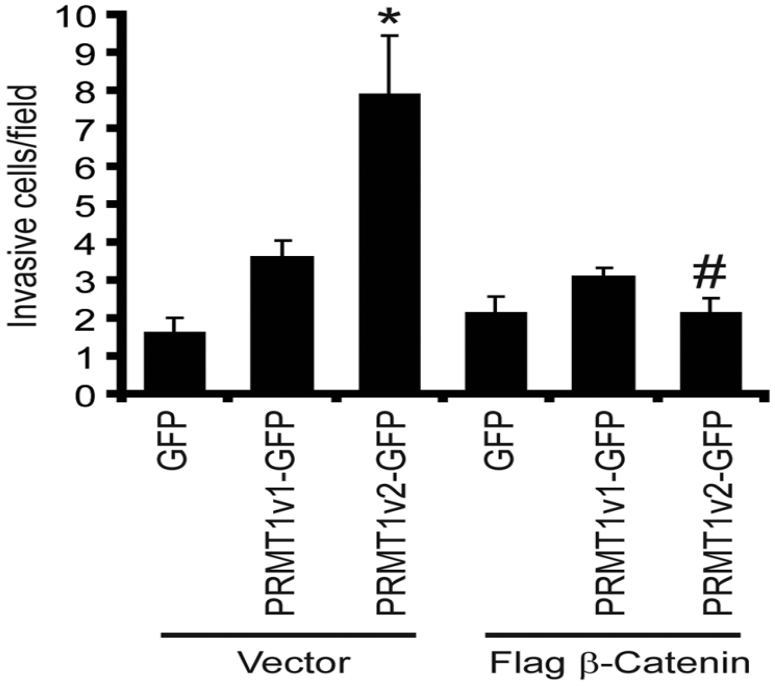
Invasive cells/field
10
9
8
7
6
5
4
3
2
1
0
*
#
GFP
PRMT1v1-GFP
PRMT1v2-GFP
GFP
PRMT1v1-GFP
PRMT1v2-GFP
Vector
Flag β-Catenin

Figure 3.21: Re-introduction of β-catenin Suppresses Invasion in MCF7 GFP-PRMT1v2 Expressing Cells

(A) MCF7 GFP, GFP-PRMT1v1, and GFP-PRMT1v2 cells were transiently transfected with an empty vector expression plasmid or an expression plasmid containing flag-tagged β-catenin for 24 h. Protein lysate were collected and Western Blot analysis was performed with an antibody against Flag. Tubulin serves as a loading control. (B) 24 h post-transfection with transiently transfected flag-tagged β-catenin, MCF7 GFP, GFP-PRMT1v1, and GFP-PRMT1v2 cells were equally plated on Transwell chambers containing matrigel for 72 h. Cells that passed through the matrigel barrier were counted. Data represents the mean +/- the standard error for three independent experiments. * denotes statistical significance $p<0.05$ comparing to control, while # denotes statistical significance $p<0.05$ comparing to PRMT1v2 vector control.

Chapter 4: Elucidating the Role of PRMT6 in Chemoresistance through its Function in Stress Granule Formation

The proteasome is a large multi-subunit complex responsible for the degradation of various proteins either through ubiquitin-dependent or –independent mechanisms (Adams, 2004a; Adams, 2004b), while proteasome inhibitors are capable of inducing apoptosis in proliferating cells (Drexler, 1997; Imajoh-Ohmi et al., 1995; Lopes et al., 1997; Sloss et al., 2008). The proteasome inhibitor bortezomib (Velcade) has been successfully used in the treatment of both mantle cell myeloma and multiple myeloma (McConkey and Zhu, 2008; Richardson et al., 2004; Richardson et al., 2003; Sterz et al., 2008). However, various solid tumors are refractory to bortezomib treatment, and this resistance is observed in cancer cell lines derived from these tumors (McConkey and Zhu, 2008; Codony-Servat et al., 2006; Rajkumar et al., 2005; Tang et al., 2008). Bortezomib treatment of certain cancer cell lines promotes the formation of stress granules, thus promoting cancer cell chemoresistance and survival (Fournier et al., 2010).

4.1 Depletion of PRMT6 Inhibits Bortezomib-Induced Stress Granule Formation

Using the paradigm of bortezomib-induced stress granule formation, PRMT6 was identified as the most promising candidate to examine the role of PRMTs in stress granule formation. To determine the effect of PRMT6 on bortezomib-induced stress granule formation, stably expressing pools of HeLa PRMT6 shRNA cell lines were established using an shRNA targeting the 3'UTR of PRMT6. PRMT6 protein levels were efficiently depleted to non-detectable levels in two stable pools of HeLa cells compared to a scramble shRNA stable cell line (Figure 4.1A). HeLa scramble and PRMT6 shRNA cells were treated with 10 μM bortezomib for 1, 2, 3, 4, and 5 h and the percentage of

cells containing stress granules was determined using TIA-1, a known stress granule marker. At 2, 3, 4, and 5 h post bortezomib treatment, a statistically significant reduction in the percentage of cells containing stress granules was observed in two PRMT6 shRNA expressing cell lines compared to a scramble shRNA expressing cell line (Figure 4.1B & 4.1C). At 1 h post treatment, a negligible number of both scramble and PRMT6 shRNA expressing cells contained stress granules, while 2 h post treatment 38% of scramble shRNA expressing cells and between 10 to 20% of PRMT6 shRNA expressing cells contained stress granules; 3, 4, and 5 h post bortezomib treatment, 75%, 79%, and 73% of scramble shRNA expressing cells compared to 45.5%, 45.3% and 32.8% of cells in one population of PRMT6 shRNA expressing cells, and 19.2%, 16%, and 11.4% in another population of PRMT6 shRNA expressing cells contained stress granules. Statistically significant results between scramble and both PRMT6 shRNA expressing cell populations with a p-value less than one percent was determined using a two way ANOVA.

Similar results were observed with two additional stress granule markers: FMRP (Figure 4.2A & 4.2B) and DDX3 (Figure 4.3A & 4.3B). Using FMRP, 0.53%, 37.6%, 82.6%, 85.6%, and 82.7% of scramble shRNA expressing cells contained bortezomib-induced stress granules 1, 2, 3, 4, and 5 h post treatment, respectively. In contrast, 0.33%, 19%, 44.9%, 46.5%, and 40.5% in one PRMT6 shRNA expressing cell population, and 2.2%, 21.8%, 29%, 24.8%, and 20.6% in another cell population contained bortezomib-induced stress granules. Using DDX3 as a marker for stress granules, in scramble shRNA expressing cells, 5.9%, 38.6%, 75.3%, 79.4%, and 72.7% of cells contained stress granules 1, 2, 3, 4, and 5 h post treatment, respectively. Contrarily, 1.6%, 21.4%, 35.2%,

4.1A)

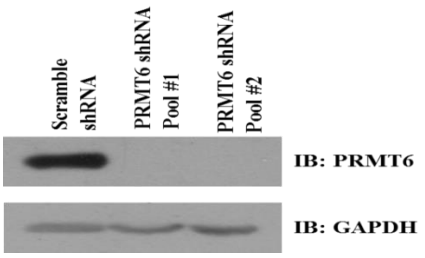
Scramble shRNA
PRMT6 shRNA Pool #1
PRMT6 shRNA Pool #2
IB: PRMT6
IB: GAPDH

B)

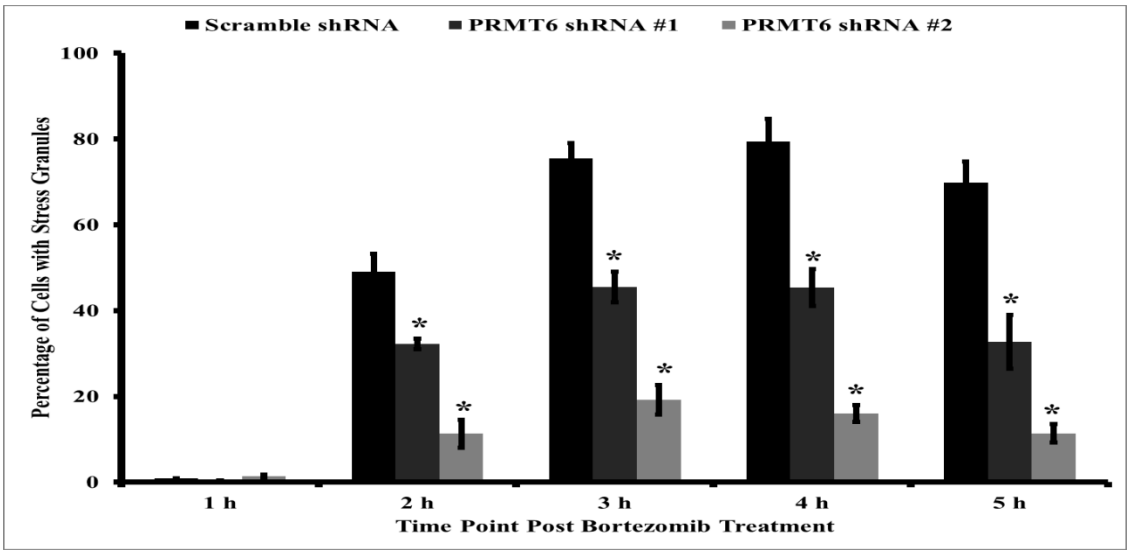
Scramble shRNA
PRMT6 shRNA #1
PRMT6 shRNA #2
Percentage of Cells with Stress Granules
100
80
60
40
20
0
1 h
2 h
3 h
4 h
5 h
Time Point Post Bortezomib Treatment

C)

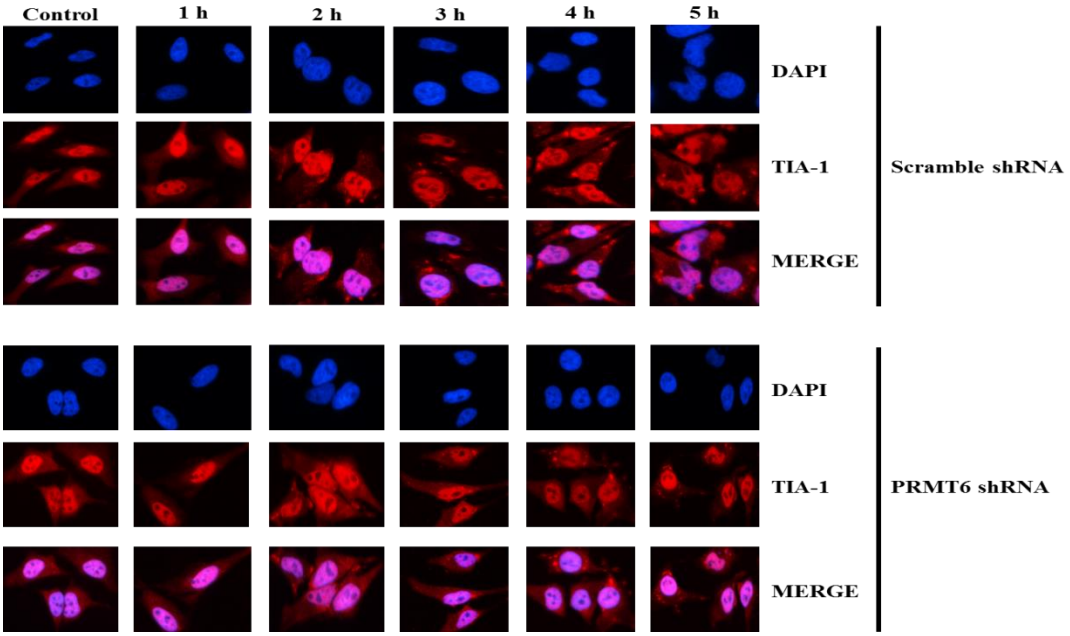
Control
1 h
2 h
3 h
4 h
5 h
DAPI
TIA-1
MERGE
Scramble shRNA
DAPI
TIA-1
MERGE
PRMT6 shRNA

Figure 4.1: Depletion of PRMT6 Results in a Reduction in Bortezomib-Induced Stress Granules in HeLa Cells using TIA-1 as Marker for Stress Granules

(A) Western blot depicting stable knockdown of PRMT6 in HeLa cells. GAPDH was utilized as a loading control. (B) HeLa scramble or two pools of PRMT6 shRNA expressing stable cell lines were treated for 1, 2, 3, 4, and 5 h with 10 μM bortezomib and immunofluorescence was performed using TIA-1 as a marker for stress granule formation. The percentage of cells containing stress granules was determined by counting at least 300 cells per coverslip. Data is the mean from three independent experiments +/- the standard error of the mean. * denotes statistical significance at a p-value <0.01 using a two way ANOVA. (C) Representative images at 40X magnification of bortezomib-induced stress granule formation in HeLa scramble and PRMT6 shRNA cell lines using TIA-1 as a marker. DAPI was used to stain the nucleus.

4.2A)

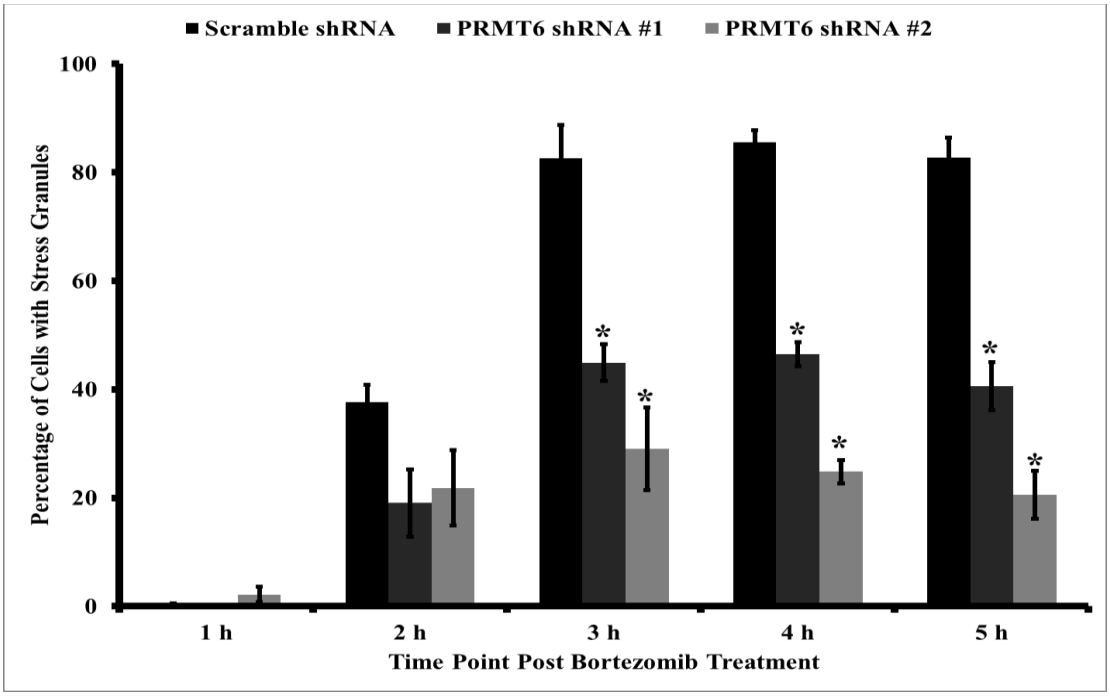
Scramble shRNA
PRMT6 shRNA #1
PRMT6 shRNA #2
Percentage of Cells with Stress Granules
100
80
60
40
20
0
1 h
2 h
3 h
4 h
5 h
Time Point Post Bortezomib Treatment

B)

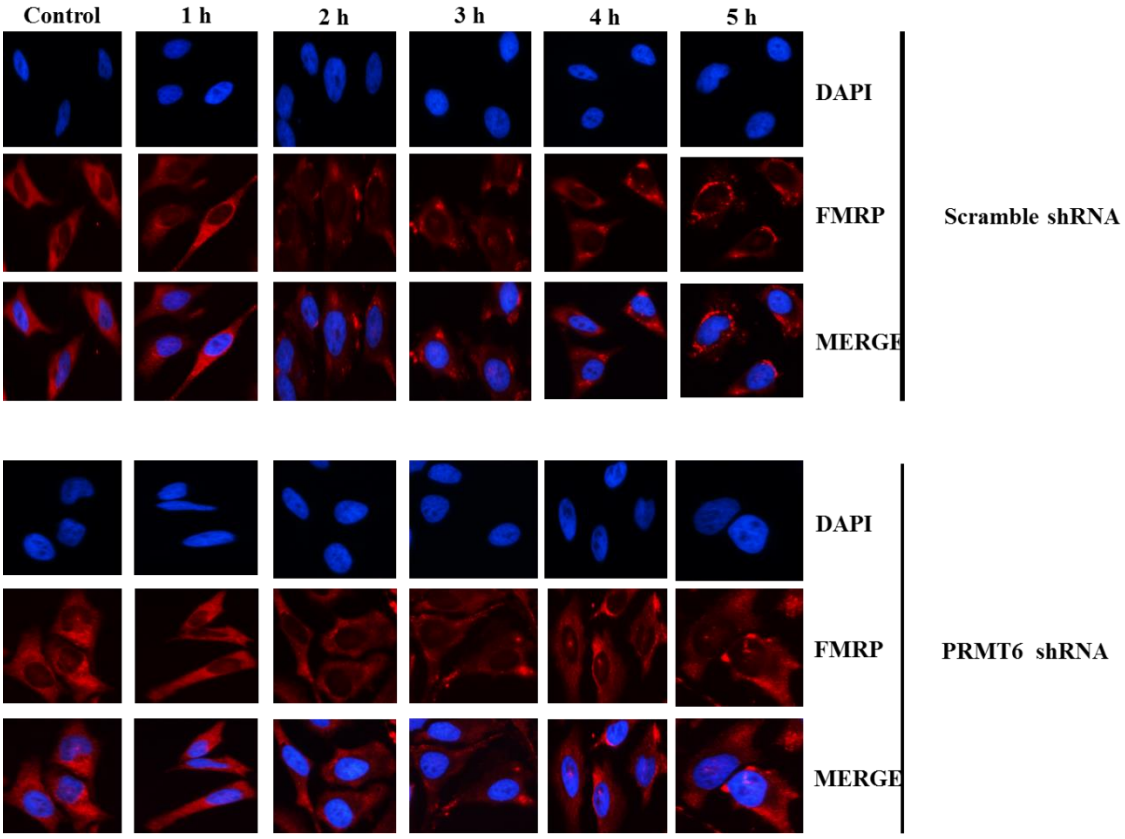
Control
1 h
2 h
3 h
4 h
5 h
DAPI
FMRP
MERGE
Scramble shRNA
DAPI
FMRP
MERGE
PRMT6 shRNA

Figure 4.2: Depletion of PRMT6 Results in a Reduction in Bortezomib-Induced Stress Granules in HeLa Cells using FMRP as Marker for Stress Granules

(A) HeLa scramble or two pools of PRMT6 shRNA expressing stable cell lines were treated for 1, 2, 3, 4, and 5 h with 10 μM bortezomib and immunofluorescence was performed using FMRP as a marker for stress granule formation. The percentage of cells containing stress granules was determined by counting at least 300 cells per coverslip. Data is the mean from three independent experiments +/- the standard error of the mean. * denotes statistical significance at a p-value <0.01 using a two way ANOVA. (B) Representative images at 40X magnification of bortezomib-induced stress granule formation in HeLa scramble and PRMT6 shRNA cell lines using FMRP as a marker. DAPI was used to stain the nucleus.

4.3A)

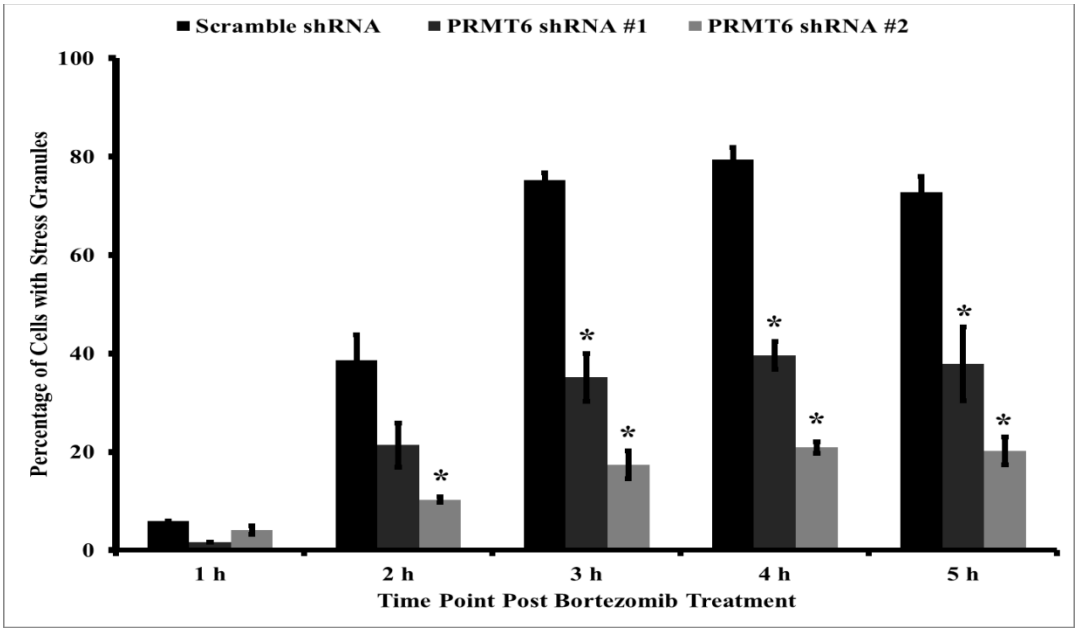
Scramble shRNA
PRMT6 shRNA #1
PRMT6 shRNA #2
Percentage of Cells with Stress Granules
100
80
60
40
20
0
1 h
2 h
3 h
4 h
5 h
Time Point Post Bortezomib Treatment

B)

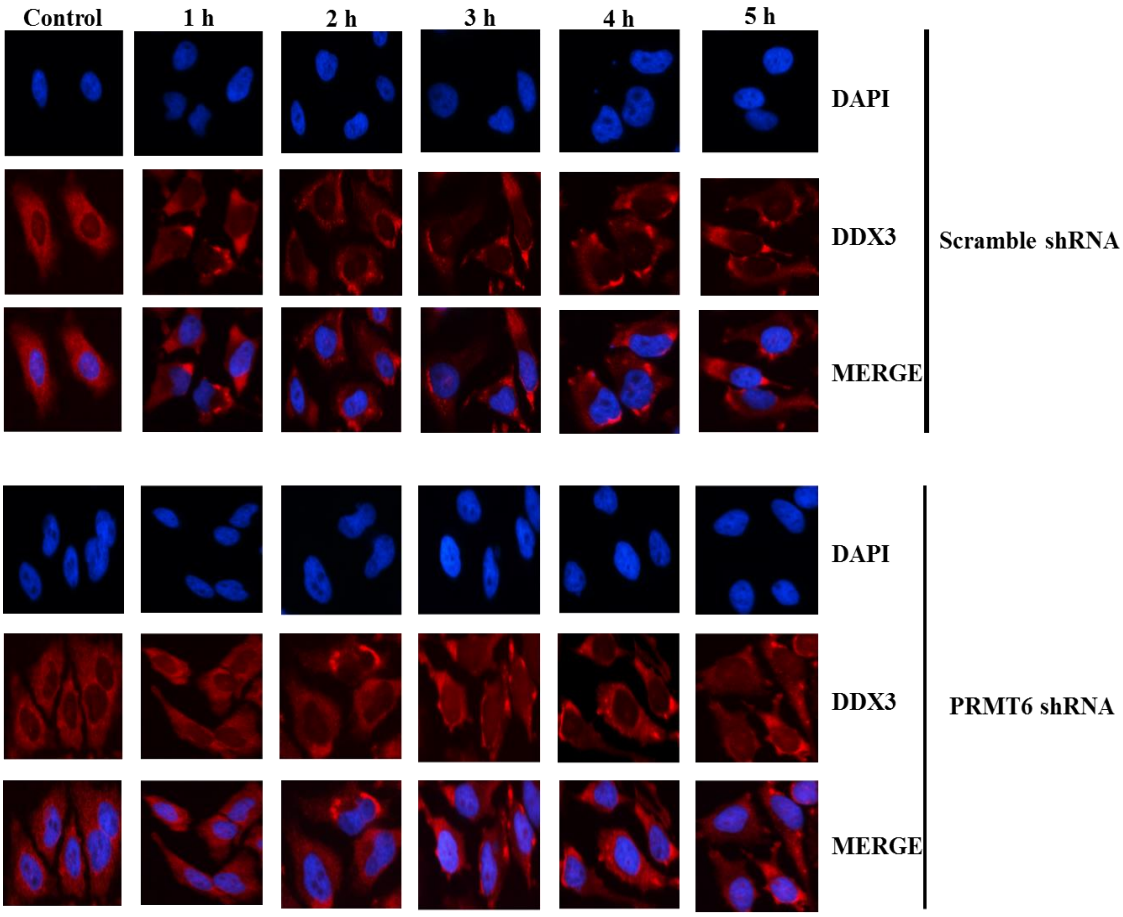
Control
1 h
2 h
3 h
4 h
5 h
DAPI
DDX3
MERGE
Scramble shRNA
DAPI
DDX3
MERGE
PRMT6 shRNA

Figure 4.3: Depletion of PRMT6 Results in a Reduction in Bortezomib-Induced Stress Granules in HeLa Cells using DDX3 as Marker for Stress Granules

(A) HeLa scramble or two pools of PRMT6 shRNA expressing stable cell lines were treated for 1, 2, 3, 4, and 5 h with 10 μM bortezomib and immunofluorescence was performed using DDX3 as a marker for stress granule formation. The percentage of cells containing stress granules was determined by counting at least 300 cells per coverslip. Data is the mean from three independent experiments +/- the standard error of the mean. * denotes statistical significance at a p-value <0.01 using a two way ANOVA. (B) Representative images at 40X magnification of bortezomib-induced stress granule formation in HeLa scramble and PRMT6 shRNA cell lines using DDX3 as a marker. DAPI was used to stain the nucleus.

39.6%, and 37.8% in one PRMT6 shRNA expressing cell population, and 4.1%, 10.3%, 17.4%, 20.9% and 20.2% in an additional cell population contained bortezomib-induced stress granules. With both FMRP and DDX3 a statistically significant result was observed using a two way ANOVA with a p-value less than one percent.

To confirm that PRMT6 depletion results in a decrease in bortezomib-induced stress granules, an additional cell line was examined. MCF7 cells are a bortezomib-resistant cell line and form stress granules upon treatment with bortezomib (Marx et al., 2007; Fournier et al., 2010). Stable MCF7 PRMT6 shRNA expressing cells were established (Figure 4.4A) and the formation of bortezomib-induced stress granules was investigated 4 h post bortezomib treatment using the same stress granule markers: TIA-1, FMRP, and DDX3 (Figure 4.4B & 4.4C). 4 h post bortezomib treatment was selected, as in HeLa cells the highest percentage of scramble shRNA expressing cells contained stress granules. Using TIA-1, 4 h post bortezomib treatment, 60.4% of scramble shRNA expressing cells contained stress granules, while in two PRMT6 depleted MCF7 cell populations 18.2% and 15.8% of cells contained stress granules, respectively. In FMRP-stained cells, 63.3% of scramble shRNA expressing cells and only 30.6% and 30.1% of PRMT6 shRNA expressing cells contained stress granules. Utilizing DDX3, 23% of cells PRMT6 depleted cell population compared to 60.4% of scramble shRNA expressing cells contained stress granules. Using a one way ANOVA, with all three stress granule markers, TIA-1, FMRP, or DDX3, a statistically significant difference with a p-value less than one percent between was observed.

In contrast to MCF7 cells, MDA MB 231 cells are bortezomib-sensitive cells and

4.4A)

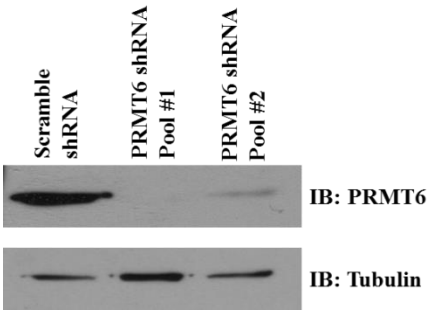
Scramble shRNA
PRMT6 shRNA Pool #1
PRMT6 shRNA Pool #2
IB: PRMT6
IB: Tubulin

B)

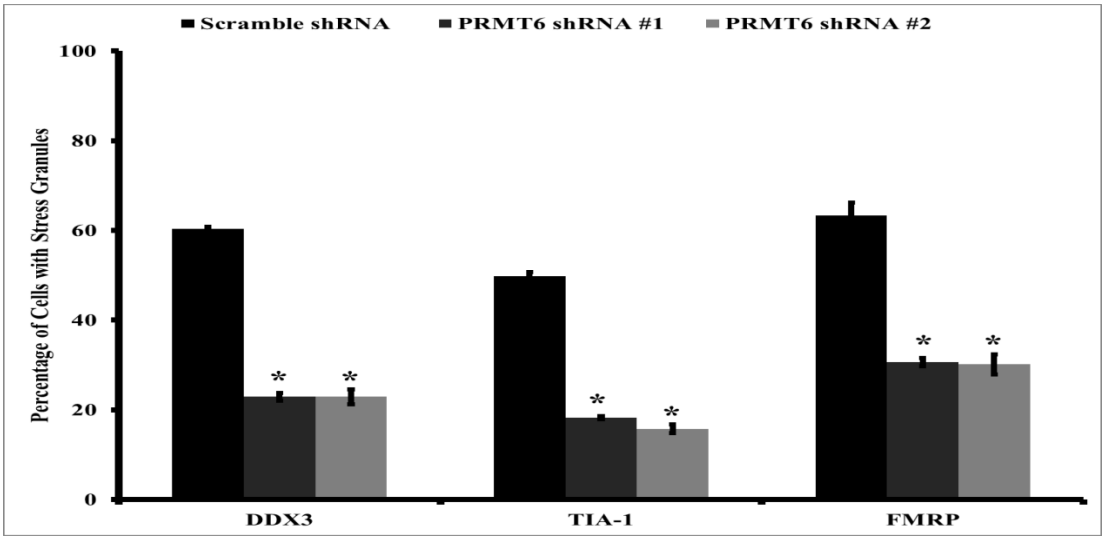
Scramble shRNA
PRMT6 shRNA #1
PRMT6 shRNA #2
Percentage of Cells with Stress Granules
100
80
60
40
20
0
*
DDX3
TIA-1
FMRP

C)

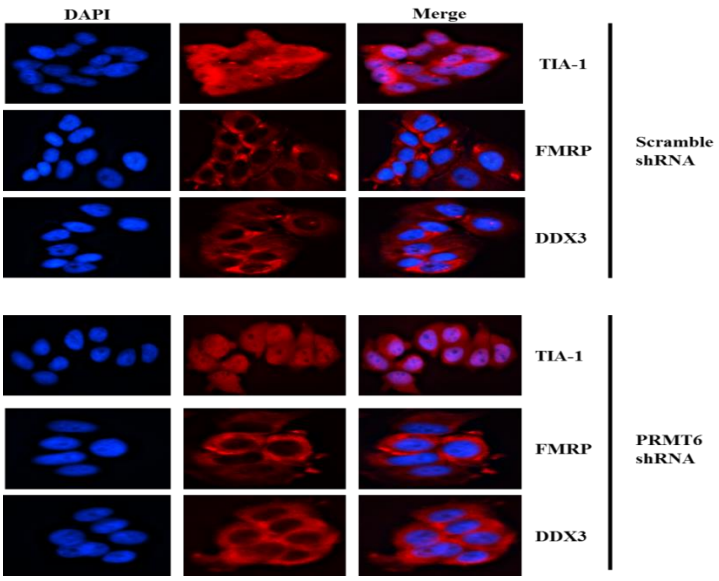
DAPI
Merge
TIA-1
FMRP
DDX3
Scramble shRNA
PRMT6 shRNA

Figure 4.4: Depletion of PRMT6 Results in a Reduction in Bortezomib-Induced Stress Granules in MCF7 Cells

A) Western Blot depicting knockdown of PRMT6 in MCF7 cells. Tubulin was used as a loading control. b) MCF7 scramble and PRMT6 shRNA expressing cells were treated for 4 h with 10 μM bortezomib and immunofluorescence was performed using TIA-1, FMRP, or DDX3 as markers for stress granule formation. The percentage of cells with stress granules was determined by counting at least 300 cells per coverslip. Data represents the average of three independent experiments +/- the standard error of the mean. * denotes statistical significance at a p-value <0.01 using a one way ANOVA. (B) Representative images at 40X magnification of bortezomib-induced stress granule formation in MCF7 scramble and PRMT6 shRNA expressing cell lines using TIA-1, FMRP, and DDX3 as markers. DAPI was used to stain the nucleus.

don’t form stress granules upon treatment with bortezomib (Tseng et al., 2012; Fournier et al., 2010). Therefore, in contrast to both HeLa and MCF7 cells where PRMT6 depletion had a significant effect on stress granule formation, no effect should be observed. MDA MB 231 PRMT6 shRNA stably-expressing cells were established (Figure 4.5A) and treated with bortezomib for 4 h, with FMRP was used as a stress granule marker. In both scramble and PRMT6 shRNA expressing cells, less than 5% cells formed stress granules upon treatment with bortezomib (Figure 4.5B & 4.5C). No statistical difference was observed between scramble and PRMT6 shRNA expressing cell lines using a one way ANOVA.

To determine if PRMT6 depletion inhibits stress granule formation upon just bortezomib treatment, or if the effect is consistent across different cellular stress, HeLa scramble and PRMT6 shRNA expressing cells were treated with sodium arsenite to induce oxidative stress. Upon cellular treatment with 500 µM for 30 min, a normal dose used to induce stress granule formation, no difference in the percentage of scramble and PRMT6 shRNA expressing cells containing stress granules was observed. This result was confirmed using the stress granule markers DDX3, FMRP, and TIA-1 (Appendix Ia). However, when cells were treated with 100 µM sodium arsenite for 30 min, a significant reduction in the percentage of PRMT6 shRNA expressing cells containing stress granules was observed. Using DDX3 as a marker, 44.6% of scramble shRNA expressing cells compared to 27.6% and 20.6% of PRMT6 shRNA expressing cells contained stress granules. Likewise, for FMRP, 61.5%, 19.7%, and 29.7%, and for TIA-1, 32.4%, 14.6%, and 21.6% of scramble shRNA and two PRMT6 shRNA expressing cells, respectively contained stress granules (Figure 4.6). Results were statistically significant as determined

4.5A)

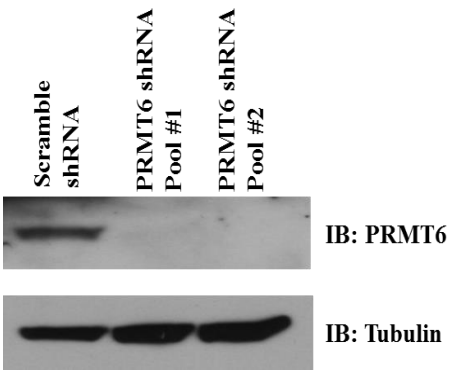
Scramble shRNA
PRMT6 shRNA Pool #1
PRMT6 shRNA Pool #2
IB: PRMT6
IB: Tubulin

B)

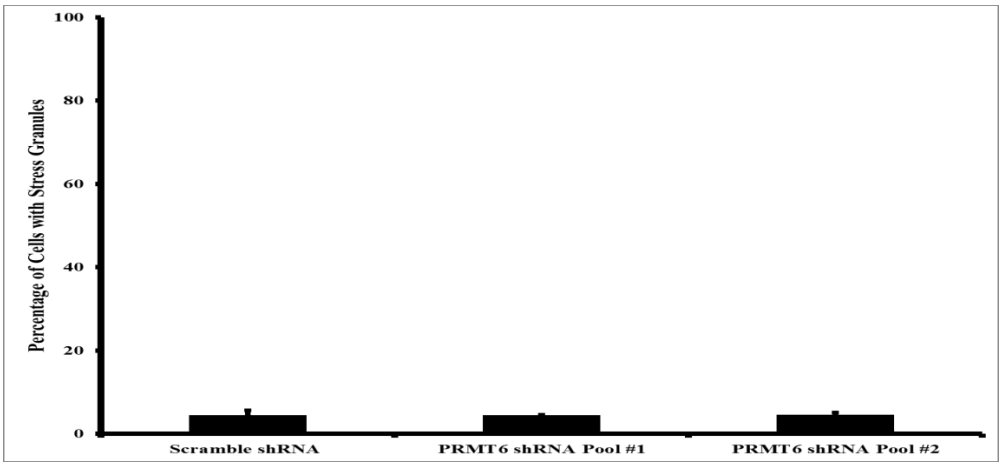
Percentage of Cells with Stress Granules
100
80
60
40
20
0
Scramble shRNA
PRMT6 shRNA Pool #1
PRMT6 shRNA Pool #2

C)

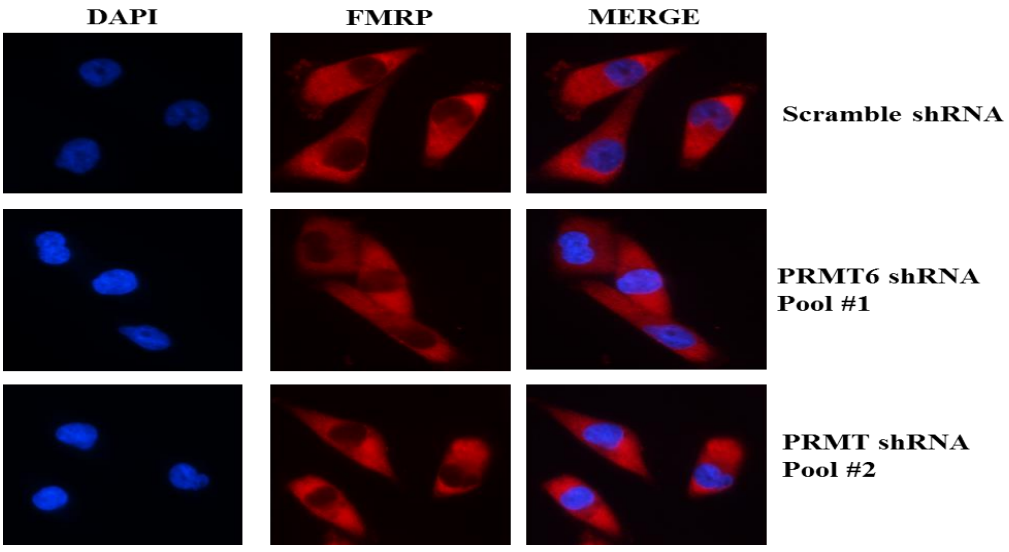
DAPI
FMRP
MERGE
Scramble shRNA
PRMT6 shRNA Pool #1
PRMT shRNA Pool #2

Figure 4.5: PRMT6 Depletion does not Influence Bortezomib-Induced Stress Granule Formation in MDA MB 231 Cells

(A) Western blot depicting knockdown of PRMT6 in MDA MB 231 cells. Tubulin was used as a loading control. (B) MDA MB 231 scramble and PRMT6 shRNA expressing cells were treated for 4 h with 10 μM bortezomib and immunofluorescence was performed using FMRP as a marker for stress granule formation. The percentage of cells with stress granules was determined by counting at least 300 cells per coverslip. Data represents the average of three independent experiments +/- the standard error of the mean. (C) Representative images at 40X magnification of bortezomib-induced stress granule formation in MDA MB 231 scramble and PRMT6 shRNA cell lines using FMRP as a marker for stress granules. DAPI was used to stain the nucleus.

using a one way ANOVA.

4.2 Re-Introduction of PRMT6 Rescues Bortezomib-Induced Stress Granules Formation

To confirm that PRMT6 is instrumental in the formation of bortezomib-induced stress granules, a rescue experiment was performed where PRMT6 was re-introduced in HeLa PRMT6 depleted cells. HeLa scramble shRNA cells were mock transfected (transfection reagent only) or transfected with an empty vector construct; while PRMT6 shRNA expressing cells were mock transfected, transfected with an empty vector construct or transfected with a flag-tagged PRMT6 construct for 48 h. Transfection of flag-tagged PRMT6 in PRMT6 depleted cells resulted in an increase of PRMT6 protein levels above the expression level of PRMT6 in the scramble shRNA cells (Figure 4.7A). Forty-eight hours post-transfection, cells were treated with 10 μM bortezomib for 4 h to induce stress granule formation. In scramble shRNA cells, 78.6% and 78.1% of cells contained stress granules in mock and empty vector transfected cells, respectively. In contrast, in PRMT6 depleted cells only 23.1% and 24.7% of mock or empty vector transfected cells, respectively contained stress granules. Re-introduction of PRMT6 resulted in a partial rescue in stress granule formation with 50.8% of cells containing stress granules (Figure 4.7B & 4.7C). Transfection of scramble and PRMT6 shRNA expressing cells with an empty vector construct resulted in the same statistical difference that was previously observed. However, re-introduction of PRMT6 resulted in a partial rescue of stress granule formation in flag-tagged PRMT6 transfected cells. Statistical significance was determined using a one way ANOVA. The PRMT6 shRNA targets the 3'-UTR of PRMT6, and therefore should not target the flag-tagged PRMT6 construct

4.6A)

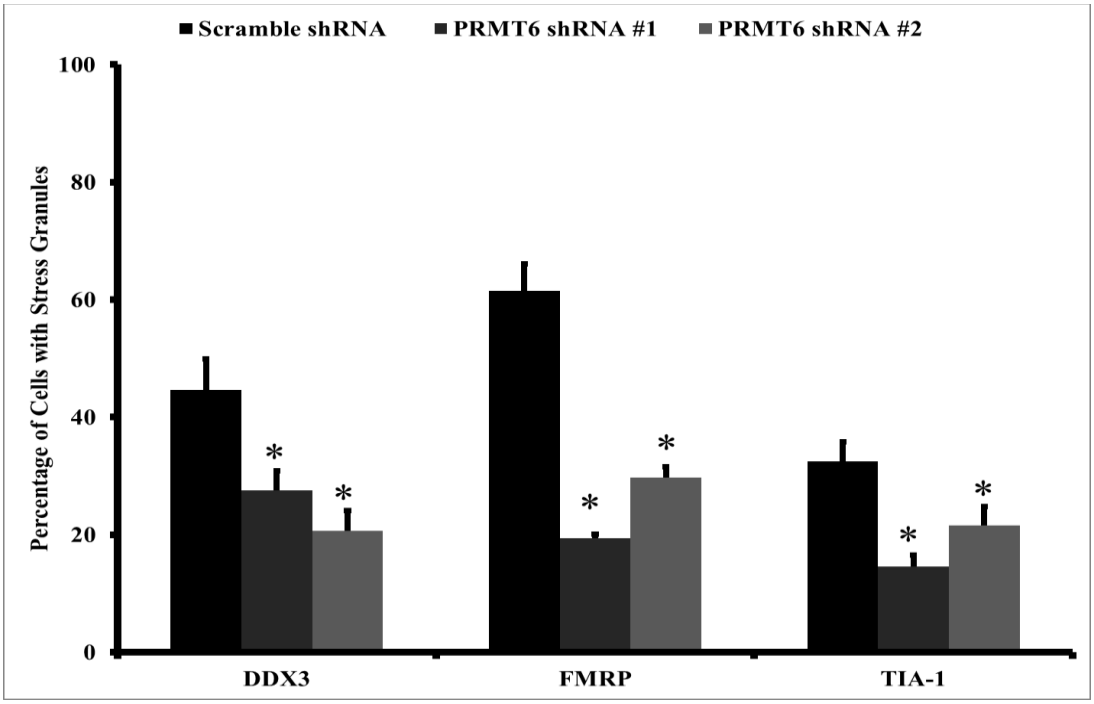
Scramble shRNA
PRMT6 shRNA #1
PRMT6 shRNA #2
Percentage of Cells with Stress Granules
100
80
60
40
20
0
*
DDX3
FMRP
TIA-1

B)

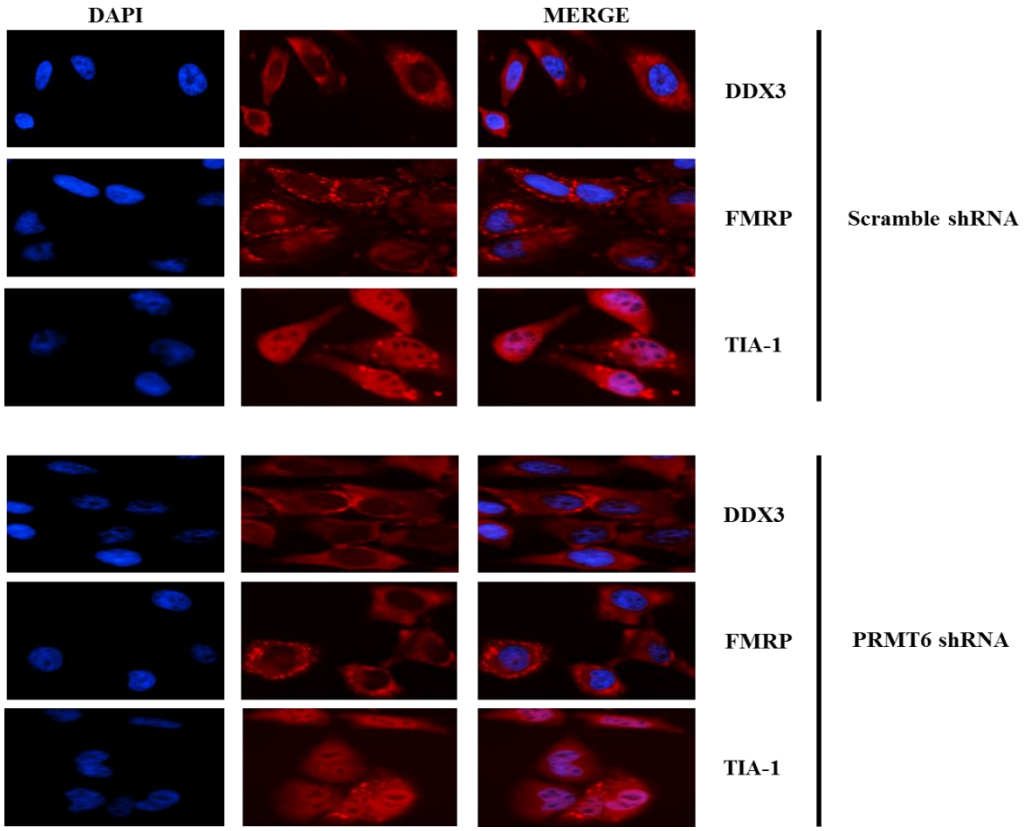
DAPI
MERGE
DDX3
FMRP
TIA-1
Scramble shRNA
DDX3
FMRP
TIA-1
PRMT6 shRNA

Figure 4.6: PRMT6 Depletion Influences Stress Granule Formation upon Low Doses of Sodium Arsenite

HeLa scramble or two pools of PRMT6 shRNA expressing stable cell lines were treated with 100μM sodium arsenite for 30 min and immunofluorescence was performed using DDX3, FMRP, and TIA-1 as markers for stress granule formation. (A) Graphical representation depicting a decrease in the percentage of PRMT6 shRNA expressing cells with stress granules. The percentage of cells containing stress granules was determined by counting at least 300 cells per coverslip. Data is the mean from three independent experiments +/- the standard error of the mean. * denotes statistical significance at a p-value <0.01 using a one way ANOVA. (B) Representative images at 40X magnification of sodium arsenite-induced stress granule formation in HeLa scramble and PRMT6 shRNA expressing cell lines using DDX3, FMRP, and TIA-1 as markers. DAPI was used to stain the nucleus.

4.7A)

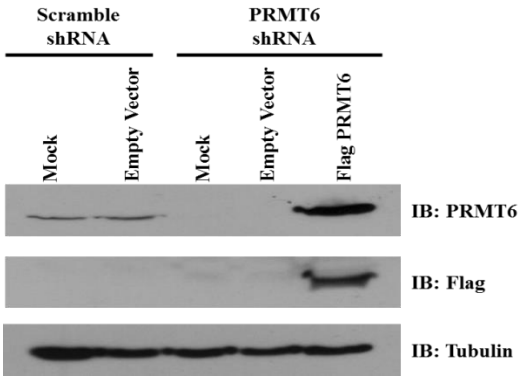
Scramble shRNA
PRMT6 shRNA
Mock
Empty Vector
Mock
Empty Vector
Flag PRMT6
IB: PRMT6
IB: Flag
IB: Tubulin

B)

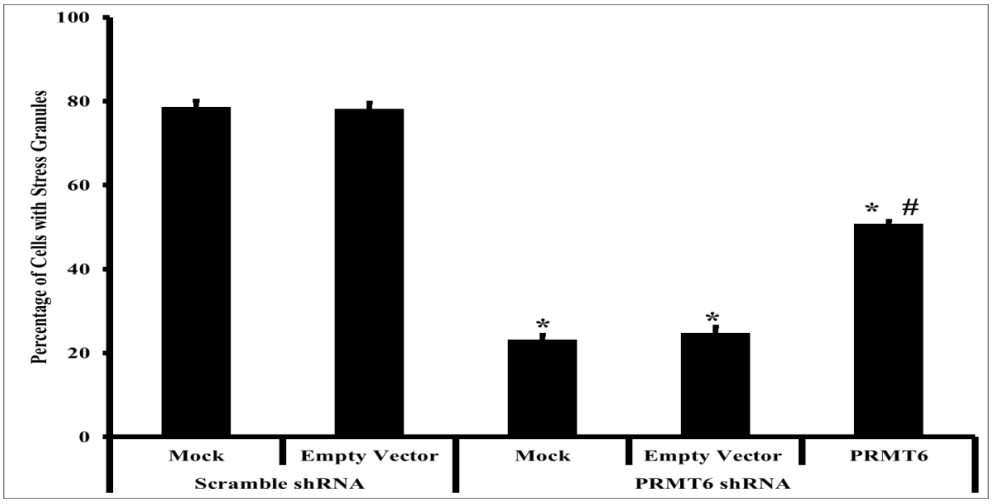
Percentage of Cells with Stress Granules
100
80
60
40
20
0
*
*
* #
Mock
Empty Vector
Mock
Empty Vector
PRMT6
Scramble shRNA
PRMT6 shRNA

C)

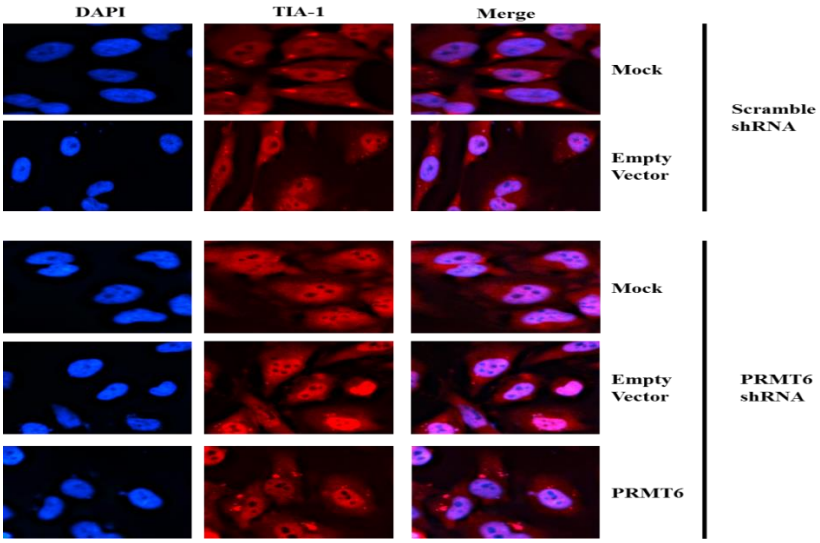
DAPI
TIA-1
Merge
Mock
Empty Vector
Scramble shRNA
Mock
Empty Vector
PRMT6
PRMT6 shRNA

Figure 4.7: Re-Introduction of PRMT6 in PRMT6 Depleted Cells Partially Rescues the Effect of Bortezomib-Induced Stress Granules

HeLa scramble shRNA stably-expressing cells were mock transfected or transfected with an empty vector while PRMT6 shRNA stably-expressing cells were mock transfected, transfected with an empty vector or transfected with a flag-tagged PRMT6 for 48 h and then treated with 10 μM bortezomib for 4 h. (A) Western Blot analysis showing PRMT6 protein levels (top panel) and Flag expression (middle panel). Tubulin is used as a loading control (bottom panel). (B) Analysis of the percentage of cells containing bortezomib-induced stress granules. Re-introduction of PRMT6 resulted in a fifty percent increase in the percentage of cells with stress granules. (C) Representative images at 40X magnification of bortezomib-induced stress granule formation in HeLa scramble and PRMT6 shRNA cell lines using TIA-1 as a marker for stress granules. DAPI was used to stain the nucleus.

illustrating the specificity of the shRNA and providing confidence that the effect of PRMT6 on stress granule formation is real. Therefore, this result implicates PRMT6 as functioning in the formation of bortezomib-induced stress granules.

4.3 Overexpression of PRMT6 does not Alter Bortezomib-Induced Stress Granule Formation

PRMT6 depletion results in reduced stress granule formation in bortezomib resistant cell lines. Therefore, the potential of PRMT6 overexpression to induce stress granule formation, and the effect of this overexpression to influence bortezomib-induced stress granule formation, was investigated. HeLa cells were transfected with a flag-tagged empty vector or flag-tagged PRMT6 for 48 h and then treated with 10 μM bortezomib for 4 h. Cells were co-stained with a flag antibody to identify cells expressing exogenous PRMT6 and the stress granule marker DDX3. Flag-tagged PRMT6 localized predominantly to the nucleus, consistent with localization of endogenous PRMT6 (Frankel et al., 2002). Alone, PRMT6 overexpression did not induce stress granule formation (Figure 4.8A). Furthermore, no difference in stress granule formation was observed in flag-tagged PRMT6 expressing cells compared to empty vector transfected cells upon bortezomib treatment. Sixty-five percent of cells contained stress granules (Figure 4.8A & 4.8B). Statistical analysis with a Student T-test showed no difference in stress granule formation in flag-tagged empty vector or flag-tagged PRMT6 transfected cells. Therefore, these results suggest that, although PRMT6 depletion does have an effect on stress granule formation, at least in HeLa cells, PRMT6 overexpression does not impact stress granule formation.

4.8A)

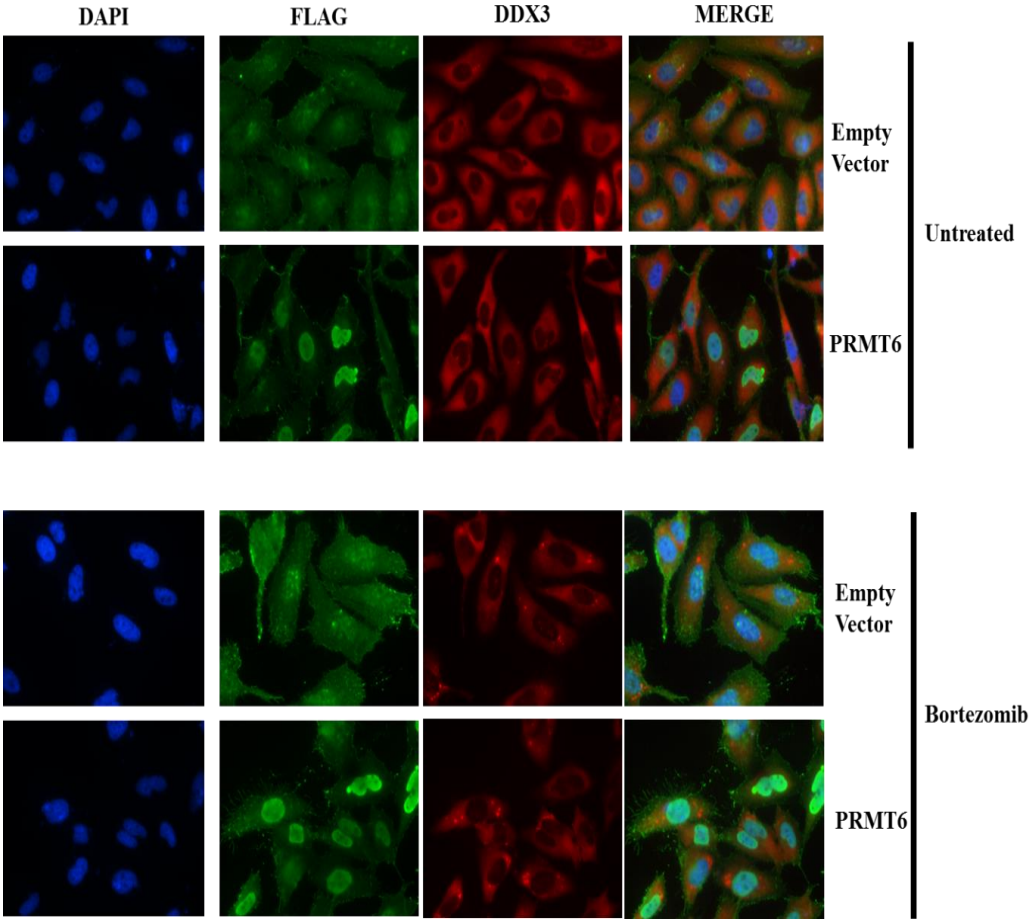
DAPI
FLAG
DDX3
MERGE
Empty Vector
PRMT6
Untreated
Empty Vector
PRMT6
Bortezomib

B)

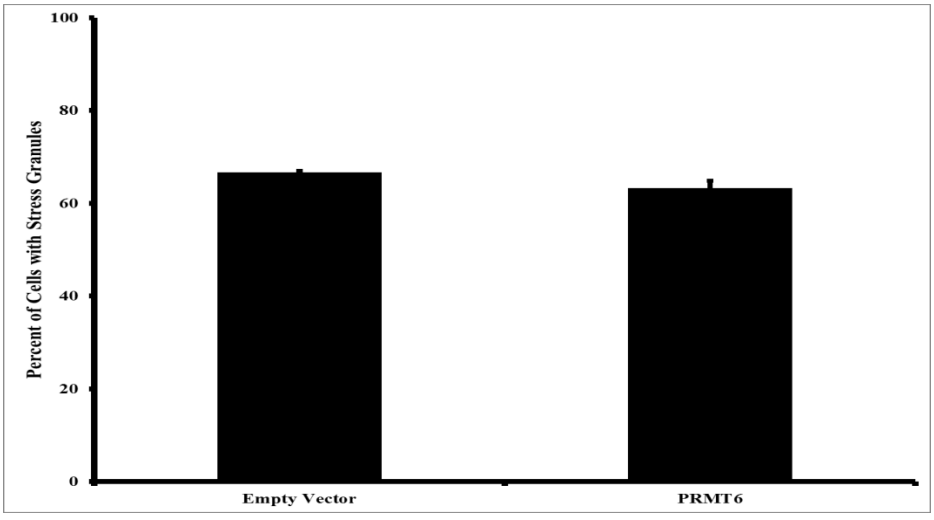
Percent of Cells with Stress Granules
100
80
60
40
20
0
Empty Vector
PRMT6

Figure 4.8: Overexpression of PRMT6 does not Influence Bortezomib-Induced Stress Granule Formation

HeLa cells were transfected with flag-tagged empty vector or flag-tagged PRMT6 for 48 h and then treated with 10 µM bortezomib for 4 h. (A) Representative images at 40X magnification of untreated or bortezomib treatment cells in HeLa cell lines using DDX3 as a marker for stress granules. DAPI was used to stain the nucleus. (B) Graphical analysis showing approximately 65% of flag-tagged empty vector or flag-tagged PRMT6 transfected cells with stress granules upon 10 µM bortezomib treatment. Results are the average +/- the standard error of the mean of three independent experiments counting at least 300 cells per coverslip.

4.4 PRMT6 Protein Expression is Induced upon Bortezomib Treatment

To gain insight into the potential mechanism by which PRMT6 functions in bortezomib-induced stress granule formation, PRMT6 protein and mRNA expression levels were examined. HeLa scramble and PRMT6 shRNA expressing cells were treated with 10 µM bortezomib for 4 h and 10 h. These time points were selected as 4 h post treatment is the time point where the highest percentage of cells contain stress granules; stress granules disassemble upon prolonged treatment with bortezomib, and 10 h post treatment, stress granules have disassembled in cell lines examined (Fournier et al., 2010). In untreated cells, PRMT6 protein levels are undetectable in PRMT6 depleted cells compared to scramble shRNA expressing cells. Upon treatment with bortezomib, a 3-fold induction in PRMT6 protein levels 4 h post treatment, and a 3.8-fold increase 10 h post treatment is observed in scramble shRNA expressing cells (Figure 4.9A & 4.9B). In both PRMT6 depleted cell populations, no detectable PRMT6 protein expression was observed 4 h or 10 h post-bortezomib treatment.

To determine if the increase in PRMT6 expression is transcriptionally or translationally regulated upon bortezomib treatment, PRMT6 mRNA levels were investigated. Similarly, as above, HeLa scramble and PRMT6 shRNA expressing cells were treated with 10 µM bortezomib for 4 h and 10 h. In scramble shRNA expressing cells, upon bortezomib treatment a 40% reduction in PRMT6 mRNA expression is observed (Figure 4.10A & 4.10B). In untreated PRMT6 shRNA expressing cells, basal PRMT6 mRNA levels are 40% lower compared to scramble shRNA expressing cells.

4.9A)

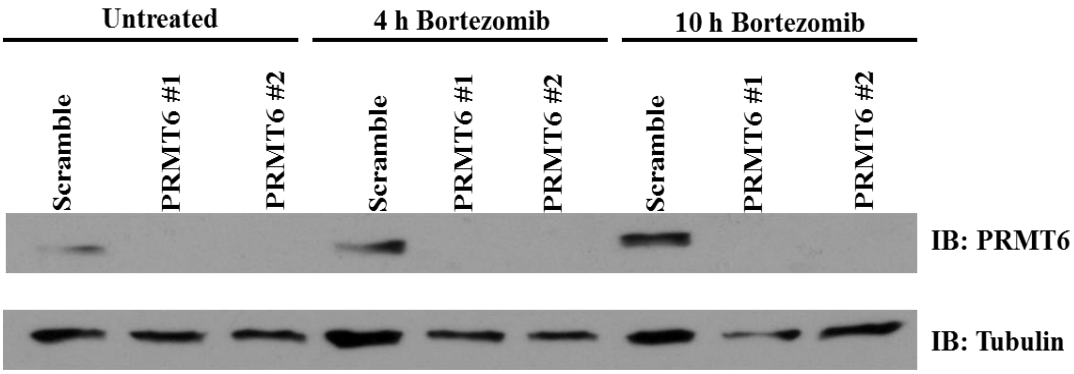
Untreated
4 h Bortezomib
10 h Bortezomib
Scramble
PRMT6 #1
PRMT6 #2
Scramble
PRMT6 #1
PRMT6 #2
Scramble
PRMT6 #1
PRMT6 #2
IB: PRMT6
IB: Tubulin

B)

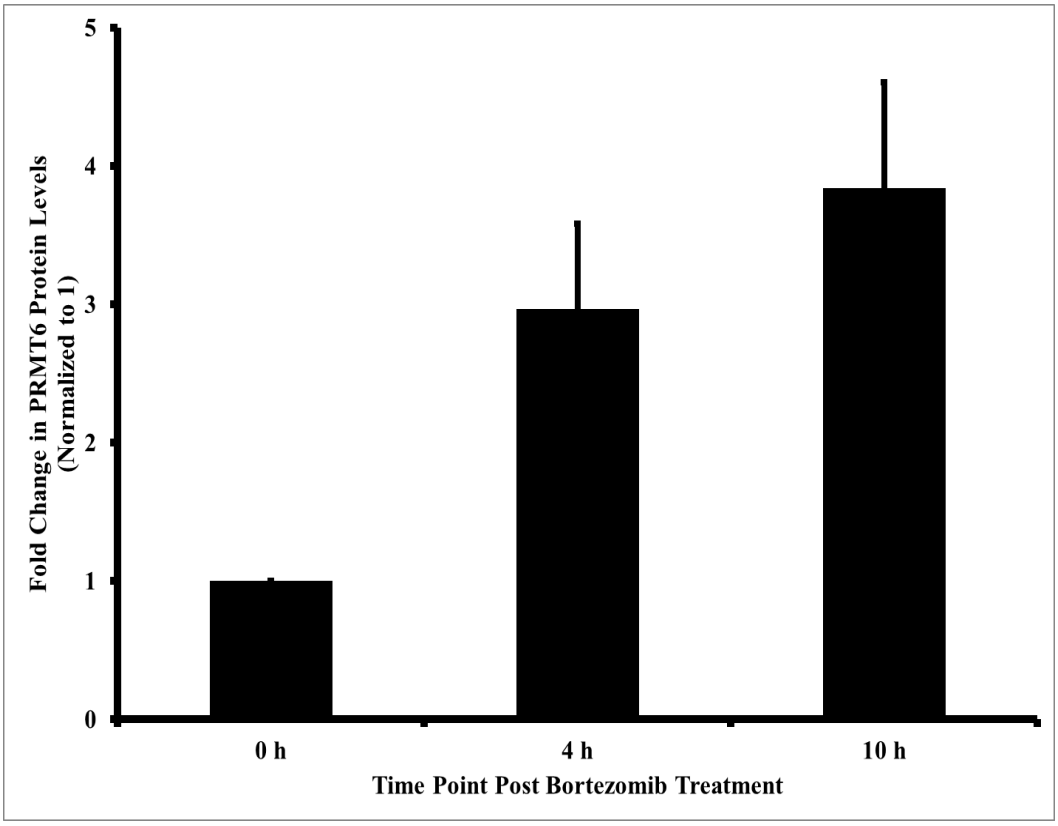
Fold Change in PRMT6 Protein Levels (Normalized to 1)
5
4
3
2
1
0
0 h
4 h
10 h
Time Point Post Bortezomib Treatment

Figure 4.9: PRMT6 Protein Expression is Induced upon Treatment with Bortezomib

(A) HeLa scramble and PRMT6 shRNA stably-expressing cells were treated with 10 μM bortezomib for 4 h and 10 h. Western blot analysis showing increased PRMT6 protein levels in scramble shRNA cells upon treatment with bortezomib. PRMT6 protein levels were undetectable in PRMT6 shRNA stably-expressing cells in untreated cells and upon treatment with bortezomib. Tubulin was used as a loading control. (B). Densitometry analysis of PRMT6 protein levels in scramble shRNA with PRMT6 protein levels normalized to tubulin levels. A 3-fold increase and a 3.8-fold increase 4h and 10 h post bortezomib treatment, respectively in PRMT6 protein levels were observed. Data represents the average from three independent experiments +/- the standard error of the mean.

4.10A)

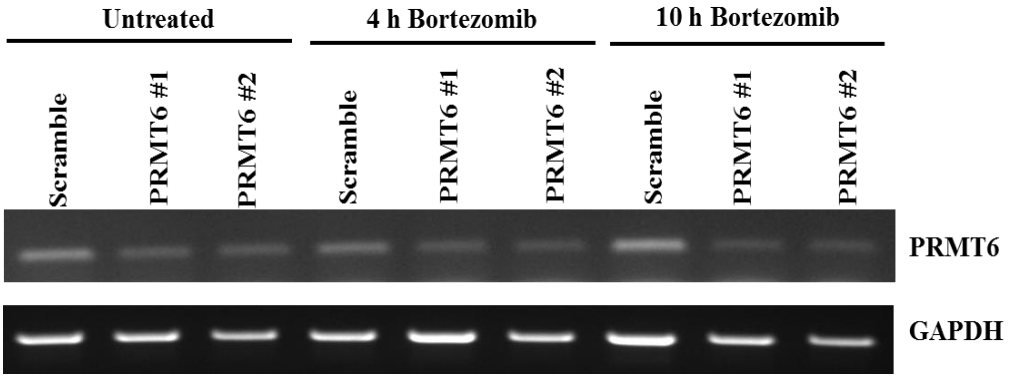
Untreated
4 h Bortezomib
10 h Bortezomib
Scramble
PRMT6 #1
PRMT6 #2
Scramble
PRMT6 #1
PRMT6 #2
Scramble
PRMT6 #1
PRMT6 #2
PRMT6
GAPDH

B)

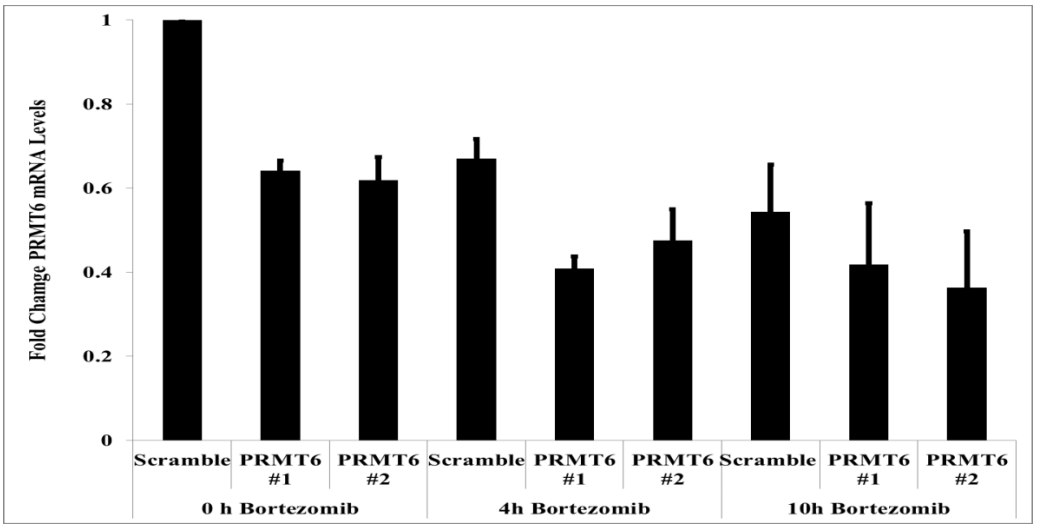
Fold Change PRMT6 mRNA Levels
1
0.8
0.6
0.4
0.2
0
Scramble
PRMT6 #1
PRMT6 #2
Scramble
PRMT6 #1
PRMT6 #2
Scramble
PRMT6 #1
PRMT6 #2
0 h Bortezomib
4h Bortezomib
10h Bortezomib

C)

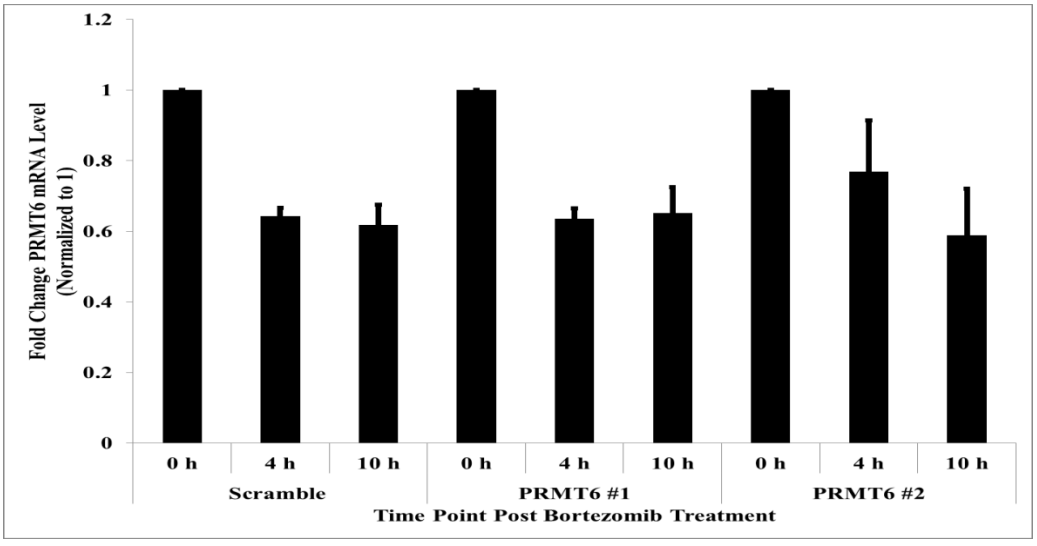
Fold Change PRMT6 mRNA Level (Normalized to 1)
1.2
1
0.8
0.6
0.4
0.2
0
0 h
4 h
10 h
0 h
4 h
10 h
0 h
4 h
10 h
Scramble
PRMT6 #1
PRMT6 #2
Time Point Post Bortezomib Treatment

Figure 4.10: PRMT6 mRNA Expression Decreases upon Treatment with Bortezomib

(A) HeLa scramble and PRMT6 shRNA stably-expressing cells were treated with 10 μM bortezomib for 4 h and 10 h. PCR analysis of cDNA generated from total RNA with PRMT6 primers shows a decrease in PRMT6 mRNA levels in both scramble and PRMT6 shRNA stably-expressing cells upon treatment with bortezomib. GAPDH was used as a loading control. (B) Densitometry analysis of PRMT6 mRNA expression in scramble and PRMT6 stably-expressing cells normalized to the loading control GAPDH (C) Data was normalized to 1 to allow for a direct comparison between PRMT6 mRNA expression in the scramble and PRMT6 shRNA stably-expressing cell lines. In both scramble and PRMT6 shRNA cells, a 40% reduction in PRMT6 mRNA levels is observed 4 h post-bortezomib treatment and this decrease continues 10 h post treatment. Data present in (B) and (C) is the average mRNA expression for three independent experiments +/- the standard error of the mean.

Upon bortezomib treatment, in PRMT6 shRNA expressing cells, a 30% decrease in mRNA expression occurs relative to untreated PRMT6 shRNA expressing cells (Figure 4.10A & 4.10B). To allow for a direct comparison between scramble and PRMT6 shRNA expressing cells, PRMT6 mRNA expression was normalized to one. Upon normalization, in both scramble and PRMT6 shRNA expressing cells, a 40% reduction in PRMT6 mRNA levels was observed 4 h post treatment, and persisted through 10 h post treatment (Figure 4.10C).

Since PRMT6 mRNA levels could have initially increased and then decreased to account for the increased PRMT6 protein levels, PRMT6 mRNA levels were examined at earlier time points. Both HeLa scramble and PRMT6 shRNA expressing cells were treated with 10 μM bortezomib for 1, 2, 3, and 4 h (Figure 4.11A & 4.11B). Upon normalization of the data, in both scramble and PRMT6 shRNA expressing cells a gradual decrease in PRMT6 mRNA levels is observed through to 4 h post treatment (Figure 4.11C).

Since bortezomib is a chemotherapeutic drug that inhibits the proteasome, it was examined whether the observed induction of PRMT6 protein expression was due to cellular stress, or if PRMT6 is a potential target of the proteasome, and therefore accumulates upon its inhibition. HeLa scramble shRNA expressing cells were treated for 1, 2, 3, and 4 h with 10 μM bortezomib, 50 μM of the proteasome inhibitor MG132, or 500 μM sodium arsenite, an inducer of oxidative stress that additionally promotes the formation of stress granules. Upon bortezomib treatment, a gradual induction of PRMT6 protein levels is observed up to 4 h post treatment (Figure 4.12). A similar increase in

4.11A)

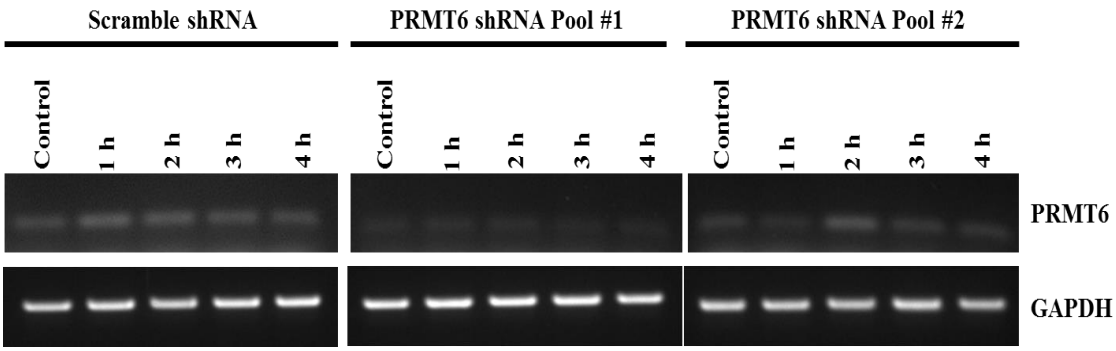
Scramble shRNA
PRMT6 shRNA Pool #1
PRMT6 shRNA Pool #2
Control
1 h
2 h
3 h
4 h
PRMT6
GAPDH

B)

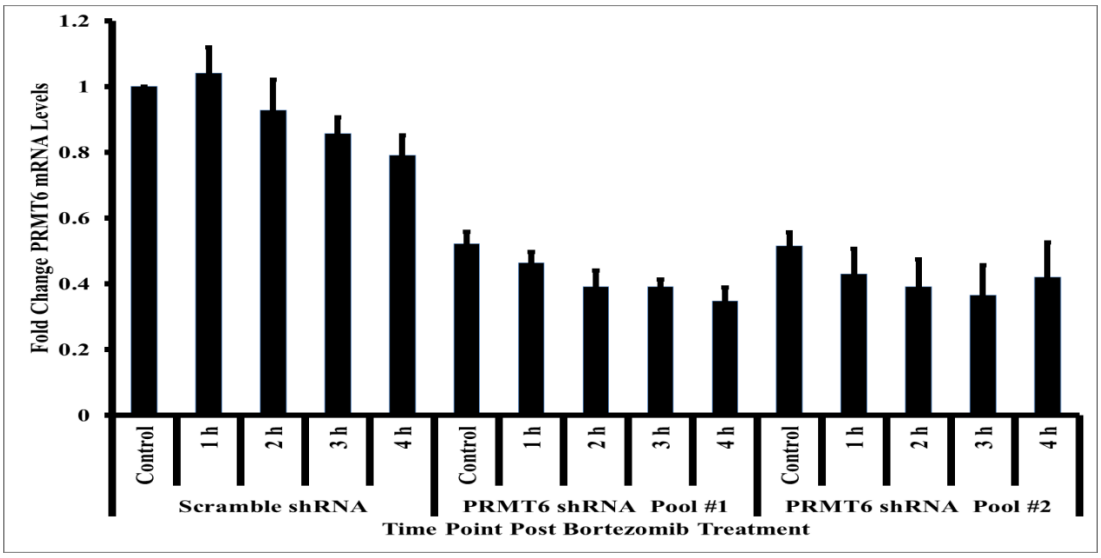
Fold Change PRMT6 mRNA Levels
1.2
1
0.8
0.6
0.4
0.2
0
Control
1 h
2 h
3 h
4 h
Scramble shRNA
PRMT6 shRNA Pool #1
PRMT6 shRNA Pool #2
Time Point Post Bortezomib Treatment

C)

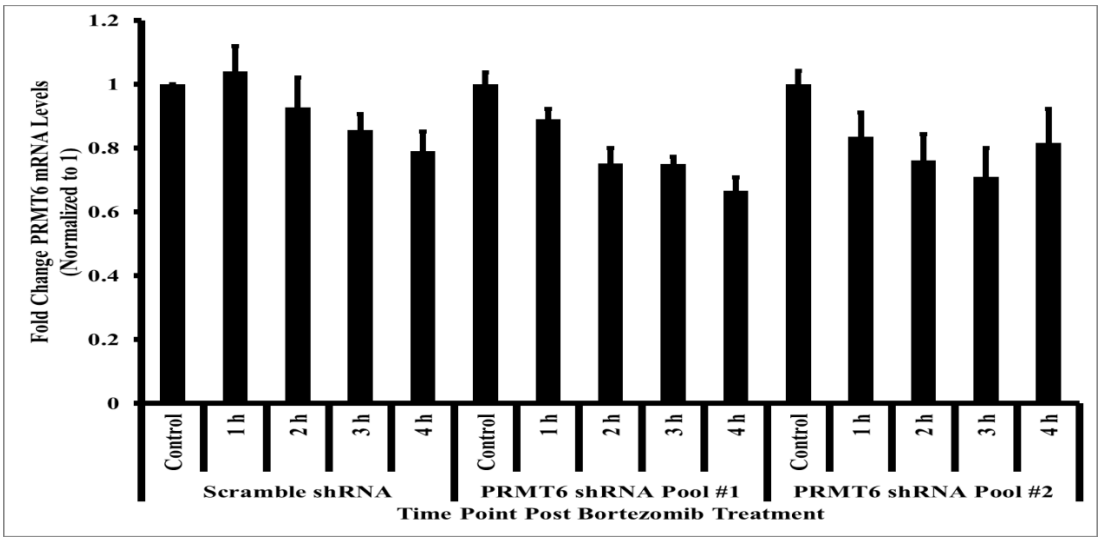
Fold Change PRMT6 mRNA Levels
(Normalized to 1)
1.2
1
0.8
0.6
0.4
0.2
0
Control
1 h
2 h
3 h
4 h
Scramble shRNA
PRMT6 shRNA Pool #1
PRMT6 shRNA Pool #2
Time Point Post Bortezomib Treatment

Figure 4.11: PRMT6 Expression is Not Transcriptionally Regulated upon Treatment with Bortezomib

(A) HeLa scramble and PRMT6 shRNA stably-expressing cells were treated for 1, 2, 3, and 4 h with 10 μM bortezomib. PCR analysis of cDNA generated from total RNA with PRMT6 primers shows a decrease in PRMT6 mRNA levels in both scramble and PRMT6 shRNA stably-expressing cells upon treatment with bortezomib. GAPDH was used as a loading control. (B) Densitometry analysis of PRMT6 mRNA expression in scramble and PRMT6 stably-expressing cells normalized to the loading control GAPDH (C) Data was normalized to 1 to allow for a direct comparison between PRMT6 mRNA expression in the scramble and PRMT6 shRNA stably-expressing cell lines. In both the scramble and PRMT6 shRNA stably-expressing cells a similar gradual decrease in PRMT6 mRNA expression was observed upon treatment with bortezomib. Data present in (B) and (C) is the average mRNA expression for three independent experiments +/- the standard error of the mean.

4.12)

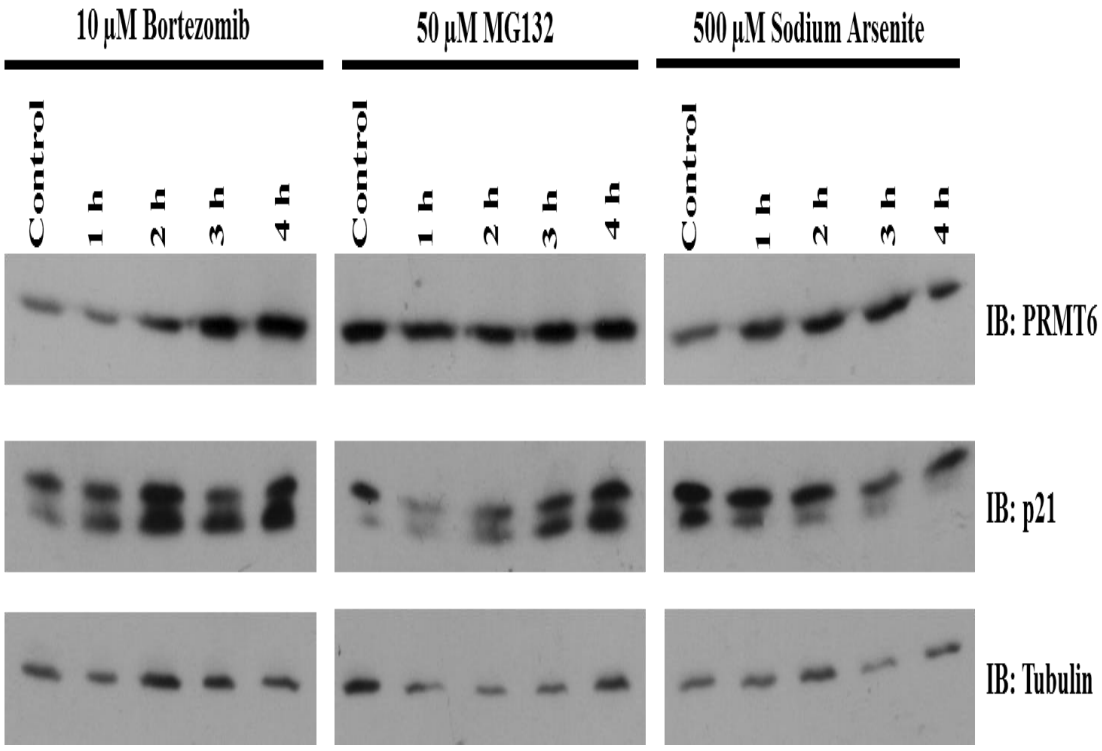
10 µM Bortezomib
50 µM MG132
500 µM Sodium Arsenite
Control
1 h
2 h
3 h
4 h
IB: PRMT6
IB: p21
IB: Tubulin

Figure 4.12: PRMT6 is not a Target of the 26S Proteasome

HeLa scramble shRNA stably-expressing cell lines were treated with 10 µM bortezomib, 50 µM MG132, or 500 µM sodium arsenite for 1, 2, 3 and 4 h. Western blot analysis shows that PRMT6 protein levels gradually increase upon treatment with bortezomib, and increase 1 h post sodium arsenite expression. However, upon treatment with MG132, PRMT6 protein levels stay constant (top panel). p21 protein levels increase upon treatment with bortezomib and MG132, and decrease with sodium arsenite (middle panel). Tubulin was used as a loading control.

PRMT6 protein levels was observed upon sodium arsenite treatment; albeit PRMT6 protein levels reached their maximum level 1 h post treatment, and persisted at this level until 4 h. However, cellular treatment with MG132 did not induce PRMT6 protein levels, suggesting that PRMT6 is not a target of the proteasome. Protein expression of p21, an established proteasome target was examined to confirm inhibition of the proteasome (Bloom et al., 2003). Additionally, decreased p21 protein expression is observed upon treatment with sodium arsenite (Lian and Gallouzi, 2009), while increased p21 protein expression is induced upon treatment with bortezomib and MG132 (Gareau et al., 2011). These results suggest that upon bortezomib treatment PRMT6 expression is translationally regulated, and that at least upon cellular treatment with bortezomib and sodium arsenite concentrations which promote stress granule formation that PRMT6 protein expression is induced.

4.5 PRMT6 Depletion Inhibits Formation of the eIF4E-eIF4G1 Complex

eIF4E plays a crucial role in translation initiation through recognition of the 5'-mRNA cap structure (7-methyl G(5')ppp(5')X, where X is any nucleoside) (Muthukrishnan et al., 1975). This interaction between eIF4E and the 5'-mRNA cap is stabilized by eIF4G, thus promoting translation initiation (Hentze, 1997). Moreover, it has been observed that the interaction between eIF4E and eIF4G is required for the formation of stress granules in a mammalian target of rapamycin complex 1 (mTORC1)-dependent manner. mTORC1 phosphorylates 4E-BP1 resulting in dissociation of 4E-BP1 from eIF4E, allowing for eIF4E association with eIF4G. Under stress conditions, eIF4E-eIF4G complexes may function as scaffolding proteins for the recruitment of yet unidentified proteins in an mTORC1-dependent manner to stress granules (Fournier et

al., 2013). Therefore, it was investigated whether depletion of PRMT6 could abrogate the interaction between eIF4E-eIF4G, thus inhibiting stress granule formation.

HeLa scramble and PRMT6 shRNA expressing cells were untreated or treated with 10 μM bortezomib for 4 h and cell lysate was incubated with m^7GTP-Sepharose beads, a mimic of the 5'mRNA cap, *in vitro*. Upon PRMT6 depletion, less eIF4E protein binds to the mRNA cap in unstressed condition (Figure 4.13) (middle panel, compare lanes 5 & 6). This is likely a result of the decreased eIF4E protein levels observed in PRMT6 depleted cells (compare lanes 1 & 2). Interestingly, treatment of either scramble or PRMT6 shRNA expressing cells with bortezomib yields a further decrease in eIF4E binding to the cap (scramble shRNA compare lanes 5 & 7; PRMT6 shRNA compare lanes 6 & 8). The decrease of eIF4E binding to the cap in PRMT6 depleted cells coincides with a decrease in eIF4G binding in untreated cells (top panel, compare lanes 5 & 6). Upon bortezomib treatment, a further reduction in eIF4G binding to the mRNA cap is observed. In contrast, DDX3, a protein which associates with eIF4E at the mRNA cap binds equally to the mRNA cap in both scramble and PRMT6 shRNA expressing cells (compare lanes 5 & 6). Though upon treatment with bortezomib, there is an increase in DDX3 binding to the mRNA cap in scramble shRNA expressing cells (compare lanes 5 & 7), which doesn't occur in PRMT6 shRNA expressing cells. These results suggest that PRMT6 mediates the eIF4E-eIF4G interaction through regulation of eIF4E.

To confirm that the results observed in the cap binding assay are attributed to a reduction in eIF4E protein levels in PRMT6 depleted cells, eIF4E protein levels were examined in two additional pools of PRMT6 shRNA expressing cell lines. Consistently, eIF4E protein levels were decreased in PRMT6 depleted cells (Figure 4.14A). This result

4.13)

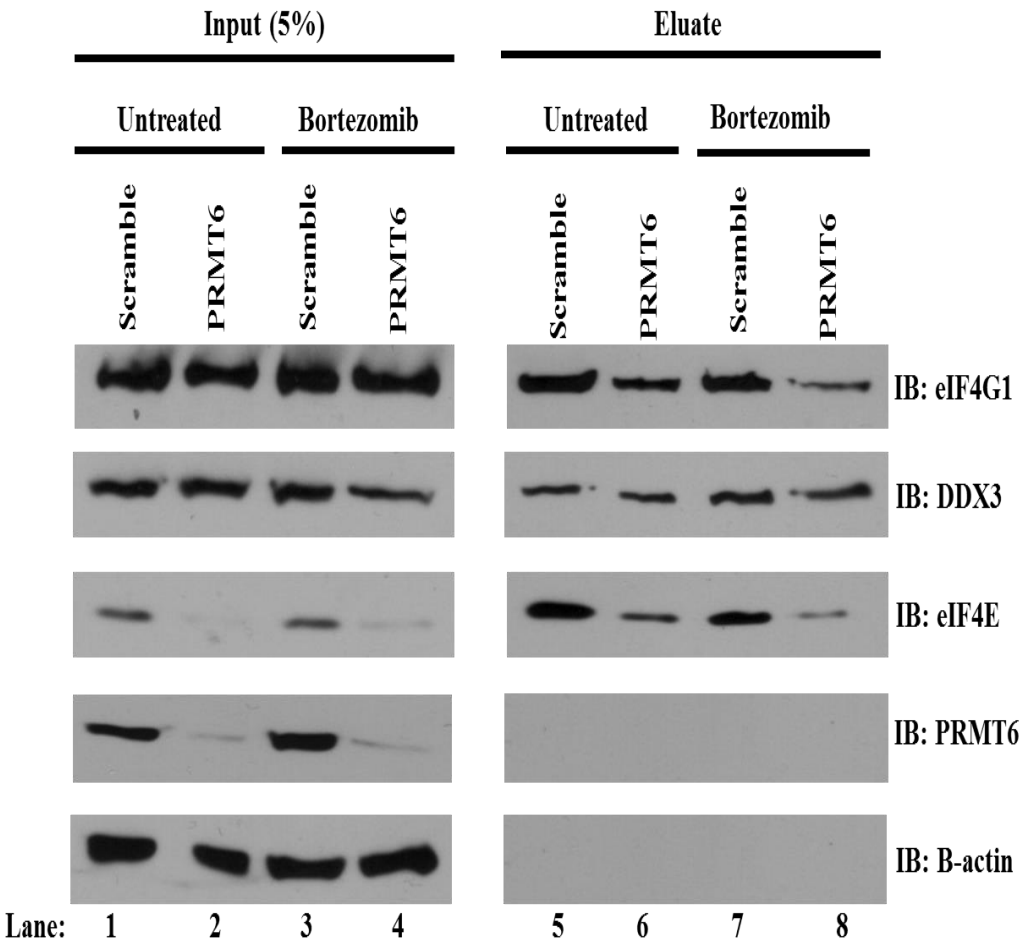
Input (5%)
Eluate
Untreated
Bortezomib
Untreated
Bortezomib
Scramble
PRMT6
Scramble
PRMT6
Scramble
PRMT6
Scramble
PRMT6
IB: eIF4G1
IB: DDX3
IB: eIF4E
IB: PRMT6
IB: B-actin
Lane: 1 2 3 4 5 6 7 8

Figure 4.13: PRMT6 Depletion Inhibits Formation of the eIF4E-eIF4G1 Complex

HeLa Scramble shRNA or PRMT6 shRNA expressing cells were untreated or treated with 10 μM bortezomib for 4 h and the cell lysate was incubated with m^7GTP-Sepharose beads. eIF4E bound proteins were eluted from the beads and resolved by SDS-PAGE and Western blotting. Five percent of the cell lysate was kept for input. β-actin was used as a loading control and to show specificity of binding to the m^7GTP-Separose beads. PRMT6 depletion results in an inhibition of formation of the eIF4E-eIF4G1 complex at the mRNA cap likely due to decreased eIF4E protein expression in PRMT6 depleted cell lines.

4.14A)

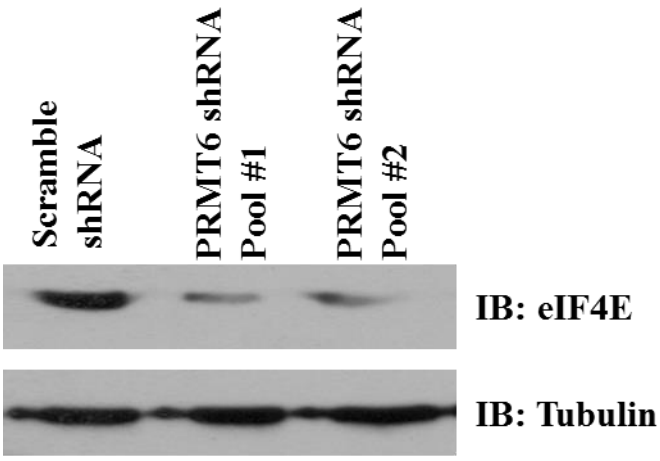
Scramble shRNA
PRMT6 shRNA Pool #1
PRMT6 shRNA Pool #2
IB: eIF4E
IB: Tubulin

B)

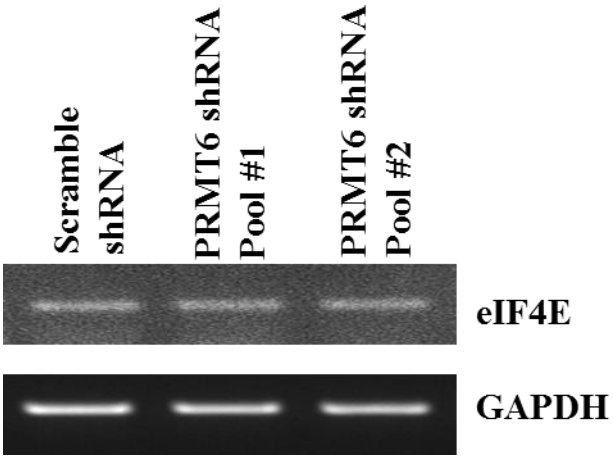
Scramble shRNA
PRMT6 shRNA Pool #1
PRMT6 shRNA Pool #2
eIF4E
GAPDH

Figure 4.14: PRMT6 Regulates eIF4E Protein Expression

Protein (A) or mRNA (B) was isolated from HeLa scramble or PRMT6 shRNA expressing cell lines. (A) Western blot depicting decreased eIF4E protein expression in PRMT6 depleted cell lines. Tubulin was used as a loading control. (B) PCR analysis of cDNA generated from total RNA with eIF4E primers showing no difference in eIF4E mRNA levels in both scramble and PRMT6 shRNA stably-expressing. GAPDH was used as a loading control.

confirms that PRMT6 regulates eIF4E expression. To determine if this regulation is at the transcriptional or translation level, eIF4E mRNA levels were examined. In PRMT6 depleted cells, eIF4E mRNA was unaffected in comparison to scramble shRNA expressing cells (Figure 4.14B), suggesting that PRMT6 regulates eIF4E post-translationally

4.6 PRMT6 Depletion Results in Decreased Cellular Survival in Bortezomib-Resistant Cancer Cells

Cancer cells form stress granules as a means of promoting cell survival upon induction of cellular stresses (Baguet et al., 2007; Mazroui et al., 2007; Arimoto et al., 2008; Eisinger-Mathason et al., 2008; Fournier et al., 2010). PRMT6 depletion in MCF7 cells, a bortezomib resistant cell line resulted in a decrease in stress granules formation. Therefore, the effect of PRMT6 depletion on cell survival was investigated to determine if there is a correlative link between a reduction in stress granule formation and cell survival. An equal number of MCF7 scramble and PRMT6 shRNA stably-expressing cells were plated and treated with 10 μM bortezomib or DMSO as a control for 24 h and a MTT assay was performed. Cell viability values were normalized to the DMSO control, with cell viability upon treatment with DMSO set to 1. Upon 10 μM bortezomib treatment of scramble shRNA stably-expressing cells, 24 h post-treatment, 81% cell viability was observed (Figure 4.15A). In contrast, upon PRMT6 depletion, 64% cell viability was observed. These results are statistically significant with a p-value less than one percent using a one way ANOVA.

MDA MB 231 cells are bortezomib-sensitive cells and form a minimal number of stress granules upon bortezomib treatment. Therefore, PRMT6 depletion should have no

effect on cell viability. An equal number of MDA MB 231 scramble and PRMT6 shRNA stably-expressing cells were plated and treated with 10 µM bortezomib or DMSO for 24 h and a MTT assay was performed. 35% cell viability was observed in the scramble shRNA expressing cells upon bortezomib treatment (Figure 4.15B). Likewise, in the PRMT6 shRNA expressing cell lines, a similar percentage of cells were viable 24h post bortezomib treatment. These results yielded no statistical difference in cell viability between the scramble and PRMT6 shRNA stably-expressing cell lines. These results show that PRMT6 depletion affects cell viability in MCF7 cells, a bortezomib resistant cell line while having no effect in bortezomib sensitive MDA MB 231 cells.

4.15A)

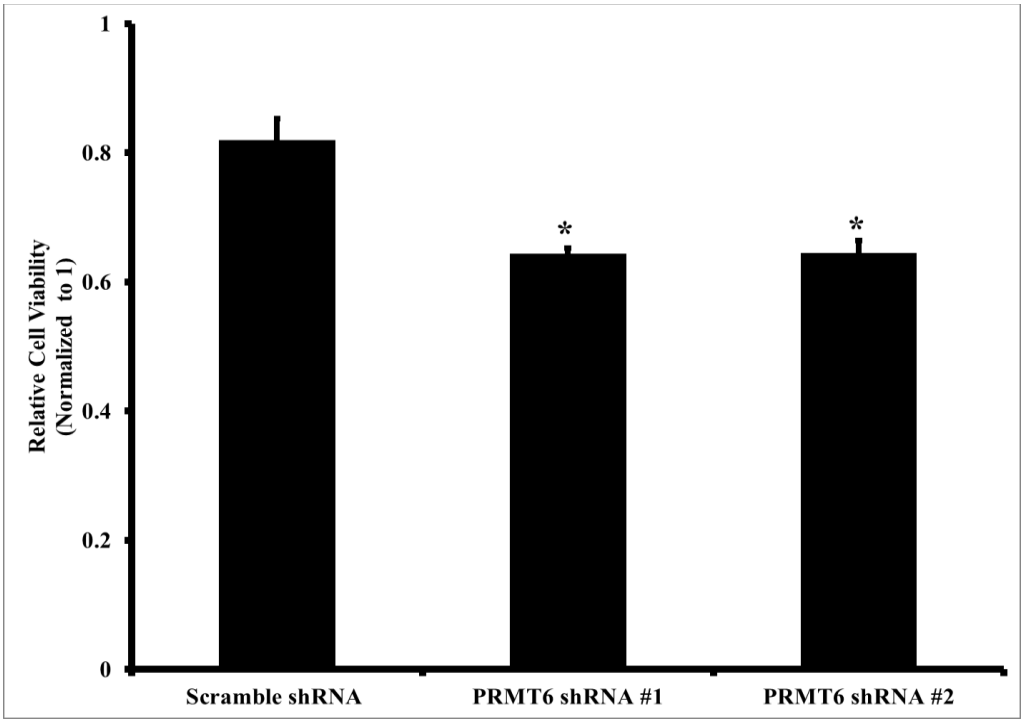
1
0.8
0.6
0.4
0.2
0
Relative Cell Viability (Normalized to 1)
*
*
Scramble shRNA
PRMT6 shRNA #1
PRMT6 shRNA #2

B)

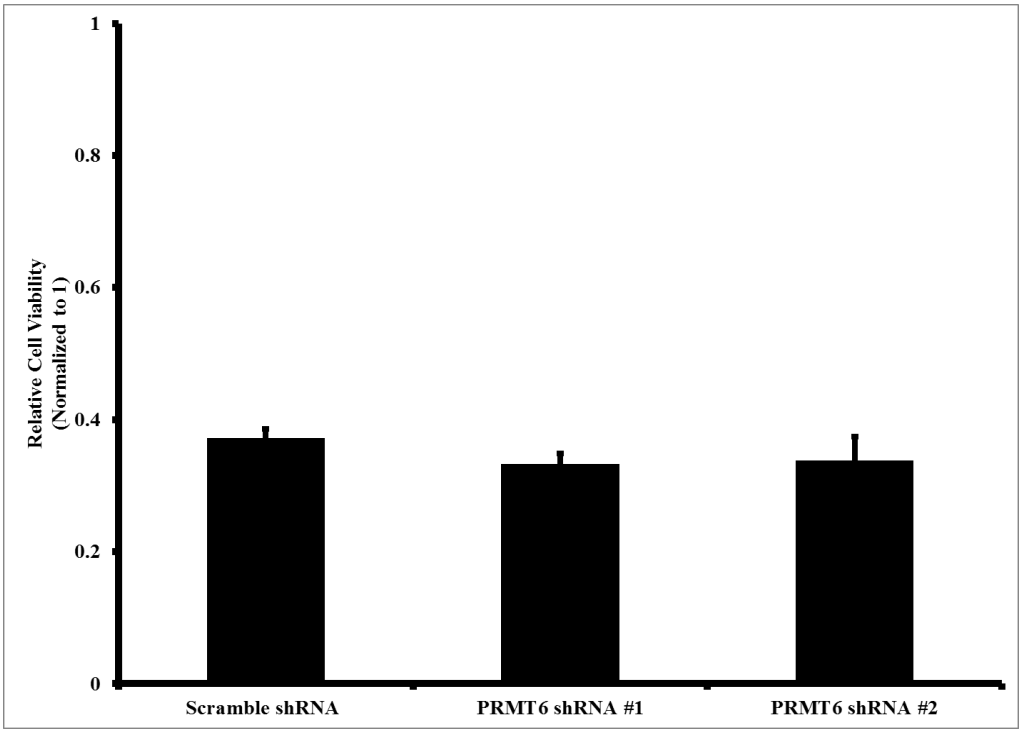
1
0.8
0.6
0.4
0.2
0
Relative Cell Viability (Normalized to 1)
Scramble shRNA
PRMT6 shRNA #1
PRMT6 shRNA #2

Figure 4.15: Depletion of PRMT6 affects Cell Viability in Bortezomib-Resistant MCF7 Cells but not in Bortezomib-Sensitive MDA MB 231 Cells

An equal number of (A) MCF7 or (B) MDA MB 231 scramble and PRMT6 shRNA stably-expressing cells were plated and treated with 10 μM bortezomib for 24 h and MTT assays were performed. Cell viability data upon treatment with bortezomib was normalized to the data for DMSO treated cells with the cell viability for DMSO treated cells set to 1. PRMT6 depletion resulted in about a 17% decrease in viability in (A) MCF7 cells, while having no effect on cell viability in (B) MDA MB 231 cells. Data is the average +/- the standard error of the mean for four independent experiments with six internal replicates per experiment. * denotes statistical significance with a p-value less than 0.01 between scramble and PRMT6 shRNA expressing cells determined using a one way ANOVA.

Chapter 5: Arginine Methylation of DEAD-box RNA Helicase DDX3

DDX3 has been implicated in the development and progression of a number of cancers including breast cancer (Chao et al., 2006; Chang et al., 2006; Huang et al., 2004; Wu et al., 2011; Botlagunta et al., 2008; Miao et al., 2013). DDX3 overexpression in normal mammary epithelial cells results in increased motility and invasion, along with down-regulation of E-cadherin. These phenotypes are indicative of an epithelial to mesenchymal transition (Botlagunta et al., 2008). Furthermore, HIF1α transcriptionally regulates DDX3 upon induction of hypoxic conditions in breast cancer cells (Botlagunta et al., 2011). Similarly to DDX3, aberrant regulation of a number of PRMTs has been observed in breast cancer (Goulet et al., 2007; Mathioudaki et al., 2011; Yoshimatsu et al., 2011; Al-Dhaheri et al., 2011; Thomassen et al., 2009). As DDX3 and a number of PRMTs are abnormally expressed in breast cancer, and DDX3 contains a number of GAR motifs, motifs characteristic of PRMT substrates, it was hypothesized that methylation of DDX3 by PRMT(s) may contribute to breast cancer etiology and/or progression.

5.1 DDX3 is an Arginine Methylated Protein

The methylation status of DDX3 was determined by performing an *in vivo* methylation assay. HeLa cells were treated with translation inhibitors cycloheximide and chloramphenicol, and then labelled with ^{3}H-methionine for 3 h, or with ^{35}S-methionine as a control to demonstrate inhibition of translation. Post-incubation with ^{3}H-methionine, DDX3 was immunoprecipitated from the cell lysate; Western Blotting was performed and the PVDF membrane was subjected to fluorography. DDX3 was determined to be methylated, *in vivo* (Figure 5.1), although the pool of methylated DDX3 relative to the amount of DDX3 immunoprecipated seemed low under normal growth conditions.

5.1)

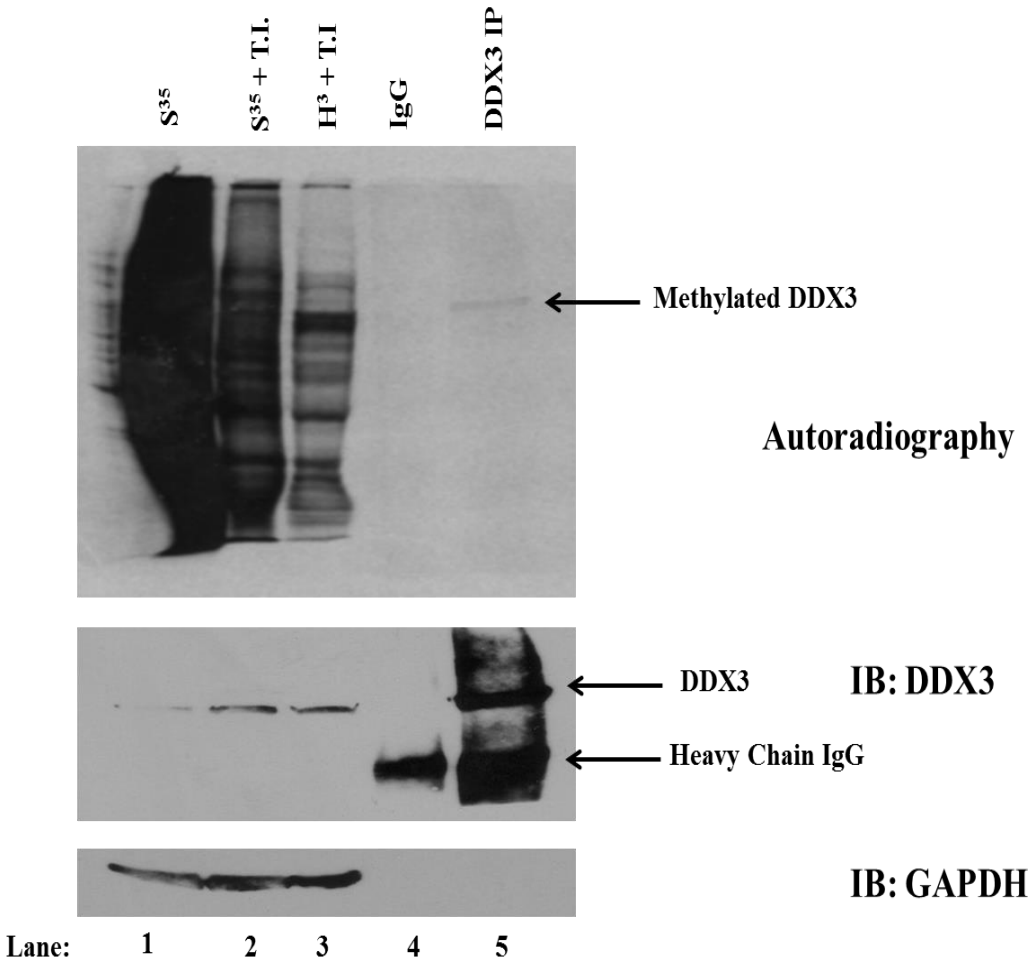
S35
S35 + T.I.
H3 + T.I
IgG
DDX3 IP
Methylated DDX3
Autoradiography
DDX3
IB: DDX3
Heavy Chain IgG
IB: GAPDH
Lane: 1 2 3 4 5

Figure 5.1: DDX3 is an Arginine Methylated Protein, *In Vivo*

HeLa cells were treated with the translation inhibitors cycloheximide and chloramphenicol and then labelled with ^{3}H-methionine or ^{35}S-methionine. Endogenous DDX3 was immunoprecipitated from the ^{3}H-methionine labelled lysates and run on a SDS-Page gel, transferred to PVDF membrane, sprayed with EN^{3}HANCE and exposed to autoradiography. The top panel shows the results from the autoradiography with the ^{3}H-labelled signal for DDX3 in lane 5. Lane 1 shows ^{35}S-methionine labelled lysate, lane 2 demonstrates inhibition of translation with cycloheximide and chloramphenicol ^{35}S-methionine labelled lysate while lane 3 exhibits cycloheximide and chloramphenicol ^{3}H-methionine labelled lysate. Ten percent of lysate was loaded in each lane. The bottom panels show immunoblotting with DDX3 confirming immunoprecipitation of DDX3, and GAPDH indicating equal loading of proteins in lanes 1, 2, and 3.

Additionally, data mining of Stable Isotope Labelling of Amino Acids in Culture (SILAC) mass spectrometry experiments, performed by Dr. Laura Trinkle-Mulcahy allowed for DDX3 arginine methylated sites to be identified. This method of identification was possible as DDX3 readily binds affinity matrices, and therefore is a common contaminant in these experiments (Trinkle-Mulcahy et al., 2008). Six arginine residues were identified as being methylated, arginine residues 101, 110, 333, 394 were characterized as being mono-methylated while residues 121 and 326 were classified as di-methylated (Figure 5.2).

5.2 PRMT1, CARM1 and PRMT6 Methylate DDX3, *In Vitro*

Subsequently, the PRMT(s) responsible for methylating DDX3 were determined by *in vitro* methylation assays. PRMTs 1, 3, 4, 5, 6, and 7 were tested to determine if they were capable of methylating DDX3, *in vitro*. Purified PRMT protein or a specific PRMT immunoprecipitated from cell lysate were incubated with either purified DDX3 protein or DDX3 immunoprecipitated from cell lysate in the presence of ^{3}H-SAM.

PRMT1

His-tagged PRMT1v1 was capable of weakly methylating GST-tagged DDX3, however, His-tagged PRMT1v2 and PRMT1v3 were not under the conditions employed here (Figure 5.3). In contrast, DDX3 immunoprecipitated from cell lysate could be methylated by both His-tagged PRMT1v1 and PRMT1v2, though His-tagged PRMT1v1 methylation was more robust than PRMT1v2 (Figure 5.4). GST-hnRNPA1 was used as a positive control, as hnRNPA1 was previously shown to be a substrate of all PRMT1 isoforms (Lim et al., 2005).

5.2)

Arginine Methylation Site	Methylation Type	Peptide	Peptide Position
R101	Methylation	GRSDYDGIGSR	100-110
R110	Methylation	GRSDYDGIGSR	100-110
R121	Di-methylation	FERGGNSRWCDK	119-130
R326	Di-methylation	GCHLLVATPGRLVDMMERGK	316-335
R333	Methylation	GCHLLVATPGRLVDMMERGK	316-335
R394	Methylation	GVRHTMMFSATFPKEIQMLAR	374-394

Figure 5.2: Identification of DDX3 Arginine Methylated Residues

Data mining of results from Stable Isotope Labelling of Amino Acids (SILAC) mass spectrometry experiments allowed for sites of methylation in DDX3 to be identified. Six peptides were identified with the methylated arginine residue indicated in red. Additionally, the type of methylation catalyzed was identified.

5.3)

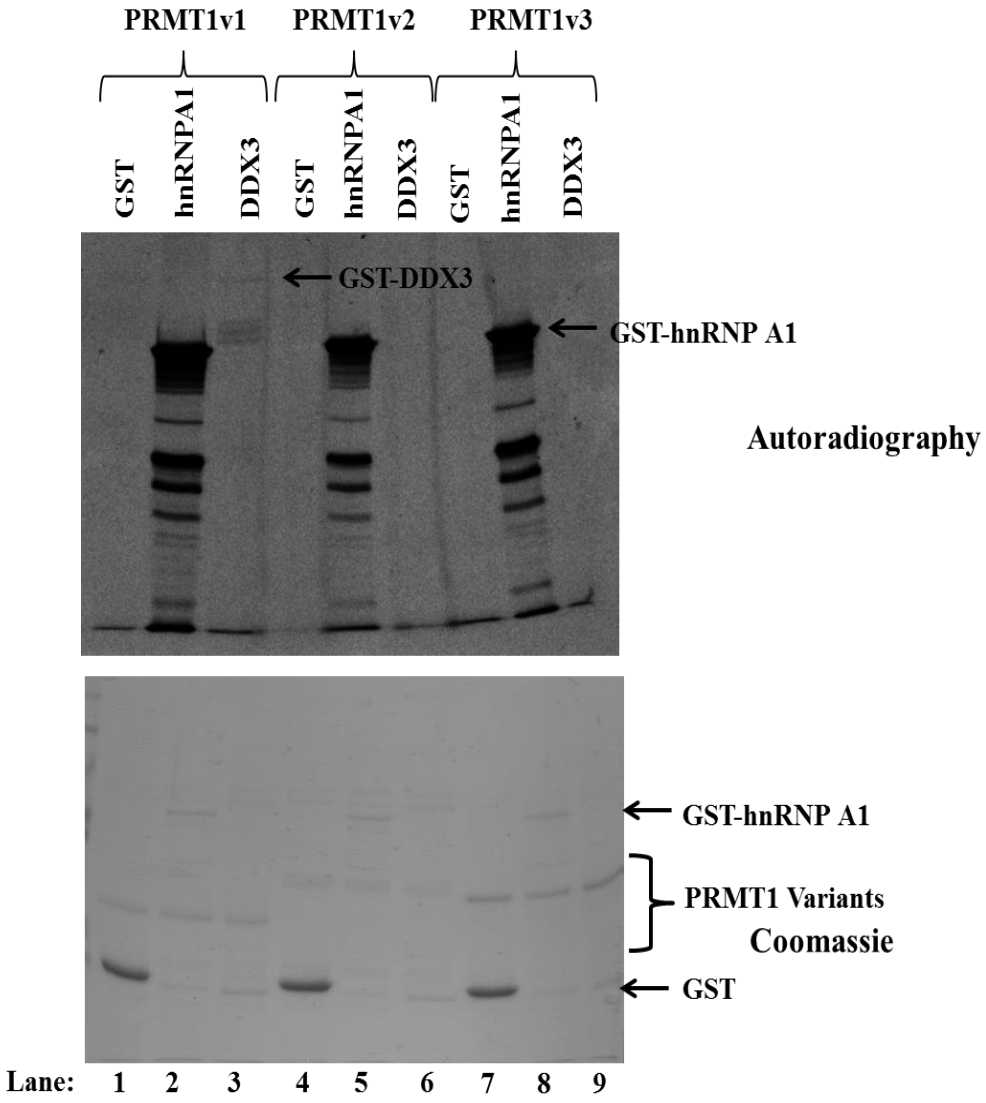
PRMT1v1
PRMT1v2
PRMT1v3
GST
hnRNPA1
DDX3
GST
hnRNPA1
DDX3
GST
hnRNPA1
DDX3
GST-DDX3
GST-hnRNP A1
Autoradiography
GST-hnRNP A1
PRMT1 Variants
Coomassie
GST
Lane: 1 2 3 4 5 6 7 8 9

Figure 5.3: PRMT1v1 Methylates Purified DDX3 Protein

Purified His-tagged PRMT1v1, PRMT1v2 or PRMT1v3 were each incubated with GST empty vector, GST-hnRNPA1 or GST-DDX3 in the presence of ^{3}H-SAM. His-tagged PRMT1v1 methylates GST-DDX3 (lane 3) while His-tagged PRMT1v2 and PRMT1v3 were unable to methylate GST-DDX3. GST-hnRNPA1 was used as a positive control while GST empty vector was used a negative control. The bottom panel shows Coomassie staining of the gel prior to exposure to autoradiography.

5.4A)

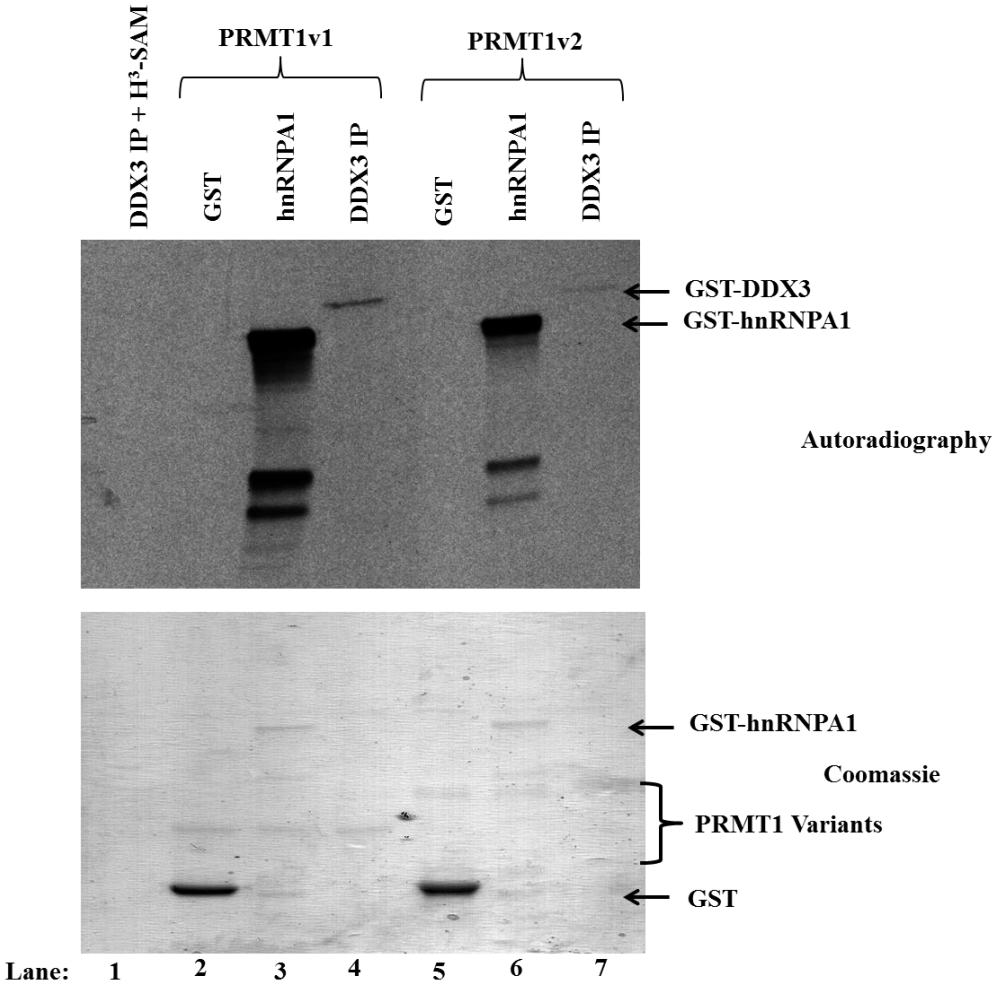
DDX3 IP + H3-SAM
PRMT1v1
PRMT1v2
GST
hnRNPA1
DDX3 IP
GST
hnRNPA1
DDX3 IP
GST-DDX3
GST-hnRNPA1
Autoradiography
GST-hnRNPA1
Coomassie
PRMT1 Variants
GST
Lane: 1 2 3 4 5 6 7

B)

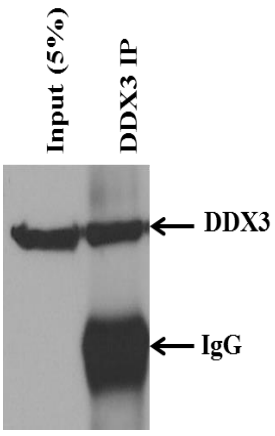
Input (5%)
DDX3 IP
DDX3
IgG

Figure 5.4: PRMT1 Methylates DDX3 Immunoprecipitated from Cell Lysate

(A) DDX3 was immunoprecipitated from HeLa cell lysate and incubated with His-tagged PRMT1v1 (lane 4) or PRMT1v2 (lane 7 in the presence of ^{3}H-SAM. Both His-tagged PRMT1v1 and PRMT1v2 were capable of methylating DDX3. DDX3 alone from cell lysate (lane 1) was not methylated. GST-hnRNPA1 was used as a positive control while empty vector GST was used as a negative control. Coomassie staining (bottom panel) shows the amount of proteins present in each reaction. (B) A large scale DDX3 immunoprecipitation was preformed from HeLa cells with the sample equally divided for each methylation assay reaction. Here, a Western blot shows immunoprecipitation of DDX3 with five percent of cell lysate used for input.

To validate that the observed methylation of DDX3 by PRMT1 was not due to increased promiscuity that PRMT1 exudes *in vitro* (Wooderchak et al., 2008), interaction studies between DDX3 and PRMT1 were performed. Myc-tagged DDX3 was transfected into 293T cells, cells were pretreated with adenosine 2', 3'-dialdehyde (Adox) and methylthioadenosine (MTA), general methylation inhibitors for 24 h, and Myc was immunoprecipitated from the cell lysate. PRMT1 interacted with myc-tagged DDX3 in untreated cells; however, the interaction was substantially enhanced upon inhibition of methylation with Adox/MTA (Figure 5.5A). This result was confirmed as an interaction between endogenous DDX3 and endogenous PRMT1 was observed when DDX3 was immunoprecipitated from 293T cell lysate (Figure 5.5B).

CARM1

GST-CARM1 was incapable of methylating GST-tagged DDX3 or DDX3 immunoprecipitated from cell lysate; however, when cells were pretreated with 20 µM of the general methylation inhibitors Adox and MTA for 24 h before lysing, GST-tagged CARM1 was able to methylate DDX3 from these cell lysates (Figure 5.6). Interestingly, in this instance when DDX3 was immunoprecipitated from Adox and MTA treated cell lysate and incubated with just ^{3}H-SAM alone, methylation of DDX3 was observed. This suggests that a PRMT was immunoprecipitated with DDX3, and thus methylated it upon addition of ^{3}H-SAM. However, upon addition of GST-CARM1, DDX3 methylation is enhanced. Furthermore, it appears that other proteins were immunoprecipitated with DDX3 that are methylated, and are potential substrates of CARM1. SmB', an identified substrate of CARM1, was used as a positive control (Cheng et al., 2007).

5.5A)

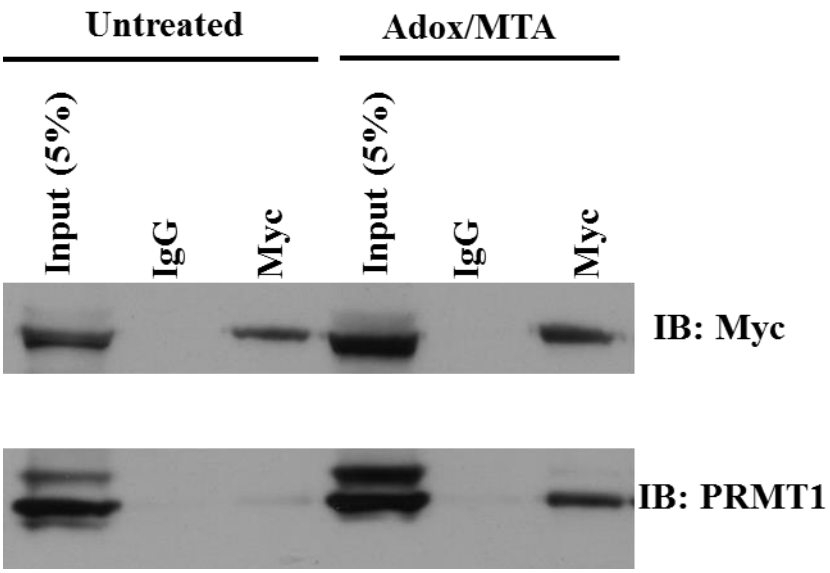
Untreated
Adox/MTA
Input (5%)
IgG
Myc
Input (5%)
IgG
Myc
IB: Myc
IB: PRMT1

B)

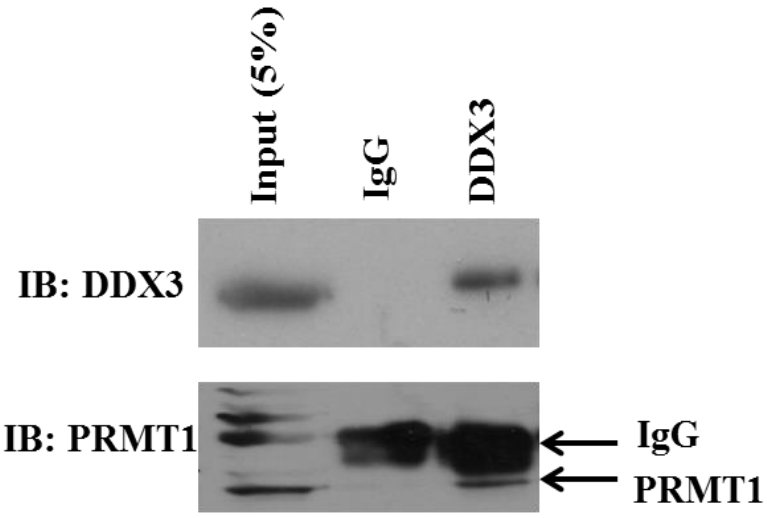
Input (5%)
IgG
DDX3
IB: DDX3
IB: PRMT1
IgG
PRMT1

Figure 5.5: PRMT1 Interacts with DDX3

(A) 293T cells were transfected with myc-tagged DDX3 for 24 h, pretreated with 20 μM each of Adox and MTA for 24 h, and myc was immunoprecipitated from the cell lysate. Western Blotting reveals an interaction between PRMT1 and myc-tagged DDX3 which is subsequently enhanced upon treatment with Adox/MTA. (B) DDX3 was immunoprecipitated from HeLa cells, with Western Blotting showing an interaction between endogenous PRMT1 and DDX3.

5.6A)

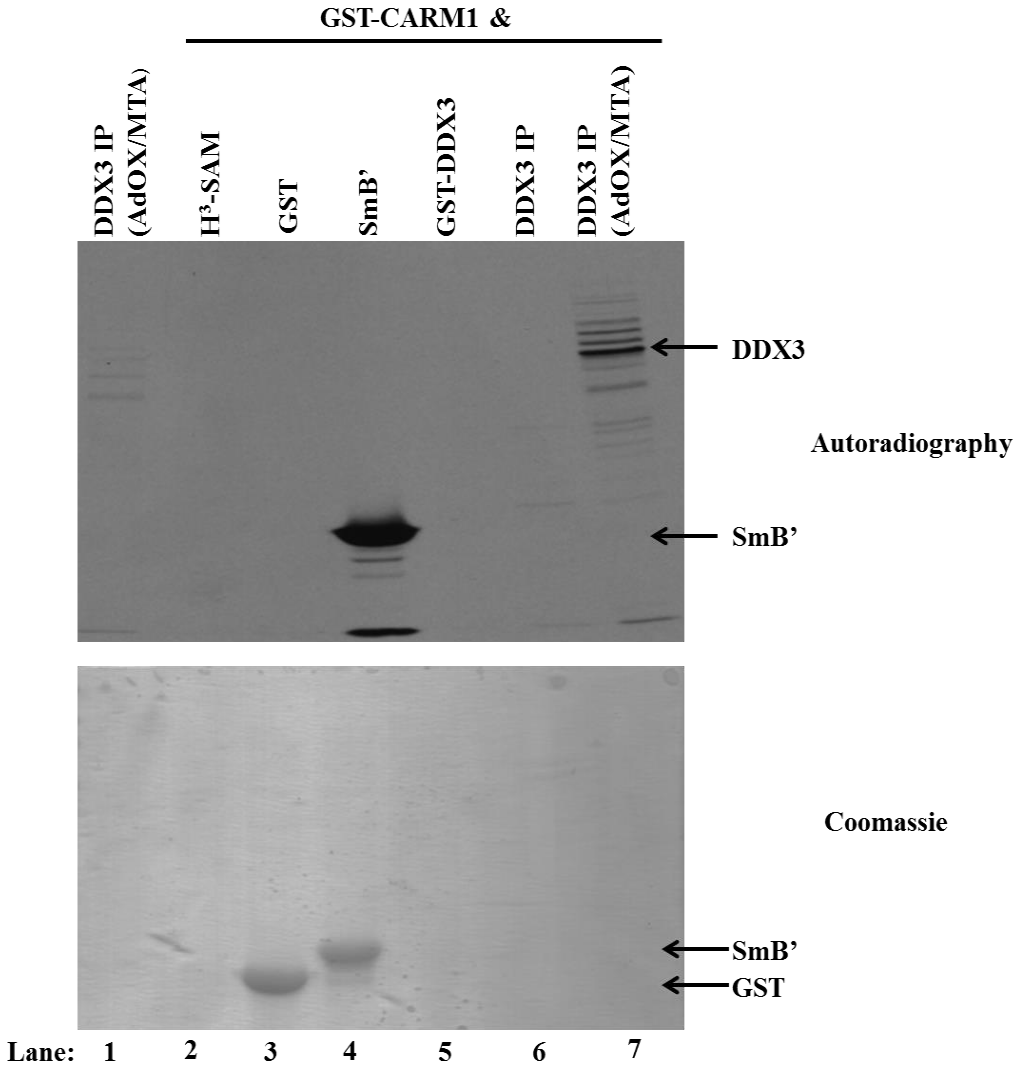
GST-CARM1 &
DDX3 IP (AdOX/MTA)
H³-SAM
GST
SmB'
GST-DDX3
DDX3 IP
DDX3 IP (AdOX/MTA)
DDX3
Autoradiography
SmB'
Coomassie
SmB'
GST
Lane: 1 2 3 4 5 6 7

B)

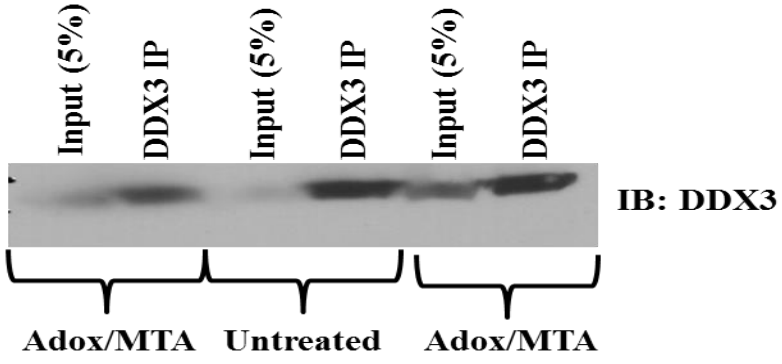
Input (5%)
DDX3 IP
Input (5%)
DDX3 IP
Input (5%)
DDX3 IP
IB: DDX3
Adox/MTA
Untreated
Adox/MTA

Figure 5.6: CARM1 Methylates DDX3 Immunoprecipitated from Cell Lysate

(A) GST-tagged CARM1 was incubated with GST-tagged DDX3 (lane 4), DDX3 immunoprecipitated from HeLa cells untreated (lane 5) or treated with 20 μM for 24 h in the presence of ^{3}H-SAM. GST-tagged CARM1 methylates DDX3 immunoprecipitated from Adox/MTA treated cells. DDX3 immunoprecipitated from Adox/MTA treated cells (lane 1) shows the enhancement of DDX3 methylation upon addition of GST-tagged CARM1. GST-SmB' was used as a positive control, while empty vector GST was used as a negative control. A Coomassie stained gel shows loading of the proteins (B) Western Blot showing DDX3 immunoprecipitated from 293T cell lysate untreated or treated with 20 μM Adox and MTA for 24 h. Five percent of cell lysate was used for input. The remaining cell lysate was used for immunoprecipitation and split in half for the methylation assay and to check the IP.

Next, utilizing CARM1 wild type and null MEF cellular extracts as a source of PRMTs, it was investigated whether differential methylation was observed. An equal amount of cell lysate from CARM1 wild type or null MEFs was incubated with 10 or 20 µg of GST-tagged DDX3 protein, and an *in vitro* methylation assay was performed. No methylation of GST-tagged DDX3 was observed using CARM1 wild type MEFs. However, GST-tagged DDX3 was methylated when using CARM1 null MEFs as a source of PRMTs (Figure 5.7). No difference in GST-SmB' methylation, the positive control, was observed because in addition to being a substrate of CARM1 (Cheng et al., 2007), SmB' is also a substrate of PRMT5 (Gonsalvez et al., 2008), and when utilizing CARM1 null MEFs was probably methylated by PRMT5. This result suggests that CARM1 methylation of DDX3 could potentially inhibit other PRMT(s) from methylating DDX3.

To confirm an interaction between CARM1 and DDX3, co-immunoprecipitation reactions were performed. 293T cells were treated with 20 µM each Adox and MTA for 24 h and DDX3 was immunoprecipitated from the lysate. CARM1 was only able to interact with DDX3 upon cellular treatment with Adox and MTA (Figure 5.8). This result coincides with those observed with the *in vitro* methylation assay, where CARM1 could only methylate DDX3 from Adox and MTA treated cells.

PRMT6

Whereas PRMT1 and CARM1 were unable to robustly methylate GST-tagged DDX3, GST-tagged PRMT6 was capable of methylating it quite readily (Figure 5.9). However, GST-tagged PRMT6 was unable to methylate DDX3 immunoprecipitated from

5.7A)

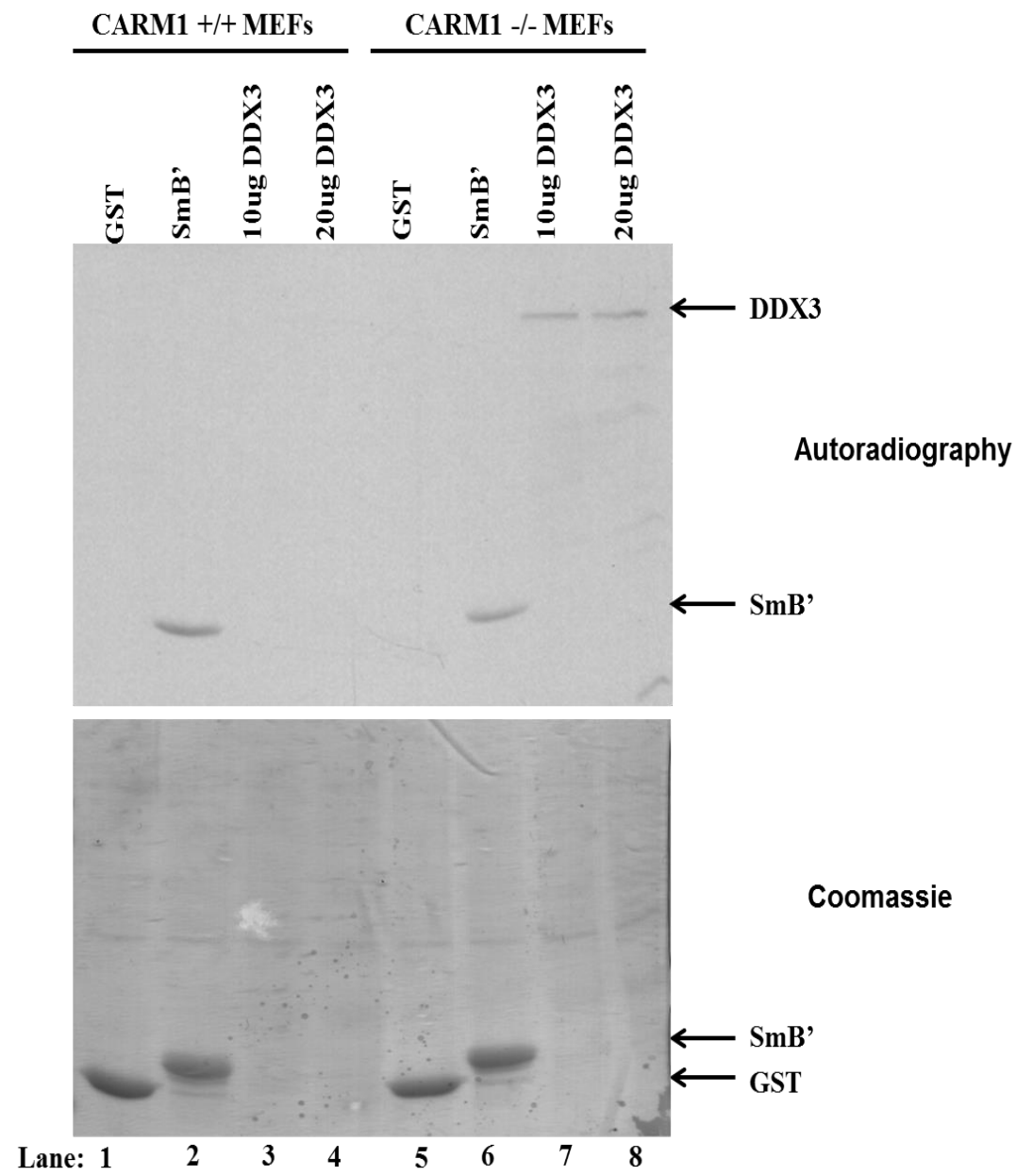
CARM1 +/+ MEFs
CARM1 -/- MEFs
GST
SmB'
10ug DDX3
20ug DDX3
GST
SmB'
10ug DDX3
20ug DDX3
DDX3
Autoradiography
SmB'
Coomassie
SmB'
GST
Lane: 1 2 3 4 5 6 7 8

B)

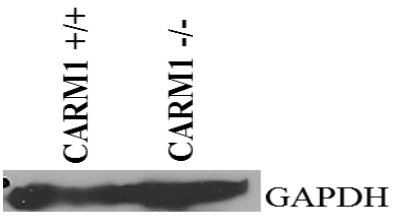
CARM1 +/+
CARM1 -/-
GAPDH

Figure 5.7: CARM1 Inhibits other PRMTs from Methylating DDX3

(A) CARM1 wild type (lanes 1-4) and null (lanes 5-8) mouse embryonic fibroblast (MEF) cell lysate was used as a source of PRMTs and incubated with 10 or 20 µg GST-tagged DDX3 protein in the presence of ^{3}H-SAM. Methylation of GST-tagged DDX3 was observed using cell lysate from CARM1 null MEFs (compare lanes 7 and 8 to lanes 3 and 4) but not using lysate from CARM1 wild type MEFs. GST-tagged SmB' was used as a positive control, while empty vector GST was used as a negative control. A Coomassie stained gel shows loading of the proteins. (B) A Western Blot shows equal loading of the lysate from CARM1 wild type and null MEFs.

5.8)

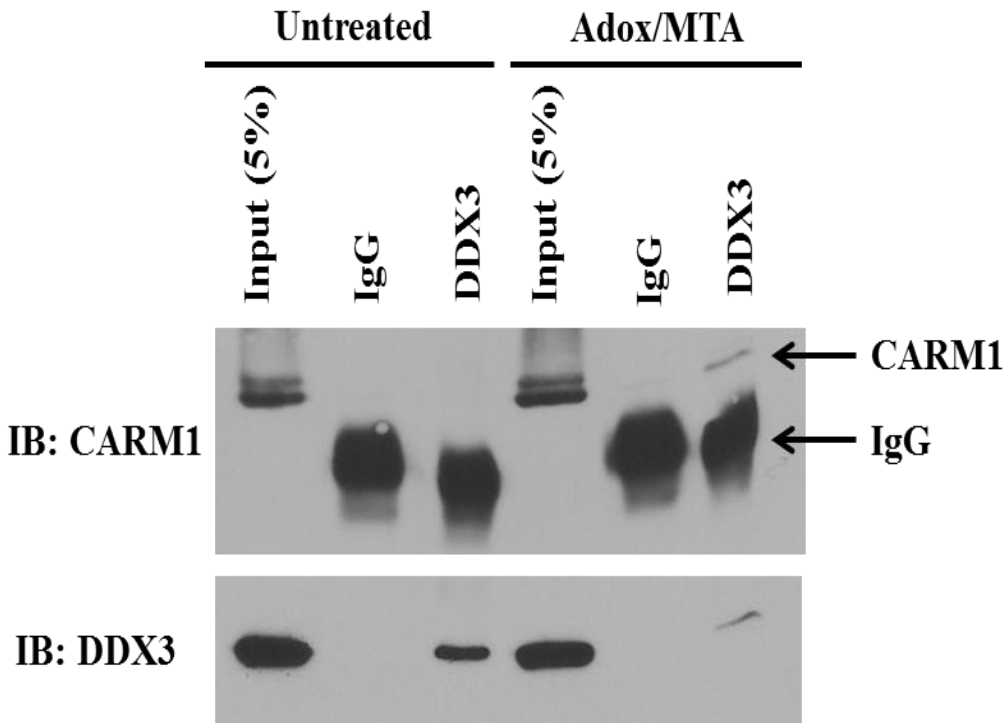
Untreated
Adox/MTA
Input (5%)
IgG
DDX3
Input (5%)
IgG
DDX3
CARM1
IgG
IB: CARM1
IB: DDX3

Figure 5.8: CARM1 Interacts with DDX3

293T cells were pretreated with 20 µM each of Adox and MTA for 24 h and DDX3 was immunoprecipitated from the cell lysate. Endogenous CARM1 was only capable of interacting with endogenous DDX3 after cells were treated with Adox/MTA for 24 h.

5.9A)

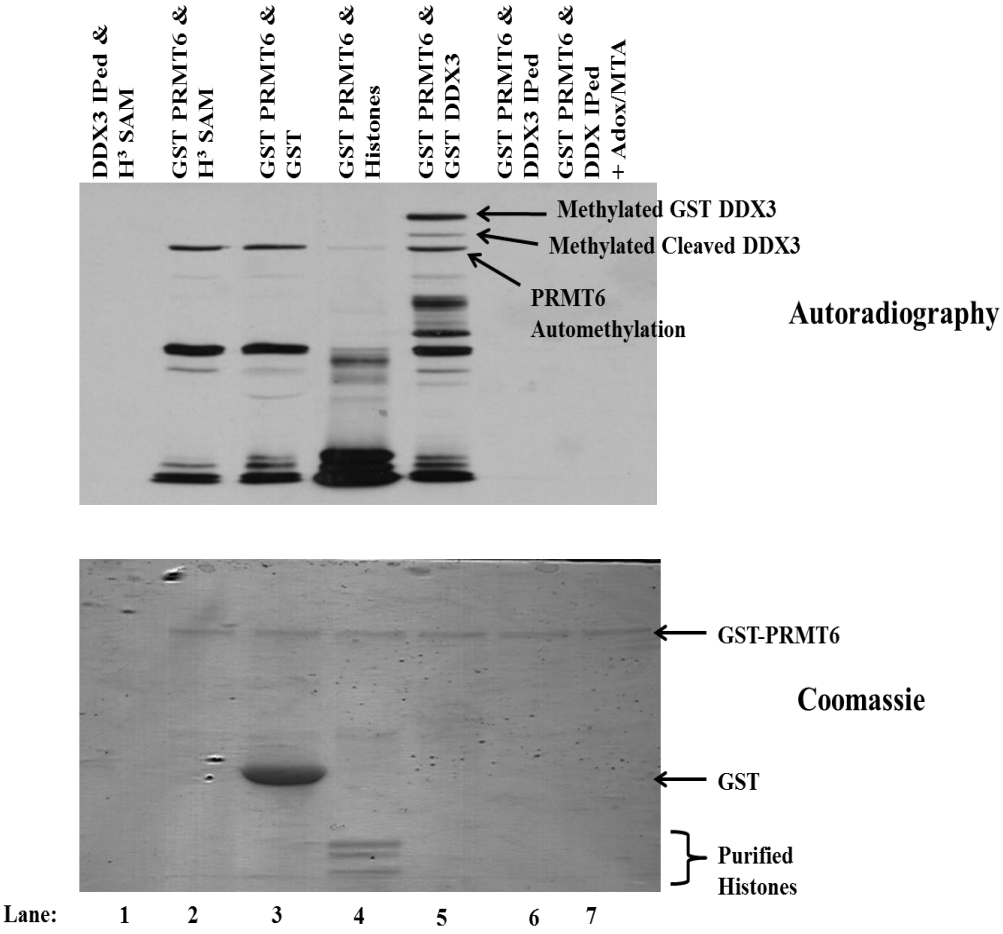
DDX3 IPed & H³ SAM
GST PRMT6 & H³ SAM
GST PRMT6 & GST
GST PRMT6 & Histones
GST PRMT6 & GST DDX3
GST PRMT6 & DDX3 IPed
GST PRMT6 & DDX IPed + Adox/MTA
Methylated GST DDX3
Methylated Cleaved DDX3
PRMT6 Automethylation
Autoradiography
GST-PRMT6
Coomassie
GST
Purified Histones
Lane: 1 2 3 4 5 6 7

B)

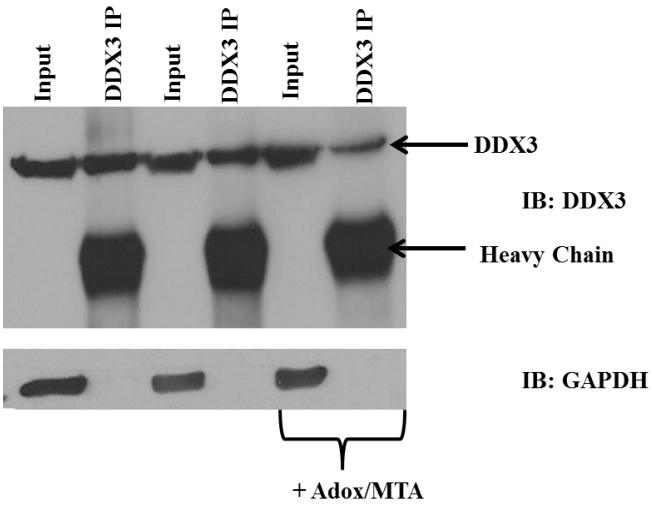
Input
DDX3 IP
Input
DDX3 IP
Input
DDX3 IP
DDX3
IB: DDX3
Heavy Chain
IB: GAPDH
+ Adox/MTA

Figure 5.9: PRMT6 Methylates DDX3, *In Vitro*

A) Purified GST-PRMT6 was incubated with either GST-DDX3 (lane 5) or DDX3 immunoprecipitated from 293T cell lysate either untreated (lane 6) or treated with 20 µM of both Adox and MTA for 24 h (lane 7) in the presence of ^{3}H-SAM. GST-PRMT6 methylates GST-DDX3 but not DDX3 immunoprecipitated from 293T cell lysates either untreated, or treated with Adox or MTA (top panel). Purified histone proteins were utilized as a positive control (lane 4) while GST purified protein (lane 3) was used as a negative control. GST-PRMT6 was incubated with ^{3}H-SAM alone to demonstrate its automethylation capability (lane 2). The bottom panel shows Coomassie staining of the gel prior to exposure to autoradiography. B) Western blot showing immunoprecipitation of DDX3 from 293T cell lysate untreated or treated with 20 µM Adox and MTA (top panel). GAPDH shows equal loading of protein (bottom panel).

cell lysate from untreated or Adox/MTA treated cells. Purified histones served as a positive control for PRMT6, as histone H3 is a substrate for PRMT6 (Guccione et al., 2007; Hyllus et al., 2007). Additionally, PRMT6 automethylation was observed as has been previously published (Frankel et al., 2002).

PRMT3, PRMT5, and PRMT7

Whereas PRMT1, CARM1, and PRMT6 methylated either purified DDX3 protein or DDX3 from cell lysate, PRMT3, PRMT5 and PRMT7 were unable to methylate DDX3. GST-tagged PRMT3 was unable to methylate purified or immunoprecipitated DDX3 (Appendix Ib), while neither PRMT5 (Appendix Ic) nor PRMT7 (Appendix Id) immunoprecipitated from cell lysate were able to methylate purified DDX3 protein or DDX3 immunoprecipitated from cell lysate. PRMT5 was immunoprecipitated from cell lysates as an interaction with the co-operator of PRMT5 protein is required to modulate PRMT5's methyltransferase activity, as purified PRMT5 protein lacks adequate methyltransferase activity (Lacroix et al., 2008). Immunoprecipitated PRMT7 was used as a purified PRMT7 protein was unavailable. These results suggest using the methods employed here, that DDX3 may not be a substrate for PRMT3, PRMT5, or PRMT7.

5.3 PRMT6 Methylates DDX3 Arginine Residues 585 and 587, *In Vitro*

The identification of the arginine residue(s) on DDX3 that PRMT6 methylates was characterized further, as *in vitro* PRMT6 methylated full length GST-tagged DDX3 purified protein more readily than either PRMT1 or CARM1. GST-tagged DDX3 truncation mutants encompassing amino acids 1-181, 182-404, and 405-662 were created, given that the data mining results identified six potential arginine methylated residues,

three within both DDX3 truncation mutants 1-181 and 182-404 (Figure 5.2). An *in vitro* methylation assay was performed and GST-tagged PRMT6 was capable of methylating both truncation mutants, 1-181 and 405-662, although methylation of 405-662 was more robust than 1-181 (Figure 5.10). Interestingly, GST-tagged PRMT6 methylated both truncation mutants to a greater extent than full length GST-tagged DDX3.

Subsequently, as methylation in the C-terminal region of DDX3 was the most robust, the arginine residue(s) methylated by PRMT6 in this region were determined. Based on the presence of four arginine residues within GAR motifs (503, 585, 587, and 632) in the C-terminal fragment of DDX3 (Figure 5.11) these residues were mutated to alanines by site-directed mutagenesis. An *in vitro* methylation assay was performed and a significant reduction in methylation was observed upon mutation of arginine residues 585 and 587 (Figure 5.12). Next, a double arginine 585/587 to alanine mutation was created to determine if mutation of both these arginine residues further reduced methylation in the C-terminus of DDX3. In fact, introduction of this mutant resulted in a further decrease in methylation by PRMT6 than was observed with either of the single mutants (Figure 5.13). Lastly, creation of single 585 or 587 mutants and the double 585/587 mutant in full length DDX3 resulted in a significant but equal decrease in methylation, though not a complete abrogation of DDX3 methylation (Figure 5.14). These results suggest that PRMT6 may methylate additional arginine residues within DDX3.

5.4 PRMT6 Methylates DDX3, *In Vivo*

Subsequently, it was investigated whether PRMT6 was responsible for methylation of DDX3 *in vivo*. HeLa scramble and PRMT6 shRNA stably expressing cell lines that were previously generated were utilized (Figure 4.1A). Myc-tagged DDX3 was

5.10)

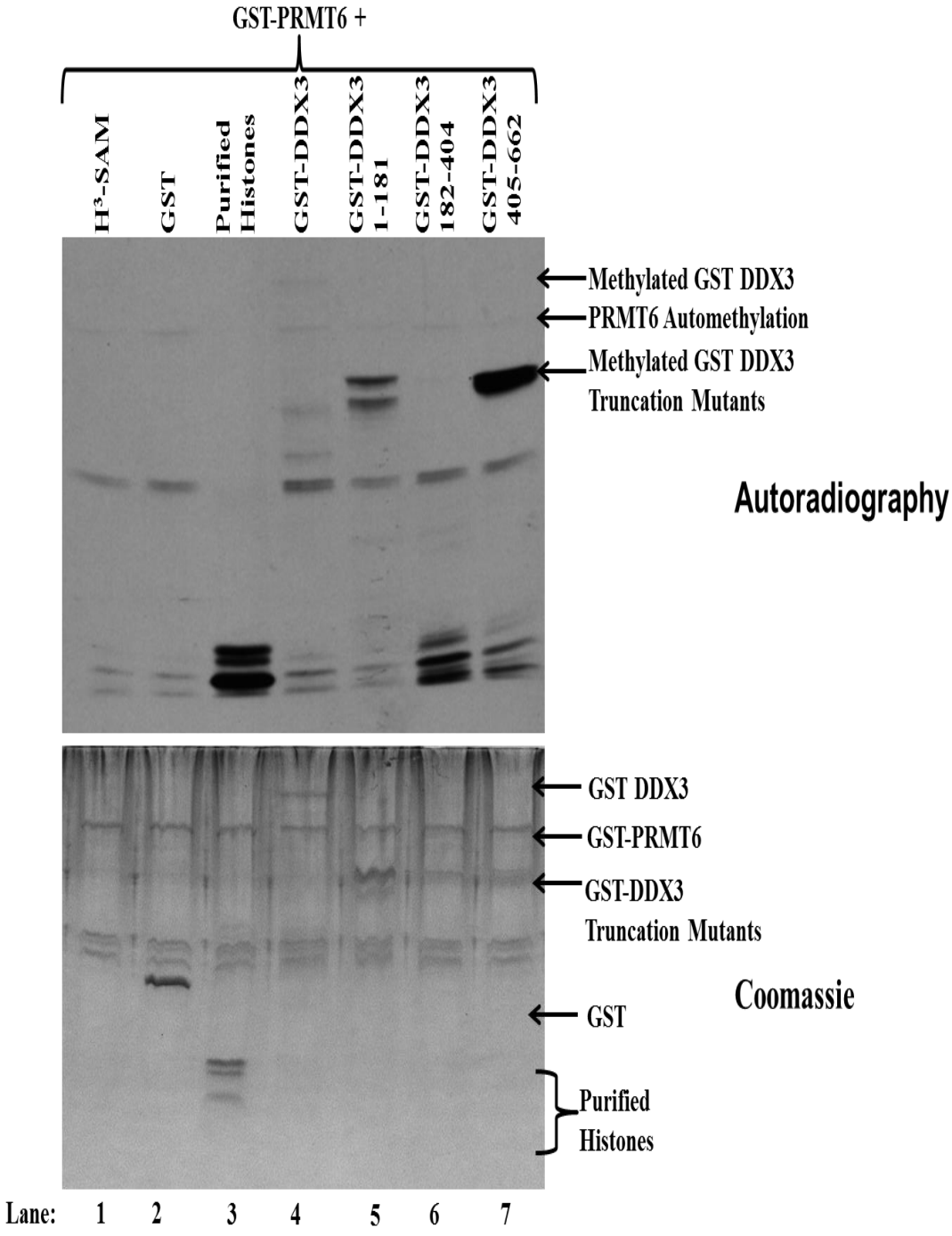
GST-PRMT6 +
H³-SAM
GST
Purified Histones
GST-DDX3
GST-DDX3 1-181
GST-DDX3 182-404
GST-DDX3 405-662
Methylated GST DDX3
PRMT6 Automethylation
Methylated GST DDX3 Truncation Mutants
Autoradiography
GST DDX3
GST-PRMT6
GST-DDX3 Truncation Mutants
GST
Purified Histones
Coomassie
Lane: 1 2 3 4 5 6 7

Figure 5.10: PRMT6 Methylates the N- and C-terminal Regions of DDX3, *In Vitro*

Purified GST-PRMT6 was incubated with either GST-DDX3 (lane 4), GST-DDX3 1-181 (lane 5), GST-DDX3 182-404 (lane 6) or GST-DDX3 405-662 (lane 7) in the presence of ^{3}H-SAM. GST-PRMT6 robustly methylates GST-DDX3 405-662 (lane 7) as well as GST-DDX3 1-181 (lane 5), both to a significantly greater level than full length GST-DDX3 (lane 4) (top panel). Purified histones were utilized as a positive control (lane 3), while GST purified protein was used as a negative control (lane 2). GST-PRMT6 was incubated with ^{3}H-SAM alone to demonstrate its automethylation capability (lane 1). The bottom panel shows Coomassie staining of the gel prior to exposure to autoradiography.

5.11)

DDX3 C-terminal Fragment

```
                                                                  410        420
                                                                  VGRVGS     TSENITQKVV
          430        440        450        460        470        480
WVEESDKRSF LLDLLNATGK DSLTLVFVET KKGADSLEDF LYHEGYACTS IHGDRSQRDR
          490        500        510        520        530        540
EEALHQFRSG KSPILVATAV AARGLDISNV KHVINFDLPS DIEEYVHRIG RTGRVGNLGL
          550        560        570        580        590        600
 ATSFFNERNI NITKDLLDLL VEAKQEVPSW LENMAYEHHY KGSSRGRSKS SRFSGGFGAR
          610        620        630        640        650        660
DYRQSSGASS SSFSSSRASS SRSGGGGHGS SRGFGGGGYG GFYNSDGYGG NYNSQGVDWW

GN
```

Figure 5.11: Potential Arginine Methylated Residues in the C-terminal Region of DDX3

Arginine residues within the C-terminal region of DDX3 were identified and mutated to alanine residues to determine the arginine residues methylated by PRMT6. The arginine residues mutated to alanine are highlighted in red.

5.12)

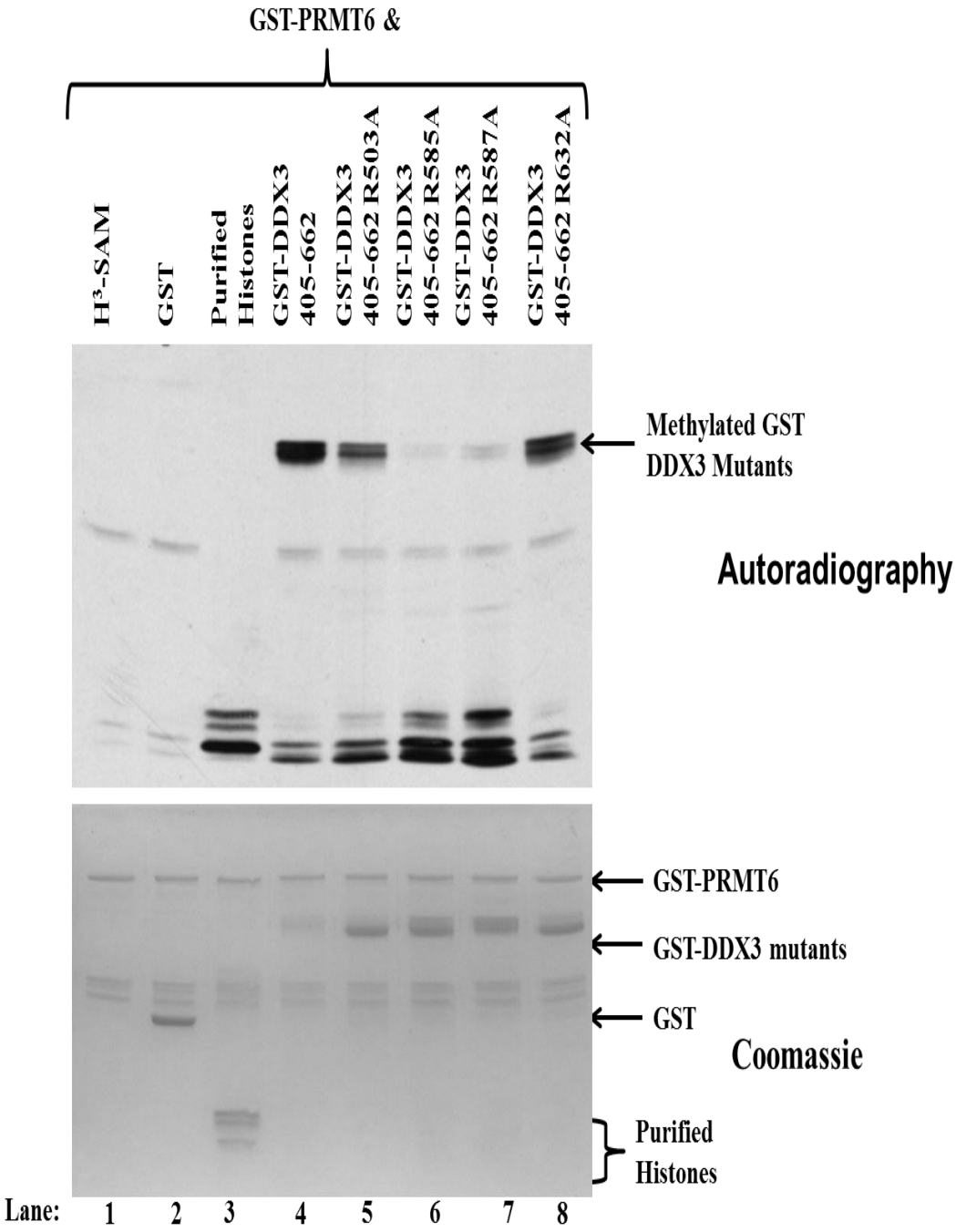
GST-PRMT6 &
H³-SAM
GST
Purified Histones
GST-DDX3 405-662
GST-DDX3 405-662 R503A
GST-DDX3 405-662 R585A
GST-DDX3 405-662 R587A
GST-DDX3 405-662 R632A
Methylated GST DDX3 Mutants
Autoradiography
GST-PRMT6
GST-DDX3 mutants
GST
Coomassie
Purified Histones
Lane: 1 2 3 4 5 6 7 8

Figure 5.12: PRMT6 Methylates Arginine Residues 585 and 587 in the C-terminal Region of DDX3*, In Vitro*

Purified GST-PRMT6 was incubated with either GST-DDX3 405-662 (lane 4), GST-DDX3 405-662 R503A (lane 5), GST-DDX3 405-662 R585A (lane 6), GST-DDX3 405-662 R587A (lane 7), or GST-DDX3 R632A (lane 8) in the presence of ^{3}H-SAM. Significantly reduced methylation of GST-DDX3 405-662 was observed upon mutation of both arginine residues 585 (lane 6) and 587 (lane 7) to alanine (top panel). Purified histones were utilized as a positive control (lane 3), while GST purified protein was used as a negative control (lane 2). GST-PRMT6 was incubated with ^{3}H-SAM alone to demonstrate its automethylation capability (lane 1). The bottom panel shows Coomassie staining of the gel prior to exposure to autoradiography.

5.13)

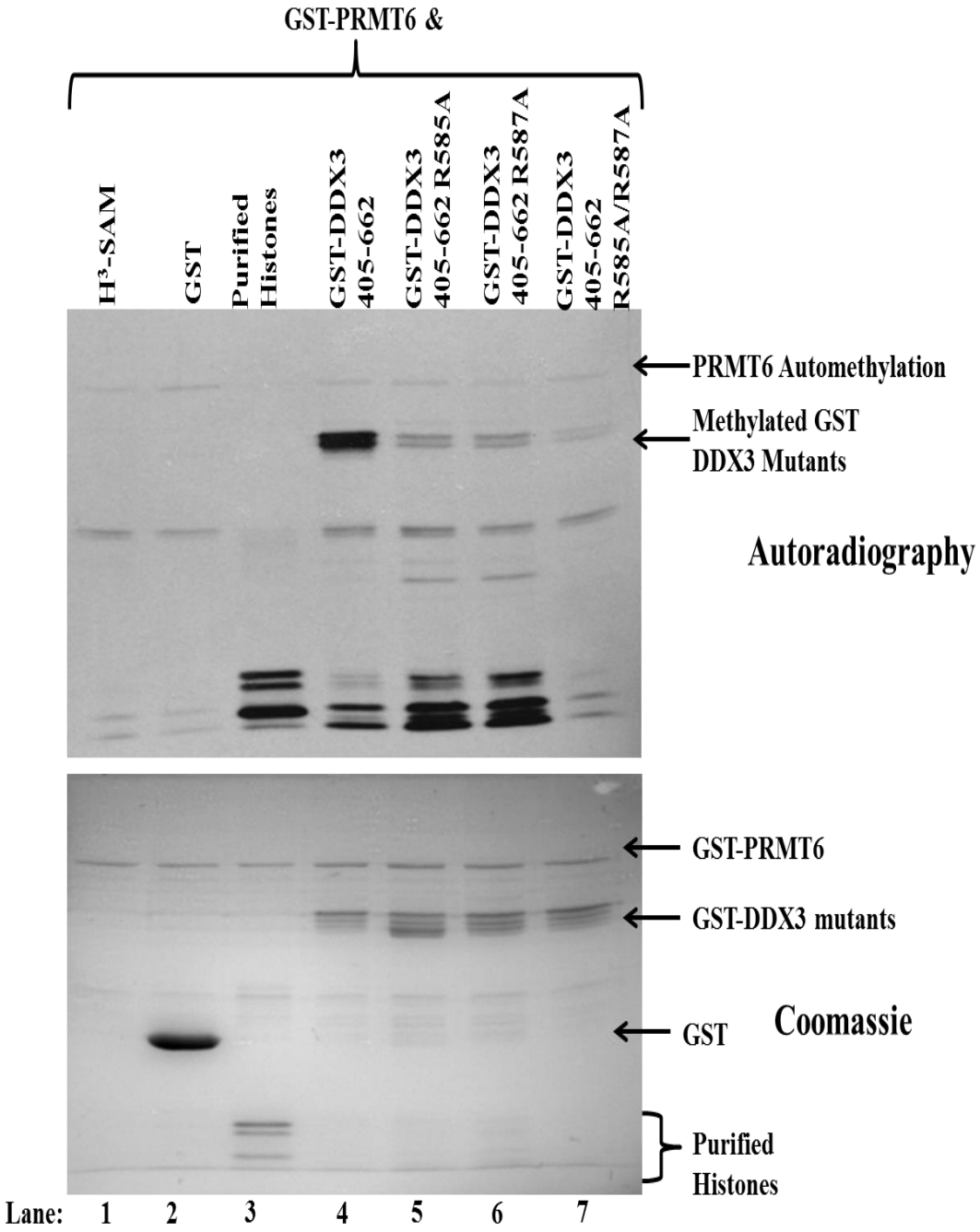
GST-PRMT6 &
H³-SAM
GST
Purified Histones
GST-DDX3 405-662
GST-DDX3 405-662 R585A
GST-DDX3 405-662 R587A
GST-DDX3 405-662 R585A/R587A
PRMT6 Automethylation
Methylated GST DDX3 Mutants
Autoradiography
GST-PRMT6
GST-DDX3 mutants
GST
Coomassie
Purified Histones
Lane: 1 2 3 4 5 6 7

Figure 5.13: Mutation of Both DDX3 Arginine Residues 585 and 587 Results in a Further Decrease in PRMT6 Methylation in the C-terminal Region of DDX3

Purified GST-PRMT6 was incubated with either GST-DDX3 405-662 (lane 4), GST-DDX3 405-662 R585A (lane 5), GST-DDX3 405-662 R587A (lane 6), or GST-DDX3 405-662 R585A/R587A (lane 7) in the presence of ^{3}H-SAM. Mutation of arginine residue 585 (lane 5) or 587 (lane 6) to alanine results in a significant decrease in PRMT6 methylation of the GST-DDX3 fragment 405-662. Mutation of both arginine residues 585 and 587 to alanines causes a further reduction in methylation of GST-DDX3 fragment 405-662 (lane 7) (top panel). Purified histones were utilized as a positive control (lane 3), while GST purified protein was used as a negative control (lane 2). GST-PRMT6 was incubated with ^{3}H-SAM alone to demonstrate its automethylation capability (lane 1). The bottom panel shows Coomassie staining of the gel prior to exposure to autoradiography.

5.14)

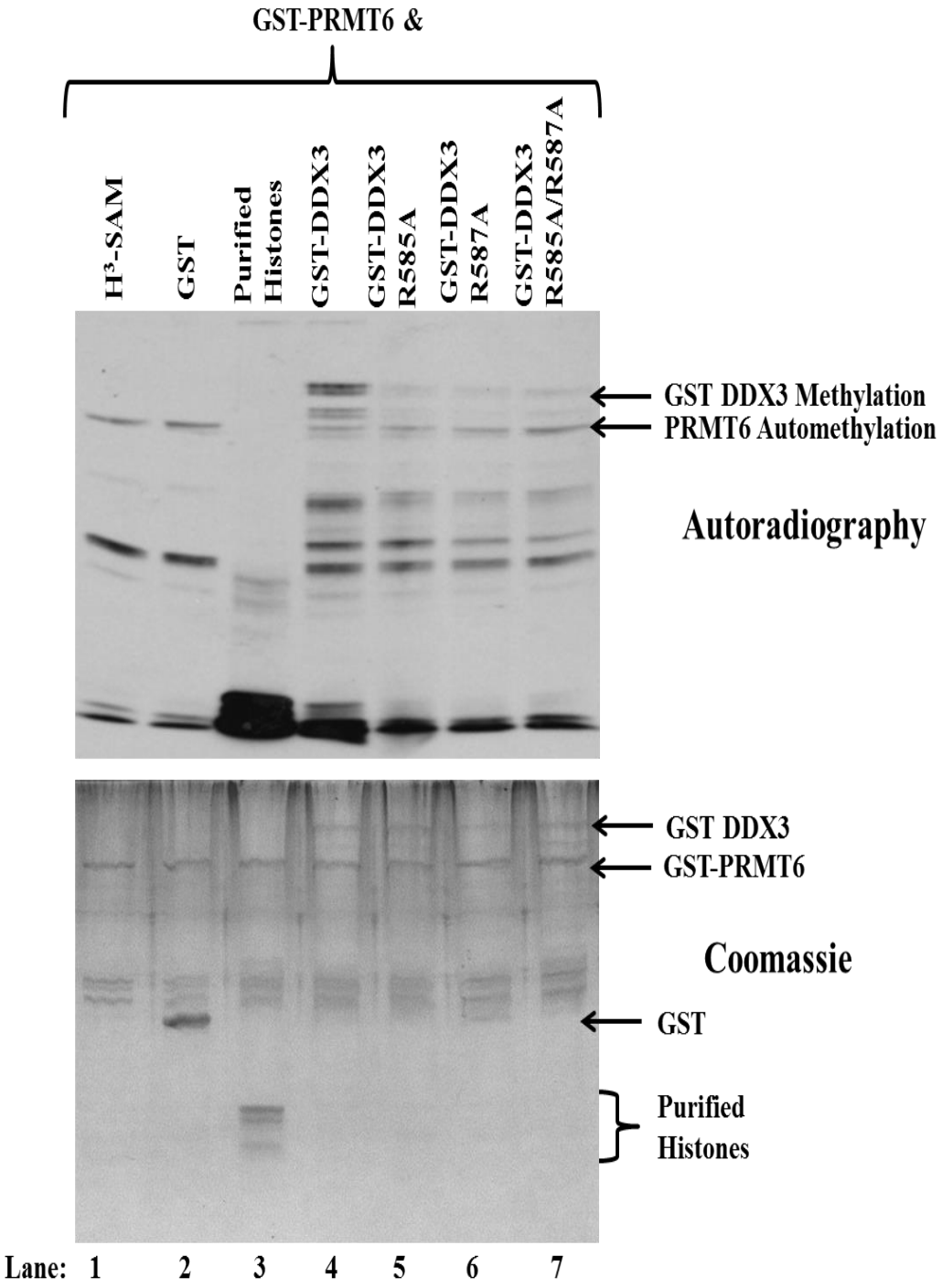
GST-PRMT6 &
H³-SAM
GST
Purified Histones
GST-DDX3
GST-DDX3 R585A
GST-DDX3 R587A
GST-DDX3 R585A/R587A
GST DDX3 Methylation
PRMT6 Automethylation
Autoradiography
GST DDX3
GST-PRMT6
Coomassie
GST
Purified Histones
Lane: 1 2 3 4 5 6 7

Figure 5.14: PRMT6 Methylates DDX3 Arginine Residues 585 and 587 in Full-Length DDX3

Purified GST-PRMT6 was incubated with either full length GST-DDX3 (lane 4), GST-DDX3 R585A (lane 5), GST-DDX3 R587A (lane 6), or GST-DDX3 R585A/R587A (lane 7) in the presence of ^{3}H-SAM. Mutation of arginine residue 585 (lane 5) or 587 (lane 6) to alanine results in a significant decrease in PRMT6 methylation of full length GST-DDX3 construct. Mutation of both arginine residues 585 and 587 did not completely abrogate methylation suggesting additional PRMT6 methylation site(s) occur within the DDX3 amino acid sequence (lane 7) (top panel). Purified histones were utilized as a positive control (lane 3), while GST purified protein was used as a negative control (lane 2). GST-PRMT6 was incubated with ^{3}H-SAM alone to demonstrate its automethylation capability (lane 1). The bottom panel shows Coomassie staining of the gel prior to exposure to autoradiography.

transfected into both scramble and PRMT shRNA expressing cell lines; cells were treated with the translational inhibitors cycloheximide and chloramphenicol, and then incubated with ^{3}H-methionine, and an *in vivo* methylation assay was performed. A significant reduction in methylated myc-tagged DDX3 was observed in the PRMT6 shRNA expressing cells compared to the scramble shRNA expressing cells, especially considering that an increased amount of myc-tagged DDX3 was immunoprecipitated from the PRMT6 shRNA expressing cells (Figure 5.15). This result suggests that, *in vivo*, PRMT6 methylates DDX3.

To validate that PRMT6 methylates DDX3 on arginine residues 585 and 587 *in vivo*, mass spectrometry was performed. Endogenous DDX3 was immunoprecipitated from both HeLa scramble and PRMT6 shRNA expressing cells and run on a SDS-Page gel. The gel was stained with Coomassie Blue and the bands corresponding to DDX3 were excised from the gel. The samples were sent to the Ottawa Hospital Research Institute Proteomics Core Facility for mass spectrometry analysis. Proteins were in-gel digested with chymotrypsin and the peptides were subjected to liquid chromatography tandem mass spectrometry. Peptides were identified using MASCOT software version 2.4. In scramble shRNA expressing samples, 72% DDX3 peptide coverage was attained, while 94% coverage was observed in the PRMT6 shRNA expressing sample. Unfortunately, peptides encompassing arginine residues 585 and 587 were not identified amongst the detected peptides in either the scramble or PRMT6 shRNA expressing samples. Nevertheless, DDX3 arginine residue 315 was identified was being methylated in both the scramble and PRMT6 shRNA samples.

5.15)

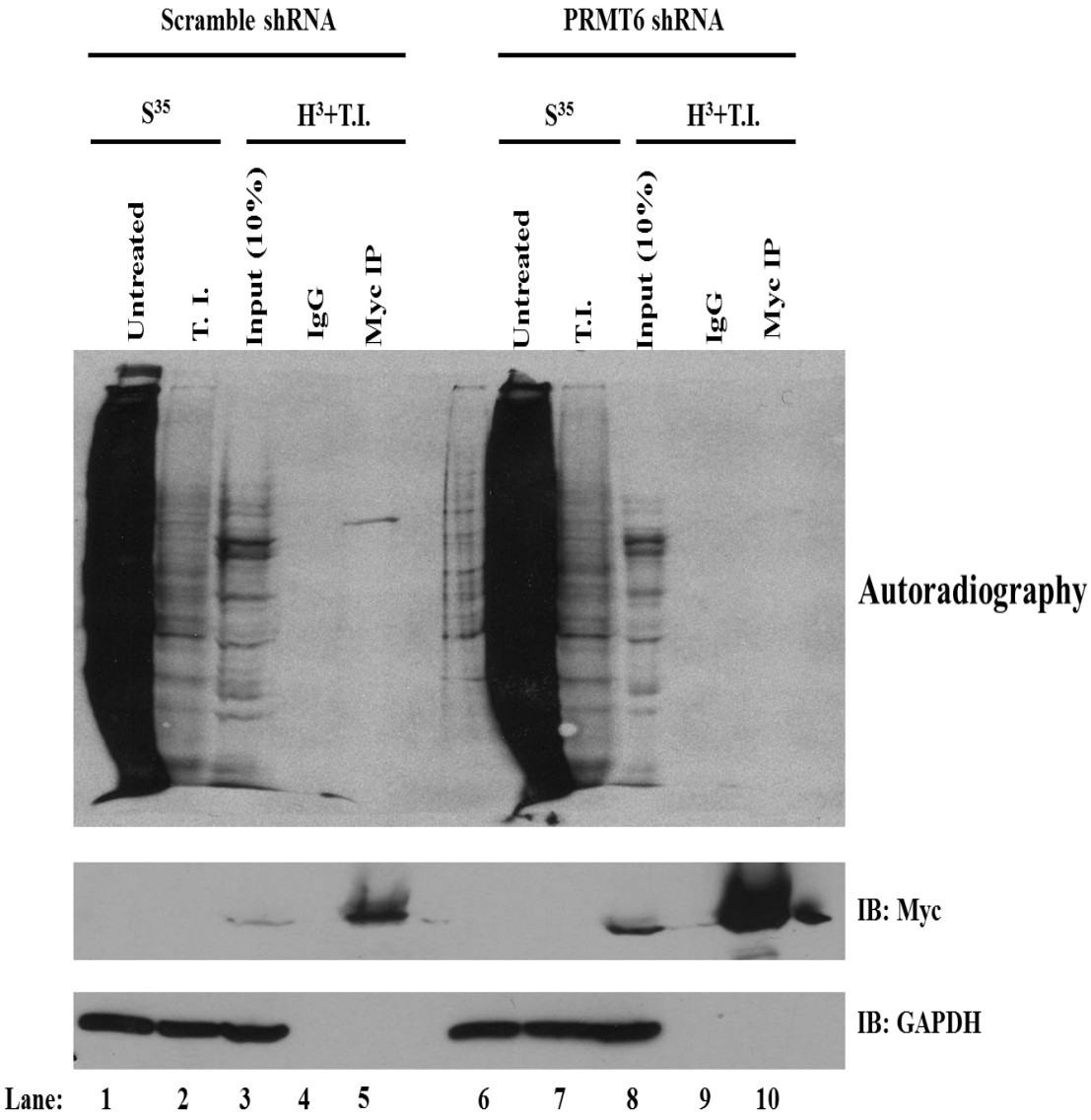
Scramble shRNA
PRMT6 shRNA
S35
H3+T.I.
S35
H3+T.I.
Untreated
T. I.
Input (10%)
IgG
Myc IP
Untreated
T.I.
Input (10%)
IgG
Myc IP
Autoradiography
IB: Myc
IB: GAPDH
Lane: 1 2 3 4 5 6 7 8 9 10

Figure 5.15: PRMT6 Methylates DDX3, *In Vivo*

HeLa scramble or PRMT6 shRNA cells were transfected with myc-tagged DDX3 for 24 h, treated with the translational inhibitors cycloheximide and chloramphenicol for 20 min, and labelled with ^{3}H-methionine for 3 h. Myc was immunoprecipitated from the cell lysate, run on an SDS-Page gel, transferred to PVDF membrane, sprayed with EN^{3}HANCE and exposed to autoradiography. The top panel (autoradiography) shows a significant decrease in methylation of myc-tagged DDX3 (compare lane 5 to lane 10) even though significantly more myc-tagged DDX3 was immunoprecipated in the HeLa PRMT6 shRNA cell lines (middle panel). Lanes 1 and 6 show ^{35}S-methionine labelled lysate, lanes 2 and 7 demonstrates inhibition of translation with cycloheximide and chloramphenicol ^{35}S-methionine labelled lysate, while lane 3 and 8 exhibit cycloheximide and chloramphenicol ^{3}H-methionine labelled lysate. Ten percent of lysate was loaded in each lane. The bottom panel presents GAPDH levels showing equal loading.

To determine any potential effect arginine 315 may have on PRMT6's ability to methylate DDX3, an *in vitro* methylation assay was performed with a full length GST-tagged DDX3 mutation of arginine residue 315 to alanine. Additionally, a triple mutation of arginine residues 315, 585, and 587 was also created. Interestingly, mutation of 315 resulted in increased DDX3 methylation relative to wild type GST-tagged DDX3 (Figure 5.16). Furthermore, triple mutation of all three residues corresponded to an increase in methylation relative to the 585/587 double mutant. This suggests that *in vitro*, arginine 315 inhibits PRMT6 methylation of additional arginine residues and further supports evidence that additional PRMT6 methylation sites besides those identified are present, most likely within the N-terminus of the protein.

5.5 Characterizing the Interaction between PRMT6 and DDX3

Since PRMT6 methylates DDX3, it would be assumed that PRMT6 would interact with DDX3. Therefore, experiments examining whether an interaction occurs between DDX3 and PRMT6 were performed both *in vitro* and *in vivo.* First, a GST pulldown assay was performed with Myc-tagged DDX3 expressed in HeLa cells and then incubated with GST-PRMT6. Myc-tagged DDX3 interacted with GST-PRMT6 but not with GST empty vector (Figure 5.17A). Furthermore, endogenously expressed DDX3 from HeLa cell lysate also interacted with GST-PRMT6 (Figure 5.17B). To further confirm the interaction between DDX3 and PRMT6, 293T cells were co-transfected with Flag-tagged PRMT6 and Myc-tagged DDX3. Upon immunoprecipitation of Myc, an interaction between Flag-tagged PRMT6 and Myc-tagged DDX3 was observed whereas Flag-tagged PRMT6 was not detected in the IPs from Myc-tagged empty vector transfected cells (Figure 5.18A). A reciprocal immunoprecipitation of Flag-tagged

5.16)

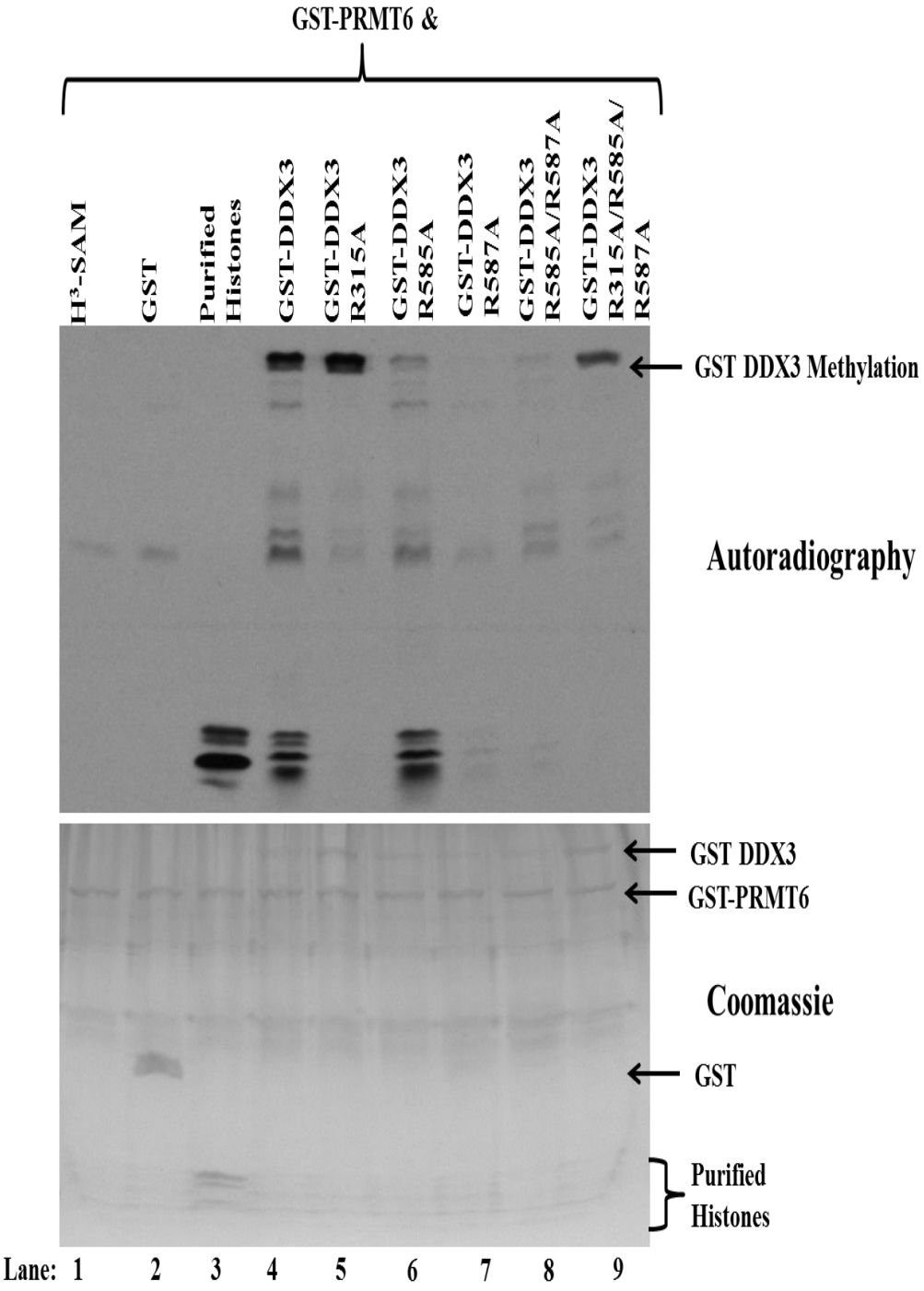
GST-PRMT6 &
H³-SAM
GST
Purified Histones
GST-DDX3
GST-DDX3 R315A
GST-DDX3 R585A
GST-DDX3 R587A
GST-DDX3 R585A/R587A
GST-DDX3 R315A/R585A/ R587A
GST DDX3 Methylation
Autoradiography
GST DDX3
GST-PRMT6
Coomassie
GST
Purified Histones
Lane: 1 2 3 4 5 6 7 8 9

Figure 5.16: Mutation of Arginine Residue 315 Results in Increased Methylation of DDX3

GST-PRMT6 was incubated with wild type GST-DDX3 (lane 4), GST-DDX3 R315A (lane 5), GST-DDX3 R585A (lane 6), GST-DDX3 R587A (lane 7), GST-DDX3 R585A/R587A (lane 8), or GST-DDX3 R315A/R585A/R587A (lane 9) in the presence of ^{3}H-SAM. Mutation of arginine residue 315 resulted in increased methylation of DDX3 by PRMT6 (lane 5), while as previously observed, mutation of residues 585 (lane 6) or 587 (lane 7) causes a decrease in methylation. Whereas mutation of both arginine residues 585 and 587 (lane 8) causes a significant reduction in methylation, mutation of all three arginine residues 315, 585, and 587 leads to an increase in methylation (lane 9) relative to the double mutant (top panel). Purified histones were utilized as a positive control (lane 3), while GST purified protein was used as a negative control (lane 2). GST-PRMT6 was incubated with ^{3}H-SAM alone to demonstrate its automethylation capability (lane 1). The bottom panel shows Coomassie staining of the gel prior to exposure to autoradiography.

5.17A) B)

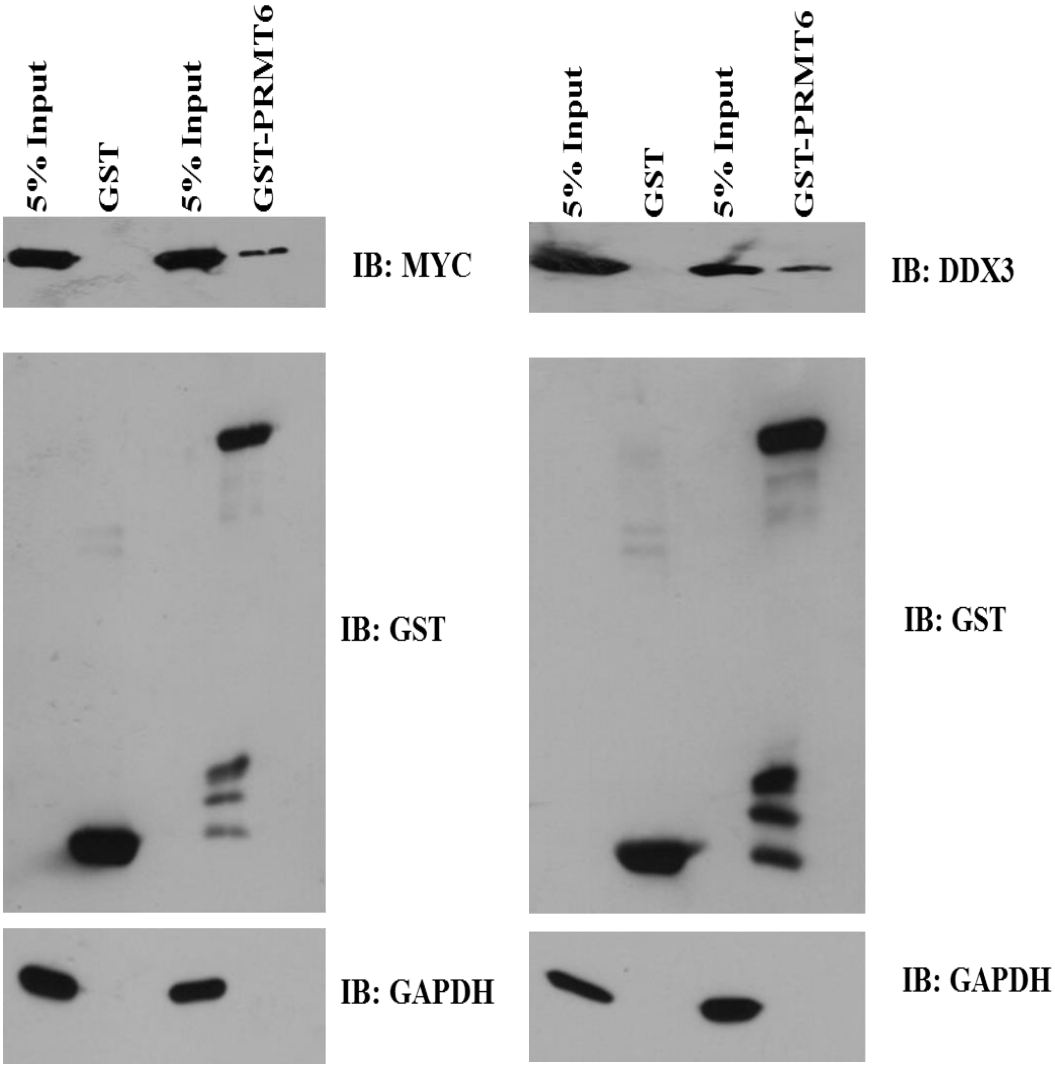
5% Input
GST
5% Input
GST-PRMT6
IB: MYC
IB: GST
IB: GAPDH
5% Input
GST
5% Input
GST-PRMT6
IB: DDX3
IB: GST
IB: GAPDH

Figure 5.17: Endogenous or Exogenously Expressed DDX3 Interacts with GST-PRMT6

(A) HeLa cells with exogenously expressed Myc-tagged DDX3 or (B) HeLa lysate with endogenously expressed DDX3 were incubated with either GST alone or GST-PRMT6 bound to GST beads. Both (A) myc-tagged DDX3 and (B) endogenous DDX3 interacted with GST-PRMT6 but not with GST alone (top panel in both (A) and (B). Western Blotting of GAPDH (bottom panel) shows comparable amounts of lysate was incubated with similar amounts of GST alone or GST-PRMT6 (middle panel).

5.18A)

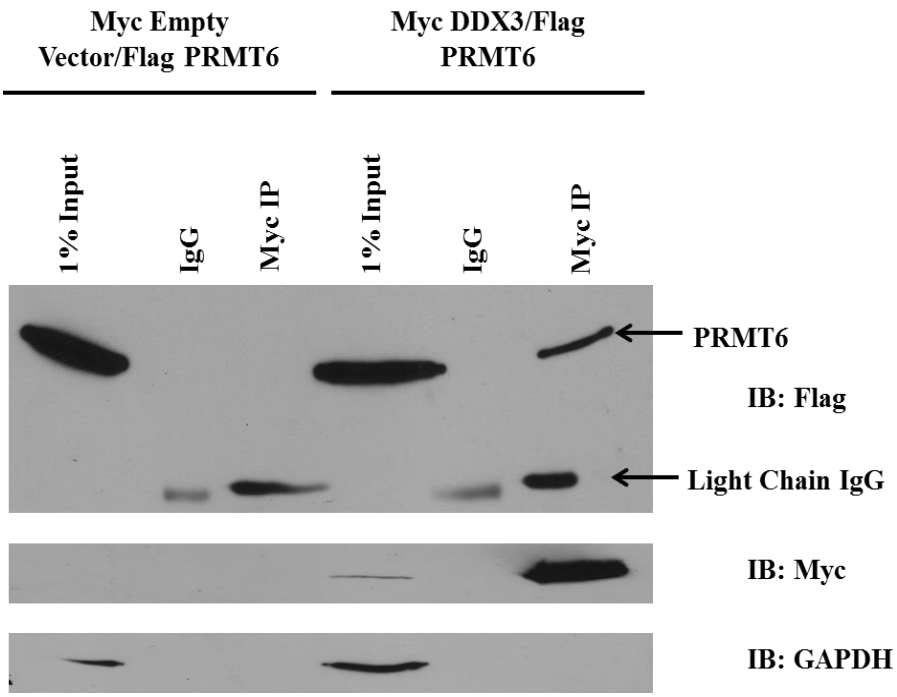
Myc Empty Vector/Flag PRMT6
Myc DDX3/Flag PRMT6
1% Input
IgG
Myc IP
1% Input
IgG
Myc IP
PRMT6
IB: Flag
Light Chain IgG
IB: Myc
IB: GAPDH

B)

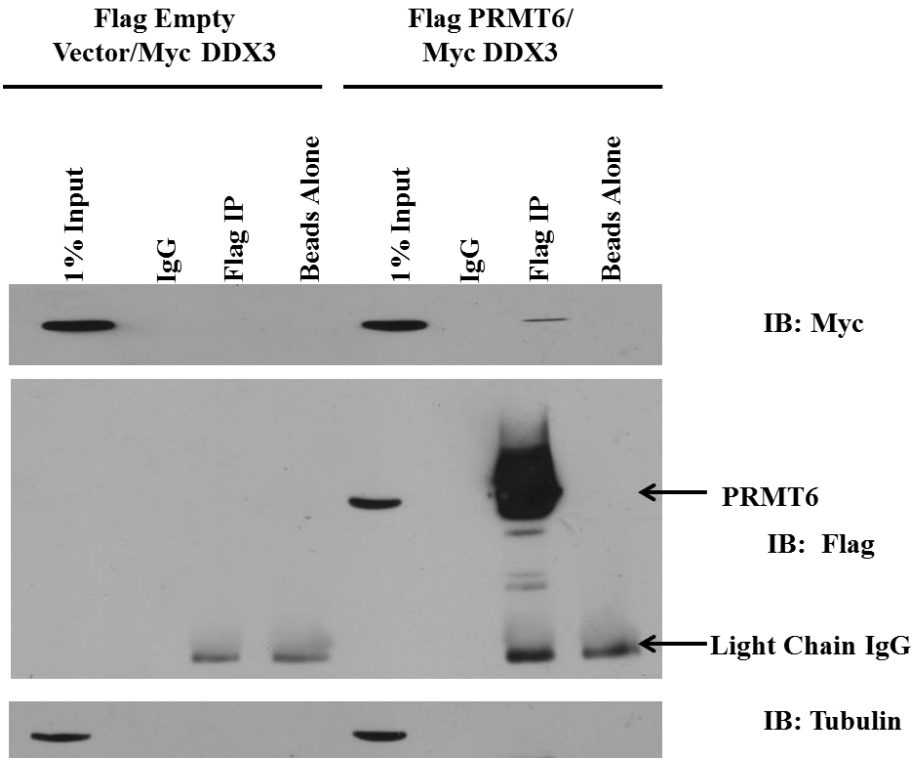
Flag Empty Vector/Myc DDX3
Flag PRMT6/ Myc DDX3
1% Input
IgG
Flag IP
Beads Alone
1% Input
IgG
Flag IP
Beads Alone
IB: Myc
PRMT6
IB: Flag
Light Chain IgG
IB: Tubulin

Figure 5.18: DDX3 Interacts with PRMT6, *In Vivo*

(A) 293T cells were co-transfected with either myc-tagged DDX3/Flag-tagged PRMT6 or myc-tagged empty vector/Flag-tagged PRMT6 with myc-tagged DDX3 immunoprecipitated from the lysate. Flag-tagged PRMT6 interacts with myc-tagged DDX3, but not with myc-tagged empty vector. (B) 293T cells were co-transfected with either myc-tagged DDX3/Flag-tagged empty vector or myc-tagged DDX3/Flag-tagged PRMT6 with Flag-tagged PRMT6 immunoprecipitated from the lysate. Myc-tagged DDX3 interacts with Flag-tagged PRMT6, but not with Flag-tagged empty vector.

PRMT6 confirmed the interaction as Myc-tagged DDX3 interacted with Flag-tagged PRMT6, but not with Flag empty vector (Figure 5.18B).

PRMT6 was observed to methylate both the N-terminus (amino acids 1-181) and the C-terminus (amino acids 405-662) of DDX3, therefore, it was determined if PRMT6 exhibits preferential binding to these regions of DDX3. A GST pulldown assay was performed with His-tagged PRMT6 incubated with wild type GST-tagged DDX3 or the three GST-tagged DDX3 truncation mutants 1-181, 182-404, or 405-662. As expected, His-tagged PRMT6 interacted with wild type GST-DDX3, but showed differential binding to the three DDX3 truncation mutants. His-tagged PRMT6 interacted with the greatest affinity to GST-tagged DDX3 405-662, less robustly to GST-tagged DDX3 1-181, and only showed a minimal interaction with GST-tagged DDX3 182-404 (Figure 5.19A). This result mimics the results observed in the methylation assay with PRMT6 and the DDX3 truncation mutants as GST-PRMT6 methylated mutant 405-662 more robustly than mutant 1-181, with minimal methylation of mutant 182-404 (Figure 5.10).

Next, it was examined whether this pattern of interaction between PRMT6 and the DDX3 truncation mutants was similar in cells. Myc-tagged DDX3 wild type and truncation mutants were expressed in 293T cells, Myc was immunoprecipitated from lysates and immunoblotting with PRMT6 was performed. PRMT6 interacted with myc-tagged wild type DDX3 and with DDX3 truncation mutants 1-181 and 405-662 (Figure 5.19B). Under the conditions utilized, an interaction with DDX3 truncation mutant 182-404 was not observed. It should be noted that the DDX3 truncation mutants expressed in

5.19A)

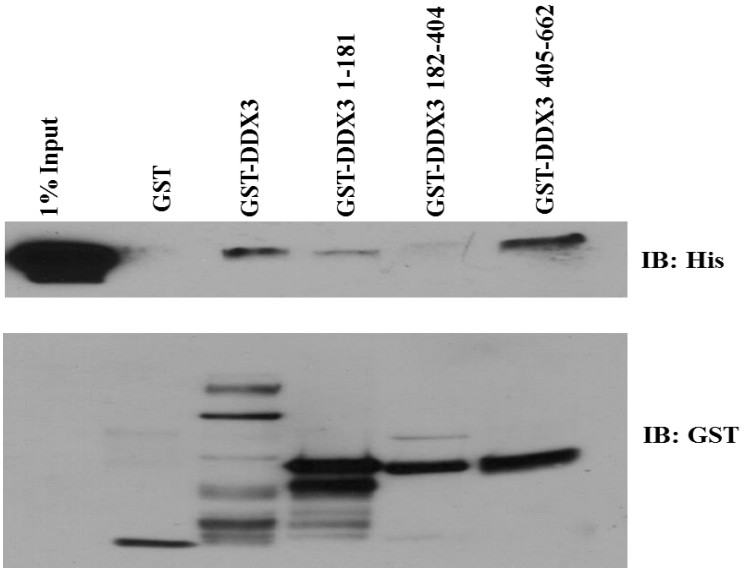
1% Input
GST
GST-DDX3
GST-DDX3 1-181
GST-DDX3 182-404
GST-DDX3 405-662
IB: His
IB: GST

B)

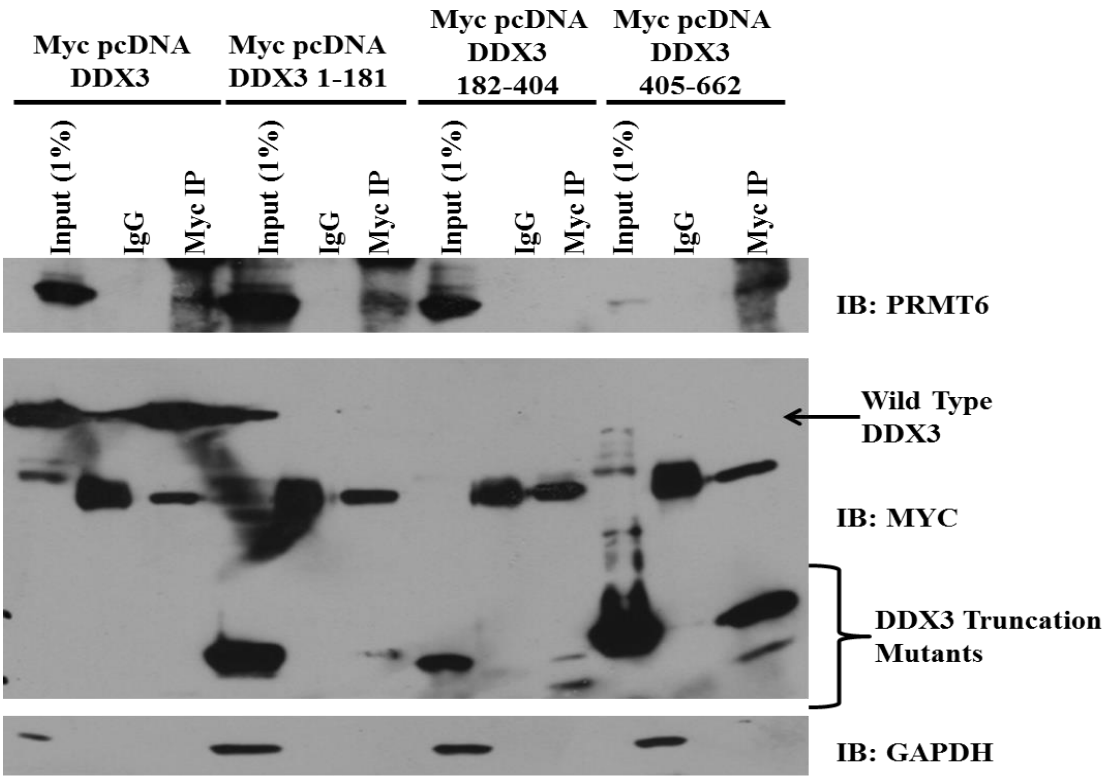
Myc pcDNA DDX3
Myc pcDNA DDX3 1-181
Myc pcDNA DDX3 182-404
Myc pcDNA DDX3 405-662
Input (1%)
IgG
Myc IP
IB: PRMT6
Wild Type DDX3
IB: MYC
DDX3 Truncation Mutants
IB: GAPDH

Figure 5.19: PRMT6 Interacts with the N-terminal and C-terminal Regions of DDX3

(A) His-tagged PRMT6 was incubated with either full length GST-DDX3, GST-DDX3 truncation mutants 1-181, 182-404 or 405-662 bound to GST beads. His-tagged PRMT6 interacts with full length GST-DDX3, along with GST-DDX3 truncation mutants 1-181 and 405-662 (top panel). The bottom panel shows the amount of GST-tagged DDX3 constructs bound to GST beads for each reaction. (B) 293T cells were transfected with full length myc-tagged DDX3, or DDX3 truncation mutants 1-181, 182-404, and 405-662 and myc-tagged DDX3 constructs were immunoprecipitated from the lysate. Endogenous PRMT6 interacts with full length myc–tagged DDX3 and myc-tagged DDX3 truncation mutants 1-181 and 405-662 (top panel). The middle panel shows the quantity of myc-tagged full length and truncated DDX3 immunoprecipitated from the lysate. GAPDH was utilized to show equal amounts of lysate from each transfection was present (bottom panel).

cells at significantly different levels, and that consistently the amount of DDX3 truncation mutant 405-662 immunoprecipitated was greater than the other mutants.

Subsequently, it was examined whether mutation of DDX3's methylated arginine residues impacts PRMT6's ability to bind to DDX3. A GST pulldown assay was performed with His-tagged PRMT6 incubated with GST-tagged wild type DDX3 and DDX3 methylation mutants R315A, R585A, R587A, R585A/R587A, and R315A/R585A/R587A. His-tagged PRMT6 equally bound to GST-tagged wild type DDX3 and each methylation mutant (Appendix Ie). This was confirmed through densitometry of three independent experiments with the amount of bound His-tagged PRMT6 normalized to GST-tagged DDX3 wild type or methylation mutants (Appendix Ie). Therefore, mutation of the PRMT6's target residues for methylation does not affect its ability to bind to DDX3. This result was confirmed using an additional GST pulldown assay as well as through a co-immunoprecipitation assay. First, Myc-tagged wild type DDX3 and methylation mutants R585A, R587A, and R585A/R587A were expressed in 293T cells and the lysates were incubated with GST-tagged PRMT6. A similar amount of myc-tagged wild type DDX3 and methylation mutants bound to GST-tagged PRMT6 (Appendix Ie). Second, Myc-tagged wild type DDX3 and methylation mutants were expressed in 293T cells and Myc was immunoprecipitated from the lysates. A comparable amount of endogenous PRMT6 interacted with myc-tagged DDX3 wild type and each methylation mutant (Appendix If).

Chapter 6: Assessing the Role of TDRD3 in Breast Cancer

TDRD3 expression has been linked with the development and/or progression of breast cancer. TDRD3 was identified as one of the most overexpressed genes in a cohort of patients who exhibited poor prognosis in ER- breast cancer (Nagahata et al., 2004). Moreover, TDRD3 was observed to be amongst 14 genes whose expression correlated with poor patient prognosis in basal-like breast cancer (Hallett et al., 2012). Additionally, in data obtained from the Cancer Genome Atlas' Data Portal, TDRD3 overexpression was seen in 58 out of 158 breast cancer patient samples (http://tcga-portal.nci.nih.gov). TDRD3 also localizes to cytoplasmic stress granules which form in the hypoxic core of tumors and develop upon treatment with chemotherapeutic drugs, thus promoting cell survival (Baguet et al., 2007; Mazroui et al., 2007; Arimoto et al., 2008; Eisinger-Mathason et al., 2008; Fournier et al., 2010). Furthermore, TDRD3 serves as a reader of methylarginine marks deposited by PRMTs whose expression and enzymatic activity are aberrantly regulated in breast cancer (Goulet et al., 2007; Thomassen et al., 2009; Mathioudaki et al., 2011; Yoshimatsu et al., 2011; Al-Dhaheri et al., 2011). Therefore, the potential role that TDRD3 may play in breast cancer etiology necessitated investigation.

6.1 TDRD3 Protein Expression is not altered in Breast Cancer Cell Lines

As TDRD3 has been incriminated in the most aggressive breast cancers, examination of TDRD3 protein levels in a panel of breast cancer cells was performed. In comparison to immortalized, normal mammary epithelial MCF10A cells, no alteration in TDRD3 protein levels were observed from weakly aggressive, ER+ MCF7 cells, to highly aggressive, ER- MDA MB 231 cells (Figure 6.1). Although no difference in protein levels is observed in breast cancer cells, the role that TDRD3 may perform in

6.1A)

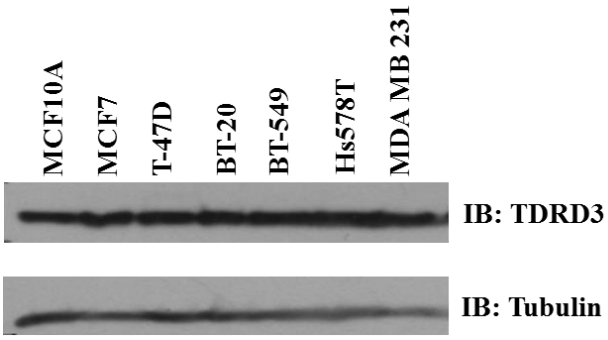
MCF10A
MCF7
T-47D
BT-20
BT-549
Hs578T
MDA MB 231
IB: TDRD3
IB: Tubulin

B)

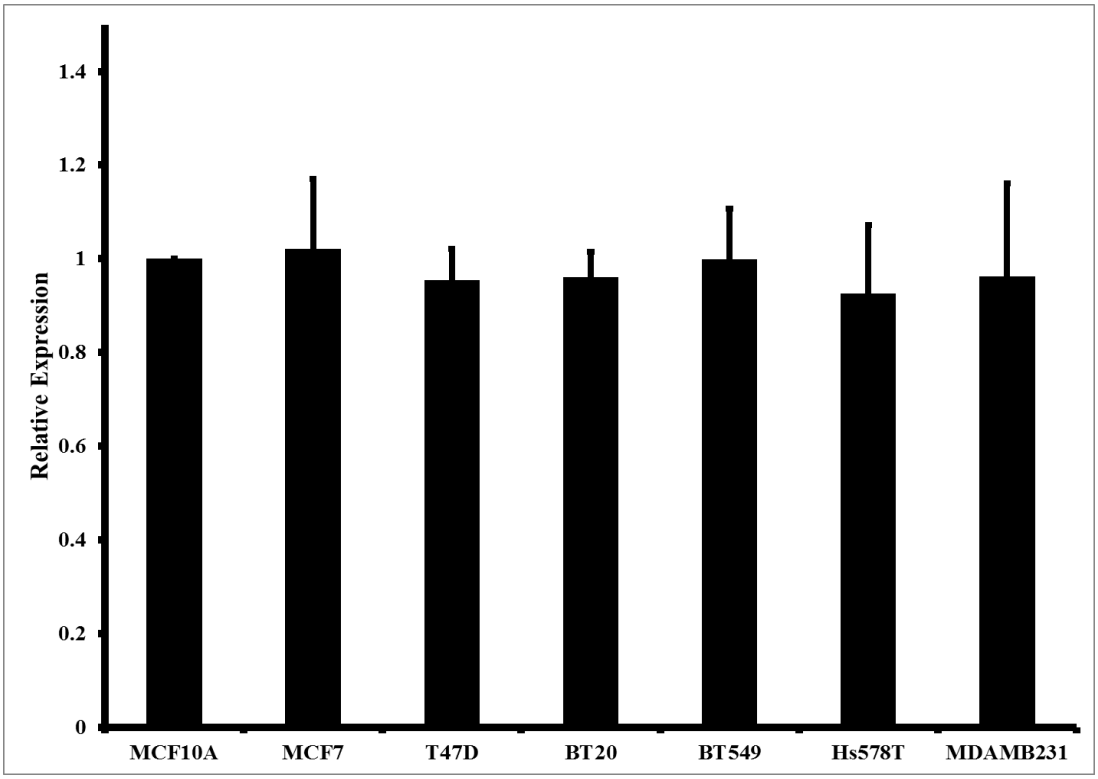
Relative Expression
1.4
1.2
1
0.8
0.6
0.4
0.2
0
MCF10A
MCF7
T47D
BT20
BT549
Hs578T
MDAMB231

Figure 6.1: TDRD3 Protein Expression is unaltered in Breast Cancer Cells

A) Representative image showing TDRD3 protein levels in a panel of breast cancer cells compared to immortalized, normal mammary epithelial cells (MCF10A). Tubulin was used a loading control. B) Densitometry analysis showing no difference in TDRD3 protein expression in breast cancer cells compared to MCF10A cells. TDRD3 protein levels were normalized to the loading control.

breast cancer etiology was still investigated as its function may be independent of its protein expression. Additionally, protein expression in cell lines is not necessarily indicative of the *in vivo* environment where the tumor microenvironment can influence tumor growth.

6.2 TDRD3 Depletion Inhibits Breast Cancer Cell Proliferation

To elucidate the role that TDRD3 performs in breast cancer, stably expressing TDRD3 shRNA pools of cells were established in MDA MB 231 and Hs578T breast cancer cell lines (Figure 6.2A). Both MDA MB 231 and Hs578T cell lines are highly aggressive, ER- breast cancer cell lines which are apt to serve as a cell culture analog to mimic the results observed in patient studies (Nagahata et al., 2004; Hallett et al., 2012), though Hs578T cells are less aggressive in nature than MDA MB 231 cells. The effect of cell proliferation upon TDRD3 depletion was investigated utilizing a MTT assay. Using two pools of TDRD3 depleted MDA MB 231 cells, cell proliferation was significantly reduced relative to the scramble shRNA expressing cells over an eight day time course, measured using a two way ANOVA (Figure 6.2B). However, in Hs578T cells, though a decrease in cell proliferation was observed, the reduction was not statistically significant (Figure 6.2C).

6.3 TDRD3 Depletion Inhibits Anchorage Independent Growth

The ability of cancer cells to sustain growth independent of their adherence to the surrounding tissue within a tumour environment is a hallmark of cancer, a phenotype indicative of cellular transformation (Hanahan and Weinberg, 2000). Therefore, the effect of TDRD3 depletion on this phenomenon was analyzed. An equal number of MDA MB 231 parental, scramble or TDRD3 shRNA expressing cells were grown in soft agar for a

6.2A)

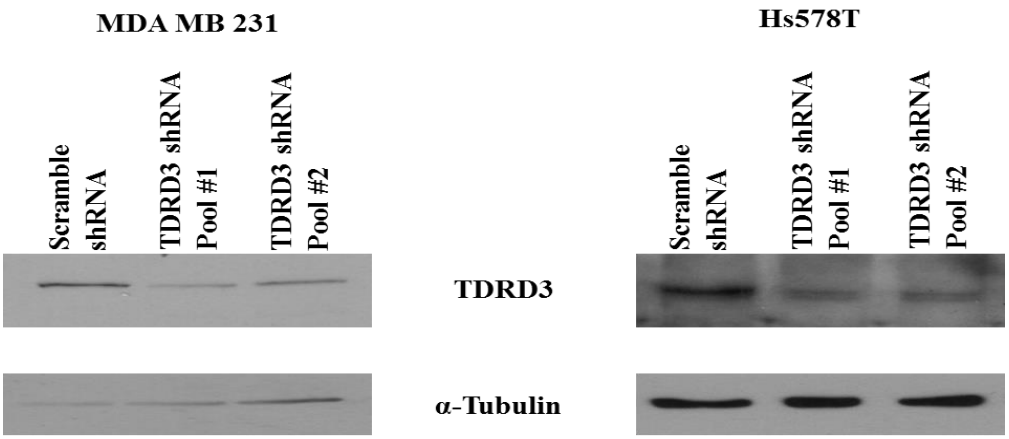
MDA MB 231
Hs578T
Scramble shRNA
TDRD3 shRNA Pool #1
TDRD3 shRNA Pool #2
TDRD3
α-Tubulin

B)

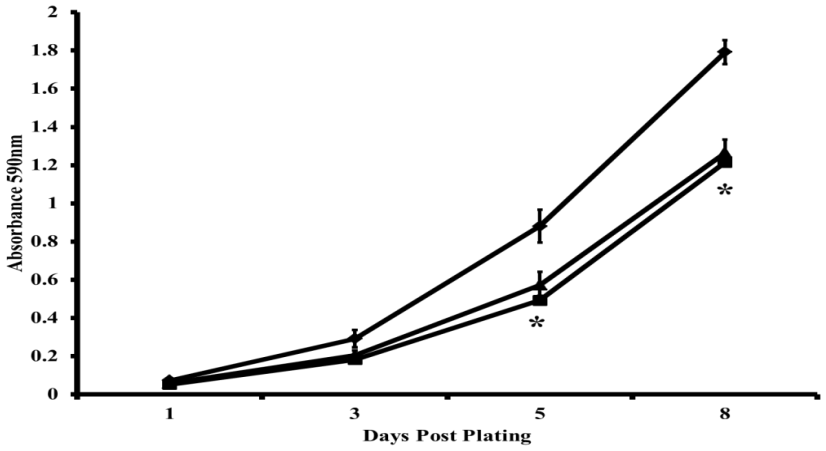
Absorbance 590nm
Days Post Plating
*
*

C)

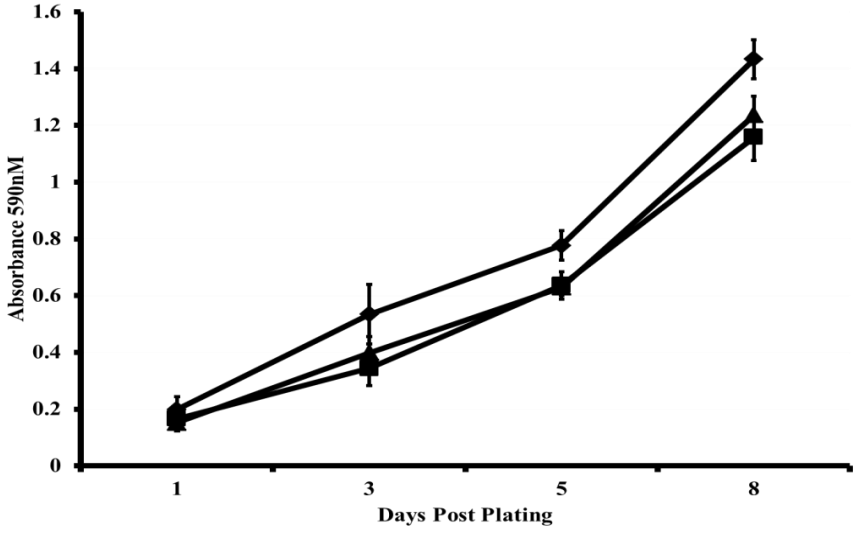
Absorbance 590nM
Days Post Plating

Figure 6.2: TDRD3 Depletion Inhibits Breast Cancer Cell Proliferation

(A) MDA MB 231 (left panel) or Hs578T (right panel) stably expressing TDRD3 shRNA were established. Western blot showing knockdown of TDRD3 protein levels in two pools of cells in MDA MB 231 and Hs578T cells. Tubulin was used as a loading control. Equal numbers of (B) MDA MB 231 or (C) Hs578T scramble and TDRD3 shRNA expressing cells were plated and cell proliferation was followed for 8 days with a MTT assay. ♦ represents the scramble shRNA expressing cells, while ■ represents TDRD3 shRNA pool #1 and ▲denotes TDRD3 shRNA pool #2. A statistically significant reduction in cell proliferation was observed in MDA MB 231 TDRD3 shRNA expressing cells but not in Hs578T TDRD3 shRNA cells as determined using a two way ANOVA.

period of three weeks, stained with crystal violet and the number of colonies were counted. TDRD3 depletion resulted in a decrease in the number of colonies that formed compared to both the MDA MB 231 parental and scramble shRNA expressing cells (Figure 6.3A). An average of 31.6 and 30 colonies formed with MDA MB 231 parental and scramble shRNA expressing cells, respectively compared to 8.6 and 19.3 colonies formed with two TDRD3 shRNA expressing cell lines. MCF10A cells, which are normal mammary epithelial cells, and therefore should not form any colonies, were used as a negative control. In addition, TDRD3 depletion corresponded to an overall decrease in colony size (Figure 6.3B). These results were statistically significant with a p-value less than one percent determined with using a one way ANOVA.

6.4 TDRD3 Depletion Impedes Breast Cancer Cell Motility and Invasion

The ability of a cell to metastasize begins with an increased propensity for a cell to move, along with its capacity to penetrate and invade through barriers. Therefore, the effect of TDRD3 depletion was investigated on these hallmarks of cancer. Motility and invasive potential were examined using Transwell chambers without or with a matrix layer, respectively. In MDA MB 231 cells, a significant decrease in motility was observed upon TDRD3 depletion (Figure 6.4A & 6.4C). An average of 103.1 MDA MB 231 scramble shRNA expressing cells passed through the Transwell chamber compared to an average of 76.3 and 75.5 TDRD3 shRNA expressing cells. Likewise, measuring cell invasion upon TDRD3 depletion yielded a significant decrease determined using a one way ANOVA (Figure 6.4B & 6.4C). An average of 63.9 MDA MB 231 scramble shRNA expressing cells passed through the Transwell chamber contrasted with 24.1 and 13.3 TDRD3 shRNA expressing cells. Interestingly, in Hs58T cells, a significant but not as

6.3A)

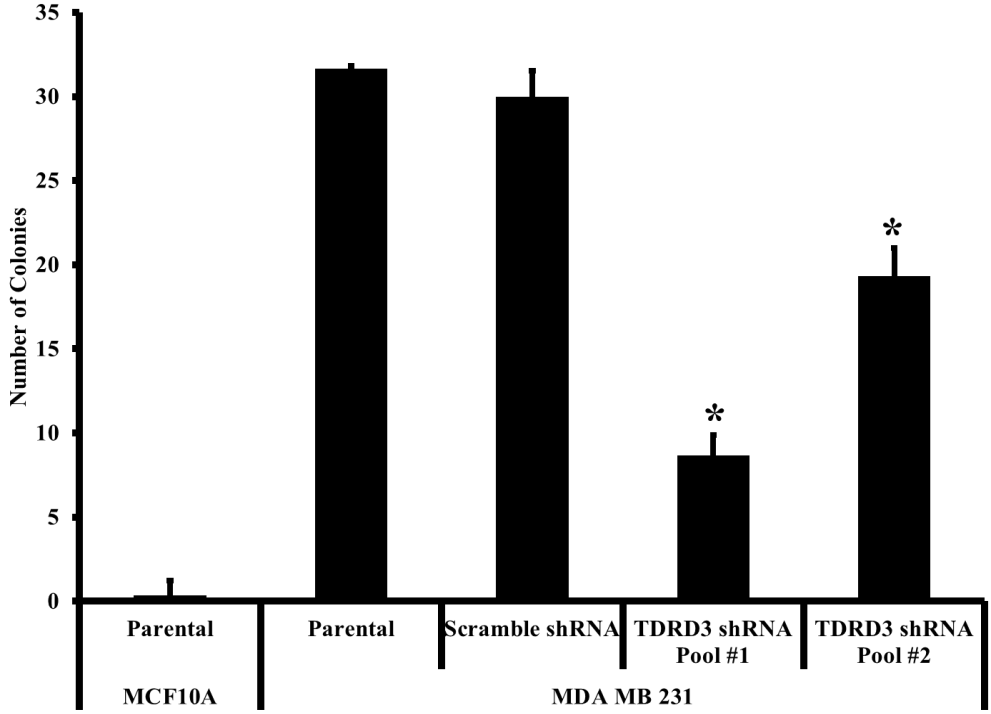
35
30
25
20
15
10
5
0
Number of Colonies
*
*
Parental
Parental
Scramble shRNA
TDRD3 shRNA Pool #1
TDRD3 shRNA Pool #2
MCF10A
MDA MB 231

B)

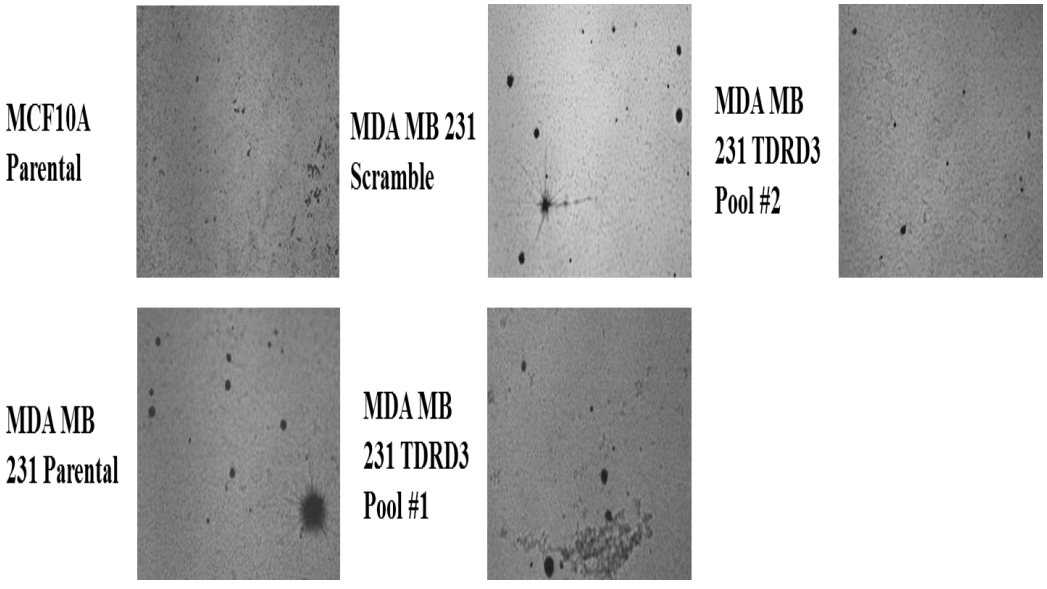
MCF10A Parental
MDA MB 231 Scramble
MDA MB 231 TDRD3 Pool #2
MDA MB 231 Parental
MDA MB 231 TDRD3 Pool #1

Figure 6.3: TDRD3 Depletion Inhibits Anchorage-Independent Colony Formation

An equal number of MCF10A and MDA MB 231 parental, scramble shRNA stably expressing or two pools of TDRD3 shRNA stably expressing cells were plated in a layer of media containing agar and grown over a period of three weeks. The colonies were stained with crystal violet and counted. (A) TDRD3 depletion results in a decrease in colony formation. Data is the mean of three independent experiments +/- the standard error of the mean. * denotes statistical significance determined with a one way ANOVA with a p-value less than 0.01. (B) Representative images of colony formation show a decrease in colony formation as well as an overall decrease in the size of colonies. Images were taken at 5X magnification.

6.4A)

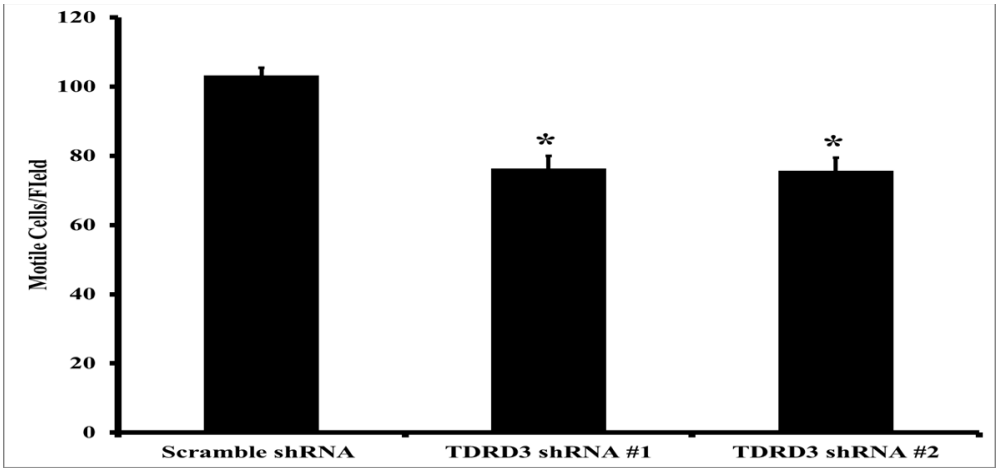
120
100
80
60
40
20
0
Motile Cells/Field
*
*
Scramble shRNA
TDRD3 shRNA #1
TDRD3 shRNA #2

B)

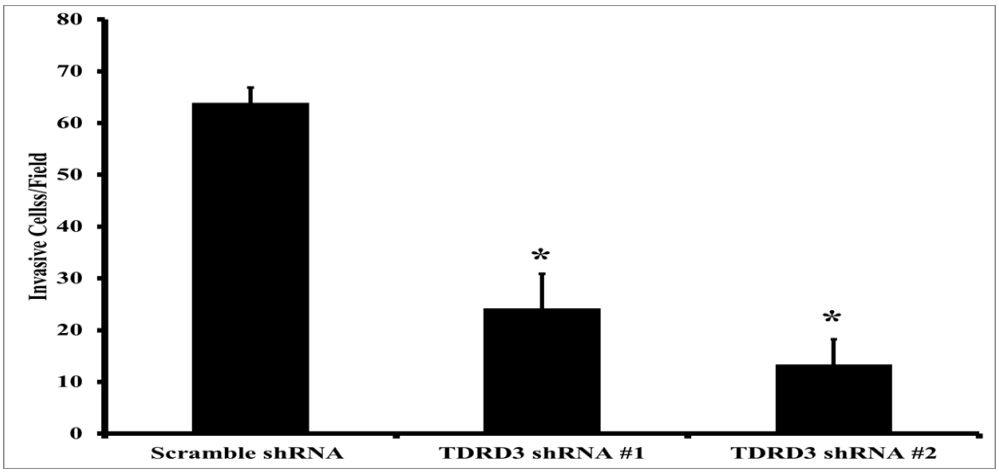
80
70
60
50
40
30
20
10
0
Invasive Cellss/Field
*
*
Scramble shRNA
TDRD3 shRNA #1
TDRD3 shRNA #2

C)

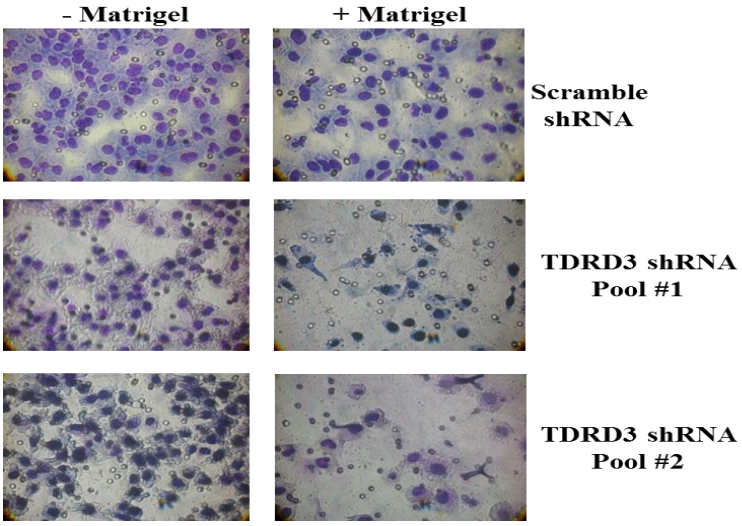
- Matrigel
+ Matrigel
Scramble shRNA
TDRD3 shRNA Pool #1
TDRD3 shRNA Pool #2

Figure 6.4: TDRD3 Depletion inhibits Cell Motility and Invasion in MDA MB 231 cells

MDA MB 231 scramble or TDRD3 shRNA expressing cells were equally plated in Transwell chambers in the absence or presence of matrigel for 24 h. Cells were removed from the top of the chamber, with the cells at the bottom of the chamber fixed, stained and counted. Six images were taken of each chamber with the results the average of six experiments +/- the standard error of the means. A statistically significant reduction in (A) motility and (B) invasion upon TDRD3 depletion was observed. (C) Representative images were taken at 20X magnification showing the number of scramble and TDRD3 shRNA expressing cells that passed through the Transwell chamber in the absence or presence of matrigel.

substantial reduction in cell invasion in TDRD3 depleted cells was observed (Figure 6.5B & 6.5C); however no difference in cell motility was discerned (Figure 6.5A & 6.5C). Measuring cell invasion, an average of 39.1 scramble shRNA expressing cells passed through the Transwell invasion chambers, while 18.3 and 16.8 TDRD3 depleted cells migrated through the chamber. For cell motility, an average of 56.5 scramble shRNA expressing cells, and 57.3 and 50.3 TDRD3 shRNA expressing cells migrated through the chambers.

To corroborate the motility data observed upon TDRD3 depletion with the Transwell chamber, motility was further assessed using a scratch wound assay. MDA MB 231 cells were grown to confluency, a wound was made with a pipette tip and the rate at which the cells closed the wound was measured 6, 12, and 24 h after the wound was made. Interestingly, 6 and 12 h after the wound was made, in TDRD3 depleted cells, the wound closed at a slower rate than in scramble shRNA expressing cells (Appendix Ig). However, 24 h after the wound was made, in both the scramble and TDRD3 shRNA expressing cell lines, the wound was closed. Even though the wound was essentially closed 24 h post-wound incision, a statistically significant difference was measured at 6 and 12 h using a two way ANOVA.

6.5 TDRD3's Promotion of Breast Cancer Cell Invasion Properties Depends on its Interaction with the RNA Binding Protein FMRP

Since the effect of TDRD3 depletion was most prominent on breast cancer cell invasion in MDA MB 231 cells, a rescue experiment was performed in this cell line to specifically demonstrate that TDRD3 expression is instrumental in regulating cell invasion. While transfection of scramble and TDRD3 shRNA expressing cells with an

6.5A)

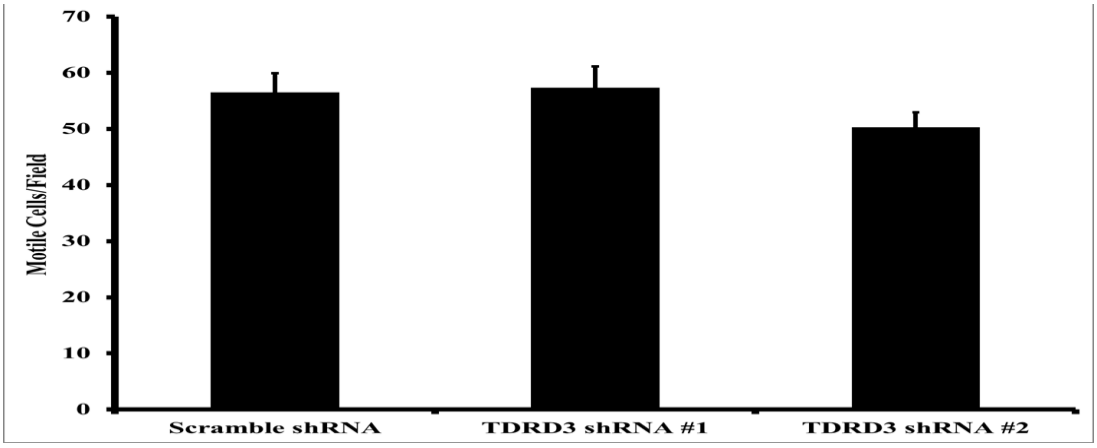
Motile Cells/Field
70
60
50
40
30
20
10
0
Scramble shRNA
TDRD3 shRNA #1
TDRD3 shRNA #2

B)

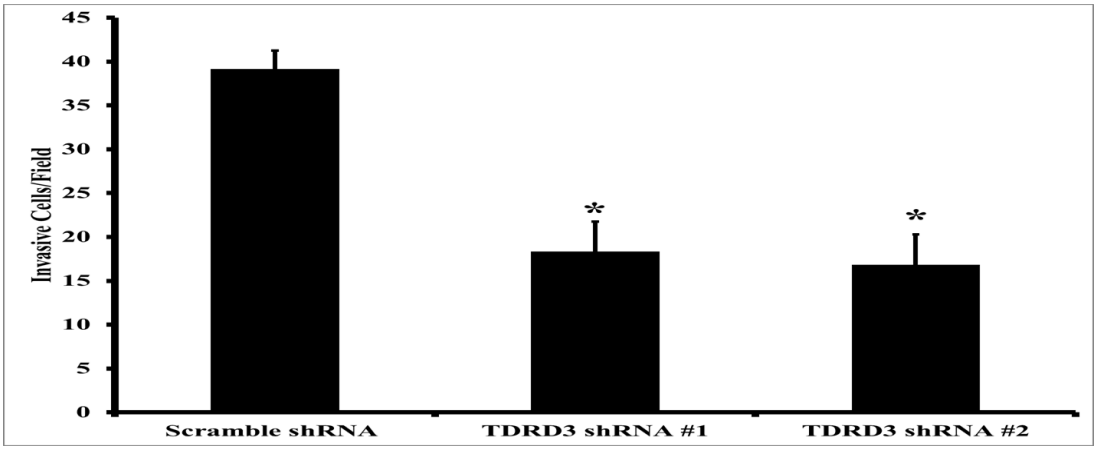
Invasive Cells/Field
45
40
35
30
25
20
15
10
5
0
*
*
Scramble shRNA
TDRD3 shRNA #1
TDRD3 shRNA #2

C)

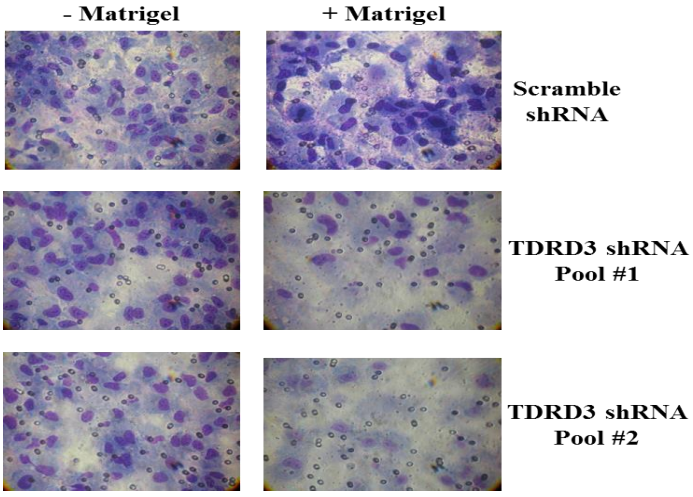
- Matrigel
+ Matrigel
Scramble shRNA
TDRD3 shRNA Pool #1
TDRD3 shRNA Pool #2

Figure 6.5: TDRD3 Depletion inhibits Cell Invasion in Hs578T cells

Hs578T scramble or TDRD3 shRNA expressing cells were equally plated in Transwell chambers in the absence or presence of matrigel for 24 h. Cells were removed from the top of the chamber, with the cells at the bottom of the chamber fixed, stained and counted. Six images were taken of each chamber with the results the average of six experiments +/- the standard error of the means. A statistically significant reduction in (B) invasion upon TDRD3 depletion was observed. (C) Representative images were taken at 20X magnification showing the number of scramble and TDRD3 shRNA expressing cells that passed through the Transwell chamber in the absence or presence of matrigel.

empty vector construct yielded similar results as were previously observed, re-introduction of a myc-tagged TDRD3 construct was sufficient to rescue the defect in cell invasion (Figure 6.6B). Likewise, re-introduction of a GFP-tagged TDRD3 construct exhibited the same phenotype (Appendix Ih).

Next, the minimal domain of TDRD3 required to rescue the defect in cell invasion was determined. Various TDRD3 deletion mutants were examined (Figure 6.6A). The E691K mutant within TDRD3's Tudor domain abrogates TDRD3's ability to bind to methylarginine motifs (Goulet et al., 2008). The TDRD3 ΔFMRP domains inhibits TDRD3 ability to interact with FMRP (Linder et al., 2008; Xu et al., 2013; Stoll et al., 2013), while TDRD3 ΔEBM prevents TDRD3 binding to the exon junction complex (Kashima et al., 2010). The TDRD3 Δ647-744 mutant lacks the Tudor, FMRP binding and EBM binding domains, whereas TDRD3 ΔN328 has the entire N-terminal region of TDRD3 including the DUF/OB fold and UBA domains deleted. The central linker construct contains the yet uncharacterized region of amino acids 329 to 646 between the UBA and Tudor domains. Lastly, TDRD3 constructs examining the C-terminal region (amino acids 647-744) were also examined: TDRD3 647-744, TDRD3 647-744 ΔFMRP, TDRD3 647-744 ΔEBM, and the region just encompassing the Tudor domain (amino acids 647-710). Interestingly, expression of TDRD3 constructs lacking the FMRP binding domain (TDRD3 ΔFMRP, TDRD3 Δ647-744, Central Linker, TDRD3 647-744 ΔFMRP, and Tudor domain) where unable to rescue TDRD3's ability to promote cell invasion (Figure 6.6B). Remarkably, TDRD3's aptitude to recognize arginine methylated motifs had no effect on its ability to regulate cell invasion as the TDRD3 E691K mutant was able to rescue cell invasion. Western blot analysis demonstrates similar expression of

all the TDRD3 constructs utilized (Figure 6.6C). These results suggest that TDRD3 promotes cell invasion through binding to FMRP.

6.6A)

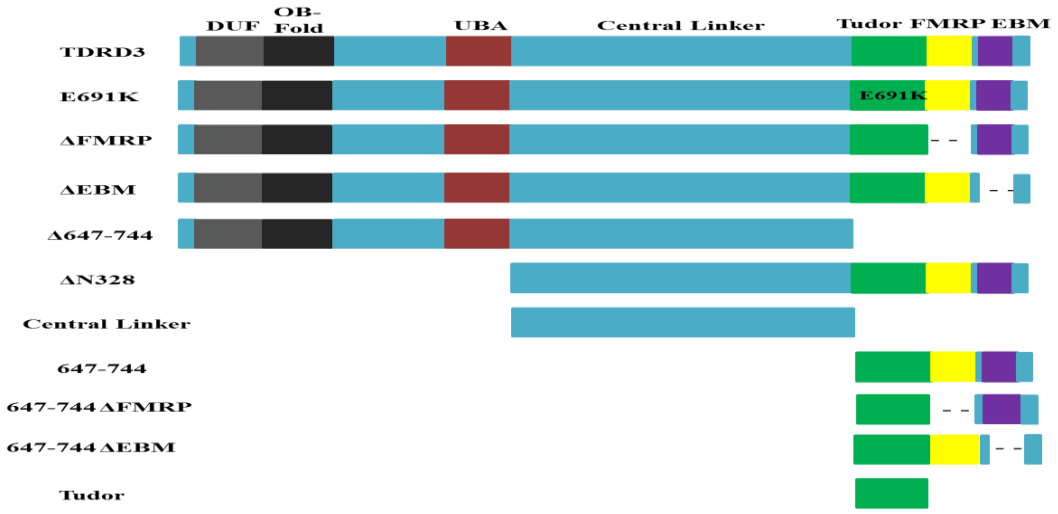
DUF
OB-Fold
UBA
Central Linker
Tudor FMRP EBM
TDRD3
E691K
ΔFMRP
ΔEBM
Δ647-744
ΔN328
Central Linker
647-744
647-744 ΔFMRP
647-744 ΔEBM
Tudor

B)

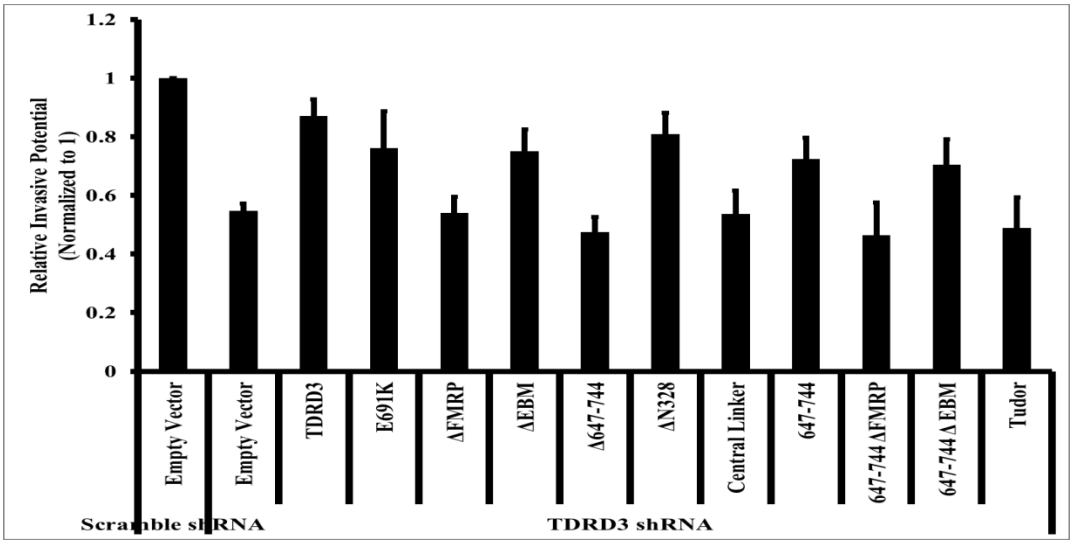
Relative Invasive Potential (Normalized to 1)
1.2
1
0.8
0.6
0.4
0.2
0
Empty Vector
Empty Vector
TDRD3
E691K
ΔFMRP
ΔEBM
Δ647-744
ΔN328
Central Linker
647-744
647-744 ΔFMRP
647-744 Δ EBM
Tudor
Scramble shRNA
TDRD3 shRNA

C)

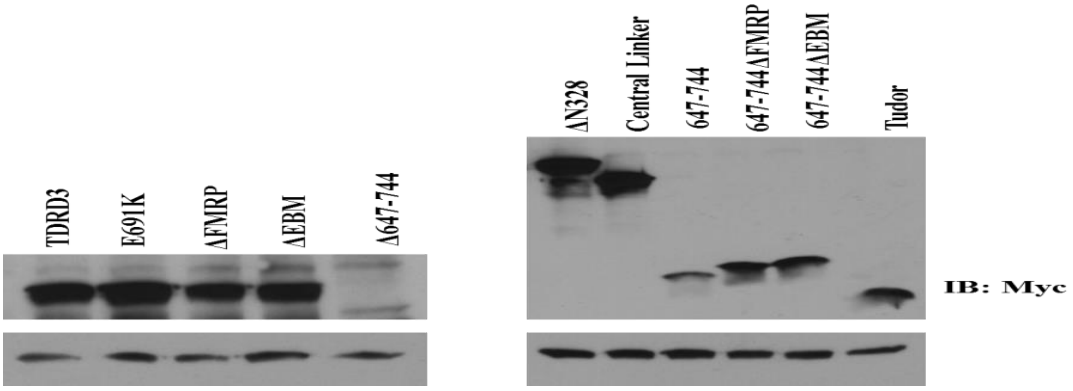
TDRD3
E691K
ΔFMRP
ΔEBM
Δ647-744
ΔN328
Central Linker
647-744
647-744ΔFMRP
647-744ΔEBM
Tudor
IB: Myc

Figure 6.6: TDRD3 Promotion of Breast Cancer Cell Invasion Properties is Dependent on its Ability to Bind the RNA Binding Protein FMRP

MDA MB 231 TDRD3 shRNA stably expressing cells were transfected with TDRD3 deletion constructs for 48 h. Cells were counted and then equally plated in Transwell invasion chambers for 24 h. The chambers were stained, and quantification of the number of cell invading through the chambers was determined by taking pictures of eight fields of view at 40X magnification (A) Representation of the TDRD3 deletion constructs that were used to determine the minimal domain responsible for rescuing TDRD3-mediated cell invasion. (B) TDRD3's ability to promote cell invasion is dependent on its capacity to bind FMRP. Data are the mean of at least three independent experiments +/- the standard error of the mean. Data for the various TDRD3 deletion constructs was normalized to the TDRD3 empty vector data to obtain the relative invasive potential of each TDRD3 construct to rescue invasion. (C)Western blotting showing that each TDRD3 deletion constructs expresses in cells, and that they exhibit similar expression levels. Tubulin was used as a loading control.

Chapter 7: Discussion

Breast cancer is the most common cancer among Canadian women, with one in nine women developing breast cancer in her lifetime. In 2013, an estimated 23 800 women were diagnosed with breast cancer with an estimated 5 000 women dying from this disease (Canadian Cancer Society). Though a number of treatments are available including surgical resection, radiation and chemotherapy, in many instances tumours are refractory or recur. Therefore, understanding the biological events that lead to the progression and therapeutic resistance of breast cancer is essential for the development of novel treatment options for this disease.

Many of the protein arginine methyltransferases, the family of enzymes responsible for the catalysis of arginine methylation, are aberrantly regulated in breast cancer. PRMT1 (Yoshimatsu et al., 2011; Mathioudaki et al., 2011), PRMT2 ((Zhong et al., 2011; Zhong et al., 2012), CARM1 (Al-Dhaheri et al., 2011), PRMT6 (Yoshimatsu et al., 2011; Dowhan et al., 2012), and PRMT7 (Thomassen et al., 2009) expression is altered in breast cancer. Furthermore, this mis-regulation in protein expression correlates with atypical regulation of crucial cell pathways, many of which are altered in breast cancer (Singh et al., 2004; El Messaoudi et al., 2006; Heller et al., 2007; Frietze et al., 2008; Le Romancer et al., 2008; Guendel et al., 2010; Zhong et al., 2011; Zhong et al., 2012; Takahashi et al., 2012). Furthermore, a number of PRMT substrates including but not limited to the estrogen receptor α (Le Romancer et al., 2008), FOXO1 (Yamagata et al., 2008), Axin (Cha et al., 2011), AIB1 (Feng et al., 2006; Naeem et al., 2007), as well as DDX3 (Botlagunta et al., 2008; Botlagunta et al., 2011) identified here as a novel substrate of PRMT1, CARM1 and PRMT6 are implicated in breast cancer development

or progression. Moreover, expression of TDRD3, one of three identified readers of arginine methylated motifs, correlates with poor patient prognosis in highly aggressive breast tumours (Nagahata et al., 2004; Hallett et al., 2012).

The data presented here further elaborates on the research linking arginine methylation with breast cancer development and progression. First, the alternatively spliced PRMT1 isoform, PRMT1v2, previously observed to be overexpressed in a panel of breast cancer cells, regulates apoptosis and cell invasion. Second, a novel role is described for PRMT6, another PRMT exhibiting altered expression in breast cancer. PRMT6 promotes chemoresistance to the drug bortezomib by mediating stress granule formation, thus promoting breast cancer cell survival. Third, DDX3, a prototypical substrate of PRMTs known to be overexpressed in breast cancer, is identified as a novel substrate of PRMT1, CARM1, and PRMT6. Lastly, TDRD3, a reader of methylated arginine motifs, also overexpressed in breast cancer regulates breast cancer cell proliferation, anchorage-independent growth and cell invasion. Therefore, it appears that there may be a link between upstream mis-regulation of PRMTs (writers of arginine methylation), and the coincidental aberrant methylation of PRMT substrates, leading to abnormal reading of the arginine methylated mark by TDRD3, thus potentially promoting breast cancer development and progression (Figure 7.1).

Protein Arginine Methyltransferase 1 isoform 2 Promotes Breast Cancer Cell Survival and Invasiveness

Aberrant PRMT1 expression has been discerned in various cancers, including breast cancer (Goulet et al., 2007; Cheung et al., 2007; Mathioudaki et al., 2011; Mathioudaki et al., 2008; Yoshimatsu et al., 2011; Papadokostopoulou et al., 2009).

7.1)

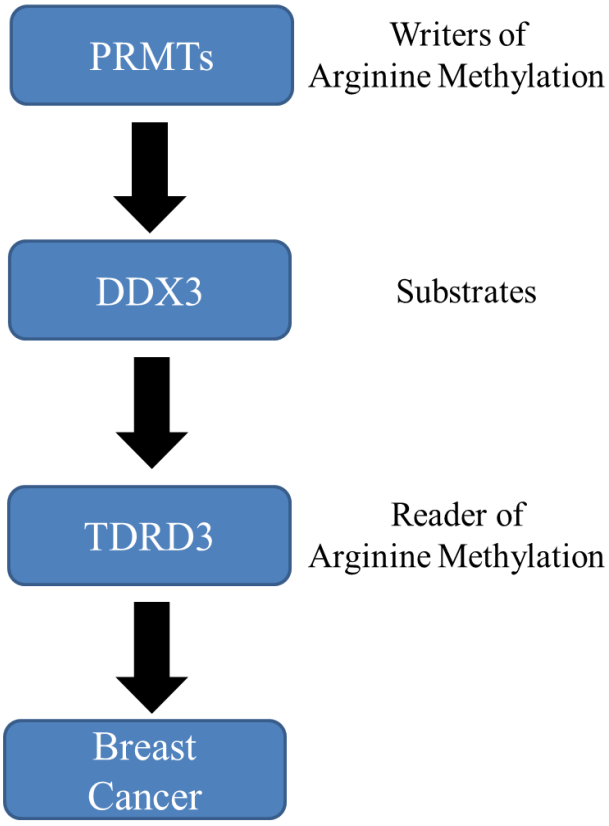
PRMTs
Writers of
Arginine Methylation
DDX3
Substrates
TDRD3
Reader of
Arginine Methylation
Breast
Cancer

Figure 7.1: Model of Regulation of Arginine Methylation in Breast Cancer

PRMTs serve as writers of arginine methylation within the cell. Aberrant regulation of PRMTs is prevalent within breast cancer cell lines and patient samples. Here, PRMT1v2, one of the PRMTs overexpressed in breast cancer has been shown to mediate apoptosis and cell invasion in breast cancer cell lines. Additionally, PRMT6, another PRMT aberrantly regulated in breast cancer mediates chemoresistance through facilitating stress granule formation, thus promoting cancer cell survival. A number of PRMTs substrates, including DDX3, identified here as a novel substrate of PRMT1, CARM1, and PRMT6 are linked with breast cancer. Additionally, TDRD3, a reader of arginine methylated motifs, overexpressed in highly aggressive breast tumors regulates breast cancer cell proliferation, anchorage-independent growth, and cell invasion. Therefore, it appears that there may a link between upstream mis-regulation of PRMTs (writers of arginine methylation), and the coincidental aberrant methylation of PRMT substrates, leading to abnormal reading of the arginine methylated mark by TDRD3, thus promoting breast cancer development and progression

Specifically, in breast cancer, expression of several PRMT1 isoforms is increased, however the mean expression of PRMT1v2 is increased to a greater extent than PRMT1v1, the most abundant isoform (Goulet et al., 2007). A clinical study examining the expression of PRMT1v1, v2, and v3 in breast cancer samples identified a strong correlation between PRMT1v1 mRNA expression and poor patient prognosis, though PRMT1v2 and v3 levels were not altered at least at the RNA level (Mathioudaki et al., 2011). In this study, immunohistological examination of total PRMT1 protein expression, not differentiating between specific isoforms, identified increased PRMT1 expression within the cytoplasm. Interestingly, PRMT1v1 displays predominant nuclear localization, while PRMT1v2 localizes to the cytoplasm (Goulet et al., 2007; Herrmann et al., 2009; Herrmann and Fackelmayer, 2009), therefore, it could be hypothesized that a significant proportion of PRMT1 observed within the cytoplasm could be PRMT1v2. Consequently, based on previous experimental data, the importance of PRMT1v2 in breast cancer was examined.

Here, it is shown that PRMT1v2 contributes to breast cancer through promoting breast cancer cell survival and invasion. Using a PRMT1v2 specific antibody raised against the peptide sequence of exon 2, a sequence unique to the coding region of PRMT1v2, specific characterization of PRMT1v2 in breast cancer was possible. PRMT1v3 and PRMT1v5 additionally retain exon 2 within their 5' UTR, although very low expression of PRMT1v3 is observed, and PRMT1v5 is undetectable in the breast cancer cell lines employed here (Goulet et al., 2007). The PRMT1v2 specific antibody distinctly recognized purified PRMT1v2 protein, as well as PRMT1v2 from MCF7 protein lysate, distinguishing from a pan-PRMT1 antibody which recognizes the main

PRMT1 isoform v1 as well as v2 (Cote et al., 2003). Furthermore, depletion of PRMT1v2 via RNA interference in four breast cancer cells lines (MCF7, T-47D, Hs578T, and MDA MB 231) resulted in specific depletion of PRMT1v2 mRNA and protein, while no decrease in PRMT1v1 mRNA or protein levels were observed. PRMT1v2 depletion required both a siRNA and shRNA targeting exon 2, as attempted depletion of PRMT1v2 with just one of these tools was incapable of sufficiently decreasing PRMT1v2 protein levels. This suggests that PRMT1v2 is crucial for cellular function and stable levels are required to ensure its normal function in cellular pathways.

Previously published data using the pan-PRMT1 antibody showed that PRMT1v2 protein expression increased in a panel of breast cancer cells compared to normal mammary epithelial cells (Goulet et al., 2007). To validate this result, PRMT1v2 protein expression was investigated using a PRMT1v2 specific antibody developed in-house. PRMT1v2 protein levels were elevated between two- and six fold in breast cancer cells compared to MCF10A immortalized, normal mammary epithelial cells. PRMT1v2 protein expression in breast cancer cells does not appear to be regulated based on the presence or absence of the estrogen receptor, a prognostic marker for breast cancer (Esteva and Hortobagyi, 2004). ER+ (MCF7, T-47D, and BT-474) as well as ER- cell lines (Hs578T, MDA MB 231, BT-20, BT-549, and SK-BR3) all exhibited increased levels of PRMT1v2 expression.

As PRMT1v2 protein expression is elevated, potentially contributing to the aberrant asymmetric methylation profiles observed in breast cancer cells (Goulet et al., 2007), the specific contribution of PRMT1v2 in breast cancer cell growth and proliferation was assessed. PRMT1v2 depletion via RNA interference resulted in

decreased cell growth, proliferation and viability in four phenotypically distinct breast cancer cell lines (MCF7, T-47D, Hs578T, and MDA MB 231). Interestingly, in some of the breast cancer cell lines examined, PRMT1v2 levels slowly recovered, and this gradual recovery coincided with a diminished effect on cell growth and viability. Previous studies have implicated PRMT1 in cell growth and viability, though the involvement of specific PRMT1 isoforms in these studies was not assessed. PRMT1 depletion in osteosarcoma, lung and bladder cancer cell lines results in a decrease in cell growth (Yoshimatsu et al., 2011). Furthermore, a reduction in cell proliferation was observed in breast cancer cells upon PRMT1 depletion through decreased estrogen-induced phosphorylation of PKB/Akt, thus inhibiting its activation (Le Romancer et al., 2008). In these studies, the observed growth arrest was due to cell cycle arrest at either the G_0/G_1 or G_2/M boundaries or both (Yoshimatsu et al., 2011; Le Romancer et al., 2008). Here, the reduction in cell growth and viability upon PRMT1v2 depletion occurred through induction of apoptosis. While the majority of apoptotic cells stained predominantly with annexin V upon PRMT1v2 depletion, there were a small percentage of cells that co-stained with both annexin V and propidium iodide, indicating a loss of membrane integrity in these cells resulting in propidium iodide staining of the DNA.

PRMT1 may additionally work in regulating cell viability through identified functions within the DNA damage response and DNA repair pathways. Upon ultraviolet (UV) irradiation, PRMT1 functions along with CARM1 as transcriptional co-activators of p53, thus regulating its target gene expression (An et al., 2004). PRMT1 methylation of the DNA damage sensing protein 53BP1 regulates its recruitment to sites of DNA double-strand breaks (Boisvert et al., 2005c). Furthermore, PRMT1 methylation of

MRE11, a component of the MRN complex, facilitates the repair of DNA double strand breaks (Boisvert et al., 2005a; Boisvert et al., 2005b). PRMT1 null MEFs exhibit spontaneous DNA damage and aberrant cell cycle regulation leading to chromosomal irregularities that eventually leads to cell death (Yu et al., 2009). PRMT1 has also been implicated in maintaining telomere length. PRMT1 methylation of TRF2, a component of the shelterin complex, controls telomere length and stability, while PRMT1 depletion in cancer cells results in telomere shortening (Mitchell et al., 2009). These studies suggest that PRMT1 performs an integral role in maintaining genomic stability. As PRMT1v2 depletion results in apoptosis, it would be intriguing to assess the potential influence PRMT1v2 may convey in DNA damage and repair pathways, as well as the maintenance of telomere integrity. Furthermore, since PRMT1v2 regulates cell survival, potentially through the maintenance of genomic stability, it would be interesting to speculate about a potential role for PRMT1v2 in promoting cell survival through chemoresistance.

The induction of apoptosis upon PRMT1v2 depletion concurs with previous, though contradictory roles for PRMT1 in apoptotic signalling. In MCF7 and MDA MB 231 cells, PRMT1 methylates ASK1, attenuating its stress-induced activation promoting cell survival (Cho et al., 2011). In contrast, similarly in MCF7 cells, PRMT1 methylation of Bad inhibits its phosphorylation by PKB/Akt, thus promoting apoptosis (Sakamaki et al., 2011). These studies identify divergent roles for PRMT1 in apoptotic signalling, though in each case, the specific isoform responsible for methylating ASK1 or Bad is unknown. Therefore, further studies are warranted to identify the precise role that PRMT1v2 may enact in apoptotic signalling.

No previous studies have linked PRMT1 with cancer cell invasion. Here it is shown that PRMT1, and more specifically PRMT1v2, is implicated in breast cancer cell invasion. PRMT1v2 depletion results in a significant reduction in motility and invasion in MDA MB 231 cells, a highly aggressive and invasive breast cancer cell line. Though it is difficult to assess the exact contribution of apoptosis upon PRMT1v2 depletion, the 68% reduction in cell invasion suggests that PRMT1v2 performs a prominent role in promoting invasion in MDA MB 231 cells. These results are supported by results showing increased cell motility and invasion in MCF7 cells, a weakly invasive breast cancer cell, through both stable and transient PRMT1v2 overexpression. Whereas PRMT1v1 overexpression also resulted in increased cell motility, only increased PRMT1v2 expression was capable of promoting increased invasion. Additionally, transient knockdown of PRMT1v2 in stably expressing PRMT1v2 MCF7 cells was sufficient to partially rescue invasion conferred through PRMT1v2 overexpression. Intriguingly, even though MCF7 cells express high levels of endogenous PRMT1v2, it appears that increased expression is required to promote increased cell invasion. This suggests that a threshold PRMT1v2 expression level must be encountered before increased invasion is attained in breast cancer cells. It is also possible that the threshold level of PRMT1v2 may vary in different cancer cell lines depending on the aberrant expression of additional cell invasion regulatory proteins. Alternatively, or concomitantly, regulation of PRMT1, an aspect of PRMT1 poorly comprehended, may influence cancer cell invasion. Interaction of PRMTs with non-methyl binding proteins can augment or inhibit their methyltransferase activity and substrate specificity (Robin-Lespinasse et al., 2007; Berthet et al., 2002). Therefore, the cellular equilibrium between

augmenting and inhibiting proteins could markedly affect the potential PRMT1v2 threshold expression level required to promote cell invasion. Consequently, expression of PRMT1v2 may not function as a suitable barometer of invasive potential.

PRMT1v2's capacity to promote invasion is also dependent on its cytoplasmic localization and methyltransferase activity, as a NES and a methyltransferase dead mutant were incapable of enhancing invasion in MCF7 cells. Strikingly, overexpression of the methyltransferase dead mutant caused a substantial decrease in cell invasion; however, this phenotype is likely due to increased cytotoxicity observed upon transfection of this mutant (Herrmann and Fackelmayer, 2009). Nevertheless, the methyltransferase dead mutant may function as a dominant negative, given that dimerization of PRMT1 is required for full catalytic activity (Herrmann and Fackelmayer, 2009; Zhang and Cheng, 2003).

MCF7 cells are typically polygonal in orientation, form tight colonies and exhibit E-cadherin positive cell-cell adherens junctions (Lacroix and Leclercq, 2004; Shtutman et al., 2006). PRMT1v2 overexpression results in a disruption in normal cell-cell adhesion, causing irregular colony formation which was characterized by an increase in loose and scattered colonies, along with an increase in F-actin positive filopodia and lamellipodia, structures whose presence is indicative of active migration (Hall, 2005; Jaffe and Hall, 2005; Schafer, 2004; Tomaskovic-Crook et al., 2009). Cellular adherens junctions are responsible for maintaining epithelial cell polarity and tissue integrity, and are characterized by an interaction between E-cadherin and catenin proteins (α, β, γ) (Yonemura, 2011). E-cadherin and β-catenin function to maintain adherens junctions, with E-cadherin, the transmembrane component, functioning extracellularly to provide

cell-cell adhesion; β-catenin, the intracellular component, binds E-cadherin to the actin cytoskeleton, providing adherens junction stability (Van Aken et al., 2001; Kemler, 1993). Loss of expression or mutation of either component of the adherens junction results in a disruption in junction stability leading to loss of cell-cell adhesion. Loss of junction stability promotes invasion and metastasis, and has been observed in numerous epithelial-derived cancers including breast cancer (Shtutman et al., 2006; Tomaskovic-Crook et al., 2009; Hiscox et al., 2006; Van Aken et al., 2001; Morrogh et al., 2012; Birchmeier and Behrens, 1994). In conjunction with loose and scattered colony formation, loss of localization of F-actin, E-cadherin, and β-catenin at the adherens junctions was observed in PRMT1v2 expressing MCF7 cells.

Examination of E-cadherin and β-catenin expression in PRMT1v2 MCF7 overexpressing cells revealed no change in E-cadherin mRNA or protein levels compared to GFP expressing cells; however, though there was no change in β-catenin mRNA levels, a 58% decrease in β-catenin protein expression was observed. Whereas PRMT1v1 overexpression promotes increased motility and causes changes in MCF7 cell morphology, no decrease in β-catenin protein expression occurred. This suggests that the mechanism by which PRMT1v1 enhances motility is functionally distinct from that whereby PRMT1v2 overexpression promotes increased motility and invasion.

β-catenin protein stability is regulated through phosphorylation of serine residues 33 and 37 and threonine residue 41 by a degradation complex composed of Axin, APC, CK1 and GSK3β (Hart et al., 1999; Latres et al., 1999; Winston et al., 1999). PRMT1 has been implicated in functioning to negatively regulate β-catenin protein expression (Cha et al., 2011). In this study, *in vitro*, both PRMT1v1 and v2 were capable of methylating

Axin, resulting in increased Axin stabilization and interaction with GSK3β, thus promoting β-catenin degradation. PRMT1 depletion leads to an increase in β-catenin-mediated transcription. Therefore, β-catenin's phosphorylation status was evaluated to determine if phosphorylation-mediated degradation was responsible for promoting increased invasion in PRMT1v2 expressing MCF7 cells. Though a lower level of β-catenin phosphorylation was observed in GFP-PRMT1v2 expressing cells, densitometry comparing the ratio of phospho-β-catenin to β-catenin in these cells revealed an increase in phosphorylation. This result suggests that phosphorylation-mediated degradation of β-catenin contributes to increased invasion. Numerous studies have shown a reduction or loss of β-catenin protein expression correlating with increased aggressiveness, metastasis, and poor patient prognosis in several cancers (Faleiro-Rodrigues et al., 2004; Faleiro-Rodrigues et al., 2005; Dolled-Filhart et al., 2006; De Leeuw et al., 1997; Yoshida et al., 2001; Nakopoulou et al., 2006; Pontes et al., 2010; Ebert et al., 2003). To validate that loss of β-catenin expression through phosphorylation-mediated degradation causes increased invasion in PRMT1v2 expressing MCF7 cells, β-catenin was re-introduced in these cells. In fact, re-introduction of β-catenin indeed resulted in decreased invasion. The above results suggest that increased invasion in PRMT1v2 expressing MCF7 cells is due to loss of β-catenin expression through phosphorylation-mediated degradation.

As previously stated, both PRMT1v1 and v2 are capable of methylating Axin promoting its stabilization (Cha et al., 2011), though this observation was discerned *in vitro* and was not tested *in vivo*. As both PRMT1v2 and Axin are predominantly cytoplasmic proteins, it could be hypothesized that *in vivo*, PRMT1v2 is responsible for methylating Axin, promoting its stability, which results in enhancing its interaction with

GSK3β. Stabilization of the Axin-GSK3β interaction promotes the formation of the β-catenin-degradation complex resulting in increased cell invasion (Figure 7.2). PRMT1 depletion results in an increase in β-catenin-dependent transcription activity (Cha et al., 2011); however, upon immunofluorescence analysis of β-catenin cellular localization in PRMT1v2 expressing MCF7 cells, increased β-catenin nuclear localization was not observed. This suggests that increased invasion in PRMT1v2 expressing MCF7 cells is due to loss of β-catenin protein expression regulating formation of adherens junctions, and not to re-localization of β-catenin to the nucleus, which promotes increased cell invasion through increased transcriptional activity (Gottardi et al., 2001; Kuphal and Behrens, 2006; Eger et al., 2000; Stockinger et al., 2001). Further experimentation will be required to determine that *in vivo*, PRMT1v2 methylates Axin leading to increased β-catenin phosphorylation, targeting it for degradation.

Although it appears that PRMT1v2 promotes increased invasion through phosphorylation-mediated degradation of β-catenin, it is plausible that PRMT1v2 may function in additional pathways. PRMT1 methylation of ERα promotes the association of PI3K with Src and FAK resulting in activation of PKB/Akt (Le Romancer et al., 2008). Expression of all of these proteins is known to promote cell migration and invasion (Hernandez-Aya and Gonzalez-Angulo, 2011; Navarro-Tito et al., 2008; Zheng et al., 2011; Ohgaki and Kleihues, 2007; Weber et al., 2011). Moreover, PRMT1 is a transcriptional co-activator of p53 (An et al., 2004), a protein which when mutated has been incriminated in regulation of cell migration and invasion (Hwang et al., 2011; Adorno et al., 2009). In both of these studies, the effect of PRMT1 in general was

7.2)

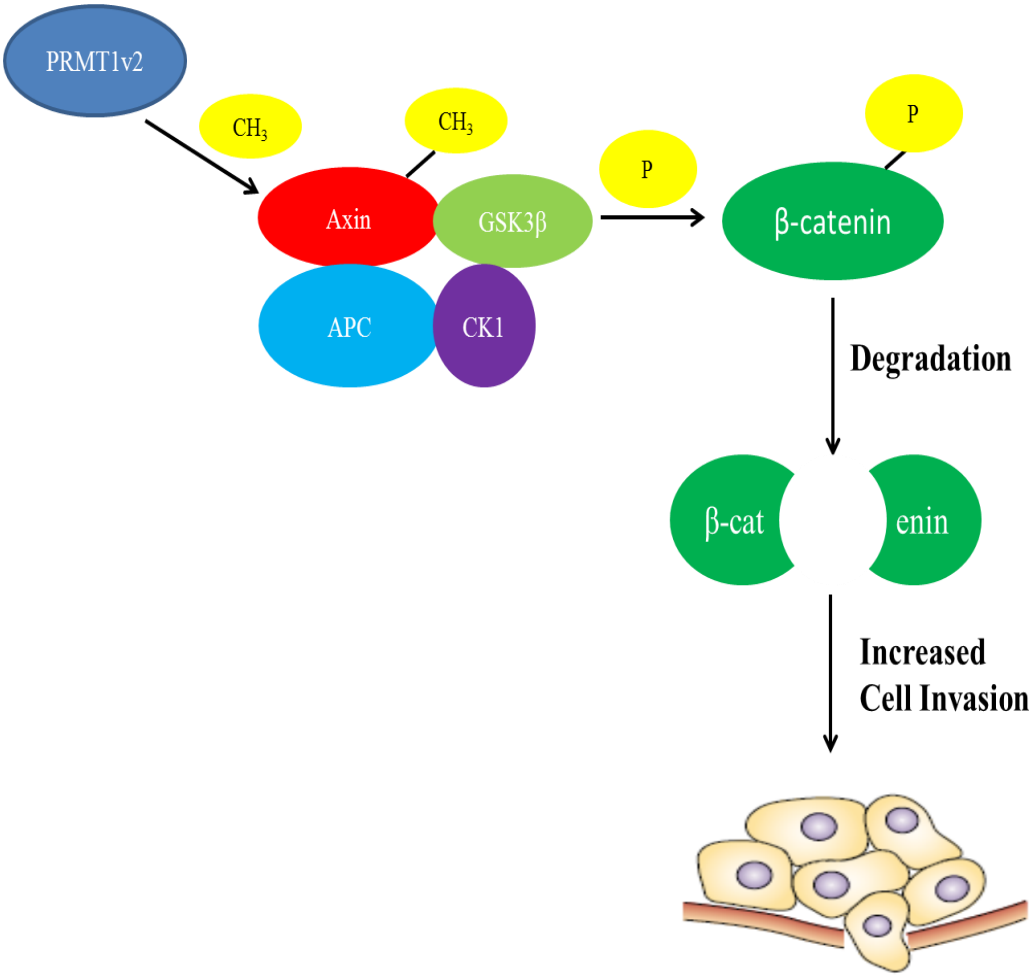
PRMT1v2
CH3
CH3
Axin
GSK3β
APC
CK1
P
P
β-catenin
Degradation
β-cat
enin
Increased
Cell Invasion

Figure 7.2: Model of PRMT1v2 Regulation of β-catenin Protein Stability

PRMT1 has been shown to methylate Axin promoting it protein stability (Cha et al., 2011). *In vitro*, both PRMT1v1 and PRMT1v2 can methylate it, though *in vivo* both PRMT1v2 and Axin are predominantly cytoplasmic protein. Therefore, it is hypothesized that *in vivo*, PRMT1v2 methylates Axin promoting its protein stability, allowing it to interact with glycogen synthase kinase 3β (GSK3β), which along with Axin forms a complex with adenomatous polyposis coli (APC) and casein kinase 1 (CK1). Within this complex GSK3β phosphorylates β-catenin, targeting it for degradation. β-catenin degradation results in increased cell invasion through abrogation of its interaction with E-cadherin, disrupting adherens junction formation.

assessed, and therefore the precise involvement of specific PRMT1 isoforms was not evaluated.

In summary, these results identify PRMT1v2 functioning to regulate cell growth, survival and invasion. Distinct functional roles for different PRMT1 isoforms within the cell are also characterized. Furthermore, they implicate a role for PRMT1v2 in breast cancer development and aggressiveness; however, additional studies will be required to assess the precise *in vivo* contribution of PRMT1v2 in breast cancer development and progression.

Elucidating the Role of PRMT6 in Chemoresistance through its Function in Stress Granule Formation

Bortezomib (Velcade) is a proteasome inhibitor that has been used effectively in the treatment of multiple myeloma and mantle cell non-Hodgkin's lymphoma (McConkey and Zhu, 2008; Richardson et al., 2003; Richardson et al., 2004; Sterz et al., 2008). Bortezomib inhibition of the proteasome results in induced G_2/M cell cycle arrest and apoptosis through Bcl-2 phosphorylation and cleavage (Ling et al., 2002). However, treatment of solid tumors with bortezomib has proven ineffective (McConkey and Zhu, 2008; Codony-Servat et al., 2006; Rajkumar et al., 2005; Tang et al., 2008). Interestingly, bortezomib treatment of cancer cell lines derived from bortezomib-resistant tumors promotes the formation of stress granules (Fournier et al., 2010; Gareau et al., 2011; Fournier et al., 2013). Formation of stress granules promotes cell survival upon induction of environmental stresses (Arimoto et al., 2008; Eisinger-Mathason et al., 2008; Baguet et al., 2007; Fournier et al., 2010). Stress granule formation upon bortezomib treatment can occur in the presence or absence of phosphorylation of the eukaryotic translation

initiation factor eIF2α (Fournier et al., 2010; Fournier et al., 2013). In the absence of eIF2α phosphorylation, mTORC1 phosphorylation of 4E-BP1 promotes eIF4Es interaction with eIF4G at the mRNA cap, which facilitates stress granule assembly. Inhibition or depletion of mTORC1, eIF4E, or eIF4G, in addition to hypo-phosphorylation of 4E-BP1 can impede stress granule formation. Although formation of an intact eIF4E-eIF4G complex is required for bortezomib-induced stress granule formation, it is hypothesized that yet to be identified scaffolding proteins are required to chaperone this complex to stress granules (Fournier et al., 2013).

Arginine methylation has been linked with stress granules as numerous substrates of PRMTs localize to stress granules, with methylation required to promote their localization (De Leeuw et al., 2007; Tradewell et al., 2012; Matsumoto et al., 2012; Yamaguchi and Kitajo, 2012; Baron et al., 2013; Lee et al., 2014). Furthermore, TDRD3, a reader of arginine methylation, also localizes to stress granules, with the Tudor domain, the region of TDRD3 responsible for methylated arginine motif recognition, necessary for its localization to occur (Goulet et al., 2008). Therefore, it is likely that PRMTs function in facilitating stress granule formation.

Although, to date, there is no direct evidence that would insinuate a direct role for PRMTs in stress granule formation, using the paradigm of bortezomib treatment to induce stress granules, the effect of PRMT6 depletion on stress granule formation was investigated. PRMT6 depletion in HeLa cells resulted in a significant reduction in stress granule formation. This observation was validated using three well known stress granule markers: TIA-1, FMRP and DDX3, and was further confirmed in MCF7 cells, a bortezomib-resistant breast cancer cell line. However, in MDA MB 231 cells, which are

sensitive to bortezomib, PRMT6 depletion had no effect on stress granule formation. Treatment of MDA MB 231 cells with other types of cellular stresses (oxidative, osmotic, and heat shock) results in stress granules forming; therefore, the inability of MDA MB 231 cells to form stress granules is due to their sensitivity to bortezomib (Yuan et al., 2014).

Low dose sodium arsenite (100 μM) treatment of PRMT6 shRNA expressing cells resulted in a decrease in the percentage of cells with stress granules, however, upon treatment with an increased dose of sodium arsenite (500 μM), PRMT6 depletion had no effect on stress granule formation. Sodium arsenite treatment of cells induces oxidative stress producing reactive oxygen species, resulting in numerous cellular pathways including but not limited to p38 MAPK, JNK/SAPK, PKC and NF-κB becoming activated (Evans et al., 2002). Inhibition of the p38 MAPK and NF-κB pathways through sequestration of RACK1 (Arimoto et al., 2008) and TRAF2 (Kim et al., 2005) into stress granules occurs upon stress granule formation. Interestingly, PRMT6 functions as a co-activator of the NF-κB pathway through its recruitment to the promoter of NF-κB target genes (Lorenzo et al., 2014). Although PRMT6 activates the NF-κB pathway, it is possible that PRMT6 could function to repress one of these stress-induced pathways either transcriptionally or through methylation. Additionally, PRMT6 probably performs a redundant role in sodium arsenite-induced stress granule formation as PRMT6 protein expression is induced upon 500 μM treatment, although no difference in the percentage of cells with stress granules is observed upon its depletion. However, in low dose sodium arsenite treatment cells, it is probable that not all stress-induced cellular pathways become activated, and therefore, the possible redundancy that may be observed in higher

dose treated cells is not present and PRMT6 depletion results in an inhibition in stress granule formation.

Re-introduction of PRMT6 was able to partially rescue the defect in stress granule formation in PRMT6 depleted cells. However, PRMT6 overexpression could not induce stress granule formation, and does not increase the rate of stress granule formation. These results suggest that, although PRMT6 can influence stress granule formation upon bortezomib and low sodium arsenite doses, PRMT6 is likely not a stress granule nucleator and cannot facilitate stress granule assembly like identified stress granule nucleators such as DDX3 (Shih et al., 2012), TIA-1 or TIAR (Gilks et al., 2004), TTP or BRF1 (Stoecklin et al., 2004), G3BP (Tourriere et al., 2003), RCK and CPEB (Wilczynska et al., 2005), caprin-1 (Solomon et al., 2007), FAST (Kedersha et al., 2005), FMRP (Mazroui et al., 2002), Argonaute-2 (Leung et al., 2006), and SMN (Hua and Zhou, 2004).

In another part of this study, DDX3 was identified as a novel substrate of PRMT6. DDX3 is a critical component of stress granule formation mediating their formation through its interaction with eIF4e (Shih et al., 2012). Therefore, it was investigated whether DDX3 depletion could further exacerbate the reduction in stress granules observed upon PRMT6 knockdown. As expected, upon bortezomib treatment, DDX3 depletion results in a decrease in stress granules; although the rate of decrease was similar in scramble and PRMT6 shRNA expressing cells indicating, that at least upon bortezomib treatment, DDX3 likely mediates stress granule formation in a PRMT6-independent manner (Appendix Ii).

Interestingly, bortezomib treatment resulted in an induction of PRMT6 protein expression. PRMT6 appears to be regulated at the post-transcriptional level, as PRMT6 mRNA levels in fact decrease upon bortezomib treatment. Furthermore, increased PRMT6 expression is likely a stress-induced response, as PRMT6 protein levels increased upon sodium arsenite treatment but did not accumulate upon treatment with the proteasome inhibitor MG132. Evidence pertaining to PRMT6 regulation is limited with the exception of PELP1 being able to modulate its function (Mann et al., 2014). However, no evidence to date has implicated PELP1 in stress granule formation or stress-induced pathways. In addition to PRMT6, other PRMTs are hypothesized to function in stress granule dynamics due to the numerous RG-containing proteins which localize to them. Though, similar to PRMT6, none of these identified PRMT regulators (BTG2 (Choi et al., 2012), hCAF1 (Robin-Lespinasse et al., 2007), DAL-1/4.1 (Singh et al., 2004; Jiang et al., 2005)) are implicated in stress granule dynamics. Therefore, further work will need to be performed to identify PRMT6 regulators, and how they function to modulate its activity.

Upon bortezomib treatment, formation of the eIF4E-eIF4G1 complex at the mRNA cap is necessary for stress granule formation (Fournier et al., 2013). Therefore, it was investigated whether this complex forms in PRMT6 depleted cells. Intriguingly, under normal conditions, eIF4E protein levels were significantly decreased in PRMT6 shRNA expressing cells. This corresponded to a decrease in eIF4E binding to the mRNA cap, which subsequently resulted in decreased eIF4G1 binding. Binding of both eIF4E and eIF4G1 to the mRNA cap was further reduced upon bortezomib treatment. PRMT6 regulates eIF4E at the protein level as its mRNA expression is unaltered in PRMT6

depleted cells. Therefore, PRMT6 likely regulates either eIF4E protein stability or mediates its translation. Formation of the eIF4F complex (eIF4E, eIF4G, and eIF4A) at the mRNA cap is essential for translation initiation, with the availability of eIF4E the rate limiting step (Merrick, 2004). Under normal physiological conditions, the availability of eIF4E is tightly regulated. eIF4E is negatively regulated by 4E-binding proteins (4E-BPs) that sequester it by occupying the same binding site as eIF4G (Poulin et al., 1998; Raught and Gingras, 1999; Rong et al., 2008). 4E-BP phosphorylation at multiple sites by components of the RAS-ERK and PI3K/mTOR signalling pathways release eIF4E from 4E-BPs, enabling the formation of the eIF4F complex, thus promoting translation (Joshi et al., 1995; Waskiewicz et al., 1999). Furthermore, eIF4E phosphorylation by MAP kinase-interacting protein kinase-1 (Mnk-1) at serine 209 leads to concomitant activation of cap-dependent translation (Ueda et al., 2004). From the results observed here, it appears that PRMT6 provides an additional layer of eIF4E regulation, likely through methylation. eIF4E contains one arginine residue within a RGG motif (R109), and three residues (R42, R112, R157) which were identified through Prediction of Protein Methylation Sites (PMeS) software (http://bioinfo.ncu.edu.cn/inquiries_PMeS.aspx). Further experimentation will be needed to determine the exact mechanism by which PRMT6 regulates eIF4E protein levels either through methylation or other means. Additionally, PRMT6 depletion inhibits cell growth and proliferation (Neault et al., 2012; Stein et al., 2012; Kleinschmidt et al., 2012; Phalke et al., 2012). This decrease may be due to an inhibition of translation due to down-regulated eIF4E levels in PRMT6 depleted cells. Likewise, further experimentation will need to be performed to determine if translation is inhibited in the absence of PRMT6.

PRMT6 depletion corresponds with a decrease in cell survival in bortezomib-resistant MCF7 cells, but has no effect on survival in bortezomib-sensitive MDA MB 231 cells. Bortezomib promotes cancer cell death through inhibition of the proteasome which induces cell cycle arrest and apoptosis (Ling et al., 2002). A number of methods conferring cellular resistance to bortezomib have been identified. The most common is a mutation in the β5 subunit of the proteasome (PSMB5). Bortezomib inhibits the chymotrypsin-like activity of PSMB5, blocking the degradation of polyubiquitinated proteins (Rajkumar et al., 2005). A glycine to alanine mutation at residue 322 results in a conformational change that disrupts contact points between the active site of PSMB5 and bortezomib, thus conferring resistance (Lu et al., 2008; Lu et al., 2009). Expression of mutated PSMB5 prevents the accumulation of unfolded proteins which would lead to excessive endoplasmic reticulum stress that would trigger apoptosis (Ri et al., 2010). Likewise, upregulated expression of proteins involved in the stress response and cell survival pathways can confer tumor cell resistance to bortezomib treatment. Expression of heat shock proteins (HSP) 27, 70, and 90 are increased in bortezomib-resistant large B-cell lymphoma cell lines compared to bortezomib-sensitive cells. Moreover, knockdown of HSP27 promotes sensitivity in resistant cell lines, while ectopic expression confers resistance in sensitive B-cell lymphoma cells (Chauhan et al., 2003; Shringarpure et al., 2006; McConkey and Zhu, 2008). Similarly, transcription factor 4, a component of the Wnt signalling pathway which is implicated in cancer development, progression and drug resistance is also upregulated in resistant B-cell lymphomas (Kale and Moore, 2012). Lastly, cellular stimulation by interleukin-6 and insulin-like growth factor can also confer resistance to bortezomib by activating NF-κB through the Ras/ERK and PI3K/mTOR

pathways (Rajkumar et al., 2005; Siegel, 2012). Interestingly, PRMT6 functions as a co-activator of NF-κB (Lorenzo et al., 2014), and its protein expression is induced upon bortezomib treatment. Therefore, it is possible that PRMT6 functions at multiple levels to regulate bortezomib-induced stress granule formation. First, PRMT6 regulates eIF4E protein expression. PRMT6 depletion results in decreased eIF4E expression, inhibiting the formation of the eIF4E-eIF4G complex at the mRNA cap. Thus, this complex, a crucial component in bortezomib-induced stress granules, does not accumulate, and therefore stress granules are unable to form, resulting in decreased cell survival (Figure 7.3a). Second, bortezomib treatment results in induction of PRMT6 by a yet unknown mechanism. This induction may stimulate NF-κB activation of its target genes, including stress response and apoptotic regulator genes, which promote cell survival. However, upon PRMT6 depletion, the NF-κB pathway is not activated, inhibiting the transcription of genes involved in the stress response and cell survival, resulting in a loss of cell viability (Figure 7.3b). Further experimentation will be required to clarify the exact mechanism(s) by which PRMT6 regulates bortezomib-induced stress granule formation.

In summary, PRMT6 depletion results in a decrease in stress granule formation in bortezomib-resistant cell lines. Re-introduction of PRMT6 was able to partially rescue this defect. Furthermore, PRMT6 protein expression is induced upon cellular treatment with bortezomib. PRMT6 regulates eIF4E protein expression, with PRMT6 knockdown inhibiting formation of the eIF4E-eIF4G complex which is required for bortezomib-induced stress granule formation. Lastly, PRMT6 depletion results in a decrease in cell survival in bortezomib-resistant cells, while having no effect in bortezomib-sensitive cells.

7.3a)

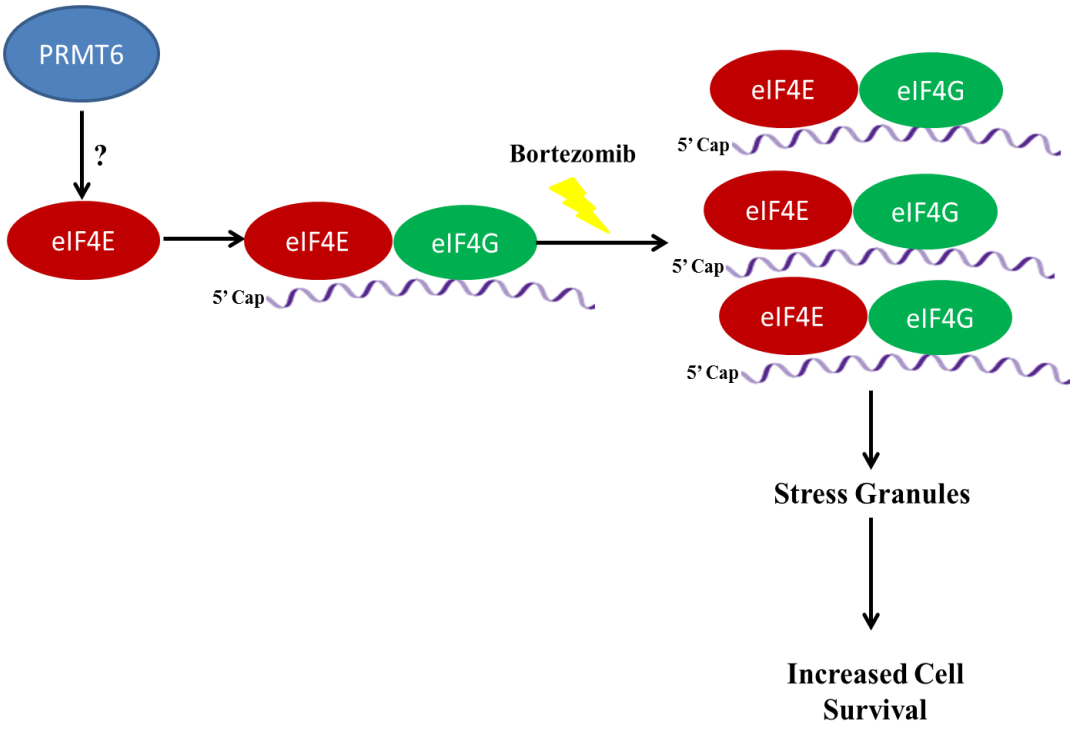
PRMT6
?
eIF4E
eIF4E
eIF4G
5' Cap
Bortezomib
eIF4E
eIF4G
5' Cap
eIF4E
eIF4G
5' Cap
eIF4E
eIF4G
5' Cap
Stress Granules
Increased Cell Survival

B)

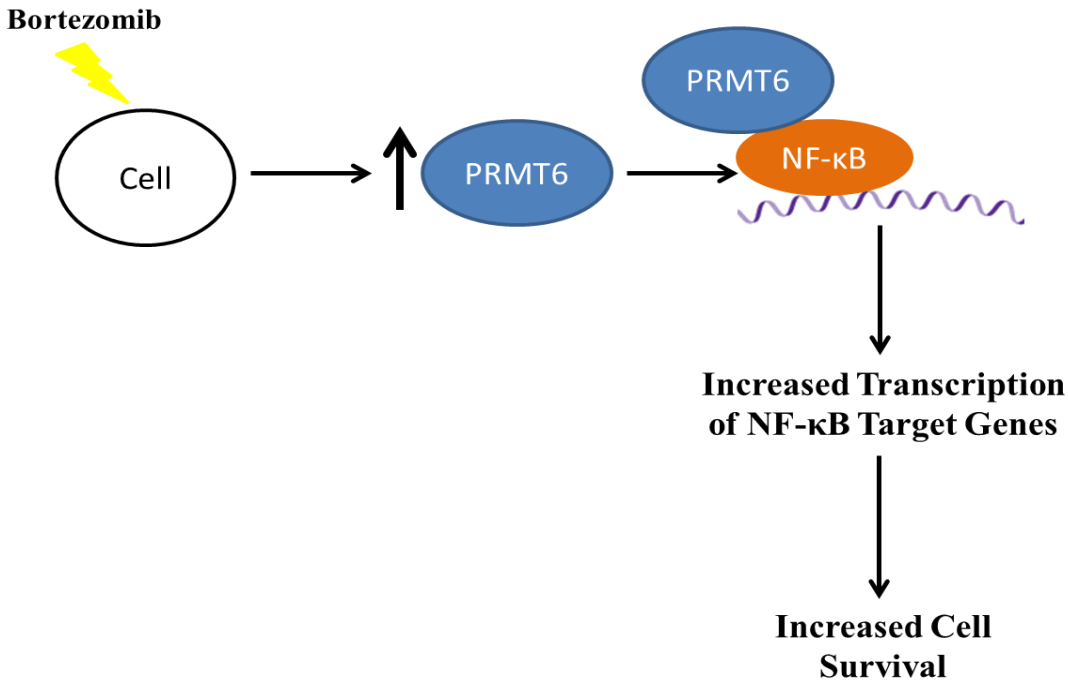
Bortezomib
Cell
PRMT6
PRMT6
NF-κB
Increased Transcription of NF-κB Target Genes
Increased Cell Survival

Figure 7.3: Model of PRMT6 Regulated Bortezomib-Induced Stress Granule Formation

(A) PRMT6 regulates eIF4E protein expression through a yet to be determined mechanism. In bortezomib-resistant breast cancer cells, PRMT6 modulation of eIF4E protein expression allows for formation of the eIF4E-eIF4G complex at the mRNA cap. Upon bortezomib treatment, eIF4E-eIF4G complexes accumulate, resulting in the formation of stress granules which promote increased cell survival. In the absence of PRMT6, eIF4E protein expression is down-regulated, resulting in inhibition of eIF4E-eIF4G formation, preventing stress granule formation, leading to decreased cell survival. (B) Bortezomib treatment induces PRMT6 protein expression through a yet unknown mechanism. PRMT6 may function as a co-activator of NF-κB, whose target genes include stress response and apoptotic regulators. Transcription of these genes may promote cell survival in bortezomib-resistant breast cancer cells lines which is abrogated in the absence of PRMT6.

Arginine Methylation of the DEAD-box RNA Helicase DDX3

DDX3, a DEAD-box RNA helicase, was examined to determine whether it is a substrate for PRMTs, since DDX3 contains numerous GAR motifs in its protein sequence, a sequence that is characteristically methylated by PRMTs. In *Trypansoma brucei*, Ded1, the DDX3 homolog is methylated by TbPRMT5 (Pasternack et al., 2007) and was identified as a potential interactor of TbPRMT6 (Fisk et al., 2010). Furthermore, PRMTs methylate numerous RNA binding proteins regulating their function (Rajpurohit et al., 1994; Nichols et al., 2000; Brahms et al., 2000; Brahms et al., 2001; Friesen et al., 2002; Selenko et al., 2001). DDX3 (Botlagunta et al., 2008; Botlagunta et al., 2011) and numerous PRMTs (Goulet et al., 2007; Thomassen et al., 2009; Mathioudaki et al., 2011; Yoshimatsu et al., 2011; Al-Dhaheri et al., 2011) are mis-regulated in breast cancer; therefore, it was hypothesized that aberrant PRMT methylation of DDX3 could promote its altered function in breast cancer cells.

Utilizing an *in vivo* methylation assay, DDX3 was identified as an arginine methylated protein. Although methylation of DDX3 was observed, the signal obtained for methylated DDX3 was not very robust even after a prolonged autoradiography exposure. This suggests that, *in vivo*, DDX3 is not robustly methylated, there is rapid turnover of methylated DDX3, or methylation of DDX3 could be associated with distinct cell states (ex. cell-cycle dependent, stress response, cell transformation). To date, no bona fide arginine demethylase has been identified, though peptidylarginine deiminase 4 can convert mono-methylarginine into citrulline, releasing a methylamine (Wang et al., 2004; Cuthbert et al., 2004). Arginine methylation has been observed to be a dynamic process. Oestrogen stimulation results in PRMT1 methylation of ERα within five minutes of

stimulation, with the methylation mark being lost ten minutes later (Le Romancer et al., 2008). Therefore, further experimentation would be required to determine if, *in vivo*, rapid turnover of arginine methylated DDX3 occurs. Data mining of SILAC mass spectrometry experiments confirmed that DDX3 is methylated *in vivo*, with six potential arginine methylated site identified; four arginine residues as mono-methylated and two residues as di-methylated. While this study was being performed, four proteomic studies were published characterizing arginine methylation of DDX3 or its homologs in *Trypanosoma brucei* and *Saccharomyces cerevisiae* with multiple arginine methylated residues identified in each study; further validating that DDX3 is an arginine methylated protein (Lott et al., 2013; Low et al., 2013; Erce et al., 2013; Bremang et al., 2013).

In vitro, it was established that PRMT1 and CARM1, along with PRMT6 were capable of methylating DDX3, while PRMT3, PRMT5, and PRMT7 were unable to methylate it using the methods employed here. Interestingly, in this study PRMT5 was unable to methylate DDX3, though its homolog in trypanosomes TbPRMT5 can methylate Ded1 (Pasternack et al., 2007). Only PRMT6 could strongly methylate purified DDX3 protein; PRMT1v1 was able to weakly methylate DDX3 but PRMT1v2, while PRMT1v3 and CARM1 were incapable of methylating purified DDX3 protein. Interestingly, PRMT1v1, PRMT1v2, and CARM1 were able to methylate DDX3 immunoprecipitated from cell lysate; CARM1 only after cells had been pre-treated with methylation inhibitors prior to the experiment being performed. While PRMT6 could methylate purified DDX3 protein, it was not able to methylate it when it was immunoprecipitated from cell lysates either untreated or pretreated with methylation inhibitors. PRMT1's inability to robustly methylate purified DDX3 protein to a similar

extent as DDX3 from cell lysate suggests that DDX3 may need to be primed by an additional post-translational modification before PRMT1 can methylate it. Similarly, this may be the case with CARM1, although CARM1 was only efficient at methylating DDX3 after cells were pretreated with methylation inhibitors. This suggests that DDX3 must be in an unmethylated state before CARM1 can methylate it. This is consistent with data showing that PRMTs are more enzymatically active towards their substrate in a hypomethylated state (Frankel et al., 2002). If, *in vivo*, multiple PRMTs do methylate DDX3, CARM1 methylation could potentially regulate the ability of other PRMTs to methylate DDX3. This is supported by evidence showing that purified DDX3 protein was methylated when using CARM1 null MEFs as a source of methyltransferases, but was not when using wild type MEFs. Furthermore, mutation of arginine residue 315, a methylated site identified through mass spectrometry resulted in increased PRMT6 methylation of DDX3, *in vitro*, suggesting that *in vivo* this site could potentially inhibit methylation by PRMT6.

DDX3 appears to be a bona fide target of both PRMT1 and CARM1 as interactions between both proteins and DDX3 was observed. With both PRMT1 and CARM1, the interaction is enhanced upon treatment with methylation inhibitors, further confirming that PRMTs preferentially interact with their substrates in a hypomethylated state (Frankel et al., 2002). It was investigated whether PRMT1 or CARM1 could influence DDX3 cellular localization. DDX3 shuttles from the nucleus to the cytoplasm, though is primarily cytoplasmic under normal physiological conditions (Yedavalli et al., 2004; Lai et al., 2008). Using PRMT1 null embryonic stem (ES) cells (Appendix Ij) or CARM1 null MEFs (Appendix Ik), DDX3 localization was still predominantly

cytoplasmic and does not appear to be affected by loss of either protein. However, low levels of PRMT1 transcripts (~1% of wild type) are still retained in null ES cells (Pawlak et al., 2000). It is likely that even this small percentage is enough for some PRMT1-mediated functions to occur in these cells, potentially even DDX3 regulation, as complete loss of PRMT1 results in loss of cell viability (Yu et al., 2009). Further experimentation will elaborate on DDX3's methylation status by both PRMT1 and CARM1 through identification of the arginine residues methylated, as well as ascertaining the functional implication of this methylation.

PRMT6 robustly methylates purified DDX3 protein but not DDX3 from cell lysates either untreated or pretreated with methylation inhibitors. In untreated cells, this could insinuate that PRMT6 may compete with other PRMTs for the same arginine residues and that these arginine residues were already methylated, therefore, PRMT6 was unable to methylate these residues.

PRMT1 and PRMT5 can methylate H4R3; PRMT1 methylation of H4R3 functions as an activating transcription mark, while PRMT5 methylation serves as a repressive transcription mark (Pal et al., 2004; Feng et al., 2011). Likewise, PRMT6 may be unable to methylate DDX3 in cells pretreated with methylation inhibitors as these residues could be potentially blocked by either methylation or other post-translation modification. For example, methylation of RIP140 on lysine residues 591, 653, and 757 inhibits the ability of the protein to be arginine methylated (Mostaqul Huq et al., 2008; Huq et al., 2009). In addition to lysine methylation influencing arginine methylation, phosphorylation also regulates it. Phosphorylation of the SRC-3 protein on a site in close proximity to an arginine methylated site reduces arginine methylation five-fold,

insinuating that at least *in vitro*, phosphorylation is able to antagonize methylation (Naeem et al., 2007). Further experiments will need to be performed to determine if PRMT1, CARM1 and/or PRMT6 can compete to methylate the same arginine residues, thus inhibiting another PRMT from doing so, and if this is the case, what are the functional consequences?

In hamster cells, DDX3 is phosphorylated on two evolutionary conserved threonine residues, 204 and 323 by cyclin B. Phosphorylation of Thr204 promotes DDX3 loss of function, coinciding with cyclin A repression and decreased ribosome biogenesis (Sekiguchi et al., 2007). The crystal structure of DDX3 amino acid residues 168-582 has been resolved (Hogbom et al., 2007), and although methylated arginine residue 315 is not in close proximity to phosphorylated residues 204 or 323, this does not preclude the possibility that arginine residues 585, 587 or 315 could be in close proximity to other yet unidentified phosphorylated or other post-translationally modified residues. In fact, arginine residue 585 is flanked N-terminal by two serine residues, while residue 587 is flanked by four serine residues. Future experimentation will need to be performed to determine if this is the case.

In vitro, PRMT6 methylates both the N- and C- terminal fragments of DDX3, with methylation of the C-terminal fragment more robust. Interestingly, methylation of both of these fragments occurs to a significantly greater extent than full length DDX3. This implies that potential methylation sites may be masked by the folding of the full length protein itself, and are more accessible in the truncation mutants. These results coincide with an increased interaction between PRMT6 and the C-terminal fragment relative to full length DDX3. Through site-directed mutagenesis, arginine residues 585

and 587 were identified to be methylated. Mutation of these two residues in the full length protein did not result in methylation being completely abrogated, thus suggesting that additional PRMT6 methylation sites at present, most likely in the N-terminus of the protein. This concurs with the three potential methylation site (R101, R110, R121) identified through data mining of mass spectrometry experiments along with other N-terminal sites identified via proteomic studies (Lott et al., 2013; Low et al., 2013; Erce et al., 2013; Bremang et al., 2013). Although, from these results, it appears that PRMT6 preferentially methylates arginine residues 585 and 587, as upon there mutation a significant proportion of DDX3 methylation is lost.

To verify that *in vivo* PRMT6 can methylate DDX3, HeLa PRMT6 knockdown cells lines were established, and an *in vivo* methylation assay was performed using an exogenously expressed DDX3. Exogenous expression was used to discern differences in PRMT6 methylation that may not have been possible with endogenous DDX3, as in HeLa cells, low levels of endogenous methylated DDX3 were observed. In fact, upon PRMT6 depletion, a reduction in methylated DDX3 was observed, even considering that significantly more DDX3 was immunoprecipitated in PRMT6 depleted cells. These results validate that *in vivo* PRMT6 is a major methyltransferase targeting DDX3. Furthermore, PRMT6 was observed to interact with DDX3 both *in vitro* and *in vivo*.

Next, a mass spectrometry based approach was used to validate that *in vivo* DDX3 arginine residues 585 and 587 are methylated. Endogenous DDX3 was immunoprecipitated from both scramble and PRMT6 shRNA expressing cells with arginine 315 identified to be methylated in the scramble shRNA sample. Unfortunately, peptides containing arginines 585 and 587 were not identified. Peptide digestion was

performed with chymotrypsin, as *in silico* analysis suggested that these sites should be detected. Analysis showed that although DDX3 was identified with high confidence in scramble and PRMT6 shRNA samples, chymotrypsin digestion was incomplete in both samples with many cleavages missed. If chymotrypsin peptide digestion was done to completion, a 12 amino acid peptide containing arginine residues 585 and 587 should be produced allowing for detection by tandem mass spectrometry. Therefore, it is possible that if digestion was incomplete, a peptide was produced too large for detection by mass spectrometry, not allowing for detection of residues 585 and 587.

Mass spectrometry identified arginine residue 315 as a methylarginine. Mutagenesis of this residue actually increased PRMT6 methylation of DDX3. Furthermore, a triple mutation of residues 315, 585, and 587 resulted in a methylation signal greater than that for mutants R585A, R587A or R585A/R587A. It could be hypothesized that, *in vivo*, arginine residue 315 is methylated by another PRMT, whose methylation inhibits the ability of PRMT6 to methylate DDX3 whether it be on arginine residues 585 and 587, or the yet to be identified residues in the N-terminus. Precedent has been set where methylation of a substrate by one PRMT inhibits methylation by another. PRMT1 methylation of the E2F-1 transcription factor hinders PRMT5 methylation, thus promoting apoptosis in DNA damaged cells. Conversely, PRMT5 methylation promotes E2F-1 binding to cyclin A, impeding PRMT1 methylation, and stimulating cell cycle progression (Zheng et al., 2013).

Attempts to identify a functional implication of PRMT6 methylation of DDX3 have thus far proved unsuccessful. DDX3 is predominantly cytoplasmic in most cells, although it shuttles from the nucleus to the cytoplasmic promoting the export of mRNAs

(Yedavalli et al., 2004; Lai et al., 2008). Mutation of arginine residues 585 and 587 does not affect DDX3 subcellular localization (Appendix Il). Likewise, these sites have no consequence on DDX3's localization to stress granules (Appendix In) (Lai et al., 2008; Shih et al., 2012). Similarly, PRMT6 depletion had no effect on DDX3 cellular localization (Appendix Im) or localization to stress granules (Appendix Io). Additionally, the influence of these sites in mediating DDX3's interaction with eIF4E (Shih et al., 2008), eIF3E (Lee et al., 2008), and eIF4G (Hilliker et al., 2011) proved inconclusive (data not shown). Although mutation of arginine residues 585 and 587 did affect DDX3 ATPase activity (Appendix Ip), attempts to determine if methylation enhanced the observed difference in ATPase activity were unsuccessful.

Although no functional significance was identified, it does not preclude the possibility that PRMT6 methylation does impact DDX3 function in some capacity. Both PRMT6 (Michaud-Levesque and Richard, 2009) and DDX3 (Botlagunta et al., 2008) influence cancer cell motility and invasion, therefore, it is intriguing to speculate that PRMT6 methylation of DDX3 affects these processes. PRMT6 methylation could also influence DDX3 functionality in mediation of HIV replication. DDX3 ATPase and helicase activity is essential for HIV replication (Yedavalli et al., 2004; Ishaq et al., 2008). Interestingly, PRMT6 methylates the HIV Tat protein, promoting its stability which allows the virus to persist in the cell and the extracellular environment for extended periods (Sivakumaran et al., 2009; Sivakumaran et al., 2013). As DDX3 ATPase activity is required for HIV replication, it could be hypothesized that PRMT6 may influence HIV replication, since mutation of arginine residues 585 and 587 results in decreased ATP hydrolysis activity (Appendix Ip). Further experimentation will be

necessary to investigate this possibility, as well as any potential influence PRMT6 may exert on cell migration and invasion through DDX3 methylation.

In summary, DDX3 is an arginine methylated protein and is a novel substrate of PRMT1, CARM1, and PRMT6. Furthermore, PRMT6 methylates arginine residues 585 and 587 within the C-terminus of DDX3, with methylation of DDX3 by PRMT6 confirmed *in vivo*. Lastly, DDX3 interacts with PRMT1, CARM1, and PRMT6.

Assessing the Role of TDRD3 in Breast Cancer

TDRD3 levels are overexpressed in recurrent ER- (Nagahata et al., 2004) and basal-like breast cancers (Hallett et al., 2012), breast cancers subtypes which are highly invasive and aggressive in nature. Furthermore, TDRD3 localizes to stress granules (Goulet et al., 2008; Linder et al., 2008), cytoplasmic foci which promote cancer cell survival upon treatment with chemotherapeutic agents (Mazroui et al., 2007; Arimoto et al., 2008; Eisinger-Mathason et al., 2008; Fournier et al., 2010) and which are also observed in the hypoxic cores of tumors (Baguet et al., 2007). Therefore, elucidating TDRD3's role in breast cancer development and progression is important.

TDRD3 mRNA levels are elevated in highly aggressive breast cancer tumors (Nagahata et al., 2004; Hallett et al., 2012), however, no difference in TDRD3 protein levels relative to normal mammary epithelial cells were observed, even in BT-549, Hs578T, and MDA MB 231 cells which are ER- breast cancer cell lines. Although no alteration in TDRD3 protein levels were observed, conditions in cell culture do not mimic conditions observed within the tumor microenvironment where TDRD3 mRNA levels were drastically elevated. Furthermore, any potential effect TDRD3 could have on cancer hallmarks in cell culture could be independent of its protein expression.

To investigate TDRD3's potential effects on cancer cell hallmarks, stably expressing TDRD3 shRNA cell lines were established in MDA MB 231 and Hs578T cell lines. TDRD3 depletion resulted in a significant decrease in cell proliferation in MDA MB 231 cells over an eight day time course; although a decrease in cell proliferation was observed in Hs578T cells, the reduction over eight days was not statistically significant. Although a significant difference in TDRD3 depleted Hs578T cells was not observed, this doesn't exclude the possibility that over a longer time frame a statistically significant reduction in cell proliferation would be observed. TDRD3 depletion also significantly inhibited anchorage-independent growth, a hallmark of cellular transformation. Lastly, TDRD3 depletion resulted in a significant reduction in cell motility in MDA MB 231 cells, while having no effect in Hs578T cells. However, TDRD3 knockdown has a very significant effect on cell invasion in both the MDA MB 231 and Hs578T cells, although the percentage reduction was greater in MDA MB 231 cells.

MDA MB 231 and Hs578T breast cancer cells are both negative for the prognostic markers of breast cancer: presence of the estrogen, progesterone, and HER2 receptors; furthermore, both cell lines exhibit low E-cadherin and claudin expression, characteristics of a loss of cell adhesion (Holliday and Speirs, 2011). Additionally, both cell lines are derived from basal-like breast tumors (Neve et al., 2006). Interestingly, TDRD3 depletion has a more significant effect on MDA MB 231 cell proliferation, motility, and invasion than on these parameters in Hs578T cells. Scramble shRNA expressing MDA MB 231 cells proliferate at a faster rate, and more cells migrated through the invasion and motility chambers than their Hs578T scramble shRNA expressing counterparts. Therefore, it could be argued that MDA MB 231 cells are a

more aggressive breast cancer cell line than Hs578T cells, and the results observed here potentially correlate with previously published *in vivo* data showing TDRD3 expression elevated in aggressive, invasive breast tumour (Nagahata et al., 2004; Hallett et al., 2012). Therefore, if this hypothesis is correct, TDRD3 depletion should have a nominal effect on cell proliferation, motility and invasion in MCF7 cells, a mildly invasive breast cancer cell line derived from a luminal breast tumour expressing both estrogen and progesterone receptors (Neve et al., 2006). Unfortunately, to date no research has examined TDRD3 expression in ER+ breast tumours which are less aggressive in nature, and generally more receptive to treatment. Further experimentation will be required to prove if this hypothesis is true.

Since TDRD3 depletion imparts the most dramatic effect on cell invasion, the minimal domain required to rescue this phenotype in MDA MB 231 cells was investigated. Surprisingly, the presence of the FMRP binding domain was required to rescue invasion. Deletion of the FMRP binding motif in full length TDRD3 or the truncated C-terminal (647-744) portion of TDRD3 was unable to rescue cell invasion. TDRD3 and FMRP both associate with actively translating polyribosomes and co-localize to stress granules (Goulet et al., 2008; Linder et al., 2008).

The FMRP protein, encoded by the gene *FXR1* is the causative agent behind Fragile X syndrome, with loss of FMRP the leading cause of inherited intellectual disability and autism (Coffee et al., 2009; Wang et al., 2010). FMRP, an mRNA binding protein facilitates the translational regulation of a subset of plasticity-related proteins by stalling ribosome translocation on target mRNAs (Siomi et al., 1993; Ashley et al., 1993; Corbin et al., 1997; Bolduc et al., 2008; Zang et al., 2009). Though the majority of

research performed concerns FMRP's function in the brain and Fragile X syndrome, FMRP is almost ubiquitously expressed, suggesting a potential role in additional diseases such as cancer (Devys et al., 1993; Tamanini et al., 1997; Bakker et al., 2000). In fact, *FMR1* mRNA is overexpressed in hepatocellular carcinoma cells (Li et al., 2003; Liu et al., 2007). Furthermore, affliction with Fragile X syndrome correlates with a decreased expression of the Wnt7A oncogene and risk of tumor incidence (Schultz-Pedersen et al., 2001; Rosales-Reynoso et al., 2010). Intriguingly, FMRP is overexpressed in breast tumors with high FMRP levels correlating with high tumor grade as well as high proliferation index (Ki67). Measurement of lung metastasis by mouse tail vein injection model, utilizing two murine breast cancer cell lines with FMRP depleted exhibited significantly less tumor nodule formation than with mice injected with control cell lines (Luca et al., 2013). Correspondingly, preliminary evidence indicates TDRD3 depletion demonstrates a similar effect in a mouse metastatic tail vein injection model (Appendix IIq). TDRD3 depletion resulted in almost a complete abrogation of lung nodule formation compared to parental cell lines, in comparison to PRMT1v2 depletion which only impedes nodule formation slightly.

In the brain, FMRP regulates a distinct subset of mRNAs relating to plasticity, while data from 4TI mouse breast cancer cells and mouse tumor samples identifies FMRP regulating mRNAs encoding proteins involved in cell adhesion, motility and invasion, as well as proteins involved in the epithelial to mesenchymal transition (Luca et al., 2013). TDRD3 serves as a scaffold protein mediating the interaction between TOP3β and FMRP, and facilitates the integration of TOP3β and FMRP into messenger ribonucleoproteins (mRNPs), which are present on actively translating polyribosomes

(Xu et al., 2013; Stoll et al., 2013). Intriguingly, TOP3β is elevated in breast carcinomas, with TOP3β expression correlating with metastasis and poor patient prognosis (Oliveira-Costa et al., 2010). Therefore, it is possibly that TDRD3 in association with TOP3β and FMRP could stimulate translation of mRNAs that promote invasion and metastasis. The interaction between TDRD3, FMRP and TOP3β was identified in HEK293 and HeLa cells, so it would be interesting to determine whether this complex also forms in MDA MB 231 and Hs578T cells. Alternatively, TDRD3 could function in conjunction with FMRP alone to promote cell invasion through regulation of target mRNAs or chaperone complexes composed of TDRD3-TOP3β-FMRP or TDRD3-FMRP to target mRNA to facilitate their translation (Figure 7.4). Further experimentation will be required to determine if mRNAs regulated by FMRP are also down-regulated in the absence of TDRD3; as well, if FMRP and TDRD3 alone promote invasion or whether TOP3β is also required.

Interestingly, neither TDRD3's Tudor domain nor its ability to recognize methyl arginines appears necessary to promote invasion, as the Tudor domain alone or a mutation abrogating TDRD3 binding to methyl arginines (E691K) were unable to rescue invasion in TDRD3 depleted cells. The Tudor domain is both necessary and sufficient for TDRD3 localization to stress granules (Goulet et al., 2008). It was originally hypothesized that TDRD3's role in stress granules was potentially linked to its function in breast cancer development and/or progression, as stress granule formation promotes cancer cell survival (Mazroui et al., 2007; Arimoto et al., 2008; Eisinger-Mathason et al., 2008; Fournier et al., 2010). Intriguingly, TDRD3 depletion accelerates stress granule formation and disassembly in MDA MB 231 and Hs578T cells upon induction of

oxidative and osmotic stress, as well as heat shock. This accelerated stress granule formation is dependent on TDRD3's ability to recognize methylated arginine motifs, as TDRD3 E691K is incapable of rescuing this defect (Fanous and Cote, unpublished data).

We hypothesize that, though stress granules form at an accelerated rate upon TDRD3 knockdown, these stress granules may not be functional entities. TDRD3 may serve as a scaffolding protein bringing arginine methylated proteins into close proximity in stress granules, and while proteins that localize to stress granules on induction of stress may shuttle to these entities, they are unable to stably situate at these sites in TDRD3's absence. Experiments looking into stress granule dynamics through Fluorescence Recovery After Photobleaching and live cell imaging in TDRD3 depleted cells will help to clarify this quandary. Furthermore, experimentation investigating cell survival will demonstrate whether TDRD3 depletion promotes cell death upon introduction of stress. Therefore, it appears that TDRD3 partakes in stress granule formation and cancer cell invasion through two distinct pathways, although this does not exclude the possibility that both of these roles may be crucial to mediate TDRD3 role's in breast cancer.

In summary, TDRD3 depletion influences numerous hallmarks of cancer including cell proliferation, anchorage-independent growth and cell motility and invasion. Furthermore, TDRD3 exerts its function on cell invasion through its interaction with FMRP, a protein known to promote cell invasion and metastasis through mRNAs traditionally altered in cancer.

7.4)

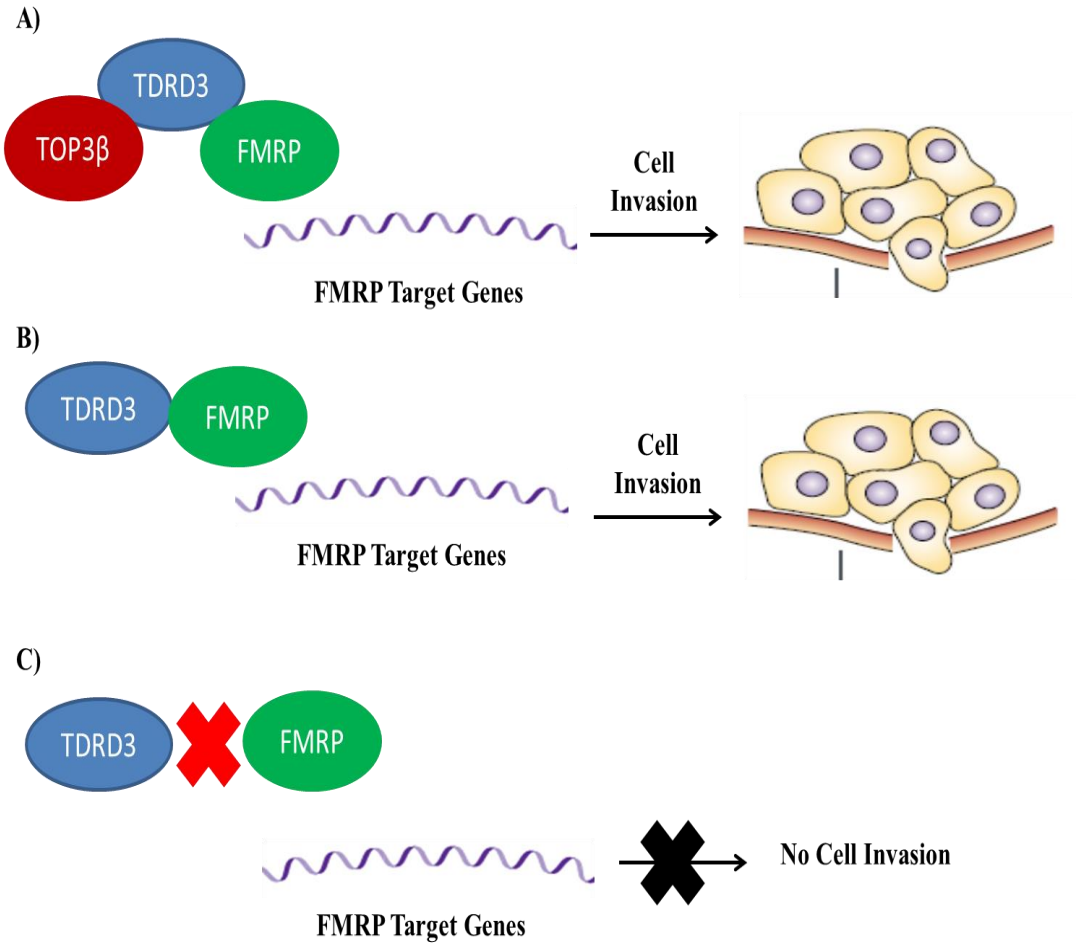
A)
TDRD3
TOP3β
FMRP
Cell Invasion
FMRP Target Genes
B)
TDRD3
FMRP
Cell Invasion
FMRP Target Genes
C)
TDRD3
FMRP
No Cell Invasion
FMRP Target Genes

Figure 7.4: Model of TDRD3-Mediated Promotion of Cell Invasion and Metastasis

A) TDRD3 serves as a scaffold protein mediating the interaction between FMRP and TOP3β. TDRD3 chaperones this TDRD3-TOP3β-FMRP complex to FMRP target mRNAs facilitating their translation. These mRNAs include those involved in cell adhesion, motility and invasion, as well as proteins involved in the epithelial to mesenchymal transition. (B) An alternative to the above model is TDRD3 promoting cell invasion and metastasis through an interaction with FMRP alone. (C) In the absence of TDRD3 interacting with FMRP, FMRP is no longer chaperoned to its target mRNA, therefore inhibiting their translation, and thus inhibiting cell invasion.

Conclusion

The results illustrated in this study provide further insight into the role of protein arginine methyltransferases in breast cancer. Specifically, a novel role is attributed to the alternatively spliced PRMT1 isoform, PRMT1v2 in the processes of apoptosis and cellular invasion, with regulation of cell invasion occurring through phosphorylation dependent degradation of β-catenin. Additionally, PRMT6, one of the PRMTs aberrantly expressed in breast cancer mediates chemoresistance through its regulation of stress granule dynamics. PRMT6 promotes bortezomib–induced stress granule formation through regulation of the eukaryotic translation initiation factor eIF4E, thus promoting cell survival in bortezomib-resistant breast cancer cells. Moreover, the RNA binding protein DDX3, a protein atypically expressed in breast cancer cells that promotes cell transformation in mammary epithelial cells is a novel substrate for PRMT1, CARM1 and PRMT6. Lastly, TDRD3, a reader of arginine methylated motifs, previously shown to be amongst the most overexpressed genes in highly aggressive estrogen receptor negative and basal-like breast tumors regulates breast cancer cell proliferation, anchorage-independent growth, and cell motility and invasion. Moreover, TDRD3 promotes cell invasion through its ability to bind FMRP, a protein known to promote breast cancer cell invasion and metastasis.

These results provide a link between PRMTs (writers of arginine methylation), DDX3 (a PRMT substrate), and TDRD3 (a reader of arginine methylation), and how upstream mis-regulation of PRMTs could contribute to downstream aberrant methylation of substrates, leading to abnormal reading of the arginine methylation mark by TDRD3, thus potentially promoting breast cancer development and progression

Appendix Ia

i)

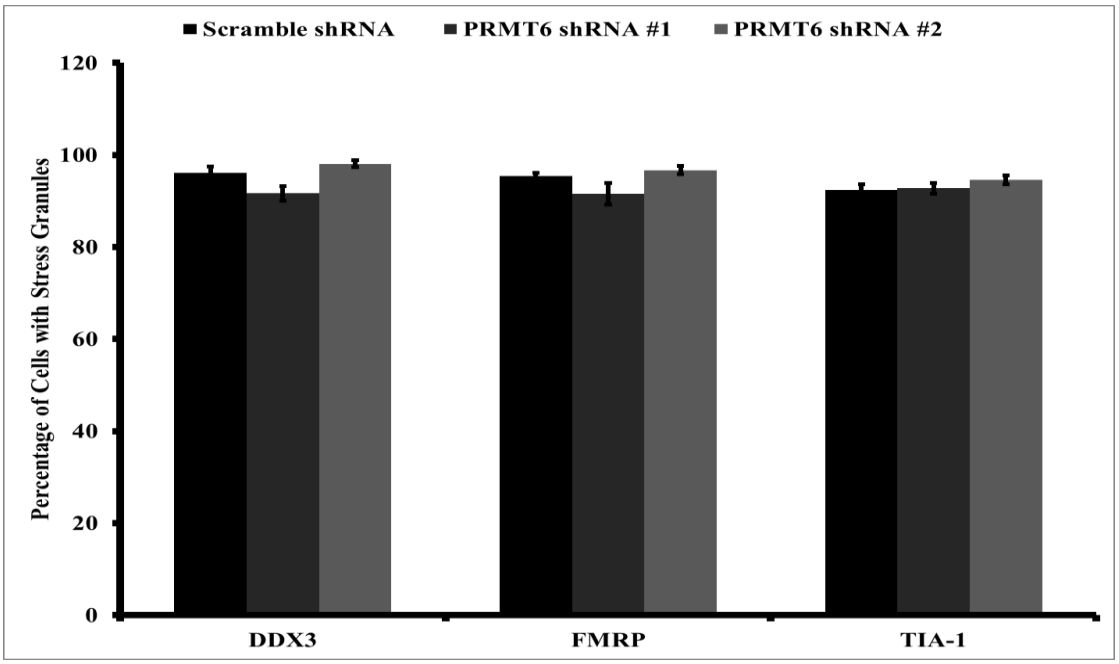

ii)

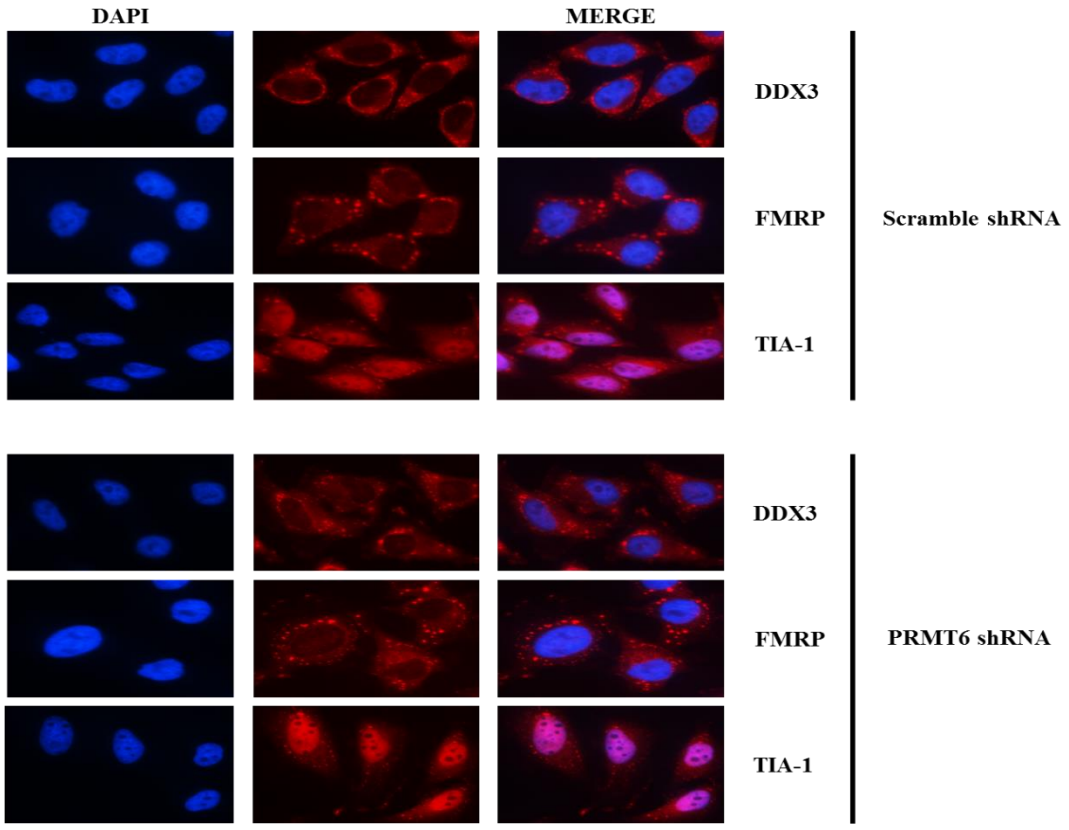

Appendix Ia: PRMT6 Depletion does not Influence Stress Granule Formation upon Normal Does of Sodium Arsenite

HeLa scramble and PRMT6 shRNA expressing cells were treated with 500 µM sodium arsenite for 30 min and were stained with the stress granule markers DDX3, FMRP, and TIA-1. The percentage of the cells containing stress granules was determined. (i) Graphical analysis showing the percentage of HeLa scramble and PRMT6 shRNA expressing cells containing stress granules. No difference in the percentage of scramble and PRMT6 shRNA expressing cells containing stress granules was observed. Data is the average +/- the standard error of the mean of three independent experiments counting at least 300 hundred cells per coverslip for each experiment. (ii) Representative images at 40X magnification using DDX3, FMRP and TIA-1 as markers for stress granule formation. DAPI was used to stain the nucleus.

Appendix Ib

i)

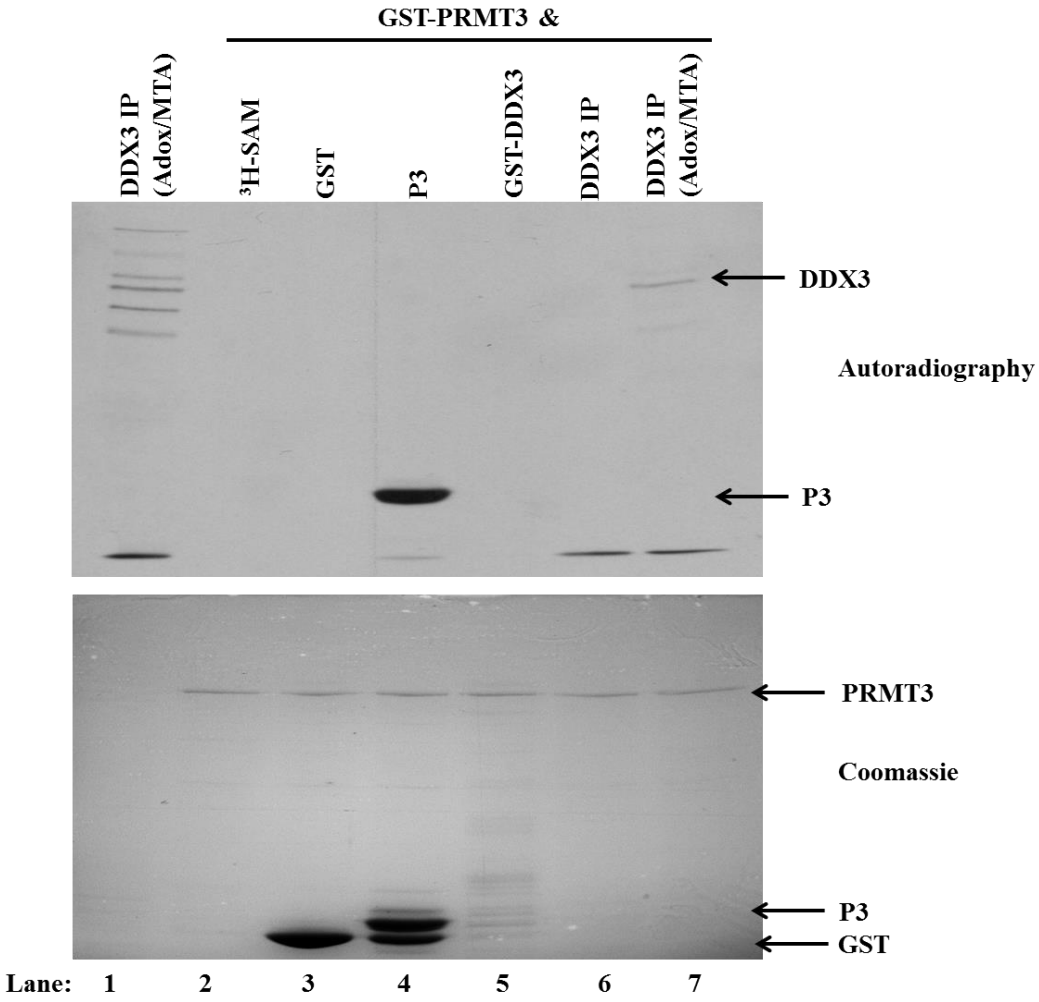

ii)

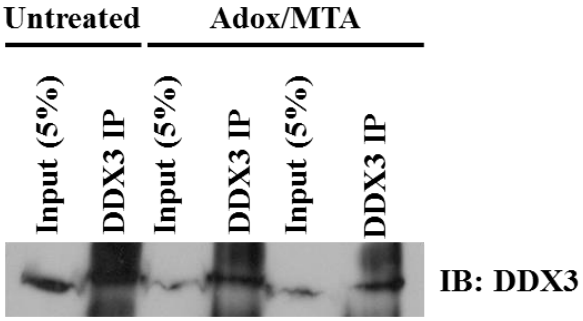

Appendix Ib: PRMT3 does not Methylate DDX3

(i) GST-tagged PRMT3 was incubated with GST-tagged DDX3 (lane 5) or DDX3 immunoprecipitated from HeLa cell lysate untreated (lane 6) or treated with Adox and MTA for 24 h (lane 7) in the presence of ^{3}H-SAM. PRMT3 was unable to methylate any form of DDX3. DDX3 immunoprecipitated from Adox/MTA treated cell lysate (lane 1) was incubated with ^{3}H-SAM as a control. GST-P3 was used as a positive control, while empty vector GST was used as a negative control. Coomassie staining was used to show loading of purified protein. (ii) Western blot showing DDX3 immunoprecipitated from HeLa cell lysate from untreated or Adox/MTA treated cells. Five percent of cell lysate was used for input, while the remaining lysate was used to immunoprecipitate DDX3 and split equally for the methylation assay and IP.

Appendix Ic

i)

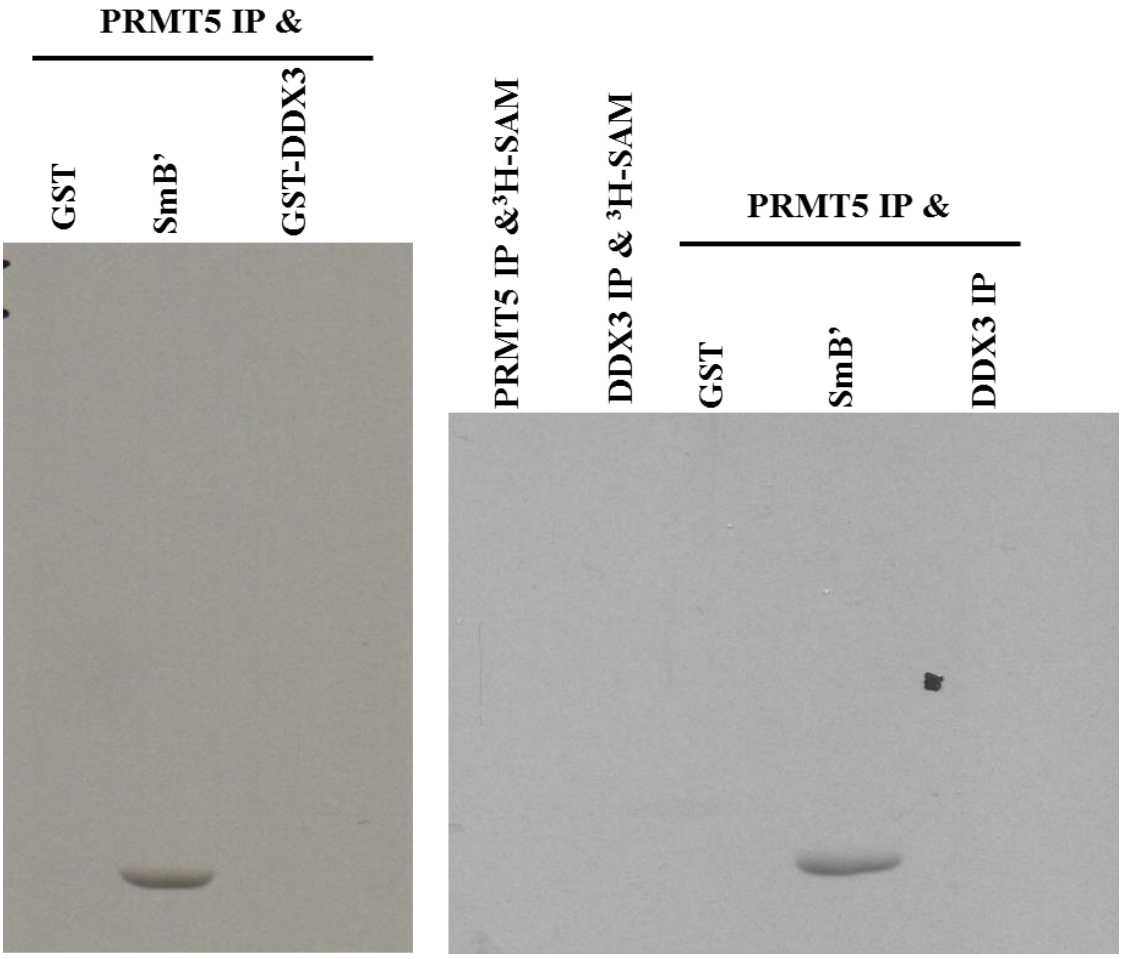

ii)

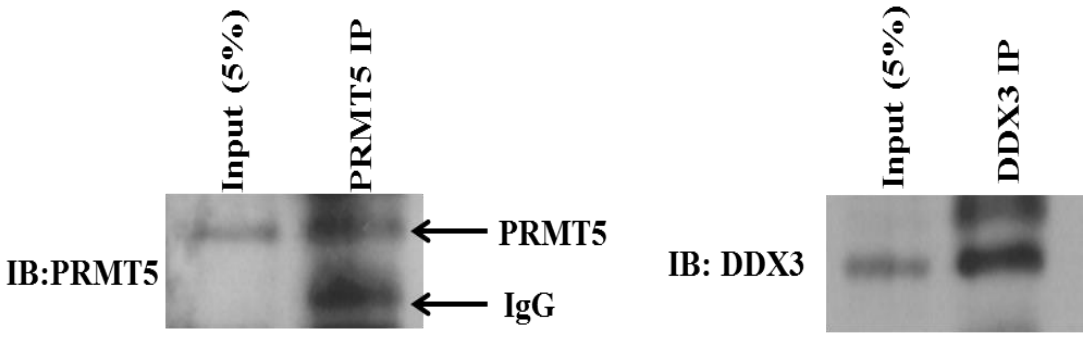

Appendix Ic: PRMT5 does not Methylate DDX3

(i) PRMT5 immunoprecipitated from HeLa lysate was incubated with GST-DDX3 (left panel) or DDX3 immunoprecipitated from HeLa lysate (right panel) in the presence of ^{3}H-SAM). PRMT5 was unable to methylate purified DDX3 protein or DDX3 immunoprecipitated from cell lysate. GST-SmB' was used as a positive control, while empty vector GST was utilized as a negative control. (ii) A Western blot showing a large scale immunoprecipitation of PRMT5 (left panel). Five percent of the cell lysate was kept for input, and twenty percent to test the IP, while the remainder was equally split for each reaction in the *in vitro* methylation assay. Western blot showing immunoprecipitation of DDX3 protein utilized in the *in vitro* methylation assay (right panel).

Appendix Id

i)

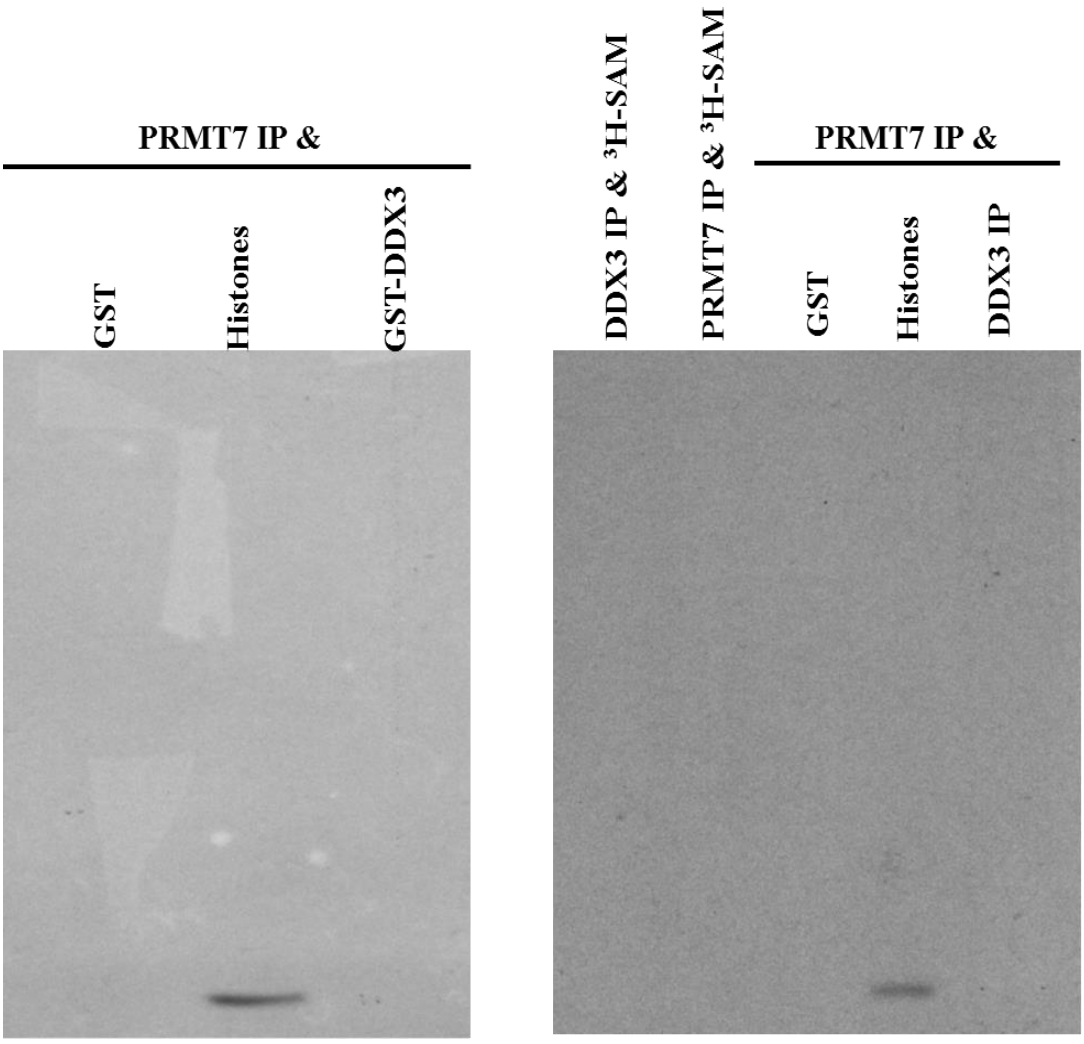

ii)

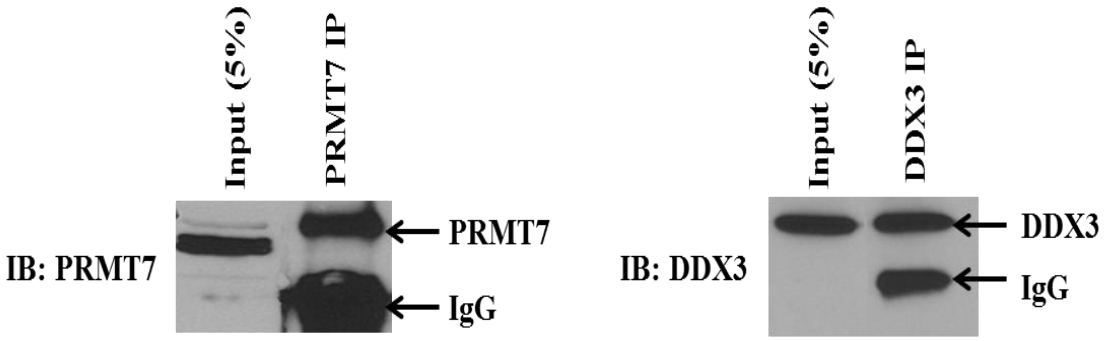

Appendix Id: PRMT7 does not Methylate DDX3

(i) PRMT7 immunoprecipitated from HeLa lysate was incubated with GST-DDX3 (left panel) or DDX3 immunoprecipitated from HeLa lysate (right panel) in the presence of ^{3}H-SAM). PRMT7 was not able to methylate purified DDX3 protein or DDX3 immunoprecipitated from cell lysate. Purified histones were used as a positive control, while empty vector GST was utilized as a negative control. (ii) A Western blot showing a large scale immunoprecipitation of PRMT7 (left panel). Five percent of the cell lysate was kept for input, and twenty percent to test the IP, while the remainder was equally split for each reaction in the *in vitro* methylation assay. A Western blot showing DDX3 immunoprecipitation (right panel).

Appendix Ie

i)

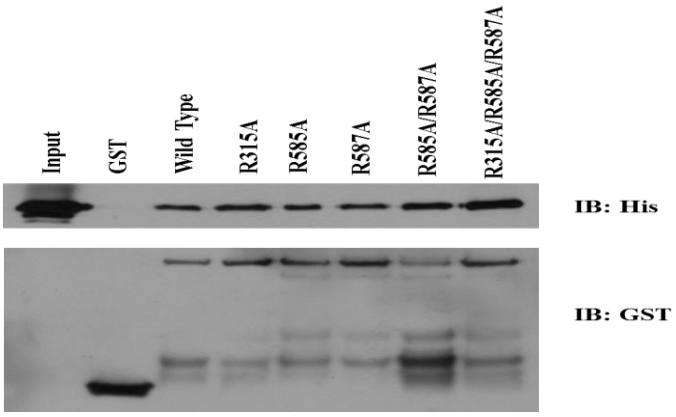

ii)

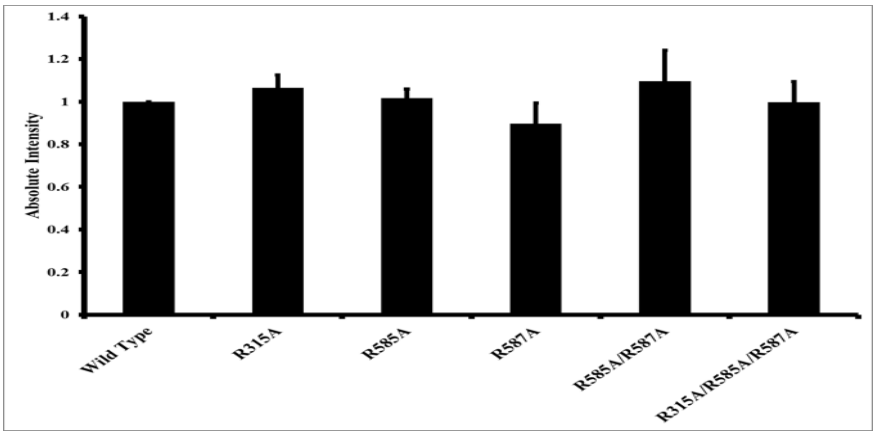

iii)

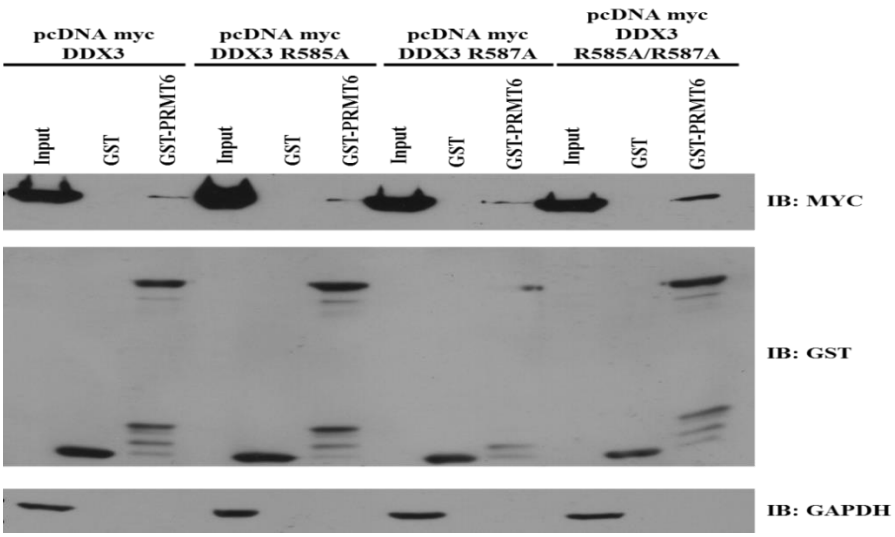

Appendix Ie: Mutation of DDX3 Methylarginine Residues Does Not Affect PRMT6 Binding, *In Vitro*

(i) His-tagged PRMT6 was incubated with GST empty vector, GST-tagged DDX3 wild type, or methylarginine mutants R315A, R585A, R587A, R585A/R587A, and R315A/R585A/R587A bound to GST beads, and a GST pulldown was performed. Immunoblotting with a His antibody shows the amount of His-tagged PRMT6 which bound to each GST-tagged DDX3 construct. A GST antibody was used to show the amount of each GST-tagged DDX3 used in the assay. (ii) Densitometry analysis shows the mean binding of PRMT6 to each GST-tagged DDX3 construct +/- the standard error of the mean for five independent experiments, whereas the amount of bound PRMT6 was normalized to the amount of each GST-tagged DDX3 construct. No difference in His-PRMT6 binding to any mutant was observed in comparison to binding to wild type GST-tagged DDX3. (iii) Myc tagged DDX3 wild type, or methylarginine mutants R585A, R587A, and R585A/R587A were expressed in 293T cells for 48 h. The cells were lysed and the lysate was incubated with either GST-tagged empty vector or GST-tagged PRMT6 bound to GST beads, and a GST pulldowm was performed. Immunoblotting with a Myc antibody shows that mutation of DDX3 arginine residues 585 or 587 to alanine does not inhibit their capacity to bind to PRMT6. A GST antibody was utilized to show the amount of GST-PRMT6 bound to GST beads for each reaction, while GAPDH shows that an equal amount of cell lysate was used in each reaction.

Appendix If

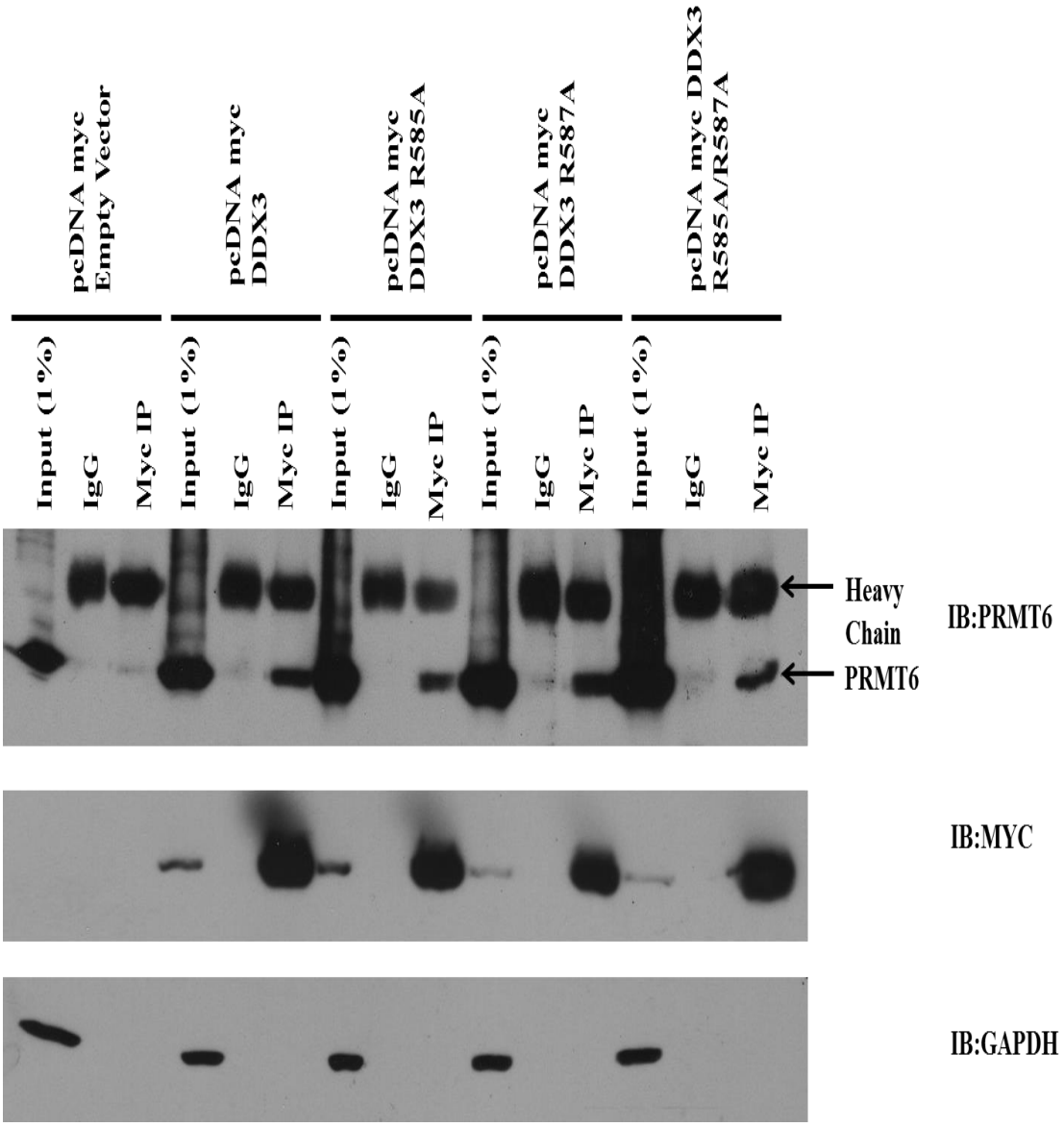
pcDNA myc Empty Vector
pcDNA myc DDX3
pcDNA myc DDX3 R585A
pcDNA myc DDX3 R587A
pcDNA myc DDX3 R585A/R587A
Input (1%)
IgG
Myc IP
Heavy Chain
PRMT6
IB:PRMT6
IB:MYC
IB:GAPDH

Appendix If: Mutation of DDX3 Methylarginine Residues Does Not Affect PRMT6 Binding, *In Vivo*

Myc-tagged wild type DDX3 or DDX3 methylarginine mutants R585A, R587A, R585A/R587A were expressed in 293T cells for 48 h. Cells were lysed and myc was immunoprecipitated from the cell lysate. Western blot analysis with a PRMT6 antibody shows that mutation of arginine residues 585 and 587 to alanine residues does not abrogate endogenous PRMT6's ability to interact with these mutants. The Myc antibody was utilized to show that a similar amount of each myc-tagged DDX3 construct was immunoprecipitated from the cell lysate, while GAPDH shows that an equivalent amount of protein was used for each reaction.

Appendix Ig

i)

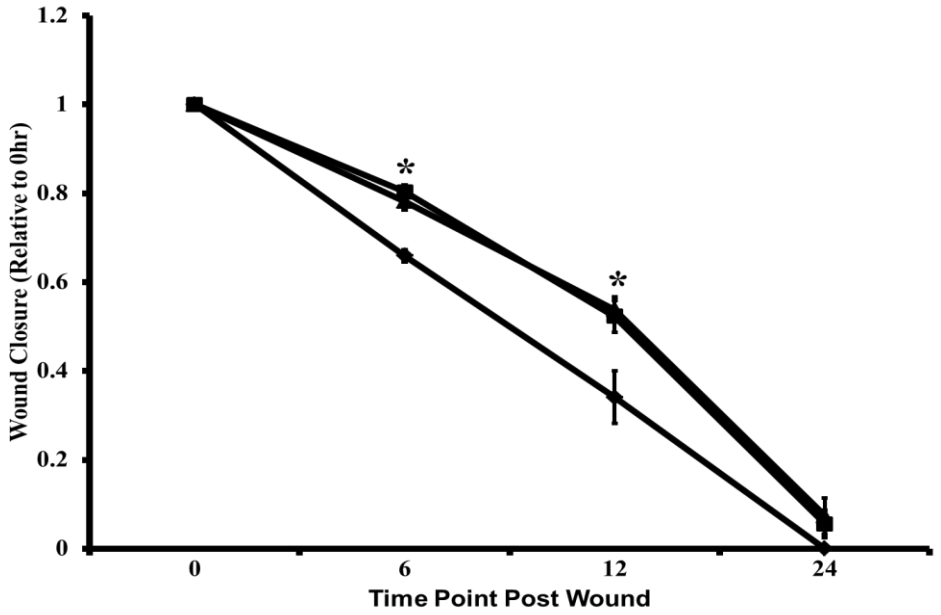

ii)

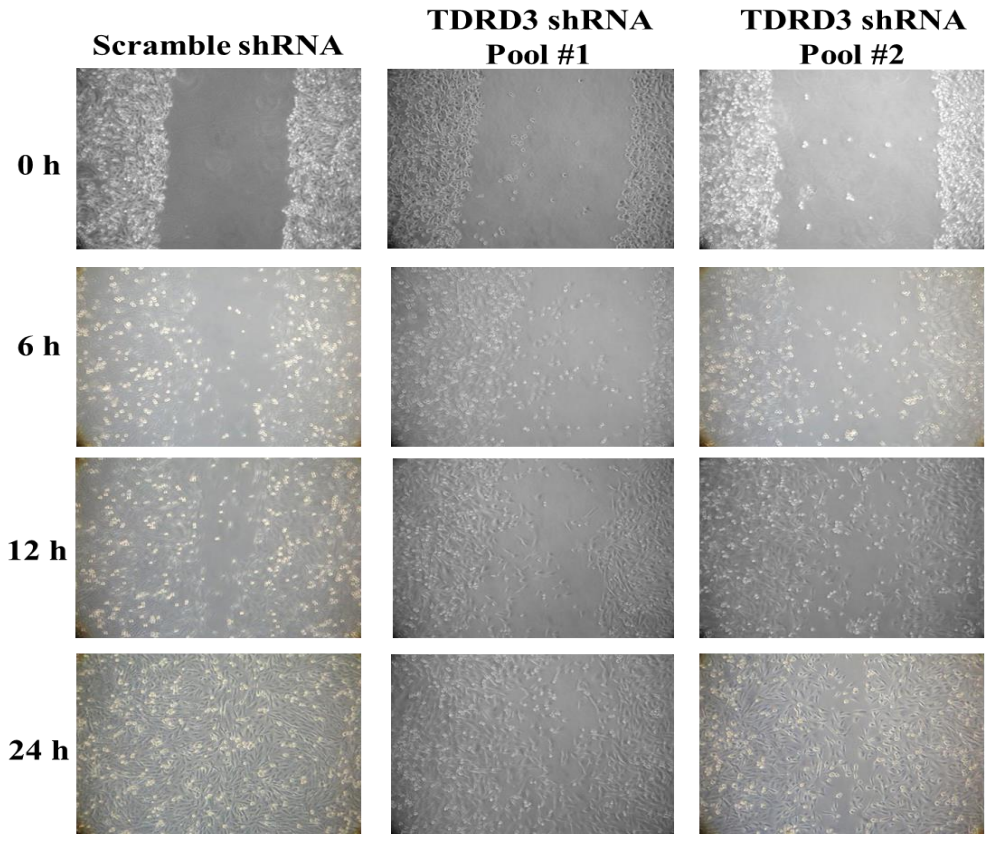

Appendix Ig: TDRD3 Depletion Inhibits MDA MB 231 Cell Motility

MDA MB 231 scramble and TDRD3 shRNA expressing cells were grown to confluency and a wound was made with a pipette tip, and the rate at which the cells closed the wound was measured 6, 12, and 24 h after the wound was made. (i) At 6 and 12 h, scramble shRNA expressing cells closed the wound at a faster rate than TDRD3 shRNA expressing cells. This difference was gone 24 h after the wound was made. (ii) Representative images of scramble and TDRD3 shRNA expressing cells at time points 0, 6, 12, and 24 h after the wound was made.

Appendix Ih

i)

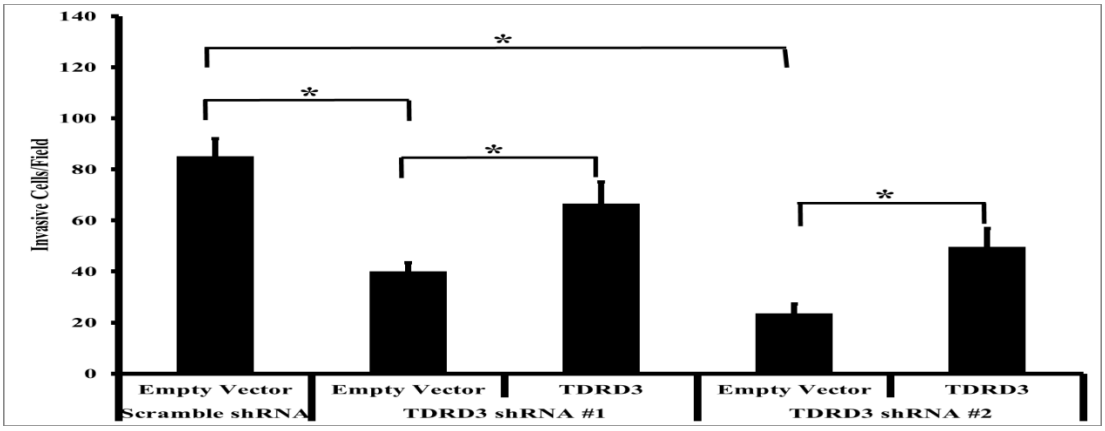

ii)

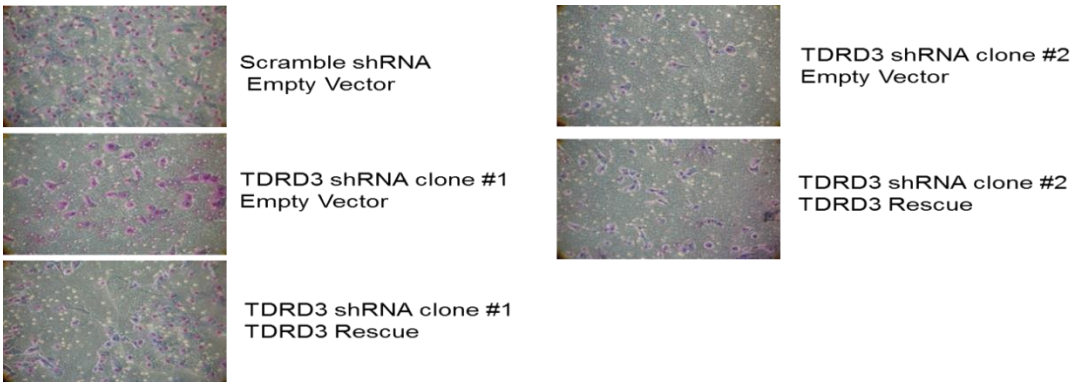

iii)

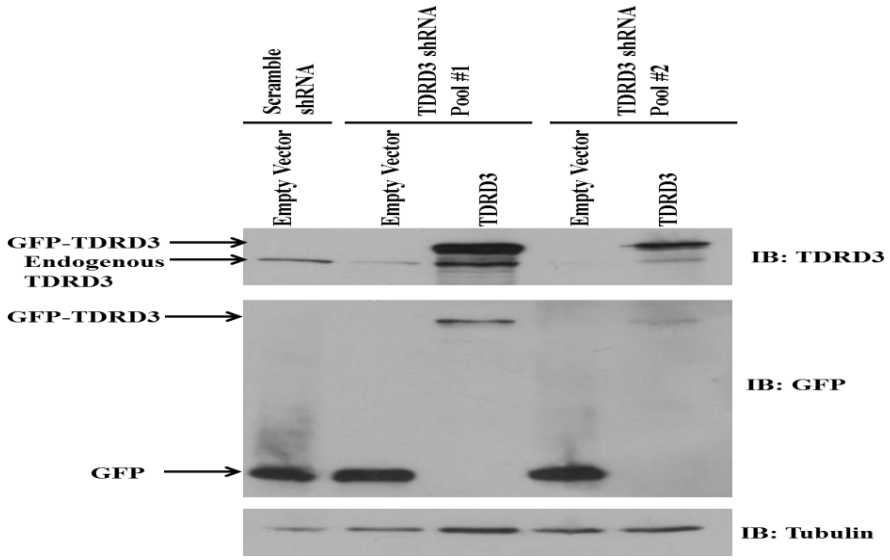

Appendix Ih: Re-introduction of GFP-tagged TDRD3 Rescues Cell Invasion

MDA MB 231 TDRD3 shRNA stably expressing cells were transfected with GFP empty vector or GFP-tagged TDRD3 for 48 h. Cells were counted and an equal number of cells were plated in Transwell invasion chambers for 24 h, stained and the number of cells invading through the chamber was determined. Six images of each chamber were taken to determine the average number of cells per field invading through the chambers. (i) Re-introduction of TDRD3 in two different pools of MDA MB 231 TDRD3 shRNA stably expressing cells results in a rescue in the invasive potential of MDA MB 231 cells. Data is the mean of three independent experiments +/- the standard error of the mean. * denotes statistical significance with a p-value less than 0.01 as determined with a one way ANOVA. (ii) Representative images of Transwell invasion chambers taken at 20X magnification. (iii) Western Blot depicting exogenous expression of GFP-tagged TDRD3 in MDA MB 231 TDRD3 shRNA stably expressing cells. Blotting with TDRD3 shows endogenous and exogenous expression of TDRD3, while immunoblotting with GFP displays expression of GFP constructs. Tubulin was used a loading control.

Appendix Ii

i)

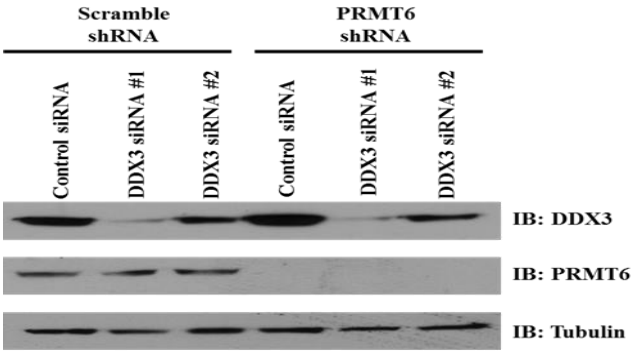

ii)

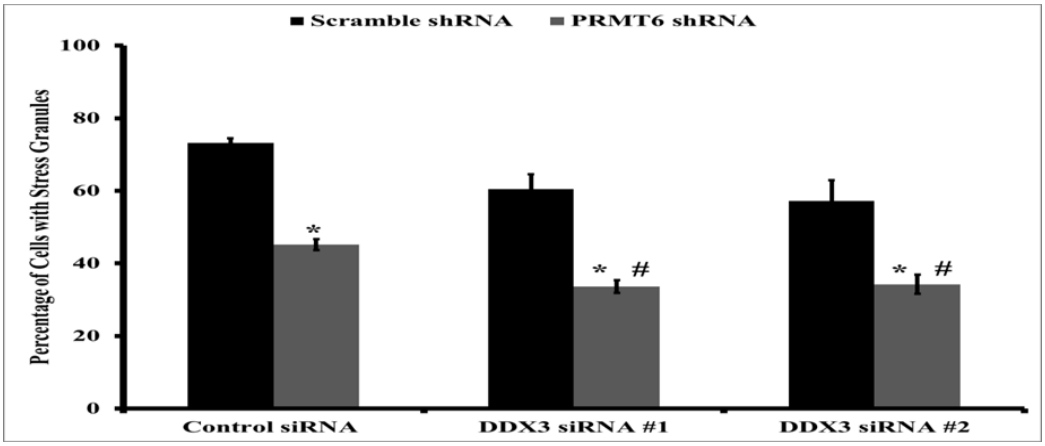

iii)

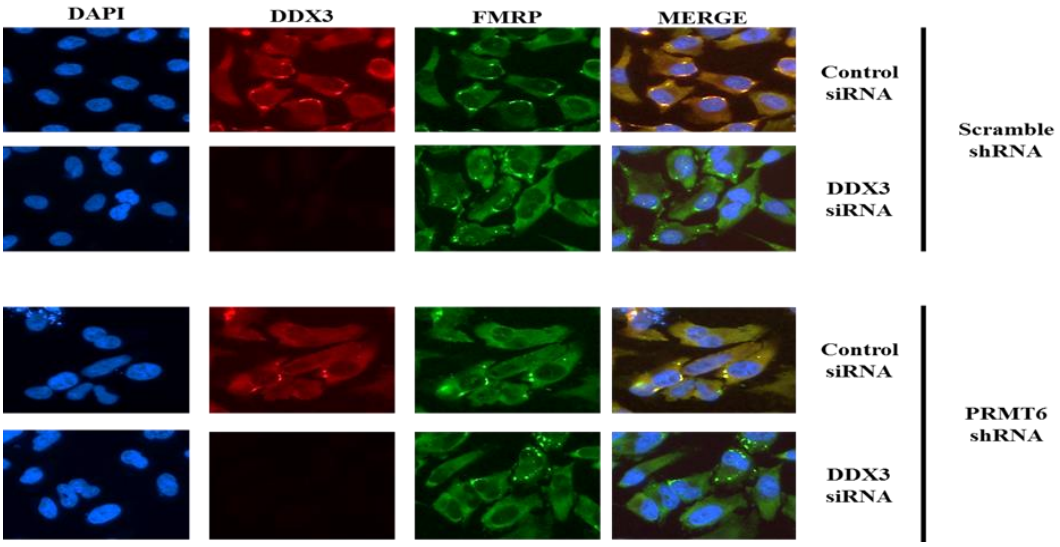

Appendix Ii: Depletion of DDX3 Decreases Bortezomib-Induced Stress Granule Formation

HeLa scramble or PRMT6 shRNA stably-expressing cells were transfected with a control siRNA or two different DDX3 siRNA (DDX3 siRNA #1 and DDX3 siRNA #2) for 24 h, and cells were treated with 10 µM bortezomib for 4 h. (i) Western blot depicting knockdown of DDX3 (top panel) in scramble and PRMT6 shRNA transfected with two different DDX3 siRNA. Tubulin was used a loading control. (ii) Graphical analysis showing the percentage of HeLa scramble and PRMT6 shRNA expressing cells upon transfection with a control siRNA or two DDX3 siRNA. DDX3 knockdown results in an equal decrease in the rate of stress granule formation in both scramble and PRMT6 shRNA stably-expressing cell lines. Data is the average +/- the standard error of the mean of three independent experiments counting at least 300 hundred cells per coverslip for each experiment. * denotes statistical significance at a p-value less than 0.05 between scramble and PRMT6 shRNA expressing cells upon transfection with either the control or DDX3 siRNA. # denotes statistical significance between control and DDX3 siRNA in PRMT shRNA expressing cell lines. Significance was determined using a one way ANOVA. (iii) Representative images taken at 40X magnification using FMRP as a marker for stress granule formation. DDX3 images were obtained using the same exposure time. DAPI was used to stain the nucleus.

Appendix Ij

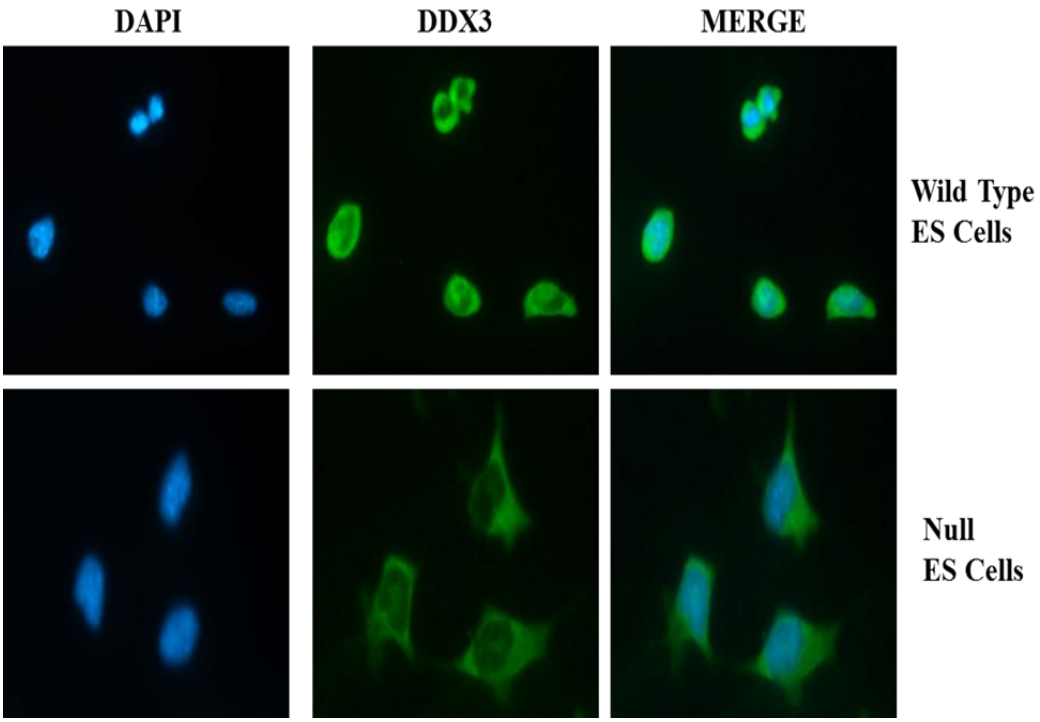

Appendix Ij: DDX3 Cellular Localization is Unaffected by PRMT1 Depletion

Immunufluorescence was performed with PRMT1 wild type and null (ES) embryonic stem cells using an antibody to stain for DDX3. DDX3 localized primarily to the cytoplasm in both wild type and null ES cells. Images were acquired at 40X magnification. DAPI was used to stain the nucleus.

Appendix Ik

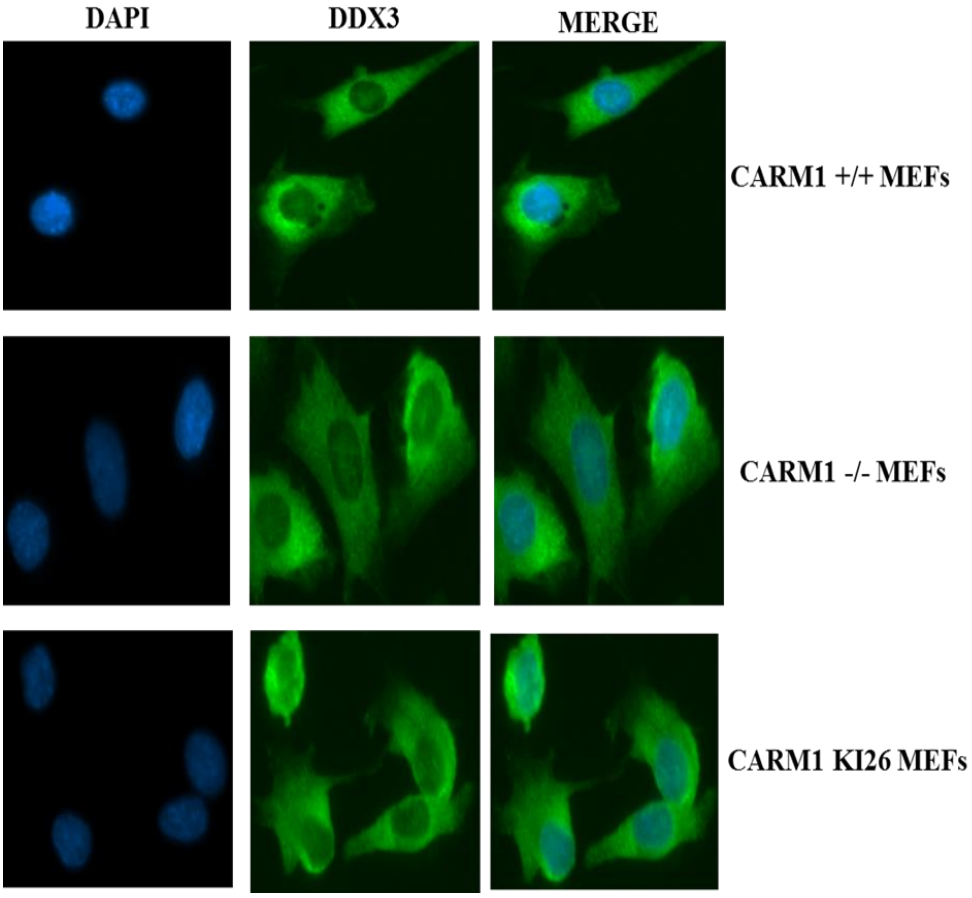

Appendix Ik: DDX3 Cellular Localization is Unaffected by CARM1 Depletion

Immunufluorescence was performed with CARM1 wild type, methyltransferase dead (KI26) and null mouse embryonic fibroblasts (MEFs) using an antibody to stain for DDX3. DDX3 localization was unaffected by CARM1 depletion and localized primarily to the cytoplasm in wild type, null and methyltransferase dead MEFs. Images were acquired at 40X magnification. DAPI was used to stain the nucleus.

Appendix Il

i)

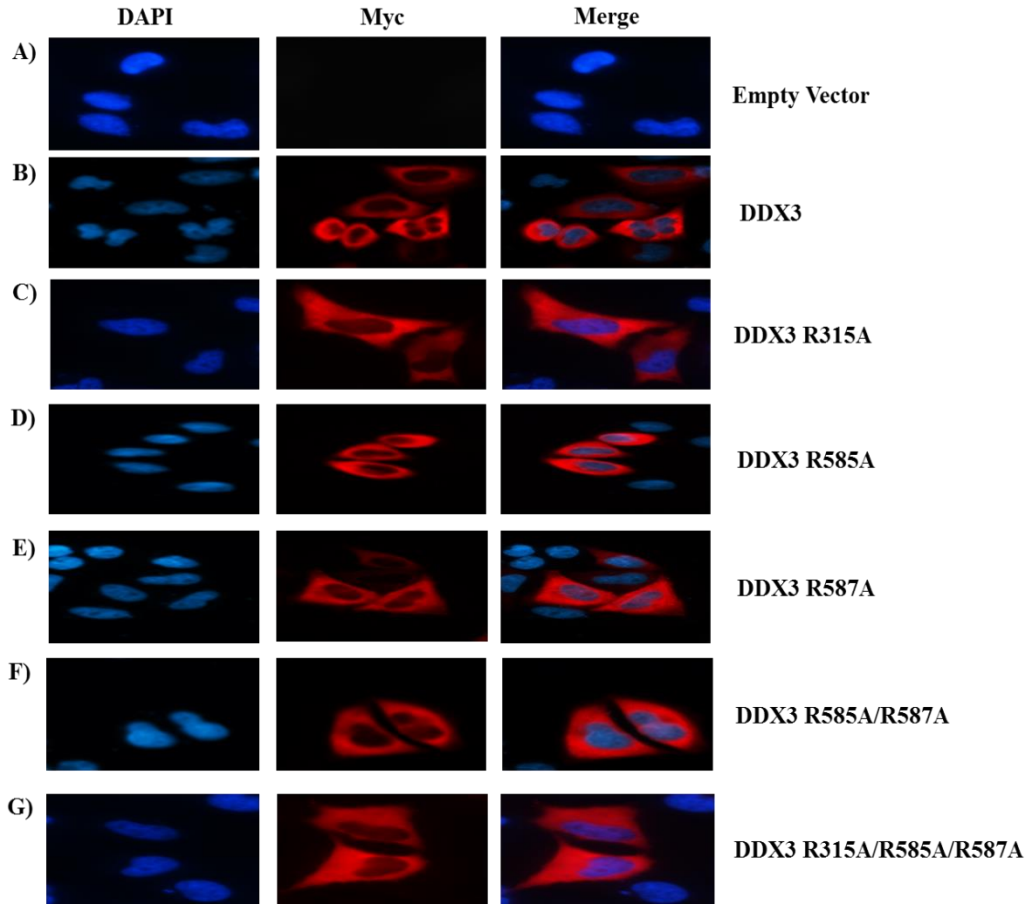

ii)

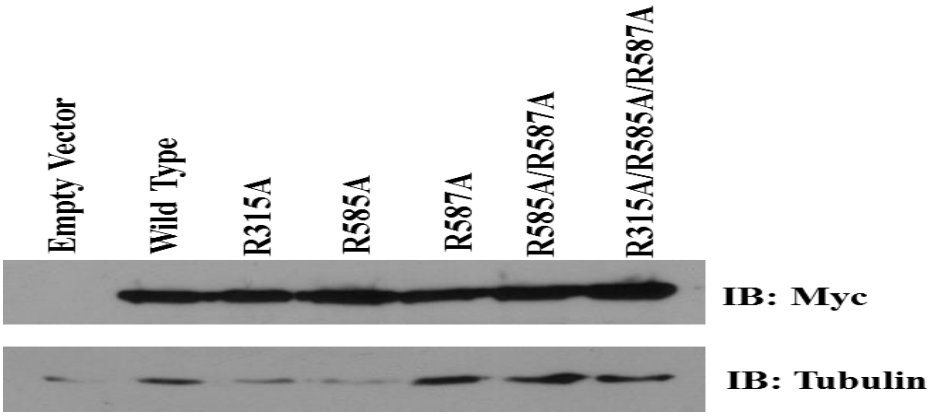

Appendix Il: Mutation of DDX3 Methylarginine Residues Does Not Affect DDX3's Cellular Localization

(i) HeLa cells were transfected with myc-tagged (B) wild type DDX3 or DDX3 methylation mutants (C) R315A, (D) R585A, (E) R587A, (F) R585A/R587A, and (G) R315A/R585A/R587A and immunofluorescence was performed with staining with a Myc antibody. DDX3 localization to the cytoplasm was unaltered upon mutation of these methylation sites to alanines. DAPI was used to stain the nucleus. (ii) Western Blot showing expression of myc-tagged DDX3 wild type and methylation mutants. Tubulin was used as a loading control.

Appendix Im:

i)

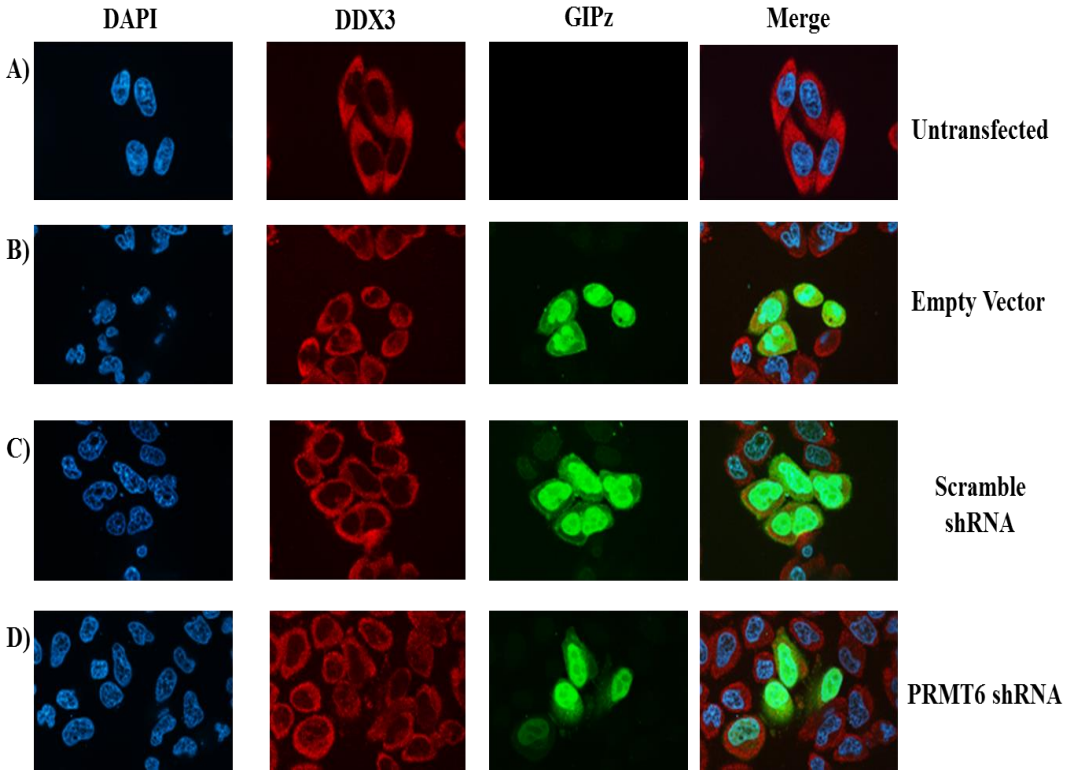

ii)

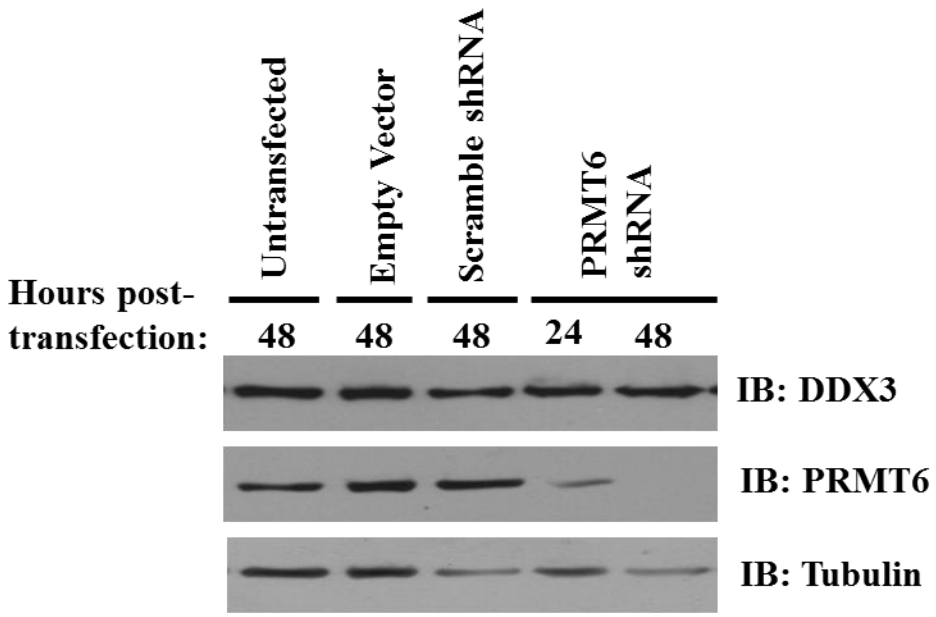

Appendix Im: Transient Knockdown of PRMT6 does not Alter DDX3 Cellular Localization

(i) HeLa cells were transiently transfected with (b) pGIPz empty vector, (c) pGIPz scramble shRNA, or (d) pGIPz PRMT6 shRNA for 48 h and immunofluorescence was performed. DDX3 cellular localization to the cytoplasm was not affected by depletion of PRMT6. Cells transfected with the pGIPz vectors were identified by staining with GFP. DAPI was used to stain the nucleus. (ii)Western blotting shows transient knockdown of PRMT6 48 h post transfection (middle panel). DDX3 protein expression was unaffected by depletion of PRMT6 protein levels (top panel). Tubulin was used to show equal protein loading (bottom panel).

Appendix In

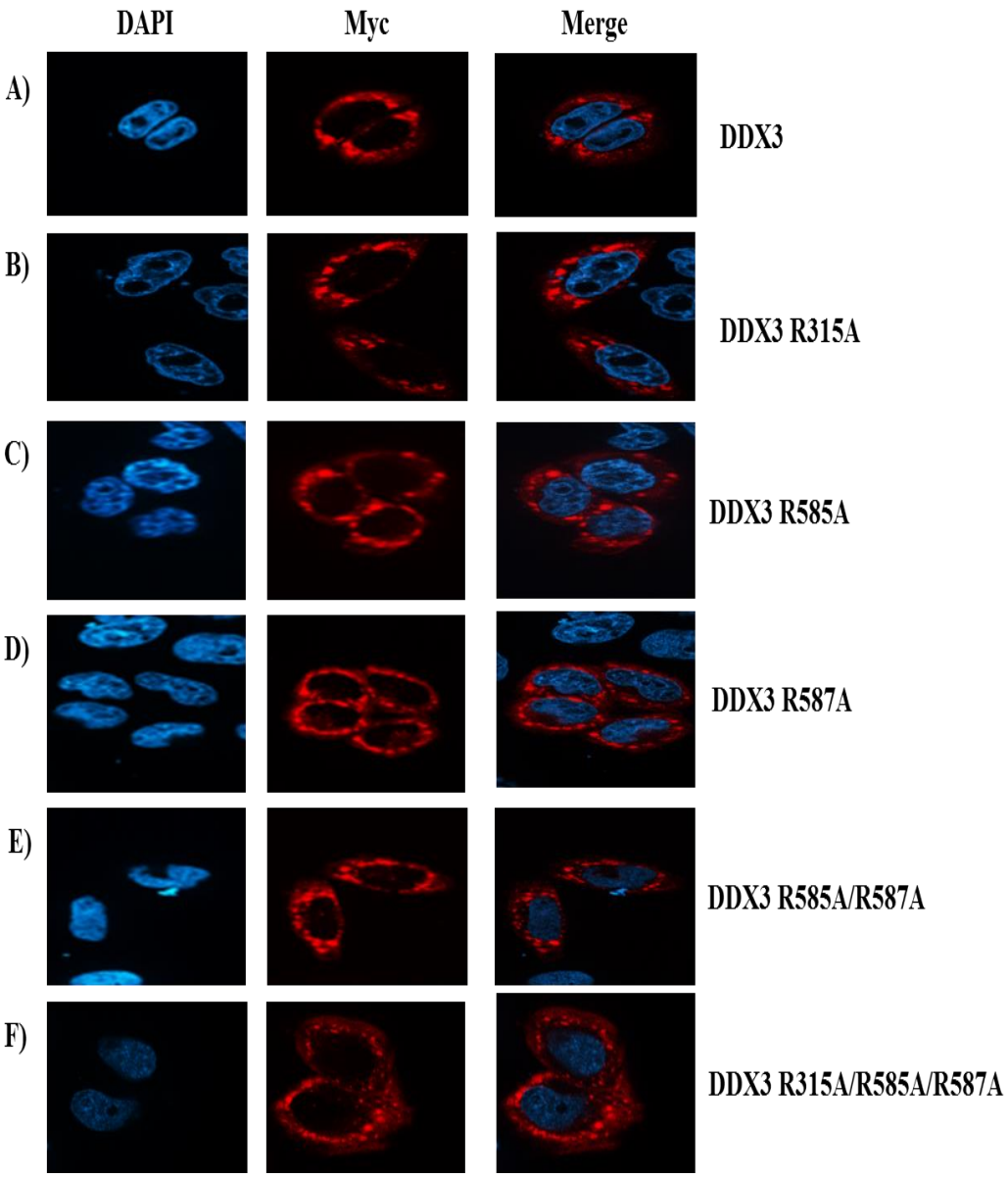
DAPI
Myc
Merge
A)
DDX3
B)
DDX3 R315A
C)
DDX3 R585A
D)
DDX3 R587A
E)
DDX3 R585A/R587A
F)
DDX3 R315A/R585A/R587A

Appendix In: Mutation of DDX3 Methylarginine Residues does not Alter DDX3 Localization to Stress Granules

HeLa cells were transfected with myc-tagged (A) wild type DDX3 or DDX3 methylation mutants (B) R315A, (C) R585A, (D) R587A, (E) R585A/R587A, and (F) R315A/R585A/R587A for 48 h, treated with 0.5 mM sodium arsenite for 1h and immunofluorescence was performed with staining with a Myc antibody. DDX3 localization to the stress granules was unaltered upon mutation of these methylation sites to alanines. DAPI was used to stain the nucleus.

Appendix Io

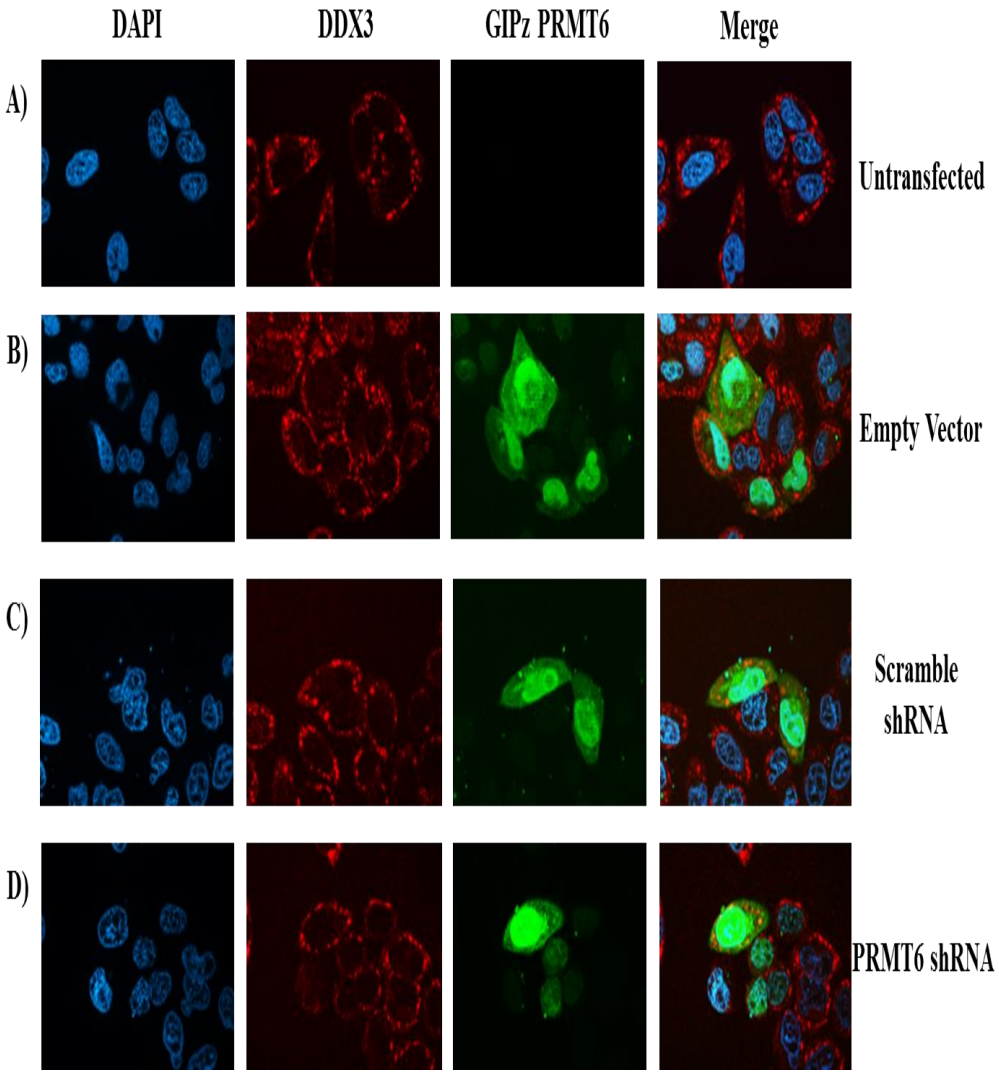
DAPI
DDX3
GIPz PRMT6
Merge
A)
Untransfected
B)
Empty Vector
C)
Scramble shRNA
D)
PRMT6 shRNA

Appendix Io: Transient Knockdown of PRMT6 does not Alter DDX3 Localization to Stress Granules

HeLa cells were transiently transfected with (b) pGIPz empty vector, (c) pGIPz scramble shRNA, or (d) pGIPz PRMT6 shRNA for 48 h, treated with 0.5 mM sodium arsenite for 1 h and immunofluorescence was performed. DDX3 cellular localization to the stress granules was not affected by depletion of PRMT6. Cells transfected with the pGIPz vectors were identified by staining with GFP. DAPI was used to stain the nucleus.

Appendix Ip

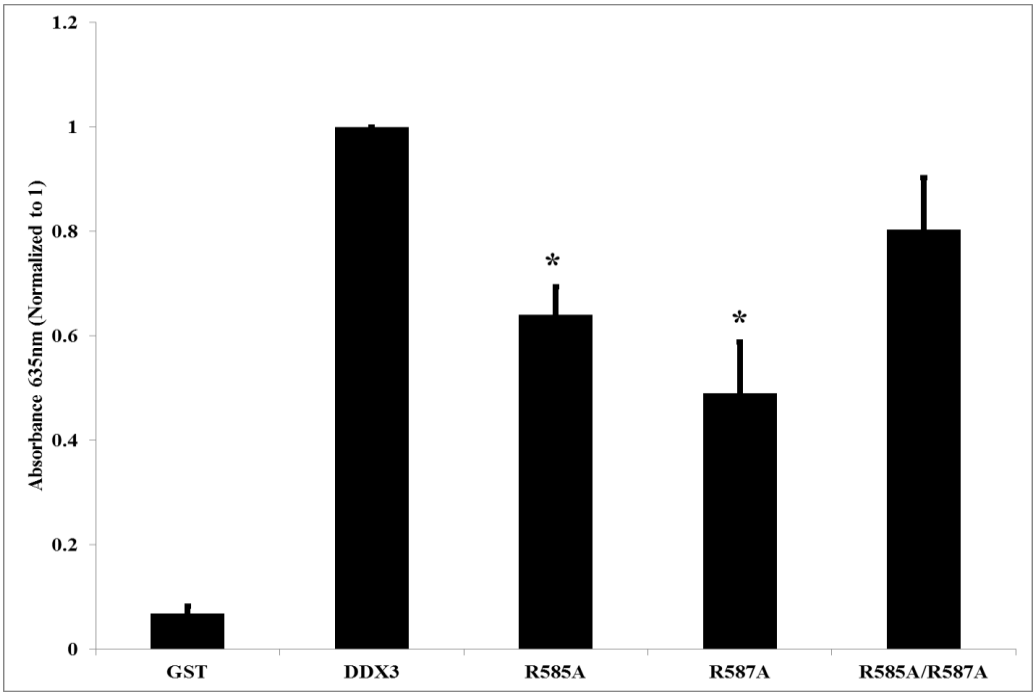
1.2
1
0.8
0.6
0.4
0.2
0
Absorbance 635nm (Normalized to 1)
*
*
GST
DDX3
R585A
R587A
R585A/R587A

Appendix Ip: Mutation of DDX3 Arginine Residues 585 and 587 Influences DDX3 ATPase Activity

GST-tagged DDX3 wild type or methylation mutants R585A, R587A, and R585A/R587A were incubated with ATP for 30 min and an ATPase assay was performed using Innova Bioscience's ATPase assay kit. The amount of hydrolyzed phosphate was measured through addition of a dye which combined with the hydrolyzed phosphate to emit a colorimetric signal which was measured at 635 nm. Mutation of arginine residues 585 or 587 to alanine resulted in a significant reduction in DDX3 ATP hydrolysis activity. Mutation of both 585 and 587 did not have a significant effect on ATP hydrolysis activity. Values were normalized to 1. GST empty vector was used as a negative control.

Appendix Iq

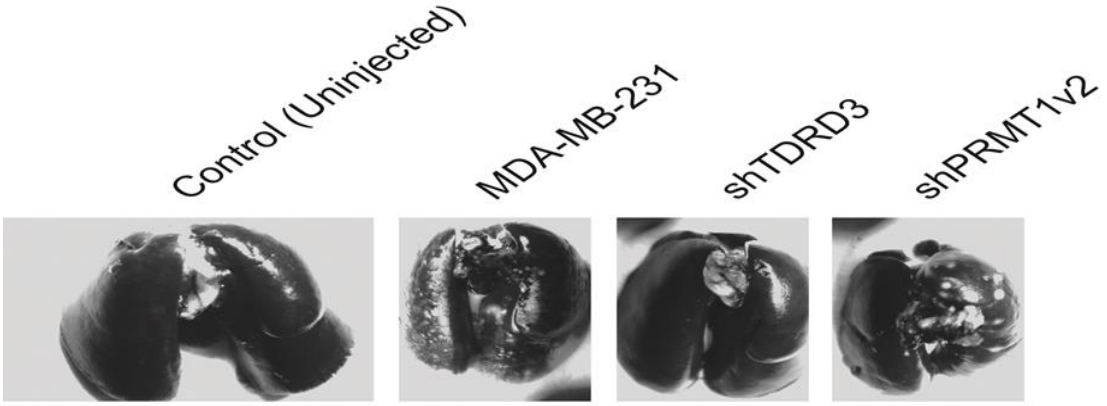
Control (Uninjected)
MDA-MB-231
shTDRD3
shPRMT1v2

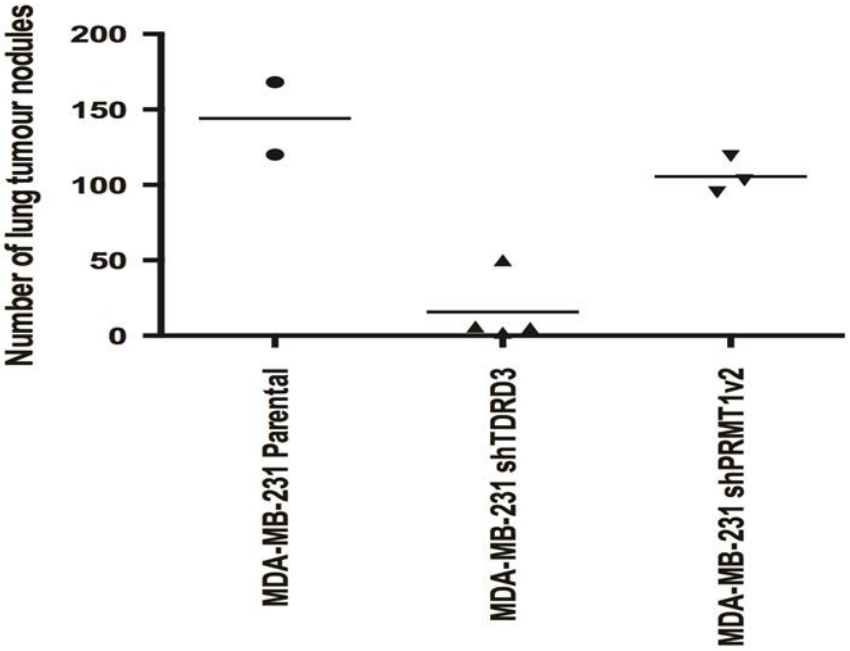
Number of lung tumour nodules
200
150
100
50
0
MDA-MB-231 Parental
MDA-MB-231 shTDRD3
MDA-MB-231 shPRMT1v2

Appendix Iq: TDRD3 Depletion Results in a Reduction in Lung Nodule Formation

An *in vivo* lung metastatic mouse model was performed with 500 000 MDA MB 231 parental, PRMT1v2 shRNA or TDRD3 shRNA stably expressing cells injected into the tail vein of nude mice. Forty days post injection, the lungs were removed and stained with India ink to allow for quantification of the number of nodules formed on the lungs. Whereas injection of PRMT1v2 shRNA stably expressing MDA MB 231 cells resulted in a slight reduction in nodule formation compared to parental MDA MB 231 cells, injection of TDRD3 shRNA stably expressing MDA MB 231 cells resulted in almost a complete abrogation of nodule formation.

Appendix II: DDX3 Site-directed Mutagenesis Primers

DDX3 R315A: Forward

(CAGCAGATTCGAGACTTGGAAGCTGGATGCCATTTGTTAG)

Reverse (CTAACAAATGGCATCCAGCTTCCAAGTCTCGAATCTGCTG)

DDX3 R503A: Forward

(TGGCTACAGCAGTAGCAGCAGCAGGACTGGACATTTC) Reverse

(GAAATGTCCAGTCCTGCTGCTGCTACTGCTGTAGCCA)

DDX3 R585A: Forward

(TGAACACCACTACAAGGGTAGCAGTGCTGGACGTTCTAAG) Reverse

(CTTAGAACGTCCAGCACTGCTACCCTTGTAGTGGTGTTCA)

DDX3 R587A: Forward

(CAAGGGTAGCAGTCGTGGAGCTTCTAAGAGTAGCAGATTT) Reverse

(AAATCTGCTACTCTTAGAAGCTCCACGACTGCTACCCTTG)

DDX3 R632A: Forward (GGCCACGGTAGCAGCGCAGGATTTGGTGGCGG)

Reverse (CCTCCACCAAATCCTGCGCTGCTACCGTGGCC)

DDX3 R585A/R587A: Forward

(CACCACTACAAGGGTAGCAGTGCTGGAGCTTCTAAGAGTAGCAGATTTAG)

Reverse

(CTAAATCTGCTACTCTTAGAAGCTCCAGCACTGCTACCCTTGTAGTGGTG)

LITERATURE CITED

Adams, J. (2004a). The development of proteasome inhibitors as anticancer drugs. Cancer Cell. 5, 417-421.

Adams, J. (2004b). The proteasome: a suitable antineoplastic target. Nature Reviews.Cancer. 4, 349-360.

Adorno, M., M. Cordenonsi, M. Montagner, et al. (2009). A Mutant-p53/Smad complex opposes p63 to empower TGFbeta-induced metastasis. Cell. 137, 87-98.

Al-Dhaheri, M., J. Wu, G.P. Skliris, et al. (2011). CARM1 is an important determinant of ERalpha-dependent breast cancer cell differentiation and proliferation in breast cancer cells. Cancer Research. 71, 2118-2128.

An, W., J. Kim, and R.G. Roeder. (2004). Ordered cooperative functions of PRMT1, p300, and CARM1 in transcriptional activation by p53. Cell. 117, 735-748.

Ancelin, K., U.C. Lange, P. Hajkova, et al. (2006). Blimp1 associates with Prmt5 and directs histone arginine methylation in mouse germ cells. Nature Cell Biology. 8, 623-630.

Anderson, P., and N. Kedersha. (2009). Stress granules. Current Biology : CB. 19, R397-8.

Anderson, P., and N. Kedersha. (2008). Stress granules: the Tao of RNA triage. Trends in Biochemical Sciences. 33, 141-150.

Anderson, P., and N. Kedersha. (2006). RNA granules. The Journal of Cell Biology. 172, 803-808.

Anderson, P., and N. Kedersha. (2002). Stressful initiations. Journal of Cell Science. 115, 3227-3234.

Arimoto, K., H. Fukuda, S. Imajoh-Ohmi, et al. (2008). Formation of stress granules inhibits apoptosis by suppressing stress-responsive MAPK pathways. Nature Cell Biology. 10, 1324-1332.

Ashley, C.T.,Jr, K.D. Wilkinson, D. Reines, et al. (1993). FMR1 protein: conserved RNP family domains and selective RNA binding. Science (New York, N.Y.). 262, 563-566.

Aubourg, S., M. Kreis, and A. Lecharny. (1999). The DEAD box RNA helicase family in Arabidopsis thaliana. Nucleic Acids Research. 27, 628-636.

Baguet, A., S. Degot, N. Cougot, et al. (2007). The exon-junction-complex-component metastatic lymph node 51 functions in stress-granule assembly. Journal of Cell Science. 120, 2774-2784.

Bakker, C.E., Y. de Diego Otero, C. Bontekoe, et al. (2000). Immunocytochemical and biochemical characterization of FMRP, FXR1P, and FXR2P in the mouse. Experimental Cell Research. 258, 162-170.

Baron, D.M., L.J. Kaushansky, C.L. Ward, et al. (2013). Amyotrophic lateral sclerosis-linked FUS/TLS alters stress granule assembly and dynamics. Molecular Neurodegeneration. 8, 30-1326-8-30.

Bashkirov, V.I., H. Scherthan, J.A. Solinger, et al. (1997). A mouse cytoplasmic exoribonuclease (mXRN1p) with preference for G4 tetraplex substrates. The Journal of Cell Biology. 136, 761-773.

Bedford, M.T., A. Frankel, M.B. Yaffe, et al. (2000). Arginine methylation inhibits the binding of proline-rich ligands to Src homology 3, but not WW, domains. The Journal of Biological Chemistry. 275, 16030-16036.

Bedford, M.T., and S. Richard. (2005). Arginine methylation an emerging regulator of protein function. Molecular Cell. 18, 263-272.

Berthet, C., F. Guehenneux, V. Revol, et al. (2002). Interaction of PRMT1 with BTG/TOB proteins in cell signalling: molecular analysis and functional aspects. Genes to Cells : Devoted to Molecular & Cellular Mechanisms. 7, 29-39.

Bezzi, M., S.X. Teo, J. Muller, et al. (2013). Regulation of constitutive and alternative splicing by PRMT5 reveals a role for Mdm4 pre-mRNA in sensing defects in the spliceosomal machinery. Genes & Development. 27, 1903-1916.

Birchmeier, W., and J. Behrens. (1994). Cadherin expression in carcinomas: role in the formation of cell junctions and the prevention of invasiveness. Biochimica Et Biophysica Acta. 1198, 11-26.

Bloom, J., V. Amador, F. Bartolini, et al. (2003). Proteasome-mediated degradation of p21 via N-terminal ubiquitinylation. Cell. 115, 71-82.

Boffa, L.C., J. Karn, G. Vidali, et al. (1977). Distribution of NG, NG,-dimethylarginine in nuclear protein fractions. Biochemical and Biophysical Research Communications. 74, 969-976.

Boisvert, F.M., J. Cote, M.C. Boulanger, et al. (2002). Symmetrical dimethylarginine methylation is required for the localization of SMN in Cajal bodies and pre-mRNA splicing. The Journal of Cell Biology. 159, 957-969.

Boisvert, F.M., U. Dery, J.Y. Masson, et al. (2005a). Arginine methylation of MRE11 by PRMT1 is required for DNA damage checkpoint control. Genes & Development. 19, 671-676.

Boisvert, F.M., M.J. Hendzel, J.Y. Masson, et al. (2005b). Methylation of MRE11 regulates its nuclear compartmentalization. Cell Cycle (Georgetown, Tex.). 4, 981-989.

Boisvert, F.M., A. Rhie, S. Richard, et al. (2005c). The GAR motif of 53BP1 is arginine methylated by PRMT1 and is necessary for 53BP1 DNA binding activity. Cell Cycle (Georgetown, Tex.). 4, 1834-1841.

Bolduc, F.V., K. Bell, H. Cox, et al. (2008). Excess protein synthesis in Drosophila fragile X mutants impairs long-term memory. Nature Neuroscience. 11, 1143-1145.

Bono, F., and N.H. Gehring. (2011). Assembly, disassembly and recycling: the dynamics of exon junction complexes. RNA Biology. 8, 24-29.

Boswell, R.E., and A.P. Mahowald. (1985). tudor, a gene required for assembly of the germ plasm in Drosophila melanogaster. Cell. 43, 97-104.

Botlagunta, M., B. Krishnamachary, F. Vesuna, et al. (2011). Expression of DDX3 is directly modulated by hypoxia inducible factor-1 alpha in breast epithelial cells. PloS One. 6, e17563.

Botlagunta, M., F. Vesuna, Y. Mironchik, et al. (2008). Oncogenic role of DDX3 in breast cancer biogenesis. Oncogene. 27, 3912-3922.

Boulanger, M.C., C. Liang, R.S. Russell, et al. (2005). Methylation of Tat by PRMT6 regulates human immunodeficiency virus type 1 gene expression. Journal of Virology. 79, 124-131.

Brahms, H., L. Meheus, V. de Brabandere, et al. (2001). Symmetrical dimethylation of arginine residues in spliceosomal Sm protein B/B' and the Sm-like protein LSm4, and their interaction with the SMN protein. RNA (New York, N.Y.). 7, 1531-1542.

Brahms, H., J. Raymackers, A. Union, et al. (2000). The C-terminal RG dipeptide repeats of the spliceosomal Sm proteins D1 and D3 contain symmetrical dimethylarginines, which form a major B-cell epitope for anti-Sm autoantibodies. The Journal of Biological Chemistry. 275, 17122-17129.

Branscombe, T.L., A. Frankel, J.H. Lee, et al. (2001). PRMT5 (Janus kinase-binding protein 1) catalyzes the formation of symmetric dimethylarginine residues in proteins. The Journal of Biological Chemistry. 276, 32971-32976.

Bremang, M., A. Cuomo, A.M. Agresta, et al. (2013). Mass spectrometry-based identification and characterisation of lysine and arginine methylation in the human proteome. Molecular bioSystems. 9, 2231-2247.

Brengues, M., and R. Parker. (2007). Accumulation of polyadenylated mRNA, Pab1p, eIF4E, and eIF4G with P-bodies in Saccharomyces cerevisiae. Molecular Biology of the Cell. 18, 2592-2602.

Carascossa, S., P. Dudek, B. Cenni, et al. (2010). CARM1 mediates the ligand-independent and tamoxifen-resistant activation of the estrogen receptor alpha by cAMP. Genes & Development. 24, 708-719.

Caruthers, J.M., and D.B. McKay. (2002). Helicase structure and mechanism. Current Opinion in Structural Biology. 12, 123-133.

Casadio, F., X. Lu, S.B. Pollock, et al. (2013). H3R42me2a is a histone modification with positive transcriptional effects. Proceedings of the National Academy of Sciences of the United States of America. 110, 14894-14899.

Cha, B., W. Kim, Y.K. Kim, et al. (2011). Methylation by protein arginine methyltransferase 1 increases stability of Axin, a negative regulator of Wnt signaling. Oncogene. 30, 2379-2389.

Chang, B., Y. Chen, Y. Zhao, et al. (2007). JMJD6 is a histone arginine demethylase. Science (New York, N.Y.). 318, 444-447.

Chang, P.C., C.W. Chi, G.Y. Chau, et al. (2006). DDX3, a DEAD box RNA helicase, is deregulated in hepatitis virus-associated hepatocellular carcinoma and is involved in cell growth control. Oncogene. 25, 1991-2003.

Chao, C.H., C.M. Chen, P.L. Cheng, et al. (2006). DDX3, a DEAD box RNA helicase with tumor growth-suppressive property and transcriptional regulation activity of the p21waf1/cip1 promoter, is a candidate tumor suppressor. Cancer Research. 66, 6579-6588.

Charier, G., J. Couprie, B. Alpha-Bazin, et al. (2004). The Tudor tandem of 53BP1: a new structural motif involved in DNA and RG-rich peptide binding. Structure (London, England : 1993). 12, 1551-1562.

Chauhan, D., G. Li, R. Shringarpure, et al. (2003). Blockade of Hsp27 overcomes Bortezomib/proteasome inhibitor PS-341 resistance in lymphoma cells. Cancer Research. 63, 6174-6177.

Chen, C., T.J. Nott, J. Jin, et al. (2011). Deciphering arginine methylation: Tudor tells the tale. Nature Reviews.Molecular Cell Biology. 12, 629-642.

Cheng, D., J. Cote, S. Shaaban, et al. (2007). The arginine methyltransferase CARM1 regulates the coupling of transcription and mRNA processing. Molecular Cell. 25, 71-83.

Cheng, H., Y. Qin, H. Fan, et al. (2013). Overexpression of CARM1 in breast cancer is correlated with poorly characterized clinicopathologic parameters and molecular subtypes. Diagnostic Pathology. 8, 129-1596-8-129.

Cheng, X., R.E. Collins, and X. Zhang. (2005). Structural and sequence motifs of protein (histone) methylation enzymes. Annual Review of Biophysics and Biomolecular Structure. 34, 267-294.

Cheung, N., L.C. Chan, A. Thompson, et al. (2007). Protein arginine-methyltransferase-dependent oncogenesis. Nature Cell Biology. 9, 1208-1215.

Cheung, W.D., K. Sakabe, M.P. Housley, et al. (2008). O-linked beta-N-acetylglucosaminyltransferase substrate specificity is regulated by myosin phosphatase targeting and other interacting proteins. The Journal of Biological Chemistry. 283, 33935-33941.

Cho, J.H., M.K. Lee, K.W. Yoon, et al. (2011). Arginine methylation-dependent regulation of ASK1 signaling by PRMT1. Cell Death and Differentiation.

Choi, K.S., J.Y. Kim, S.K. Lim, et al. (2012). TIS21(/BTG2/PC3) accelerates the repair of DNA double strand breaks by enhancing Mre11 methylation and blocking damage signal transfer to the Chk2(T68)-p53(S20) pathway. DNA Repair. 11, 965-975.

Chuang, R.Y., P.L. Weaver, Z. Liu, et al. (1997). Requirement of the DEAD-Box protein ded1p for messenger RNA translation. Science (New York, N.Y.). 275, 1468-1471.

Chuang, T.W., P.J. Peng, and W.Y. Tarn. (2011). The exon junction complex component Y14 modulates the activity of the methylosome in biogenesis of spliceosomal small nuclear ribonucleoproteins. The Journal of Biological Chemistry. 286, 8722-8728.

Ciriello, G., C. Gallina, and C. Guerra. (2010). Analysis of interactions between ribosomal proteins and RNA structural motifs. BMC Bioinformatics. 11 Suppl 1, S41-2105-11-S1-S41.

Codony-Servat, J., M.A. Tapia, M. Bosch, et al. (2006). Differential cellular and molecular effects of bortezomib, a proteasome inhibitor, in human breast cancer cells. Molecular Cancer Therapeutics. 5, 665-675.

Coffee, B., K. Keith, I. Albizua, et al. (2009). Incidence of fragile X syndrome by newborn screening for methylated FMR1 DNA. American Journal of Human Genetics. 85, 503-514.

Corbin, F., M. Bouillon, A. Fortin, et al. (1997). The fragile X mental retardation protein is associated with poly(A)+ mRNA in actively translating polyribosomes. Human Molecular Genetics. 6, 1465-1472.

Cordin, O., J. Banroques, N.K. Tanner, et al. (2006). The DEAD-box protein family of RNA helicases. Gene. 367, 17-37.

Cote, J., F.M. Boisvert, M.C. Boulanger, et al. (2003). Sam68 RNA binding protein is an in vivo substrate for protein arginine N-methyltransferase 1. Molecular Biology of the Cell. 14, 274-287.

Cote, J., and S. Richard. (2005). Tudor domains bind symmetrical dimethylated arginines. The Journal of Biological Chemistry. 280, 28476-28483.

Cuthbert, G.L., S. Daujat, A.W. Snowden, et al. (2004). Histone deimination antagonizes arginine methylation. Cell. 118, 545-553.

Dang, Y., N. Kedersha, W.K. Low, et al. (2006). Eukaryotic initiation factor 2alpha-independent pathway of stress granule induction by the natural product pateamine A. The Journal of Biological Chemistry. 281, 32870-32878.

Daujat, S., U.M. Bauer, V. Shah, et al. (2002). Crosstalk between CARM1 methylation and CBP acetylation on histone H3. Current Biology : CB. 12, 2090-2097.

Davis, M.B., X. Liu, S. Wang, et al. (2013). Expression and sub-cellular localization of an epigenetic regulator, co-activator arginine methyltransferase 1 (CARM1), is associated with specific breast cancer subtypes and ethnicity. Molecular Cancer. 12, 40-4598-12-40.

de la Cruz, J., I. Iost, D. Kressler, et al. (1997). The p20 and Ded1 proteins have antagonistic roles in eIF4E-dependent translation in Saccharomyces cerevisiae. Proceedings of the National Academy of Sciences of the United States of America. 94, 5201-5206.

de la Cruz, J., D. Kressler, and P. Linder. (1999). Unwinding RNA in Saccharomyces cerevisiae: DEAD-box proteins and related families. Trends in Biochemical Sciences. 24, 192-198.

De Leeuw, F., T. Zhang, C. Wauquier, et al. (2007). The cold-inducible RNA-binding protein migrates from the nucleus to cytoplasmic stress granules by a methylation-dependent mechanism and acts as a translational repressor. Experimental Cell Research. 313, 4130-4144.

De Leeuw, W.J., G. Berx, C.B. Vos, et al. (1997). Simultaneous loss of E-cadherin and catenins in invasive lobular breast cancer and lobular carcinoma in situ. The Journal of Pathology. 183, 404-411.

Devys, D., Y. Lutz, N. Rouyer, et al. (1993). The FMR-1 protein is cytoplasmic, most abundant in neurons and appears normal in carriers of a fragile X premutation. Nature Genetics. 4, 335-340.

Dillon, M.B., H.L. Rust, P.R. Thompson, et al. (2013). Automethylation of Protein Arginine Methyltransferase 8 Regulates Activity by Impeding AdoMet Sensitivity. The Journal of Biological Chemistry.

Dolled-Filhart, M., A. McCabe, J. Giltnane, et al. (2006). Quantitative in situ analysis of beta-catenin expression in breast cancer shows decreased expression is associated with poor outcome. Cancer Research. 66, 5487-5494.

Dolzhanskaya, N., G. Merz, and R.B. Denman. (2006). Oxidative stress reveals heterogeneity of FMRP granules in PC12 cell neurites. Brain Research. 1112, 56-64.

Dowhan, D.H., M.J. Harrison, N.A. Eriksson, et al. (2012). Protein arginine methyltransferase 6-dependent gene expression and splicing: association with breast cancer outcomes. Endocrine-Related Cancer. 19, 509-526.

Drexler, H.C. (1997). Activation of the cell death program by inhibition of proteasome function. Proceedings of the National Academy of Sciences of the United States of America. 94, 855-860.

Du, K., S. Arai, T. Kawamura, et al. (2011). TLS and PRMT1 synergistically coactivate transcription at the survivin promoter through TLS arginine methylation. Biochemical and Biophysical Research Communications. 404, 991-996.

Ebert, M.P., J. Yu, J. Hoffmann, et al. (2003). Loss of beta-catenin expression in metastatic gastric cancer. Journal of Clinical Oncology : Official Journal of the American Society of Clinical Oncology. 21, 1708-1714.

Eger, A., A. Stockinger, B. Schaffhauser, et al. (2000). Epithelial mesenchymal transition by c-Fos estrogen receptor activation involves nuclear translocation of beta-catenin and upregulation of beta-catenin/lymphoid enhancer binding factor-1 transcriptional activity. The Journal of Cell Biology. 148, 173-188.

Eisinger-Mathason, T.S., J. Andrade, A.L. Groehler, et al. (2008). Codependent functions of RSK2 and the apoptosis-promoting factor TIA-1 in stress granule assembly and cell survival. Molecular Cell. 31, 722-736.

El Messaoudi, S., E. Fabbrizio, C. Rodriguez, et al. (2006). Coactivator-associated arginine methyltransferase 1 (CARM1) is a positive regulator of the Cyclin E1 gene. Proceedings of the National Academy of Sciences of the United States of America. 103, 13351-13356.

El-Andaloussi, N., T. Valovka, M. Toueille, et al. (2007). Methylation of DNA polymerase beta by protein arginine methyltransferase 1 regulates its binding to proliferating cell nuclear antigen. FASEB Journal : Official Publication of the Federation of American Societies for Experimental Biology. 21, 26-34.

El-Andaloussi, N., T. Valovka, M. Toueille, et al. (2006). Arginine methylation regulates DNA polymerase beta. Molecular Cell. 22, 51-62.

Ellis, J.J., M. Broom, and S. Jones. (2007). Protein-RNA interactions: structural analysis and functional classes. Proteins. 66, 903-911.

Erce, M.A., D. Abeygunawardena, J.K. Low, et al. (2013). Interactions affected by arginine methylation in the yeast protein-protein interaction network. Molecular & Cellular Proteomics : MCP.

Esteva, F.J., and G.N. Hortobagyi. (2004). Prognostic molecular markers in early breast cancer. Breast Cancer Research : BCR. 6, 109-118.

Evans, J.L., I.D. Goldfine, B.A. Maddux, et al. (2002). Oxidative stress and stress-activated signaling pathways: a unifying hypothesis of type 2 diabetes. Endocrine Reviews. 23, 599-622.

Eystathioy, T., E.K. Chan, S.A. Tenenbaum, et al. (2002). A phosphorylated cytoplasmic autoantigen, GW182, associates with a unique population of human mRNAs within novel cytoplasmic speckles. Molecular Biology of the Cell. 13, 1338-1351.

Fabbrizio, E., S. El Messaoudi, J. Polanowska, et al. (2002). Negative regulation of transcription by the type II arginine methyltransferase PRMT5. EMBO Reports. 3, 641-645.

Faleiro-Rodrigues, C., I. Macedo-Pinto, D. Pereira, et al. (2004). Loss of beta-catenin is associated with poor survival in ovarian carcinomas. International Journal of Gynecological Pathology : Official Journal of the International Society of Gynecological Pathologists. 23, 337-346.

Faleiro-Rodrigues, C., I.M. Macedo-Pinto, S.S. Maia, et al. (2005). Biological relevance of E-cadherin-catenin complex proteins in primary epithelial ovarian tumours. Gynecologic and Obstetric Investigation. 60, 75-83.

Feng, Q., B. He, S.Y. Jung, et al. (2009). Biochemical control of CARM1 enzymatic activity by phosphorylation. The Journal of Biological Chemistry. 284, 36167-36174.

Feng, Q., P. Yi, J. Wong, et al. (2006). Signaling within a coactivator complex: methylation of SRC-3/AIB1 is a molecular switch for complex disassembly. Molecular and Cellular Biology. 26, 7846-7857.

Feng, Y., R. Maity, J.P. Whitelegge, et al. (2013). Mammalian protein arginine methyltransferase 7 (PRMT7) specifically targets RXR sites in lysine- and arginine-rich regions. The Journal of Biological Chemistry. 288, 37010-37025.

Feng, Y., J. Wang, S. Asher, et al. (2011). Histone H4 acetylation differentially modulates arginine methylation by an in Cis mechanism. The Journal of Biological Chemistry. 286, 20323-20334.

Ferbeyre, G., E. de Stanchina, E. Querido, et al. (2000). PML is induced by oncogenic ras and promotes premature senescence. Genes & Development. 14, 2015-2027.

Fisk, J.C., C. Zurita-Lopez, J. Sayegh, et al. (2010). TbPRMT6 is a type I protein arginine methyltransferase that contributes to cytokinesis in Trypanosoma brucei. Eukaryotic Cell. 9, 866-877.

Fournier, M.J., L. Coudert, S. Mellaoui, et al. (2013). Inactivation of the mTORC1-eukaryotic translation initiation factor 4E pathway alters stress granule formation. Molecular and Cellular Biology. 33, 2285-2301.

Fournier, M.J., C. Gareau, and R. Mazroui. (2010). The chemotherapeutic agent bortezomib induces the formation of stress granules. Cancer Cell International. 10, 12-2867-10-12.

Frankel, A., N. Yadav, J. Lee, et al. (2002). The novel human protein arginine N-methyltransferase PRMT6 is a nuclear enzyme displaying unique substrate specificity. The Journal of Biological Chemistry. 277, 3537-3543.

Friesen, W.J., and G. Dreyfuss. (2000). Specific sequences of the Sm and Sm-like (Lsm) proteins mediate their interaction with the spinal muscular atrophy disease gene product (SMN). The Journal of Biological Chemistry. 275, 26370-26375.

Friesen, W.J., S. Massenet, S. Paushkin, et al. (2001a). SMN, the product of the spinal muscular atrophy gene, binds preferentially to dimethylarginine-containing protein targets. Molecular Cell. 7, 1111-1117.

Friesen, W.J., S. Paushkin, A. Wyce, et al. (2001b). The methylosome, a 20S complex containing JBP1 and pICln, produces dimethylarginine-modified Sm proteins. Molecular and Cellular Biology. 21, 8289-8300.

Friesen, W.J., A. Wyce, S. Paushkin, et al. (2002). A novel WD repeat protein component of the methylosome binds Sm proteins. The Journal of Biological Chemistry. 277, 8243-8247.

Frietze, S., M. Lupien, P.A. Silver, et al. (2008). CARM1 regulates estrogen-stimulated breast cancer growth through up-regulation of E2F1. Cancer Research. 68, 301-306.

Fukumura, J., E. Noguchi, T. Sekiguchi, et al. (2003). A temperature-sensitive mutant of the mammalian RNA helicase, DEAD-BOX X isoform, DBX, defective in the transition from G1 to S phase. Journal of Biochemistry. 134, 71-82.

Gareau, C., M.J. Fournier, C. Filion, et al. (2011). p21(WAF1/CIP1) upregulation through the stress granule-associated protein CUGBP1 confers resistance to bortezomib-mediated apoptosis. PloS One. 6, e20254.

Geissler, R., R.P. Golbik, and S.E. Behrens. (2012). The DEAD-box helicase DDX3 supports the assembly of functional 80S ribosomes. Nucleic Acids Research.

Gilks, N., N. Kedersha, M. Ayodele, et al. (2004). Stress granule assembly is mediated by prion-like aggregation of TIA-1. Molecular Biology of the Cell. 15, 5383-5398.

Gonsalvez, G.B., K. Praveen, A.J. Hicks, et al. (2008). Sm protein methylation is dispensable for snRNP assembly in Drosophila melanogaster. RNA (New York, N.Y.). 14, 878-887.

Gottardi, C.J., E. Wong, and B.M. Gumbiner. (2001). E-cadherin suppresses cellular transformation by inhibiting beta-catenin signaling in an adhesion-independent manner. The Journal of Cell Biology. 153, 1049-1060.

Goulet, I., S. Boisvenue, S. Mokas, et al. (2008). TDRD3, a novel Tudor domain-containing protein, localizes to cytoplasmic stress granules. Human Molecular Genetics. 17, 3055-3074.

Goulet, I., G. Gauvin, S. Boisvenue, et al. (2007). Alternative splicing yields protein arginine methyltransferase 1 isoforms with distinct activity, substrate specificity, and subcellular localization. The Journal of Biological Chemistry. 282, 33009-33021.

Guccione, E., C. Bassi, F. Casadio, et al. (2007). Methylation of histone H3R2 by PRMT6 and H3K4 by an MLL complex are mutually exclusive. Nature. 449, 933-937.

Guderian, G., C. Peter, J. Wiesner, et al. (2011). RioK1, a new interactor of protein arginine methyltransferase 5 (PRMT5), competes with pICln for binding and modulates PRMT5 complex composition and substrate specificity. The Journal of Biological Chemistry. 286, 1976-1986.

Guendel, I., L. Carpio, C. Pedati, et al. (2010). Methylation of the tumor suppressor protein, BRCA1, influences its transcriptional cofactor function. PloS One. 5, e11379.

Habashy, H.O., E.A. Rakha, I.O. Ellis, et al. (2013). The oestrogen receptor coactivator CARM1 has an oncogenic effect and is associated with poor prognosis in breast cancer. Breast Cancer Research and Treatment. 140, 307-316.

Hall, A. (2005). Rho GTPases and the control of cell behaviour. Biochemical Society Transactions. 33, 891-895.

Hallett, R.M., G. Pond, and J.A. Hassell. (2012). A target based approach identifies genomic predictors of breast cancer patient response to chemotherapy. BMC Medical Genomics. 5, 16-8794-5-16.

Hanahan, D., and R.A. Weinberg. (2000). The hallmarks of cancer. Cell. 100, 57-70.

Harding, H.P., I. Novoa, Y. Zhang, et al. (2000a). Regulated translation initiation controls stress-induced gene expression in mammalian cells. Molecular Cell. 6, 1099-1108.

Harding, H.P., Y. Zhang, A. Bertolotti, et al. (2000b). Perk is essential for translational regulation and cell survival during the unfolded protein response. Molecular Cell. 5, 897-904.

Harrison, M.J., Y.H. Tang, and D.H. Dowhan. (2010). Protein arginine methyltransferase 6 regulates multiple aspects of gene expression. Nucleic Acids Research. 38, 2201-2216.

Hart, M., J.P. Concordet, I. Lassot, et al. (1999). The F-box protein beta-TrCP associates with phosphorylated beta-catenin and regulates its activity in the cell. Current Biology : CB. 9, 207-210.

Harvey, J.M., G.M. Clark, C.K. Osborne, et al. (1999). Estrogen receptor status by immunohistochemistry is superior to the ligand-binding assay for predicting response to adjuvant endocrine therapy in breast cancer. Journal of Clinical Oncology : Official Journal of the American Society of Clinical Oncology. 17, 1474-1481.

Hassa, P.O., M. Covic, M.T. Bedford, et al. (2008). Protein arginine methyltransferase 1 coactivates NF-kappaB-dependent gene expression synergistically with CARM1 and PARP1. Journal of Molecular Biology. 377, 668-678.

Heller, G., J. Geradts, B. Ziegler, et al. (2007). Downregulation of TSLC1 and DAL-1 expression occurs frequently in breast cancer. Breast Cancer Research and Treatment. 103, 283-291.

Hentze, M.W. (1997). eIF4G: a multipurpose ribosome adapter? Science (New York, N.Y.). 275, 500-501.

Herglotz, J., O.N. Kuvardina, S. Kolodziej, et al. (2013). Histone arginine methylation keeps RUNX1 target genes in an intermediate state. Oncogene. 32, 2565-2575.

Hernandez-Aya, L.F., and A.M. Gonzalez-Angulo. (2011). Targeting the phosphatidylinositol 3-kinase signaling pathway in breast cancer. The Oncologist. 16, 404-414.

Herrmann, F., and F.O. Fackelmayer. (2009). Nucleo-cytoplasmic shuttling of protein arginine methyltransferase 1 (PRMT1) requires enzymatic activity. Genes to Cells : Devoted to Molecular & Cellular Mechanisms. 14, 309-317.

Herrmann, F., P. Pably, C. Eckerich, et al. (2009). Human protein arginine methyltransferases in vivo--distinct properties of eight canonical members of the PRMT family. Journal of Cell Science. 122, 667-677.

Higashimoto, K., P. Kuhn, D. Desai, et al. (2007). Phosphorylation-mediated inactivation of coactivator-associated arginine methyltransferase 1. Proceedings of the National Academy of Sciences of the United States of America. 104, 12318-12323.

Hilliker, A., Z. Gao, E. Jankowsky, et al. (2011). The DEAD-box protein Ded1 modulates translation by the formation and resolution of an eIF4F-mRNA complex. Molecular Cell. 43, 962-972.

Hiscox, S., W.G. Jiang, K. Obermeier, et al. (2006). Tamoxifen resistance in MCF7 cells promotes EMT-like behaviour and involves modulation of beta-catenin phosphorylation. International Journal of Cancer.Journal International Du Cancer. 118, 290-301.

Hogbom, M., R. Collins, S. van den Berg, et al. (2007). Crystal structure of conserved domains 1 and 2 of the human DEAD-box helicase DDX3X in complex with the mononucleotide AMP. Journal of Molecular Biology. 372, 150-159.

Holliday, D.L., and V. Speirs. (2011). Choosing the right cell line for breast cancer research. Breast Cancer Research : BCR. 13, 215.

Hou, Z., H. Peng, K. Ayyanathan, et al. (2008). The LIM protein AJUBA recruits protein arginine methyltransferase 5 to mediate SNAIL-dependent transcriptional repression. Molecular and Cellular Biology. 28, 3198-3207.

Hoyle, N.P., L.M. Castelli, S.G. Campbell, et al. (2007). Stress-dependent relocalization of translationally primed mRNPs to cytoplasmic granules that are kinetically and spatially distinct from P-bodies. The Journal of Cell Biology. 179, 65-74.

Hua, Y., and J. Zhou. (2004). Survival motor neuron protein facilitates assembly of stress granules. FEBS Letters. 572, 69-74.

Huang, J.S., C.C. Chao, T.L. Su, et al. (2004). Diverse cellular transformation capability of overexpressed genes in human hepatocellular carcinoma. Biochemical and Biophysical Research Communications. 315, 950-958.

Hubers, L., H. Valderrama-Carvajal, J. Laframboise, et al. (2011). HuD interacts with survival motor neuron protein and can rescue spinal muscular atrophy-like neuronal defects. Human Molecular Genetics. 20, 553-579.

Huq, M.D., S.G. Ha, H. Barcelona, et al. (2009). Lysine methylation of nuclear co-repressor receptor interacting protein 140. Journal of Proteome Research. 8, 1156-1167.

Hurley, J.H., S. Lee, and G. Prag. (2006). Ubiquitin-binding domains. The Biochemical Journal. 399, 361-372.

Hwang, C.I., J. Choi, Z. Zhou, et al. (2011). MET-dependent cancer invasion may be preprogrammed by early alterations of p53-regulated feedforward loop and triggered by stromal cell-derived HGF. Cell Cycle (Georgetown, Tex.). 10, 3834-3840.

Hyllus, D., C. Stein, K. Schnabel, et al. (2007). PRMT6-mediated methylation of R2 in histone H3 antagonizes H3 K4 trimethylation. Genes & Development. 21, 3369-3380.

Iacovides, D.C., C.C. O'Shea, J. Oses-Prieto, et al. (2007). Critical role for arginine methylation in adenovirus-infected cells. Journal of Virology. 81, 13209-13217.

Imajoh-Ohmi, S., T. Kawaguchi, S. Sugiyama, et al. (1995). Lactacystin, a specific inhibitor of the proteasome, induces apoptosis in human monoblast U937 cells. Biochemical and Biophysical Research Communications. 217, 1070-1077.

Ingelfinger, D., D.J. Arndt-Jovin, R. Luhrmann, et al. (2002). The human LSm1-7 proteins colocalize with the mRNA-degrading enzymes Dcp1/2 and Xrnl in distinct cytoplasmic foci. RNA (New York, N.Y.). 8, 1489-1501.

Invernizzi, C.F., B. Xie, F.A. Frankel, et al. (2007). Arginine methylation of the HIV-1 nucleocapsid protein results in its diminished function. AIDS (London, England). 21, 795-805.

Invernizzi, C.F., B. Xie, S. Richard, et al. (2006). PRMT6 diminishes HIV-1 Rev binding to and export of viral RNA. Retrovirology. 3, 93.

Ishaq, M., J. Hu, X. Wu, et al. (2008). Knockdown of cellular RNA helicase DDX3 by short hairpin RNAs suppresses HIV-1 viral replication without inducing apoptosis. Molecular Biotechnology. 39, 231-238.

Jaffe, A.B., and A. Hall. (2005). Rho GTPases: biochemistry and biology. Annual Review of Cell and Developmental Biology. 21, 247-269.

Jiang, W., M.E. Roemer, and I.F. Newsham. (2005). The tumor suppressor DAL-1/4.1B modulates protein arginine N-methyltransferase 5 activity in a substrate-specific manner. Biochemical and Biophysical Research Communications. 329, 522-530.

Jin, J., X. Xie, C. Chen, et al. (2009). Eukaryotic protein domains as functional units of cellular evolution. Science Signaling. 2, ra76.

Jones, S., D.T. Daley, N.M. Luscombe, et al. (2001). Protein-RNA interactions: a structural analysis. Nucleic Acids Research. 29, 943-954.

Joshi, B., A.L. Cai, B.D. Keiper, et al. (1995). Phosphorylation of eukaryotic protein synthesis initiation factor 4E at Ser-209. The Journal of Biological Chemistry. 270, 14597-14603.

Kale, A.J., and B.S. Moore. (2012). Molecular mechanisms of acquired proteasome inhibitor resistance. Journal of Medicinal Chemistry. 55, 10317-10327.

Kashima, I., S. Jonas, U. Jayachandran, et al. (2010). SMG6 interacts with the exon junction complex via two conserved EJC-binding motifs (EBMs) required for nonsense-mediated mRNA decay. Genes & Development. 24, 2440-2450.

Katz, J.E., M. Dlakic, and S. Clarke. (2003). Automated identification of putative methyltransferases from genomic open reading frames. Molecular & Cellular Proteomics : MCP. 2, 525-540.

Kedersha, N., S. Chen, N. Gilks, et al. (2002). Evidence that ternary complex (eIF2-GTP-tRNA(i)(Met))-deficient preinitiation complexes are core constituents of mammalian stress granules. Molecular Biology of the Cell. 13, 195-210.

Kedersha, N., G. Stoecklin, M. Ayodele, et al. (2005). Stress granules and processing bodies are dynamically linked sites of mRNP remodeling. The Journal of Cell Biology. 169, 871-884.

Kedersha, N.L., M. Gupta, W. Li, et al. (1999). RNA-binding proteins TIA-1 and TIAR link the phosphorylation of eIF-2 alpha to the assembly of mammalian stress granules. The Journal of Cell Biology. 147, 1431-1442.

Kemler, R. (1993). From cadherins to catenins: cytoplasmic protein interactions and regulation of cell adhesion. Trends in Genetics : TIG. 9, 317-321.

Kim, H., E. Jeong, S.W. Lee, et al. (2003). Computational analysis of hydrogen bonds in protein-RNA complexes for interaction patterns. FEBS Letters. 552, 231-239.

Kim, J., J. Daniel, A. Espejo, et al. (2006a). Tudor, MBT and chromo domains gauge the degree of lysine methylation. EMBO Reports. 7, 397-403.

Kim, N.H., S.N. Kim, D.W. Seo, et al. (2013). PRMT6 overexpression upregulates TSP-1 and downregulates MMPs: its implication in motility and invasion. Biochemical and Biophysical Research Communications. 432, 60-65.

Kim, S.H., W.K. Dong, I.J. Weiler, et al. (2006b). Fragile X mental retardation protein shifts between polyribosomes and stress granules after neuronal injury by arsenite stress

or in vivo hippocampal electrode insertion. The Journal of Neuroscience : The Official Journal of the Society for Neuroscience. 26, 2413-2418.

Kim, W.J., S.H. Back, V. Kim, et al. (2005). Sequestration of TRAF2 into stress granules interrupts tumor necrosis factor signaling under stress conditions. Molecular and Cellular Biology. 25, 2450-2462.

Kim, Y.S., S.G. Lee, S.H. Park, et al. (2001). Gene structure of the human DDX3 and chromosome mapping of its related sequences. Molecules and Cells. 12, 209-214.

Kleinschmidt, M.A., P. de Graaf, H.A. van Teeffelen, et al. (2012). Cell cycle regulation by the PRMT6 arginine methyltransferase through repression of cyclin-dependent kinase inhibitors. PloS One. 7, e41446.

Klinge, C.M., S.C. Jernigan, K.A. Mattingly, et al. (2004). Estrogen response element-dependent regulation of transcriptional activation of estrogen receptors alpha and beta by coactivators and corepressors. Journal of Molecular Endocrinology. 33, 387-410.

Kohler, A., and E. Hurt. (2007). Exporting RNA from the nucleus to the cytoplasm. Nature Reviews.Molecular Cell Biology. 8, 761-773.

Kuhn, P., R. Chumanov, Y. Wang, et al. (2011). Automethylation of CARM1 allows coupling of transcription and mRNA splicing. Nucleic Acids Research. 39, 2717-2726.

Kuphal, F., and J. Behrens. (2006). E-cadherin modulates Wnt-dependent transcription in colorectal cancer cells but does not alter Wnt-independent gene expression in fibroblasts. Experimental Cell Research. 312, 457-467.

Lacroix, M., S. El Messaoudi, G. Rodier, et al. (2008). The histone-binding protein COPR5 is required for nuclear functions of the protein arginine methyltransferase PRMT5. EMBO Reports. 9, 452-458.

Lacroix, M., and G. Leclercq. (2004). Relevance of breast cancer cell lines as models for breast tumours: an update. Breast Cancer Research and Treatment. 83, 249-289.

Lai, M.C., W.C. Chang, S.Y. Shieh, et al. (2010). DDX3 regulates cell growth through translational control of cyclin E1. Molecular and Cellular Biology. 30, 5444-5453.

Lai, M.C., Y.H. Lee, and W.Y. Tarn. (2008). The DEAD-box RNA helicase DDX3 associates with export messenger ribonucleoproteins as well as tip-associated protein and participates in translational control. Molecular Biology of the Cell. 19, 3847-3858.

Lasko, P. (2010). Tudor domain. Current Biology : CB. 20, R666-7.

Latres, E., D.S. Chiaur, and M. Pagano. (1999). The human F box protein beta-Trcp associates with the Cul1/Skp1 complex and regulates the stability of beta-catenin. Oncogene. 18, 849-854.

Le Romancer, M., I. Treilleux, N. Leconte, et al. (2008). Regulation of estrogen rapid signaling through arginine methylation by PRMT1. Molecular Cell. 31, 212-221.

Lee, C.S., A.P. Dias, M. Jedrychowski, et al. (2008). Human DDX3 functions in translation and interacts with the translation initiation factor eIF3. Nucleic Acids Research. 36, 4708-4718.

Lee, J., and M.T. Bedford. (2002). PABP1 identified as an arginine methyltransferase substrate using high-density protein arrays. EMBO Reports. 3, 268-273.

Lee, J., J. Sayegh, J. Daniel, et al. (2005). PRMT8, a new membrane-bound tissue-specific member of the protein arginine methyltransferase family. The Journal of Biological Chemistry. 280, 32890-32896.

Lee, Y.H., M.T. Bedford, and M.R. Stallcup. (2011). Regulated recruitment of tumor suppressor BRCA1 to the p21 gene by coactivator methylation. Genes & Development. 25, 176-188.

Lee, Y.J., W.Y. Hsieh, L.Y. Chen, et al. (2012). Protein arginine methylation of SERBP1 by protein arginine methyltransferase 1 affects cytoplasmic/nuclear distribution. Journal of Cellular Biochemistry. 113, 2721-2728.

Lee, Y.J., H.M. Wei, L.Y. Chen, et al. (2014). Localization of SERBP1 in stress granules and nucleoli. The FEBS Journal. 281, 352-364.

Lejeune, D., N. Delsaux, B. Charloteaux, et al. (2005). Protein-nucleic acid recognition: statistical analysis of atomic interactions and influence of DNA structure. Proteins. 61, 258-271.

Leung, A.K., J.M. Calabrese, and P.A. Sharp. (2006). Quantitative analysis of Argonaute protein reveals microRNA-dependent localization to stress granules. Proceedings of the National Academy of Sciences of the United States of America. 103, 18125-18130.

Li, Y., Y. Tang, L. Ye, et al. (2003). Establishment of a hepatocellular carcinoma cell line with unique metastatic characteristics through in vivo selection and screening for metastasis-related genes through cDNA microarray. Journal of Cancer Research and Clinical Oncology. 129, 43-51.

Lian, X.J., and I.E. Gallouzi. (2009). Oxidative Stress Increases the Number of Stress Granules in Senescent Cells and Triggers a Rapid Decrease in p21waf1/cip1 Translation. The Journal of Biological Chemistry. 284, 8877-8887.

Lim, Y., Y.H. Kwon, N.H. Won, et al. (2005). Multimerization of expressed protein-arginine methyltransferases during the growth and differentiation of rat liver. Biochimica Et Biophysica Acta. 1723, 240-247.

Limm, K., C. Ott, S. Wallner, et al. (2013). Deregulation of protein methylation in melanoma. European Journal of Cancer (Oxford, England : 1990). 49, 1305-1313.

Lin, W.J., J.D. Gary, M.C. Yang, et al. (1996). The mammalian immediate-early TIS21 protein and the leukemia-associated BTG1 protein interact with a protein-arginine N-methyltransferase. The Journal of Biological Chemistry. 271, 15034-15044.

Linder, B., O. Plottner, M. Kroiss, et al. (2008). Tdrd3 is a novel stress granule-associated protein interacting with the Fragile-X syndrome protein FMRP. Human Molecular Genetics. 17, 3236-3246.

Linder, P., P.F. Lasko, M. Ashburner, et al. (1989). Birth of the D-E-A-D box. Nature. 337, 121-122.

Ling, Y.H., L. Liebes, B. Ng, et al. (2002). PS-341, a novel proteasome inhibitor, induces Bcl-2 phosphorylation and cleavage in association with G2-M phase arrest and apoptosis. Molecular Cancer Therapeutics. 1, 841-849.

Liu, F., X. Zhao, F. Perna, et al. (2011). JAK2V617F-mediated phosphorylation of PRMT5 downregulates its methyltransferase activity and promotes myeloproliferation. Cancer Cell. 19, 283-294.

Liu, K., C. Chen, Y. Guo, et al. (2010). Structural basis for recognition of arginine methylated Piwi proteins by the extended Tudor domain. Proceedings of the National Academy of Sciences of the United States of America. 107, 18398-18403.

Liu, K., Y. Guo, H. Liu, et al. (2012). Crystal Structure of TDRD3 and Methyl-Arginine Binding Characterization of TDRD3, SMN and SPF30. PloS One. 7, e30375.

Liu, Y., X. Zhu, J. Zhu, et al. (2007). Identification of differential expression of genes in hepatocellular carcinoma by suppression subtractive hybridization combined cDNA microarray. Oncology Reports. 18, 943-951.

Lopes, U.G., P. Erhardt, R. Yao, et al. (1997). P53-Dependent Induction of Apoptosis by Proteasome Inhibitors. The Journal of Biological Chemistry. 272, 12893-12896.

Lorenzo, A.D., Y. Yang, M. Macaluso, et al. (2014). A gain-of-function mouse model identifies PRMT6 as a NF-kappaB coactivator. Nucleic Acids Research.

Lott, K., J. Li, J.C. Fisk, et al. (2013). Global proteomic analysis in trypanosomes reveals unique proteins and conserved cellular processes impacted by arginine methylation. Journal of Proteomics. 91C, 210-225.

Low, J.K., G. Hart-Smith, M.A. Erce, et al. (2013). Analysis of the Proteome of Saccharomyces cerevisiae for Methylarginine. Journal of Proteome Research.

Lu, S., J. Yang, Z. Chen, et al. (2009). Different mutants of PSMB5 confer varying bortezomib resistance in T lymphoblastic lymphoma/leukemia cells derived from the Jurkat cell line. Experimental Hematology. 37, 831-837.

Lu, S., J. Yang, X. Song, et al. (2008). Point mutation of the proteasome beta5 subunit gene is an important mechanism of bortezomib resistance in bortezomib-selected variants of Jurkat T cell lymphoblastic lymphoma/leukemia line. The Journal of Pharmacology and Experimental Therapeutics. 326, 423-431.

Luca, R., M. Averna, F. Zalfa, et al. (2013). The fragile X protein binds mRNAs involved in cancer progression and modulates metastasis formation. EMBO Molecular Medicine. 5, 1523-1536.

Mamiya, N., and H.J. Worman. (1999). Hepatitis C virus core protein binds to a DEAD box RNA helicase. The Journal of Biological Chemistry. 274, 15751-15756.

Mann, M., Y. Zou, Y. Chen, et al. (2014). PELP1 oncogenic functions involve alternative splicing via PRMT6. Molecular Oncology. 8, 389-400.

Marchione, R., S.A. Leibovitch, and J.L. Lenormand. (2013). The translational factor eIF3f: the ambivalent eIF3 subunit. Cellular and Molecular Life Sciences : CMLS.

Martin, G., A. Ostareck-Lederer, A. Chari, et al. (2010). Arginine methylation in subunits of mammalian pre-mRNA cleavage factor I. RNA (New York, N.Y.). 16, 1646-1659.

Martin, S.J., C.P. Reutelingsperger, A.J. McGahon, et al. (1995). Early redistribution of plasma membrane phosphatidylserine is a general feature of apoptosis regardless of the initiating stimulus: inhibition by overexpression of Bcl-2 and Abl. The Journal of Experimental Medicine. 182, 1545-1556.

Marx, C., C. Yau, S. Banwait, et al. (2007). Proteasome-regulated ERBB2 and estrogen receptor pathways in breast cancer. Molecular Pharmacology. 71, 1525-1534.

Masuda, S., R. Das, H. Cheng, et al. (2005). Recruitment of the human TREX complex to mRNA during splicing. Genes & Development. 19, 1512-1517.

Mathioudaki, K., A. Papadokostopoulou, A. Scorilas, et al. (2008). The PRMT1 gene expression pattern in colon cancer. British Journal of Cancer. 99, 2094-2099.

Mathioudaki, K., A. Scorilas, A. Ardavanis, et al. (2011). Clinical evaluation of PRMT1 gene expression in breast cancer. Tumour Biology : The Journal of the International Society for Oncodevelopmental Biology and Medicine. 32, 575-582.

Matsumoto, K., H. Nakayama, M. Yoshimura, et al. (2012). PRMT1 is required for RAP55 to localize to processing bodies. RNA Biology. 9, 610-623.

Maurer-Stroh, S., N.J. Dickens, L. Hughes-Davies, et al. (2003). The Tudor domain 'Royal Family': Tudor, plant Agenet, Chromo, PWWP and MBT domains. Trends in Biochemical Sciences. 28, 69-74.

Mazroui, R., S. Di Marco, R.J. Kaufman, et al. (2007). Inhibition of the ubiquitin-proteasome system induces stress granule formation. Molecular Biology of the Cell. 18, 2603-2618.

Mazroui, R., M.E. Huot, S. Tremblay, et al. (2002). Trapping of messenger RNA by Fragile X Mental Retardation protein into cytoplasmic granules induces translation repression. Human Molecular Genetics. 11, 3007-3017.

Mazroui, R., R. Sukarieh, M.E. Bordeleau, et al. (2006). Inhibition of ribosome recruitment induces stress granule formation independently of eukaryotic initiation factor 2alpha phosphorylation. Molecular Biology of the Cell. 17, 4212-4219.

McConkey, D.J., and K. Zhu. (2008). Mechanisms of proteasome inhibitor action and resistance in cancer. Drug Resistance Updates : Reviews and Commentaries in Antimicrobial and Anticancer Chemotherapy. 11, 164-179.

McEwen, E., N. Kedersha, B. Song, et al. (2005). Heme-regulated inhibitor kinase-mediated phosphorylation of eukaryotic translation initiation factor 2 inhibits translation, induces stress granule formation, and mediates survival upon arsenite exposure. The Journal of Biological Chemistry. 280, 16925-16933.

Meerzaman, D.M., C. Yan, Q.R. Chen, et al. (2014). Genome-wide Transcriptional Sequencing Identifies Novel Mutations in Metabolic Genes in Human Hepatocellular Carcinoma. Cancer Genomics & Proteomics. 11, 1-12.

Meister, G., S. Hannus, O. Plottner, et al. (2001). SMNrp is an essential pre-mRNA splicing factor required for the formation of the mature spliceosome. The EMBO Journal. 20, 2304-2314.

Merrick, W.C. (2004). Cap-dependent and cap-independent translation in eukaryotic systems. Gene. 332, 1-11.

Merz, C., H. Urlaub, C.L. Will, et al. (2007). Protein composition of human mRNPs spliced in vitro and differential requirements for mRNP protein recruitment. RNA (New York, N.Y.). 13, 116-128.

Metivier, R., G. Penot, M.R. Hubner, et al. (2003). Estrogen receptor-alpha directs ordered, cyclical, and combinatorial recruitment of cofactors on a natural target promoter. Cell. 115, 751-763.

Miao, X., Z.L. Yang, L. Xiong, et al. (2013). Nectin-2 and DDX3 are biomarkers for metastasis and poor prognosis of squamous cell/adenosquamous carcinomas and adenocarcinoma of gallbladder. International Journal of Clinical and Experimental Pathology. 6, 179-190.

Michaud-Levesque, J., and S. Richard. (2009). Thrombospondin-1 is a transcriptional repression target of PRMT6. The Journal of Biological Chemistry. 284, 21338-21346.

Mitchell, T.R., K. Glenfield, K. Jeyanthan, et al. (2009). Arginine methylation regulates telomere length and stability. Molecular and Cellular Biology. 29, 4918-4934.

Mokas, S., J.R. Mills, C. Garreau, et al. (2009). Uncoupling stress granule assembly and translation initiation inhibition. Molecular Biology of the Cell. 20, 2673-2683.

Morettin,A., Baldwin,RM., Cote,J. (In Press). Arginine Methyltransferases as Novel Therapeutic Targets for Breast Cancer. Mutagenesis.

Morrogh, M., V.P. Andrade, D. Giri, et al. (2012). Cadherin-catenin complex dissociation in lobular neoplasia of the breast. Breast Cancer Research and Treatment. 132, 641-652.

Mostaqul Huq, M.D., P. Gupta, and L.N. Wei. (2008). Post-translational modifications of nuclear co-repressor RIP140: a therapeutic target for metabolic diseases. Current Medicinal Chemistry. 15, 386-392.

Muthukrishnan, S., G.W. Both, Y. Furuichi, et al. (1975). 5'-Terminal 7-methylguanosine in eukaryotic mRNA is required for translation. Nature. 255, 33-37.

Naeem, H., D. Cheng, Q. Zhao, et al. (2007). The activity and stability of the transcriptional coactivator p/CIP/SRC-3 are regulated by CARM1-dependent methylation. Molecular and Cellular Biology. 27, 120-134.

Nagahata, T., M. Onda, M. Emi, et al. (2004). Expression profiling to predict postoperative prognosis for estrogen receptor-negative breast cancers by analysis of 25,344 genes on a cDNA microarray. Cancer Science. 95, 218-225.

Nakopoulou, L., E. Mylona, I. Papadaki, et al. (2006). Study of phospho-beta-catenin subcellular distribution in invasive breast carcinomas in relation to their phenotype and the clinical outcome. Modern Pathology : An Official Journal of the United States and Canadian Academy of Pathology, Inc. 19, 556-563.

Navarro-Tito, N., T. Robledo, and E.P. Salazar. (2008). Arachidonic acid promotes FAK activation and migration in MDA-MB-231 breast cancer cells. Experimental Cell Research. 314, 3340-3355.

Neault, M., F.A. Mallette, G. Vogel, et al. (2012). Ablation of PRMT6 reveals a role as a negative transcriptional regulator of the p53 tumor suppressor. Nucleic Acids Research.

Neve, R.M., K. Chin, J. Fridlyand, et al. (2006). A collection of breast cancer cell lines for the study of functionally distinct cancer subtypes. Cancer Cell. 10, 515-527.

Nichols, R.C., X.W. Wang, J. Tang, et al. (2000). The RGG domain in hnRNP A2 affects subcellular localization. Experimental Cell Research. 256, 522-532.

Ohgaki, H., and P. Kleihues. (2007). Genetic pathways to primary and secondary glioblastoma. The American Journal of Pathology. 170, 1445-1453.

Ohkura, N., M. Takahashi, H. Yaguchi, et al. (2005). Coactivator-associated arginine methyltransferase 1, CARM1, affects pre-mRNA splicing in an isoform-specific manner. The Journal of Biological Chemistry. 280, 28927-28935.

Oliveira-Costa, J.P., J. Zanetti, L.R. Oliveira, et al. (2010). Significance of topoisomerase IIIbeta expression in breast ductal carcinomas: strong associations with disease-specific survival and metastasis. Human Pathology. 41, 1624-1630.

Pahlich, S., R.P. Zakaryan, and H. Gehring. (2006). Protein arginine methylation: Cellular functions and methods of analysis. Biochimica Et Biophysica Acta. 1764, 1890-1903.

Pak, M.L., T.M. Lakowski, D. Thomas, et al. (2011). A protein arginine N-methyltransferase 1 (PRMT1) and 2 heteromeric interaction increases PRMT1 enzymatic activity. Biochemistry. 50, 8226-8240.

Pal, S., S.N. Vishwanath, H. Erdjument-Bromage, et al. (2004). Human SWI/SNF-associated PRMT5 methylates histone H3 arginine 8 and negatively regulates expression of ST7 and NM23 tumor suppressor genes. Molecular and Cellular Biology. 24, 9630-9645.

Pal, S., R. Yun, A. Datta, et al. (2003). mSin3A/histone deacetylase 2- and PRMT5-containing Brg1 complex is involved in transcriptional repression of the Myc target gene cad. Molecular and Cellular Biology. 23, 7475-7487.

Papadokostopoulou, A., K. Mathioudaki, A. Scorilas, et al. (2009). Colon cancer and protein arginine methyltransferase 1 gene expression. Anticancer Research. 29, 1361-1366.

Park, S.H., S.G. Lee, Y. Kim, et al. (1998). Assignment of a human putative RNA helicase gene, DDX3, to human X chromosome bands p11.3-->p11.23. Cytogenetics and Cell Genetics. 81, 178-179.

Pasternack, D.A., J. Sayegh, S. Clarke, et al. (2007). Evolutionarily divergent type II protein arginine methyltransferase in Trypanosoma brucei. Eukaryotic Cell. 6, 1665-1681.

Pawlak, M.R., C.A. Scherer, J. Chen, et al. (2000). Arginine N-methyltransferase 1 is required for early postimplantation mouse development, but cells deficient in the enzyme are viable. Molecular and Cellular Biology. 20, 4859-4869.

Phalke, S., S. Mzoughi, M. Bezzi, et al. (2012). p53-Independent regulation of p21Waf1/Cip1 expression and senescence by PRMT6. Nucleic Acids Research.

Pintucci, G., N. Quarto, and D.B. Rifkin. (1996). Methylation of high molecular weight fibroblast growth factor-2 determines post-translational increases in molecular weight and affects its intracellular distribution. Molecular Biology of the Cell. 7, 1249-1258.

Pontes, J.,Jr, M. Srougi, P.M. Borra, et al. (2010). E-cadherin and beta-catenin loss of expression related to bone metastasis in prostate cancer. Applied Immunohistochemistry & Molecular Morphology : AIMM / Official Publication of the Society for Applied Immunohistochemistry. 18, 179-184.

Ponting, C.P. (1997). Tudor domains in proteins that interact with RNA. Trends in Biochemical Sciences. 22, 51-52.

Poulin, F., A.C. Gingras, H. Olsen, et al. (1998). 4E-BP3, a new member of the eukaryotic initiation factor 4E-binding protein family. The Journal of Biological Chemistry. 273, 14002-14007.

Powers, M.A., M.M. Fay, R.E. Factor, et al. (2011). Protein arginine methyltransferase 5 accelerates tumor growth by arginine methylation of the tumor suppressor programmed cell death 4. Cancer Research. 71, 5579-5587.

Qi, C., J. Chang, Y. Zhu, et al. (2002). Identification of protein arginine methyltransferase 2 as a coactivator for estrogen receptor alpha. The Journal of Biological Chemistry. 277, 28624-28630.

Rajkumar, S.V., P.G. Richardson, T. Hideshima, et al. (2005). Proteasome inhibition as a novel therapeutic target in human cancer. Journal of Clinical Oncology : Official Journal of the American Society of Clinical Oncology. 23, 630-639.

Rajpurohit, R., W.K. Paik, and S. Kim. (1994). Effect of enzymic methylation of heterogeneous ribonucleoprotein particle A1 on its nucleic-acid binding and controlled proteolysis. The Biochemical Journal. 304 (Pt 3), 903-909.

Rappsilber, J., P. Ajuh, A.I. Lamond, et al. (2001). SPF30 is an essential human splicing factor required for assembly of the U4/U5/U6 tri-small nuclear ribonucleoprotein into the spliceosome. The Journal of Biological Chemistry. 276, 31142-31150.

Rappsilber, J., W.J. Friesen, S. Paushkin, et al. (2003). Detection of arginine dimethylated peptides by parallel precursor ion scanning mass spectrometry in positive ion mode. Analytical Chemistry. 75, 3107-3114.

Raught, B., and A.C. Gingras. (1999). eIF4E activity is regulated at multiple levels. The International Journal of Biochemistry & Cell Biology. 31, 43-57.

Rezai-Zadeh, N., X. Zhang, F. Namour, et al. (2003). Targeted recruitment of a histone H4-specific methyltransferase by the transcription factor YY1. Genes & Development. 17, 1019-1029.

Ri, M., S. Iida, T. Nakashima, et al. (2010). Bortezomib-resistant myeloma cell lines: a role for mutated PSMB5 in preventing the accumulation of unfolded proteins and fatal ER stress. Leukemia. 24, 1506-1512.

Richardson, P.G., T. Hideshima, and K.C. Anderson. (2003). Bortezomib (PS-341): a novel, first-in-class proteasome inhibitor for the treatment of multiple myeloma and other cancers. Cancer Control : Journal of the Moffitt Cancer Center. 10, 361-369.

Richardson, P.G., T. Hideshima, C. Mitsiades, et al. (2004). Proteasome inhibition in hematologic malignancies. Annals of Medicine. 36, 304-314.

Robin-Lespinasse, Y., S. Sentis, C. Kolytcheff, et al. (2007). hCAF1, a new regulator of PRMT1-dependent arginine methylation. Journal of Cell Science. 120, 638-647.

Rocak, S., and P. Linder. (2004). DEAD-box proteins: the driving forces behind RNA metabolism. Nature Reviews.Molecular Cell Biology. 5, 232-241.

Rong, L., M. Livingstone, R. Sukarieh, et al. (2008). Control of eIF4E cellular localization by eIF4E-binding proteins, 4E-BPs. RNA (New York, N.Y.). 14, 1318-1327.

Rosales-Reynoso, M.A., A.B. Ochoa-Hernandez, A. Aguilar-Lemarroy, et al. (2010). Gene expression profiling identifies WNT7A as a possible candidate gene for decreased cancer risk in fragile X syndrome patients. Archives of Medical Research. 41, 110-118.e2.

Sakabe, K., and G.W. Hart. (2010). O-GlcNAc transferase regulates mitotic chromatin dynamics. The Journal of Biological Chemistry. 285, 34460-34468.

Sakamaki, J., H. Daitoku, K. Ueno, et al. (2011). Arginine methylation of BCL-2 antagonist of cell death (BAD) counteracts its phosphorylation and inactivation by Akt. Proceedings of the National Academy of Sciences of the United States of America. 108, 6085-6090.

Sayegh, J., K. Webb, D. Cheng, et al. (2007). Regulation of protein arginine methyltransferase 8 (PRMT8) activity by its N-terminal domain. The Journal of Biological Chemistry. 282, 36444-36453.

Schafer, D.A. (2004). Cell biology: barbed ends rule. Nature. 430, 734-735.

Schultz-Pedersen, S., H. Hasle, J.H. Olsen, et al. (2001). Evidence of decreased risk of cancer in individuals with fragile X. American Journal of Medical Genetics. 103, 226-230.

Sekiguchi, T., Y. Kurihara, and J. Fukumura. (2007). Phosphorylation of threonine 204 of DEAD-box RNA helicase DDX3 by cyclin B/cdc2 in vitro. Biochemical and Biophysical Research Communications. 356, 668-673.

Selenko, P., R. Sprangers, G. Stier, et al. (2001). SMN tudor domain structure and its interaction with the Sm proteins. Nature Structural Biology. 8, 27-31.

Seligson, D.B., S. Horvath, T. Shi, et al. (2005). Global histone modification patterns predict risk of prostate cancer recurrence. Nature. 435, 1262-1266.

Sgarra, R., J. Lee, M.A. Tessari, et al. (2006). The AT-hook of the chromatin architectural transcription factor high mobility group A1a is arginine-methylated by protein arginine methyltransferase 6. The Journal of Biological Chemistry. 281, 3764-3772.

Shattuck-Eidens, D., M. McClure, J. Simard, et al. (1995). A collaborative survey of 80 mutations in the BRCA1 breast and ovarian cancer susceptibility gene. Implications for presymptomatic testing and screening. JAMA : The Journal of the American Medical Association. 273, 535-541.

Shen, E.C., M.F. Henry, V.H. Weiss, et al. (1998). Arginine methylation facilitates the nuclear export of hnRNP proteins. Genes & Development. 12, 679-691.

Shih, J.W., T.Y. Tsai, C.H. Chao, et al. (2008). Candidate tumor suppressor DDX3 RNA helicase specifically represses cap-dependent translation by acting as an eIF4E inhibitory protein. Oncogene. 27, 700-714.

Shih, J.W., W.T. Wang, T.Y. Tsai, et al. (2012). Critical roles of RNA helicase DDX3 and its interactions with eIF4E/PABP1 in stress granule assembly and stress response. The Biochemical Journal. 441, 119-129.

Shringarpure, R., L. Catley, D. Bhole, et al. (2006). Gene expression analysis of B-lymphoma cells resistant and sensitive to bortezomib. British Journal of Haematology. 134, 145-156.

Shtutman, M., E. Levina, P. Ohouo, et al. (2006). Cell adhesion molecule L1 disrupts E-cadherin-containing adherens junctions and increases scattering and motility of MCF7 breast carcinoma cells. Cancer Research. 66, 11370-11380.

Siegel, D.S. (2012). Relapsed/Refractory multiple myeloma: defining refractory disease and identifying strategies to overcome resistance. Seminars in Hematology. 49 Suppl 1, S3-15.

Sikorsky, T., F. Hobor, E. Krizanova, et al. (2012). Recognition of asymmetrically dimethylated arginine by TDRD3. Nucleic Acids Research. 40, 11748-11755.

Singh, V., T.B. Miranda, W. Jiang, et al. (2004). DAL-1/4.1B tumor suppressor interacts with protein arginine N-methyltransferase 3 (PRMT3) and inhibits its ability to methylate substrates in vitro and in vivo. Oncogene. 23, 7761-7771.

Singhroy, D.N., T. Mesplede, A. Sabbah, et al. (2013). Automethylation of protein arginine methyltransferase 6 (PRMT6) regulates its stability and its anti-HIV-1 activity. Retrovirology. 10, 73-4690-10-73.

Siomi, H., M.C. Siomi, R.L. Nussbaum, et al. (1993). The protein product of the fragile X gene, FMR1, has characteristics of an RNA-binding protein. Cell. 74, 291-298.

Siomi, M.C., T. Mannen, and H. Siomi. (2010). How does the royal family of Tudor rule the PIWI-interacting RNA pathway? Genes & Development. 24, 636-646.

Sivakumaran, H., M.H. Lin, A. Apolloni, et al. (2013). Overexpression of PRMT6 does not suppress HIV-1 Tat transactivation in cells naturally lacking PRMT6. Virology Journal. 10, 207-422X-10-207.

Sivakumaran, H., A. van der Horst, A.J. Fulcher, et al. (2009). Arginine methylation increases the stability of human immunodeficiency virus type 1 Tat. Journal of Virology. 83, 11694-11703.

Sloss, C.M., F. Wang, R. Liu, et al. (2008). Proteasome inhibition activates epidermal growth factor receptor (EGFR) and EGFR-independent mitogenic kinase signaling pathways in pancreatic cancer cells. Clinical Cancer Research : An Official Journal of the American Association for Cancer Research. 14, 5116-5123.

Solomon, S., Y. Xu, B. Wang, et al. (2007). Distinct structural features of caprin-1 mediate its interaction with G3BP-1 and its induction of phosphorylation of eukaryotic translation initiation factor 2alpha, entry to cytoplasmic stress granules, and selective interaction with a subset of mRNAs. Molecular and Cellular Biology. 27, 2324-2342.

Soto-Rifo, R., P.S. Rubilar, T. Limousin, et al. (2012). DEAD-box protein DDX3 associates with eIF4F to promote translation of selected mRNAs. The EMBO Journal. 31, 3745-3756.

Srivastava, S.P., K.U. Kumar, and R.J. Kaufman. (1998). Phosphorylation of eukaryotic translation initiation factor 2 mediates apoptosis in response to activation of the double-stranded RNA-dependent protein kinase. The Journal of Biological Chemistry. 273, 2416-2423.

Stein, C., S. Riedl, D. Ruthnick, et al. (2012). The arginine methyltransferase PRMT6 regulates cell proliferation and senescence through transcriptional repression of tumor suppressor genes. Nucleic Acids Research.

Sterz, J., I. von Metzler, J.C. Hahne, et al. (2008). The potential of proteasome inhibitors in cancer therapy. Expert Opinion on Investigational Drugs. 17, 879-895.

Stockinger, A., A. Eger, J. Wolf, et al. (2001). E-cadherin regulates cell growth by modulating proliferation-dependent beta-catenin transcriptional activity. The Journal of Cell Biology. 154, 1185-1196.

Stoecklin, G., and N. Kedersha. (2013). Relationship of GW/P-bodies with stress granules. Advances in Experimental Medicine and Biology. 768, 197-211.

Stoecklin, G., T. Stubbs, N. Kedersha, et al. (2004). MK2-induced tristetraprolin:14-3-3 complexes prevent stress granule association and ARE-mRNA decay. The EMBO Journal. 23, 1313-1324.

Stoll, G., O.P. Pietilainen, B. Linder, et al. (2013). Deletion of TOP3beta, a component of FMRP-containing mRNPs, contributes to neurodevelopmental disorders. Nature Neuroscience. 16, 1228-1237.

Sun, M., L. Song, Y. Li, et al. (2008). Identification of an antiapoptotic protein complex at death receptors. Cell Death and Differentiation. 15, 1887-1900.

Sun, M., L. Song, T. Zhou, et al. (2011). The role of DDX3 in regulating Snail. Biochimica Et Biophysica Acta. 1813, 438-447.

Sun, M., T. Zhou, E. Jonasch, et al. (2013). DDX3 regulates DNA damage-induced apoptosis and p53 stabilization. Biochimica Et Biophysica Acta. 1833, 1489-1497.

Takahashi, Y., M. Iwai, T. Kawai, et al. (2012). Aberrant expression of tumor suppressors CADM1 and 4.1B in invasive lesions of primary breast cancer. Breast Cancer (Tokyo, Japan). 19, 242-252.

Tamanini, F., R. Willemsen, L. van Unen, et al. (1997). Differential expression of FMR1, FXR1 and FXR2 proteins in human brain and testis. Human Molecular Genetics. 6, 1315-1322.

Tang, J., A. Frankel, R.J. Cook, et al. (2000). PRMT1 is the predominant type I protein arginine methyltransferase in mammalian cells. The Journal of Biological Chemistry. 275, 7723-7730.

Tang, Z.Y., Y.L. Wu, S.L. Gao, et al. (2008). Effects of the proteasome inhibitor bortezomib on gene expression profiles of pancreatic cancer cells. The Journal of Surgical Research. 145, 111-123.

Tanner, N.K. (2003). The newly identified Q motif of DEAD box helicases is involved in adenine recognition. Cell Cycle (Georgetown, Tex.). 2, 18-19.

Tanner, N.K., and P. Linder. (2001). DExD/H box RNA helicases: from generic motors to specific dissociation functions. Molecular Cell. 8, 251-262.

Tarn, W.Y., and T.H. Chang. (2009). The current understanding of Ded1p/DDX3 homologs from yeast to human. RNA Biology. 6, 17-20.

Taverna, S.D., H. Li, A.J. Ruthenburg, et al. (2007). How chromatin-binding modules interpret histone modifications: lessons from professional pocket pickers. Nature Structural & Molecular Biology. 14, 1025-1040.

Theobald, D.L., R.M. Mitton-Fry, and D.S. Wuttke. (2003). Nucleic acid recognition by OB-fold proteins. Annual Review of Biophysics and Biomolecular Structure. 32, 115-133.

Thomassen, M., Q. Tan, and T.A. Kruse. (2009). Gene expression meta-analysis identifies chromosomal regions and candidate genes involved in breast cancer metastasis. Breast Cancer Research and Treatment. 113, 239-249.

Tomaskovic-Crook, E., E.W. Thompson, and J.P. Thiery. (2009). Epithelial to mesenchymal transition and breast cancer. Breast Cancer Research : BCR. 11, 213.

Topisirovic, I., N. Siddiqui, V.L. Lapointe, et al. (2009). Molecular dissection of the eukaryotic initiation factor 4E (eIF4E) export-competent RNP. The EMBO Journal. 28, 1087-1098.

Tourriere, H., K. Chebli, L. Zekri, et al. (2003). The RasGAP-associated endoribonuclease G3BP assembles stress granules. The Journal of Cell Biology. 160, 823-831.

Tradewell, M.L., Z. Yu, M. Tibshirani, et al. (2012). Arginine methylation by PRMT1 regulates nuclear-cytoplasmic localization and toxicity of FUS/TLS harbouring ALS-linked mutations. Human Molecular Genetics. 21, 136-149.

Treger, M., and E. Westhof. (2001). Statistical analysis of atomic contacts at RNA-protein interfaces. Journal of Molecular Recognition : JMR. 14, 199-214.

Trinkle-Mulcahy, L., S. Boulon, Y.W. Lam, et al. (2008). Identifying specific protein interaction partners using quantitative mass spectrometry and bead proteomes. The Journal of Cell Biology. 183, 223-239.

Tripsianes, K., T. Madl, M. Machyna, et al. (2011). Structural basis for dimethylarginine recognition by the Tudor domains of human SMN and SPF30 proteins. Nature Structural & Molecular Biology. 18, 1414-1420.

Tseng, L.M., C.Y. Liu, K.C. Chang, et al. (2012). CIP2A is a target of bortezomib in human triple negative breast cancer cells. Breast Cancer Research : BCR. 14, R68.

Ueda, T., R. Watanabe-Fukunaga, H. Fukuyama, et al. (2004). Mnk2 and Mnk1 are essential for constitutive and inducible phosphorylation of eukaryotic initiation factor 4E but not for cell growth or development. Molecular and Cellular Biology. 24, 6539-6549.

Van Aken, E., O. De Wever, A.S. Correia da Rocha, et al. (2001). Defective E-cadherin/catenin complexes in human cancer. Virchows Archiv : An International Journal of Pathology. 439, 725-751.

van Dijk, E., N. Cougot, S. Meyer, et al. (2002). Human Dcp2: a catalytically active mRNA decapping enzyme located in specific cytoplasmic structures. The EMBO Journal. 21, 6915-6924.

Wada, K., K. Inoue, and M. Hagiwara. (2002). Identification of methylated proteins by protein arginine N-methyltransferase 1, PRMT1, with a new expression cloning strategy. Biochimica Et Biophysica Acta. 1591, 1-10.

Waldmann, T., A. Izzo, K. Kamieniarz, et al. (2011). Methylation of H2AR29 is a novel repressive PRMT6 target. Epigenetics & Chromatin. 4, 11-8935-4-11.

Wang, L.W., E. Berry-Kravis, and R.J. Hagerman. (2010). Fragile X: leading the way for targeted treatments in autism. Neurotherapeutics : The Journal of the American Society for Experimental NeuroTherapeutics. 7, 264-274.

Wang, X., Y. Huang, J. Zhao, et al. (2012). Suppression of PRMT6-mediated arginine methylation of p16 protein potentiates its ability to arrest A549 cell proliferation. The International Journal of Biochemistry & Cell Biology.

Wang, Y., J. Wysocka, J. Sayegh, et al. (2004). Human PAD4 regulates histone arginine methylation levels via demethylimination. Science (New York, N.Y.). 306, 279-283.

Waskiewicz, A.J., J.C. Johnson, B. Penn, et al. (1999). Phosphorylation of the cap-binding protein eukaryotic translation initiation factor 4E by protein kinase Mnk1 in vivo. Molecular and Cellular Biology. 19, 1871-1880.

Webby, C.J., A. Wolf, N. Gromak, et al. (2009). Jmjd6 catalyses lysyl-hydroxylation of U2AF65, a protein associated with RNA splicing. Science (New York, N.Y.). 325, 90-93.

Weber, G.L., M.O. Parat, Z.A. Binder, et al. (2011). Abrogation of PIK3CA or PIK3R1 reduces proliferation, migration, and invasion in glioblastoma multiforme cells. Oncotarget. 2, 833-849.

Wek, S.A., S. Zhu, and R.C. Wek. (1995). The histidyl-tRNA synthetase-related sequence in the eIF-2 alpha protein kinase GCN2 interacts with tRNA and is required for

activation in response to starvation for different amino acids. Molecular and Cellular Biology. 15, 4497-4506.

Wilczynska, A., C. Aigueperse, M. Kress, et al. (2005). The translational regulator CPEB1 provides a link between dcp1 bodies and stress granules. Journal of Cell Science. 118, 981-992.

Winston, J.T., P. Strack, P. Beer-Romero, et al. (1999). The SCFbeta-TRCP-ubiquitin ligase complex associates specifically with phosphorylated destruction motifs in IkappaBalpha and beta-catenin and stimulates IkappaBalpha ubiquitination in vitro. Genes & Development. 13, 270-283.

Wooderchak, W.L., T. Zang, Z.S. Zhou, et al. (2008). Substrate profiling of PRMT1 reveals amino acid sequences that extend beyond the "RGG" paradigm. Biochemistry. 47, 9456-9466.

Wu, D.W., M.C. Lee, J. Wang, et al. (2013). DDX3 loss by p53 inactivation promotes tumor malignancy via the MDM2/Slug/E-cadherin pathway and poor patient outcome in non-small-cell lung cancer. Oncogene.

Wu, D.W., W.S. Liu, J. Wang, et al. (2011). Reduced p21(WAF1/CIP1) via alteration of p53-DDX3 pathway is associated with poor relapse-free survival in early-stage human papillomavirus-associated lung cancer. Clinical Cancer Research : An Official Journal of the American Association for Cancer Research. 17, 1895-1905.

Xie, B., C.F. Invernizzi, S. Richard, et al. (2007). Arginine methylation of the human immunodeficiency virus type 1 Tat protein by PRMT6 negatively affects Tat Interactions with both cyclin T1 and the Tat transactivation region. Journal of Virology. 81, 4226-4234.

Xu, D., W. Shen, R. Guo, et al. (2013). Top3beta is an RNA topoisomerase that works with fragile X syndrome protein to promote synapse formation. Nature Neuroscience. 16, 1238-1247.

Yadav, N., D. Cheng, S. Richard, et al. (2008). CARM1 promotes adipocyte differentiation by coactivating PPARgamma. EMBO Reports. 9, 193-198.

Yadav, N., J. Lee, J. Kim, et al. (2003). Specific protein methylation defects and gene expression perturbations in coactivator-associated arginine methyltransferase 1-deficient mice. Proceedings of the National Academy of Sciences of the United States of America. 100, 6464-6468.

Yamagata, K., H. Daitoku, Y. Takahashi, et al. (2008). Arginine methylation of FOXO transcription factors inhibits their phosphorylation by Akt. Molecular Cell. 32, 221-231.

Yamaguchi, A., and K. Kitajo. (2012). The effect of PRMT1-mediated arginine methylation on the subcellular localization, stress granules, and detergent-insoluble aggregates of FUS/TLS. PloS One. 7, e49267.

Yang, Y., Y. Lu, A. Espejo, et al. (2010). TDRD3 is an effector molecule for arginine-methylated histone marks. Molecular Cell. 40, 1016-1023.

Yedavalli, V.S., C. Neuveut, Y.H. Chi, et al. (2004). Requirement of DDX3 DEAD box RNA helicase for HIV-1 Rev-RRE export function. Cell. 119, 381-392.

Yonemura, S. (2011). Cadherin-actin interactions at adherens junctions. Current Opinion in Cell Biology. 23, 515-522.

Yoshida, R., N. Kimura, Y. Harada, et al. (2001). The loss of E-cadherin, alpha- and beta-catenin expression is associated with metastasis and poor prognosis in invasive breast cancer. International Journal of Oncology. 18, 513-520.

Yoshimatsu, M., G. Toyokawa, S. Hayami, et al. (2011). Dysregulation of PRMT1 and PRMT6, Type I arginine methyltransferases, is involved in various types of human cancers. International Journal of Cancer.Journal International Du Cancer. 128, 562-573.

Yu, Z., T. Chen, J. Hebert, et al. (2009). A mouse PRMT1 null allele defines an essential role for arginine methylation in genome maintenance and cell proliferation. Molecular and Cellular Biology. 29, 2982-2996.

Yuan, L., Y. Xiao, Q. Zhou, et al. (2014). Proteomic analysis reveals that MAEL, a component of nuage, interacts with stress granule proteins in cancer cells. Oncology Reports. 31, 342-350.

Yue, W.W., M. Hassler, S.M. Roe, et al. (2007). Insights into histone code syntax from structural and biochemical studies of CARM1 methyltransferase. The EMBO Journal. 26, 4402-4412.

Zang, J.B., E.D. Nosyreva, C.M. Spencer, et al. (2009). A mouse model of the human Fragile X syndrome I304N mutation. PLoS Genetics. 5, e1000758.

Zhang, X., and X. Cheng. (2003). Structure of the predominant protein arginine methyltransferase PRMT1 and analysis of its binding to substrate peptides. Structure (London, England : 1993). 11, 509-520.

Zhao, X., V. Jankovic, A. Gural, et al. (2008). Methylation of RUNX1 by PRMT1 abrogates SIN3A binding and potentiates its transcriptional activity. Genes & Development. 22, 640-653.

Zheng, S., J. Huang, K. Zhou, et al. (2011). 17beta-Estradiol enhances breast cancer cell motility and invasion via extra-nuclear activation of actin-binding protein ezrin. PloS One. 6, e22439.

Zheng, S., J. Moehlenbrink, Y.C. Lu, et al. (2013). Arginine methylation-dependent reader-writer interplay governs growth control by E2F-1. Molecular Cell. 52, 37-51.

Zhong, J., R.X. Cao, T. Hong, et al. (2011). Identification and expression analysis of a novel transcript of the human PRMT2 gene resulted from alternative polyadenylation in breast cancer. Gene. 487, 1-9.

Zhong, J., R.X. Cao, X.Y. Zu, et al. (2012). Identification and characterization of novel spliced variants of PRMT2 in breast carcinoma. The FEBS Journal. 279, 316-335.

Zhou, Z., L.J. Licklider, S.P. Gygi, et al. (2002). Comprehensive proteomic analysis of the human spliceosome. Nature. 419, 182-185.

Zou, L., H. Zhang, C. Du, et al. (2012). Correlation of SRSF1 and PRMT1 expression with clinical status of pediatric acute lymphoblastic leukemia. Journal of Hematology & Oncology. 5, 42.

Zurita-Lopez, C.I., T. Sandberg, R. Kelly, et al. (2012). Human protein arginine methyltransferase 7 (PRMT7) is a type III enzyme forming omega-NG-monomethylated arginine residues. The Journal of Biological Chemistry. 287, 7859-7870.

Alan James Morettin

Education

University of Ottawa
Candidate for Doctor of Philosophy in Cellular and Molecular Medicine, May 2014

University of Windsor
Masters of Science in Biology, Apr. 2008

Lake Superior State University
Bachelor of Science in Biology, May 2003

Experience

Sept. 2008-Present **Department of Cellular and Molecular Medicine, University of Ottawa, Ottawa, ON**

- Involved in novel research projects leading to the publication of peer reviewed articles
- Designed, performed, and analyzed data pertaining to multiple research projects
- Involved in the supervision of undergraduate and Master's students through assisting in experimental design for research projects

Apr. 2008-Aug. 2008 **Research Technician, Department of Biology, University of Windsor,**

Windsor, ON

- Assisted in research projects leading to the publication of articles in peer reviewed journal
- Responsible for the day to day operation of the lab

Sept. 2005-Apr. 2008 **Department of Biology, University of Windsor, Windsor, ON**

- Undertook novel research in projects that lead to publication in a peer reviewed article
- Designed, performed, and analyzed data pertaining to a novel research project

Sept. 2005-Apr.2008 **Teaching Assistant, Department of Biology, University of Windsor, Windsor, ON**

- Teaching Assistant in the Department of Biology for courses in genetics and biotechnology

- Responsible for introducing laboratory concepts to undergraduate students and directing them through to the completion of the lab
- Responsible for evaluating students and providing constructive feedback to improve academic performance

Publications

- Morettin A, Baldwin RM, Cote J. Arginine Methyltransferase as novel therapeutic targets in breast cancer. *Mutagenesis* In Press

- Baldwin RM, Morettin A, Cote J. The role of PRMTs in cancer: Could minor isoforms be leaving a mark (2014). *World J. of Biol. Chem.* **5** (2): 115-129

- Baldwin RM, Morettin A, Paris G, Goulet I, Cote J. Alternatively spliced protein arginine methyltransferase 1 isoform PRMT1v2 promotes the survival and invasiveness of breast cancer cells (2013). *Cell Cycle* **11**(24): 1-16.

- Ward A, Morettin A, Shum B, Hudson JW. Aberrant methylation of polo-like kinase CpG islands in *Plk4* heterozygous mice (2011). *BMC Cancer* **11**: 71.

- Morettin A, Ward A, Nantais J, Hudson JW. Gene expression patterns in heterozygous *Plk4* murine embryonic fibroblasts. (2009). *BMC Genomics* **10**: 319.

Awards

- Faculty of Graduate Studies Admission Scholarship, University of Ottawa, Ottawa, ON (Sept. 2008-Aug. 2012)

- Faculty of Graduate Studies Admission Scholarship, University of Windsor, Windsor, ON (Sept. 2005-Aug. 2007)

- All American Collegiate Scholarship Award, Lake Superior State University, Sault Ste. Marie, MI

- National College Honour Scholarship, Alpha Chi Honour Society, Lake Superior State University, Sault Ste. Marie, MI

- Board of Trustees Scholarship, Lake Superior State University, Sault Ste. Marie, MI (Sept. 1999-May 2003)

Presentations

Oral Presentations

- RNA Club, University of Ottawa, Ottawa, ON (Apr. 2012 and Dec. 2013)

Poster Presentations

- FASEB Biological Methylation: Regulation of Chromatin, Epigenetics, and Disease, Nassau, Bahamas July 6-11, 2014